EFFECT OF THE ADJACENT SPAN ON THE LATERAL-TORSIONAL BUCKLING CAPACITY OF OVERHANG BEAMS

SIMON HERMAN VENTER

A project dissertation submitted in partial fulfilment of the requirement for the degree of

MASTER OF ENGINEERING (STRUCTURAL ENGINEERING)

In the

FACULTY OF ENGINEERING

UNIVERSITY OF PRETORIA

December 2016

PROJECT DISSERTATION SUMMARY

EFFECT OF THE ADJACENT SPAN ON THE LATERAL-TORSIONAL BUCKLING CAPACITY OF OVERHANG BEAMS

SIMON HERMAN VENTER

Supervisor:	Ms SA Skorpen
Co-supervisor:	Professor BWJ van Rensburg
Department:	Civil Engineering
University:	University of Pretoria
Degree:	Master of Engineering (Structural engineering)

Lateral-torsional buckling is a possible instability failure in slender beams. Therefore, codes such as SANS 10162-1 and BS 5950-1 provide methods to determine the buckling capacity of a beam. For overhang beams, SANS 10162-1 and BS 5950-1 have a single set of effective length factors. This single set of factors implies either that the adjacent segment was not considered or that it had no effect on the lateral-torsional buckling capacity. Factors such as warping allow interaction buckling. Hence, the adjacent span has an effect on the buckling capacity of an overhang beam. The aim of the study was to develop a design equation for the elastic critical buckling moment M_{cr}, to include the effect of the adjacent span.

A different approach for designers to determine the buckling capacities of specialised high-risk beam is to use finite element (FE) analysis. The validity of FE result from the models depends on the analysis assumptions made by the designer. Thus each designer very often obtains different results. The purpose of the study was, therefore, to try to refine current design methods to allow a designer to calculate quickly and effectively the elastic critical buckling moment of overhang beams without using FE modelling.

The beams tested and analysed were hot-rolled, uniform, doubly symmetric steel I-sections with no lateral bracing, other than at the supports; with a point load at the free end.

By comparing current methods in calculating LTB, it was noted that the effective length approach of SANS 10162-1 was conservative for overhang beams. The current method employed by SANS 10162-1 and BS 5950-1 could be refined by altering the effective length factors, which is a non-dimensional parameter.

Two methods were employed to refine the design approach: physical experiments and FE modelling. Physical experiments aided and verified the accuracy of FE models. FE analyses were used to conduct a parametric study, in which the overhang length, beam size, load height and the backspan to overhang ratio were varied. With the results obtained, it was possible to simplify and standardise the design method. Standardising allows the method to apply to a large variety of I-beams, regardless of the lengths of each span. A simplified design calculation could eliminate the need for FE modelling (due to the difference in assumptions), allowing consistent results. Instead of effective length factors, a non-dimensional buckling parameter was utilised.

The conclusions show that the buckling parameter is dependent on the size of the beam; the distance between applied load and shear centre; the length of the overhanging segment; and the ratio of backspan to overhang length. Larger overhanging segment lengths and larger backspan to overhang ratios decreases the buckling capacity. The reduced buckling capacity due to top flange loading decreases as the overhang to backspan ratio increases. The design equation developed in this study facilitates calculations for any I-beam size within the calibrated limits. The design equation is up to 13 % conservative compared to FE analyses.

DECLARATION

I, the undersigned hereby declare that:

- I understand what plagiarism is and I am aware of the University's policy in this regard;

- The work contained in this dissertation is my own original work;

- I did not refer to work of current or previous students, lecture notes, handbooks or any other study material without proper referencing;

- Where other people's work has been used this has been properly acknowledged and referenced;

- I have not allowed anyone to copy any part of my dissertation;

- I have not previously in its entirety or in part submitted this dissertation at any university for a degree.

DISCLAIMER:

The work presented in this report is that of the student alone. Students were encouraged to take ownership of their projects and to develop and execute their experiments with limited guidance and assistance. The content of the research does not necessarily represent the views of the supervisor or any staff member of the University of Pretoria, Department of Civil Engineering. The supervisor did not read or edit the final report and is not responsible for any technical inaccuracies, statements or errors. The conclusions and recommendations given in the report are also not necessarily that of the supervisor, sponsors or companies involved in the research.

Name of student: Simon Herman Venter

Student number: 10689550

Date: 1 December 2016

Number of words in report: 32365 words

ACKNOWLEDGEMENT

I wish to express my appreciation to the following organisations and persons who made this project dissertation possible:

a) The University of Pretoria for providing the required materials, computer software and laboratory facilities during the course of the study.

b) Ms J Callanan, for providing assistance in obtaining the required materials from the suppliers.

c) NJR Steel, who provided the $IPE_{AA}100$ steel beams and steel plates used in the experiments.

d) The following persons are gratefully acknowledged for their assistance to ensure that the experimental setup and testing was a success:

   i)   Mr J Scholtz
   ii)   Mr D Mostert
   iii) Mr J Botha
   iv)   Mr J Nkosi

e) Ms SA Skorpen, my supervisor and Professor BWJ van Rensburg, my co-supervisor for their guidance and support throughout the year.

f) Mr RS Peterson for proof reading the dissertation.

TABLE OF CONTENTS

LIST OF TABLES

LIST OF FIGURES

LIST OF ALPHABETICAL SYMBOLS

A	=	Expression used to calculate ω_2 or α; factor.
B	=	Expression used to calculate ω_2; factor.
B_1 & B_2	=	Expression used to calculate α.
B_r	=	Factored bearing resistance of member or component.
C	=	Torsional rigidity; factor.
C_1	=	Warping rigidity.
C_1 & C_2	=	Expressions used to calculate the buckling moment.
C_B	=	Effect of bracing coefficient.
C_H	=	Effect of load height coefficient.
C_L	=	Moment distribution coefficient.
C_w	=	Warping torsional constant.
d	=	Depth of steel cross-section; distance between flange centroids.
E	=	Elastic modulus of steel.
{F}	=	Global load vector.
f_u	=	Ultimate strength of steel.
f_y	=	Specified minimum yield stress.
f_{y_l}	=	Lower yield strength.
f_{y_u}	=	Upper yield strength.
G	=	Shear modulus of steel.
h	=	Distance between shear centre and load applied; measured height of the beam.
h_s	=	Distance between flange centroids.
I	=	Interaction factor.
I_t	=	St. Venant torsion constant of a cross-section (Equivalent to J).
$I_{t,spring}$	=	Converted torsional constant of a spring element.
I_w	=	Warping torsional constant (Equivalent to C_w).
I_y	=	Moment of inertia about y-axis.
I_z	=	Moment of inertia about z-axis (European equivalent for I_y).
i_z	=	Radius of gyration about z-axis (Equivalent to r_y).
J	=	St. Venant torsion constant of a cross-section.
K	=	Torsional parameter of a segment.
$\overline{K}$	=	Modified torsional parameter.
[K]	=	Global stiffness matrix.
k	=	Effective length factor, taking into account distance between shear centre and load.

k_b	=	Effective length factor of the beam.
k_c	=	Effective length factor of cantilever (overhang) segment.
k_s	=	Effective length factor for shear centre loading.
k_{spring}	=	Rotation spring stiffness.
k_t	=	Effective length factor for top flange loading.
k_w	=	Effective length factor for end warping restraint.
K_y	=	Effective length factor about y-axis.
K_z	=	Effective length factor about z-axis.
k_z	=	Effective length factor for end reactions about the z-axis.
L	=	Length of beam between restraints.
l	=	Length of the element.
L_b	=	Length of backspan segment.
L_c	=	Length of cantilever (overhang) segment.
$(M_0)_{cr}$	=	Effective elastic critical buckling moment of a simply supported beam.
M_b	=	Critical moment of backspan segment that is free to warp (simply supported beam).
M_c	=	Maximum moment; critical moment of cantilever segment that is free to warp.
M_{cr}	=	Critical elastic moment of laterally unbraced beam.
M_{cru}	=	Elastic critical buckling moment of a simply supported beam.
M_I	=	Inelastic beam buckling moment.
M_L	=	Limiting end moment on a crooked and twisted beam at first yield.
M_p	=	Plastic moment of cross-section.
M_r	=	Bending resistance.
M_u	=	Critical bending moment.
M_{ult}	=	Ultimate buckling moment.
M_y	=	Yield moment of cross-section.
M_{yz}	=	Elastic lateral buckling moment of a simply supported beam in uniform bending.
N	=	Length of bearing of an applied load.
P_{cr}	=	Elastic critical buckling load of a cantilever.
Q	=	Critical point load at free end.
q	=	Uniformly distributed load.
R	=	Torsional slenderness parameter.
r	=	Ratio relating distance between shear centre and load applied to the cross-section depth.
r_y	=	Radius of gyration about y-axis.
S	=	Non-dimensional buckling parameter.
t_{bf}	=	Thickness of bottom flange.

t_f	=	Flange thickness.
t_{tf}	=	Thickness of top flange.
t_w	=	Web thickness.
{U}	=	Global displacement vector.
u	=	Lateral deflection.
X	=	Torsional parameter (Equivalent to K).
x	=	Lateral axis.
y	=	Vertical axis.
y_Q	=	Distance between the shear centre and the load applied below the shear centre.
z_g	=	Distance between shear centre and load applied.
z	=	Longitudinal axis; longitudinal position along the beam.

LIST OF GREEK SYMBOLS

α	=	Lateral buckling coefficient.
α_m	=	Moment modification factor.
Γ	=	Warping torsional constant (equivalent to C_w).
γ	=	Buckling coefficient; dimensionless factor.
γ_2	=	Dimensionless factor.
γ_e	=	Effective buckling coefficient.
$\gamma_{q\lambda_{cr}}$	=	Non-dimensional parameter.
δ_{L_B}	=	Lateral deflection of the backspan segment.
δ_{L_b}	=	Lateral deflection of bottom flange.
δ_{L_C}	=	Lateral deflection of the overhanging segment.
δ_{L_t}	=	Lateral deflection of top flange.
δ_{V_B}	=	Vertical deflection of the backspan segment.
δ_{V_C}	=	Vertical deflection of the overhanging segment.
ε	=	Dimensionless load height parameter.
ϕ	=	0.9, Resistance factor for structural steel; longitudinal twist.
ϕ_B	=	Twist of the backspan segment.
ϕ_{be}	=	0.75, Resistance factor for beam web bearing, end.
ϕ_C	=	Twist of the overhanging segment.
ω_2	=	Equivalent moment factor (C_b in American literature).

1. INTRODUCTION

1.1 BACKGROUND

A slender cantilevered beam may fail due to instability, explicitly known as a buckling failure. Buckling is determined by various beam parameters. Steel design specifications each have different approaches to calculating the buckling capacity. Unbraced cantilevered beams are more susceptible to buckling than ordinary simply supported beams, as it has no vertical support at the free end of the beam; hence, the capacity in resisting a load is reduced. Cantilevers and overhang beams, of which both have a cantilevered segment, are either part of a permanent structure or act as temporary structure during the construction phase. Therefore, the buckling capacity of a cantilevered beam is an important beam characteristic as it is considered for both construction and design loads.

In the last century, the growth of the urban environment has expanded rapidly and often leaving designers with a limited amount of space to build new structures. Cantilevers and overhang beams are used in structures to avoid compromising the available space. With current design technology, architects are designing more complex façades to improve the aesthetics of a building. Thus engineers often rely on overhang beams to meet the architect's design requirements. Examples include small overhangs such as viewing decks, balconies and swimming pools to significant overhang length such as a roof structure of a sports stadium.

As with the examples mentioned above, designers often prefer using continuous overhang beams rather than a separate built-in cantilever beam and an interior span beam. A continuous beam reduces the design and construction time as the connection at the support is simplified. Simplified connections at the supports reduce the probability of failure. Because overhang beams are continuous, warping in the beams is not restricted at the supports. Therefore, the adjacent span (backspan) may have an effect on the buckling capacity of the cantilevered segment, be it either beneficial or detrimental.

Buckling, especially lateral-torsional buckling (LTB) is an instability bound failure that occurs before the material strength of the beam is reached. Lateral-torsional buckling is recognisable by the entire cross-section of the beam twisting and deflecting laterally when the beam buckles, hence the terms 'lateral' and 'torsional'. Figure 1.1 illustrates a built-in cantilever in the unloaded and buckled position. LTB could occur if the beam is slender along the length, even if the cross-section of the beam is large enough to withstand the force applied. By bracing the beam to the structure, it is possible to prevent buckling. The buckling capacity and mode are required to determine the position of the beam that needs bracing.
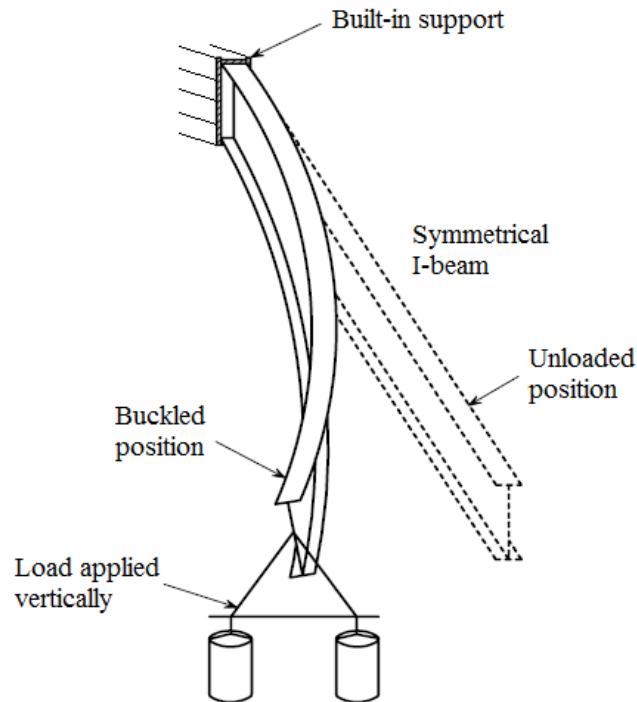
Figure 1.1: Buckled shape of a built-in cantilever.

The buckling capacities of cantilevers were extensively investigated, usually resulting in governing equations or curve fitting polynomials. Difficulties arise when calculating the LTB capacity of an overhang beam. Overhang beams have many variables, each that could affect the buckling capacity. Unlike cantilevers, the length of the adjacent span must be considered, in addition to the warping effect of the internal support.

Current solutions rely on limiting the effective length of the cantilevered segment to at least the length of the adjacent span, allowing methods such as those given by Kirby and Nethercot (1979). The effective length factors provided by Kirby and Nethercot (1979) were adopted by Ziemian (2010), the British Standards (BS 5950-1:2000, 2008) and the South African National Standards (SANS 10162:1, 2011). However, neither Ziemian (2010) nor SANS 10162-1 stipulated this lower limit on cantilevered segment effective lengths, even though similar effective length factors to Kirby and Nethercot (1979) were used.

Each overhang beam is unique and therefore, has unique properties and dimensions. The problem arose when the critical buckling strength of the beam needed to be calculated. Currently, SANS 10162:1, BS 5950-1 and Ziemian (2010) provide a method to calculate the critical buckling strength of an overhang beam using the effective length of the overhanging segment. However, these methods do not take into account the ratio of backspan to overhang. SANS 10162-1, BS 5950-1 and Ziemian (2010) assume that

the buckling capacity of the overhanging segment is independent of the backspan length. That means the buckling capacity calculated for the overhanging segment could be either over-conservative or non-conservative. The Canadian Code (CAN/CSA-S16-01, 2004) does not have any effective length factors. Comparing CAN/CSA-S16-01 to SANS 10162-1 and BS 5950-1 could result in a difference in buckling capacity.

The designer has at least two options: ensuring that the effective overhang length is at least as long as the backspan for each beam throughout the structure, which may result in over-conservative buckling capacities, or, use finite element modelling (FEM) for specialised high-risk beams. These options are either impractical for the designer or are expensive regarding cost or computational power. With the latest advancement in computer resources, FEM is often used by designers when determining LTB of specialised high-risk beams. Currently, there are numerous FE software packages available, for example, Strand7 (2010) and DIANA (Maljaars *et al*., 2004), which are orientated for design purposes and Abaqus (2015), which is mostly used for research. Special-purposed FE software concentrating on a smaller scope of solutions, such as buckling analysis, is also available. This type of FE software includes the Buckling Analysis of Stiffened Plates (BASP) program and Plane Rigid Frame Elastic Lateral Buckling (PRFELB). BASP is an FE software specifically designed to analyse the buckling behaviour of beams (Dowswell, 2004). PRFELB is a user-friendly program that assists designers in designing beams, beam-columns and plane frames, regarding lateral-torsional buckling (Papangelis *et al*., 1998).

1.2   OBJECTIVES OF THE STUDY

The aim of the study was to determine the effect that the adjacent span has on the lateral-torsional buckling strength of an overhang beam. The effect was investigated by varying the ratio of the length of the adjacent span to the length of the overhang span using I-beams typically available in South Africa.

The purpose was to obtain an equation that would allow a designer to determine the buckling capacity of an overhang beam by taking into account the backspan length. The buckling capacity of a beam determines the maximum load it can withstand before the beam becomes unstable. Thus knowing the buckling capacities of beams is crucial in the design of a structure. The difficulty is obtaining these buckling capacities when the beam is a continuous overhang beam.

In practice, for specialised high-risk beams, designers sometimes use FE modelling to analyse each beam individually, often by trial and error. In a large structure, beams may have different sizes, support conditions and span lengths. Using FE modelling for each beam can become time-consuming and

expensive (regarding costs and computational resources). Additionally, the accuracy of any FE model relies on the assumptions made by the designer. Therefore, different designers may have different answers for the same problem. A method to *refine*, *simplify* and *standardise* the calculation of the elastic buckling capacity of an overhang beam is therefore required and serves as the main objective of this report.

A literature study was conducted to understand the buckling mechanism of beams and which factors influence the buckling capacity. Cantilevers formed the initial subject of the literature study, upon which the investigation expanded to overhang beams. The study included overhang beams with and without the backspan being a parameter. For overhang beams, fewer design methods were available to determine the buckling capacity. The objectives in refining the calculations were to compare existing methods to determine the differences in assumptions, limitations and results and then from these comparisons, determine a method to adjust the calculations when determining the critical moment M_{cr}.

Once a method of adjusting the calculations was obtained, physical experiments were built and tested to understand how the adjacent span affects M_{cr} for the beam. To facilitate physical experiments, FE models were also constructed. Using FE modelling had its set of objectives:

- Determining if FEA is a viable option for buckling analysis, especially lateral-torsional buckling in overhang beams.
- The techniques required to best model an FE problem.
- Comparing FE results to experiment results for validation and calibration purposes.

Standardising the calculation for M_{cr} allowed the method to be applicable to any beam size, span length and ratio of backspan to overhang. A parametric study was performed allowing variation in the dimensions of the beam to determine a relationship between the dimensions of the beam and the buckling capacity. The objective was to use this relationship to standardise the calculation method.

The implication of a standardised calculation eliminates the need for a designer to rely on FE analysis for specialised high-risk beams or ensuring that the effective overhang length is at least as long as the backspan. A single equation is more consistent than FE modelling. Regarding overhang beams, SANS 10162-1 or similar structural steel codes, therefore, could have provisions for a backspan to overhang ratio, thus increasing the accuracy of lateral-torsional buckling calculations.

1.3 SCOPE OF THE STUDY

A few key parameter were investigated to determine the effect that the adjacent span has on the LTB capacity of an overhang beam. These parameters include the distance between the shear centre and the applied load, overhang length, backspan to overhang ratio and beam size.

The investigation of current methods was limited to cantilevers and two-spanned beams (with a backspan and overhanging segment), with emphasis on single point loads at the free end. The supports of the beams analysed were restricted to lateral and torsional restraints at the fulcrum and root support, while the free end of the beam was completely unrestrained. These support conditions are often used for overhang beams, especially in shallow beams. Warping was considered in the study, including its effect in continuous (overhang) beams, as it has an influence on the buckling capacity of a beam.

The buckling capacity was the only strength parameter investigated, which forms part of the bending resistance of a beam. The buckling analyses were limited to uniform symmetrical I-beams commonly available in South Africa. The accuracy, assumptions and limitations of existing methods and techniques were investigated to refine, if possible, the method of determining the LTB capacity currently provided by SANS 10162-1. For convenience, the approach of SANS 10162-1 regarding LTB is described in Appendix B.

Two approaches were employed to determine the *elastic* LTB capacity of a beam: physical experiments and FEA. Therefore, the scope included techniques to build a setup capable of physical experiments and methods to construct accurate FE models. The experiments were limited to $IPE_{AA}100$ I-beams, as these beams were the smallest beams available, reducing material cost and the load required for buckling of the beam.

The investigation of this study *excluded* buckling in the inelastic range or loading beyond the buckling capacity, i.e. post-buckling. Only concentrated point loads at the tip of the free end of the beam were considered. The equivalent moment factors approach was not considered. Though local buckling and lateral-distortion buckling were researched, it was only to determine methods to avoid these modes of buckling; its effects remained beyond the scope of this study. Tapered beams and flanges, unsymmetrical cross-sections and an initial twist of the beam were also not part of the scope.

1.4 METHODOLOGY

Both physical experiments and finite element analysis were utilised to investigate the effect of the adjacent span on the lateral-torsional buckling capacity of overhang beams. The results obtained were compared to determine a relationship between the critical moment and the dimensions of the overhang beams.

A literature study was performed to determine existing knowledge on buckling of beams. Key concepts on LTB of I-beams were discussed and methods to determine the LTB capacity. Also, local and lateral-distortion buckling were investigated to provide methods to avoid these modes of buckling, thus concentrating purely on LTB. Assumptions, limitations and shortcomings of current methods to determine the LTB capacities were highlighted. The literature study included methods to understand and improve FE models and physical experiments.

Preliminary FE *shell* element models were constructed for basic, built-in cantilevers and overhang beams to determine the LTB capacity. The purpose of these simple FE models was to compare the results to current methods. By comparing the results, the viability and accuracy of using numerical methods, especially FEA, were established. With the data available, a method to refine the calculations when determining the critical moment was set up for a single beam size. This method initially refined the effective length factors. Preliminary FE shell element analyses provided critical buckling moments for overhang beams with various lengths. These results facilitated the design of the physical experiments, as the length of beams and buckling loads were known. Lastly, conducting FEA before experiments reduced potential problems in the design and execution of the experiments.

Physical experiments were performed on full-scale $IPE_{AA}100$ I-beams. Twenty-four experiments were carried out with the objective to determine the buckling capacity of the beam as the length of the adjacent span increased. Four of these experiments were cantilevers to serve as a control when comparing to current methods. Each test was duplicated to improve the accuracy of the results; hence, twelve unique setups were tested. Only point loads at the free end of the cantilevered segment were investigated. The loads were applied either at the shear centre or on the top flange. The results obtained formed the platform for the calibration of the FE *solid* element models that followed.

Upon calibrating the FE solid element models, a detailed parametric study was conducted with the objectives to varying the overhang length of the beam, the backspan to overhang ratio and the beam size. The physical experiments were limited to a single sized beam with a constant overhang length. Finite element analyses provided buckling capacities for a large range of beam setups. Instead of

refining effective length factors, it proved beneficial to utilise a non-dimensional buckling parameter that was dependent on the beam parameters and thus formulated a design equation.

1.5   ORGANISATION OF THE REPORT

The report consists of the following chapters:

Chapter 1 described the background of the report, including the objectives, scope and the research methodology.

Chapter 2 is a literature study on the topic of LTB in both cantilevers and overhang beams. The study included various effects that contribute to the buckling capacity of a beam. Also, includes methods to improve the physical experiments and FE models.

Chapter 3 contains the results of the FE shell element analyses conducted to verify the experiment. A discussion is provided comparing the FE results to various current methods.

Chapter 4 explains the experimental method and setup.

Chapter 5 is a detailed discussion based on the observations and results of the experimental method.

Chapter 6 presents and discuss the results obtained from the parametric study conducted using FE solid element analyses. The formulation of a design equation and its factors, for overhang beams, were discussed.

Chapter 7 contains the conclusions of the study and recommendations for future work.

A list of references used throughout this report is attached, after Chapter 7.

Appendix A contains the results of the parametric study.

Appendix B provides an explanation of the SANS 10162-1 approach.

Appendix C provides the nominal dimensions of the beams used in this study.

Appendix D contains worked out examples using the proposed design equation and the current SANS 10162-1 method.

2   LITERATURE REVIEW

2.1   INTRODUCTION

A literature review forms the basis of any research project. Its purpose was to serve as a foundation for this project. A literature study summarises the current knowledge on a topic. The objectives were to highlight existing knowledge in this field, to point out uncertainties, the relevance of subtopics and the implication of this study. Some of the most important points of discussion included the theories of lateral-torsional buckling and finite element analysis; the differences between cantilevers and overhang beams; load conditions and method of analysis.

This literature review presented a summary of the existing knowledge on lateral-torsional buckling (LTB) of overhang beams. From the initial work done by Timoshenko and Gere to the latest numerical modelling conducted presently. The literature review was divided into four main sections: bending resistance of beams, lateral-torsional buckling of cantilevers and overhang beams, numerical modelling of overhang beams and experimental studies.

The bending resistance of beams was a discussion on the possible modes of buckling; the various effective length factors used depending on the load height and support conditions; and the effect of residual stresses on the bending resistance. The discussion on LTB of both cantilevers and overhang beams included alternative design equations, which included the methods of Essa and Kennedy (1994), Dowswell (2004), Andrade *et al*. (2007) and Trahair *et al*. (2008). A brief overview of the numerical modelling performed by Maljaars *et al*. (2004), Aalberg (2015) and Dessouki *et al*. (2015) was included to improve the FE models that were analysed in this study. Finally, the experimental work done by Zirakian and Showkati (2007) and Ozbasaran *et al.* (2015) were discussed to improve and simplify the experimental setup.

The aim of the study was to refine the current method of determining the lateral-torsional buckling capacity given by SANS 10162-1 and CAN/CSA-S16-1, by including the ratio of the backspan segment length to the overhanging segment length. Currently, SANS 10162-1 have a single set of effective length factors for overhang beams that are free at the tip and loaded at the shear centre or on the top flange. Thus, the effect of the adjacent span was omitted.

2.2 BENDING RESISTANCE OF BEAMS

Buckling is a term that refers to a member failing before the yield stress was reached. Buckling may control the strength of a beam; hence, it is termed a limit state. It is thus important to determine the buckling capacity of a beam, be it either local, lateral-torsional or lateral-distortional buckling. The width-to-thickness ratios of the beam govern the buckling failure. The bending resistance of a beam depends on the mode of buckling; the effective length; the load height; the support conditions and the residual stresses within the beam. Each of these aspects was discussed in detail below.

2.2.1 LOCAL BUCKLING

When a member becomes short, the individual elements of the beam, i.e. the flange or web, could buckle in a local area. In other words, the buckling strength of the beam was governed by a small portion of the beam, not the entire beam as preferred. In short beams with a point load, the mode of local buckling is often either web crippling or web buckling. Crippling of the web occurs if the web was too slender to support the shear load applied, generally reducing the buckling capacity. Therefore, web crippling occurred before the lateral-torsional buckling capacity was reached. Local buckling is irreversible, as the beam element has buckled past the yield point. The cross-section of structural steel beams is divided into four classes, based on the width-to-thickness ratio. These classes are 1: Plastic, 2: Compact, 3: Non-compact and 4: Slender. For this study, slender beams that were not Class 4 were used, to avoid web buckling.

A large point load or support load could induce web crippling or yielding. In this study, checks were performed to ensure that these concentrated loads did not exceed the web crippling or yielding force. The end reaction force required for web crippling and yielding B_r according to SANS 10162-1 or CAN/CSA-S16-1 are given by Eqs. 2.1 and 2.2, respectively. Similar equations for interior loads are also given by SANS 10162-1.

$$B_r = \phi_{be} t_w f_y (N + 4t_f) \qquad\qquad \text{Eq. 2.1}$$
$$B_r = 0.60\, \phi_{be} t_w{}^2 \sqrt{f_y E} \qquad\qquad \text{Eq. 2.2}$$

Where:

B_r = Factored bearing resistance of member or component.

ϕ_{be} = 0.75, Resistance factor for beam web bearing, end.

t_w = Web thickness.

f_y = Specified minimum yield stress.

N = Length of bearing of an applied load.

t_f = Flange thickness.

E = Elastic modulus of steel.

2.2.2 LATERAL-TORSIONAL BUCKLING

Unlike the buckling behaviour of compression members, lateral-torsional instability in beams consists of both an unstable compression region and a stable tension region (Mahachi, 2013). Due to the compatibility between tension and compression regions, the beam twists during buckling (if laterally unrestrained) as the stable tension region resists the lateral deflection of the unstable compression region (Mahachi, 2013). Therefore, there are two types of resistances in a lateral-torsional buckling scenario: lateral buckling resistance and twist of the beam section.

Salmon *et al*. (2009) stated that regarding resistance, the unstable compression flange is braced in its weak direction by the stable tension flange via the web. Salmon *et al*. (2009) also stated that the connection between the web and the flange provides lateral and torsional resistance, i.e. the flange is considered continuously restrained. The connection enables the web to transfer its bending stiffness to the entire section during lateral movement (Salmon *et al*., 2009).

Since the formulation of the original theory, numerous advancement in the field of lateral-torsional buckling were accomplished. Most notably was the work done by Timoshenko and Gere (1961) who derived fundamental differential equations for symmetric I-beams, which included the effect of warping. Warping is the longitudinal deflection (along the z-axis) of the flanges and causes rotation about the vertical axis (about the y-axis) of the beam at the supports. Timoshenko and Gere (1961) formulated a closed-form solution for the case of I-beams that were bent in single curvature with end moments that were equal and opposite, given by Eq. 2.3 and illustrated in Figure 2.1.

$$M_{cru} = \frac{\pi}{L}\sqrt{EI_y GJ}\sqrt{1+\gamma} \qquad\qquad \text{Eq. 2.3}$$

Where:

γ = $\pi^2 EC_w/L^2 GJ$

M_{cru} = Elastic critical moment of a simply supported beam.

L = Length of beam between restraints.

I_y = Moment of inertia about y-axis.

G = Shear modulus of steel.

J = St. Venant torsion constant of a cross-section.

C_w = Warping torsional constant.
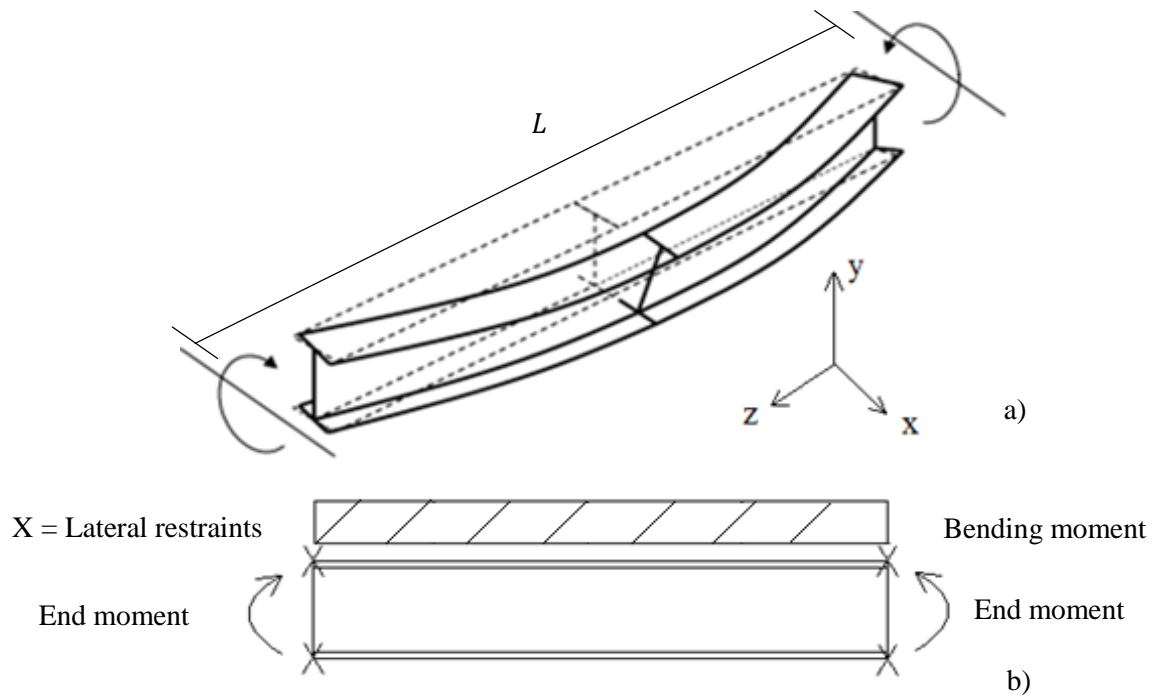
Figure 2.1: a) Buckling of I-beam with equal but opposite end moments b) bending moment diagram.

x = Lateral axis (European equivalent is y-axis).

y = Vertical axis (European equivalent is z-axis).

z = Longitudinal axis (European equivalent is x-axis).

Buckling of beams is classified as elastic, inelastic or plastic, depending on the lateral slenderness, as shown in Figure 2.2. Lateral torsional buckling could occur in both the elastic and inelastic ranges. Once the beam became less slender (shorter), factors such as imperfections and residual stresses had an increasingly adverse effect on the buckling capacity of the beam.
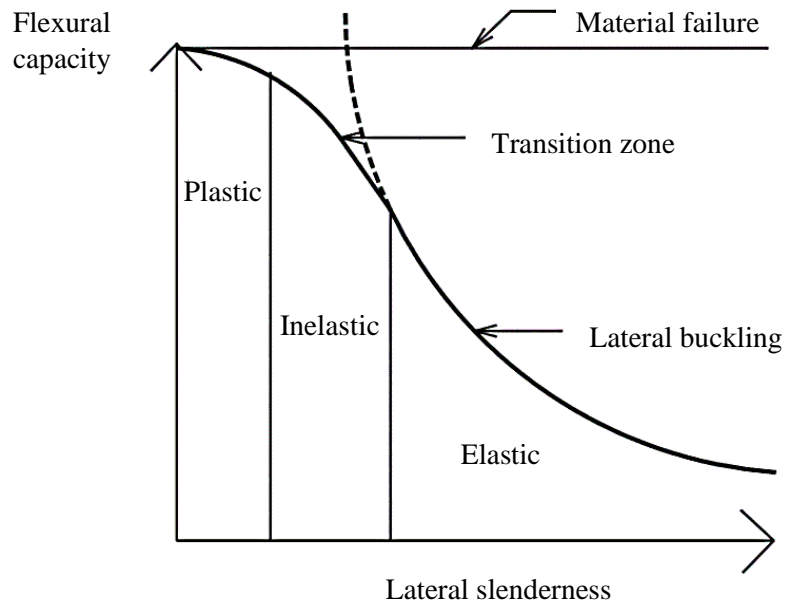
Figure 2.2: Failure modes in beams (Adapted from Mahachi, 2013).

Design codes such as CAN/CSA-S16-01 specifies a limit on the elastic range and reduces the bending resistance of the beam when in the inelastic range. The critical buckling moment is required to determine the design bending resistance of the beam for both the elastic and inelastic range.

According to CAN/CSA-S16-01 (which was also adopted by SANS 10162-1) when the critical moment is in the elastic range, i.e. $M_u \leq 0.67M_p$, the bending resistance of the beam is simply $M_r = \phi M_u$. For the inelastic range, the critical moment is reduced using Eq. 2.4, but must be smaller than the upper limit of ϕM_p.

$$M_r = 1.15 \, \phi M_p \left(1 - \frac{0.28M_p}{M_u}\right) \qquad \text{Eq. 2.4}$$

Where:

ϕ = 0.9, Resistance factor for structural steel.

M_p = Plastic moment of cross-section.

M_r = Bending resistance.

M_u = Critical bending moment.

Trahair (2010) showed that current design codes were limited in providing guidance in determining the inelastic buckling behaviour of cantilevers. Cantilevers refer to beams that are free on one side and completely restrained at the other end. Therefore, the support conditions of cantilevers and simply supported beams are different. Trahair (2010) formulated alternative design equations for inelastic

buckling of simply supported beams, in addition, formulated inelastic buckling equations for cantilevers. The inelastic buckling equation for cantilevers was not based on simply supported beams, such as the method described above, but was based on the critical moment equation for a cantilever by Trahair *et al*. (2008).

2.2.3 LATERAL-DISTORTIONAL BUCKLING

When inelastic buckling occurs, it is a combination of lateral-distortional and lateral-torsional buckling. Lateral-distortional buckling refers to the bending (distortion) of the web. Figure 2.3 illustrates web distortion. Distortion of the web usually occurs when the beam was partially restrained, i.e. only the bottom flange was restrained (Bradford, 1994). A method available to overcome web distortion is to add web stiffeners at the point of concentrated loads or supports.
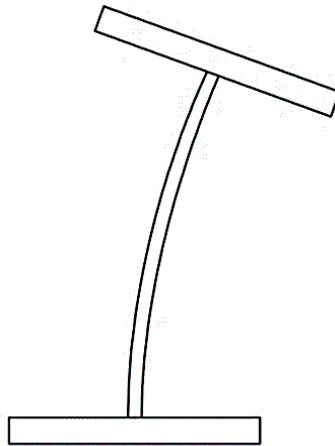
Figure 2.3: Cross-section of a beam when lateral-distortional buckling occurs.

Bradford (1994) investigated both lateral-distortional buckling and LTB for overhang beams. The investigation included the difference between the two buckling modes; the critical loads at which the two buckling modes occurred; and the effects of the two modes on overall buckling. Knowing the contribution of lateral-distortional buckling to the overall buckling failure enabled the calculation of the reduced buckling capacity of a beam due to web distortion. Bradford (1992) showed that distortion might be significant for cantilevers, especially when loaded above the shear centre, reducing the buckling load considerably.

In the FE analyses conducted by Dowswell (2004); and Essa and Kennedy (1993), transverse beam web stiffeners were added to the models at points of concentrated loads. Adding web stiffeners allowed shorter beams to fail by LTB, thus investigating a larger range of beam lengths was possible. Web stiffeners did not always remove the effect of web distortion but reduced the contribution to the overall

buckling capacity. Dowswell (2004) used the FE program Buckling Analysis of Stiffened Plates (BASP) and compared the critical loads to the cantilever equation of Timoshenko and Gere (1961). A ratio between the FE results and the calculated load were determined. The ratio varied from 0.76 to 1.07. According to Dowswell (2004), the variation in critical load was due to the distortion of the web, which was not taken into account by the Timoshenko and Gere equation (Eq. 2.3).

In the FE analyses conducted by Bradford (1994), when lateral-distortional buckling was not considered, the elastic and geometric stiffness matrix were modified to allow suppression of distortion which enabled accurate predictions of LTB loads. According to the results from Bradford (1994), a reduction in the effects of distortion was observed when the web became less slender; the flange was narrower and when lateral and torsional restraint was provided at the top flange of the internal support.

In this study, buckling in the elastic range was investigated to ensure that the beam failed due to instability (lateral-torsional buckling) and not as a material failure (yielding). In addition, elastic buckling excludes lateral-distortional buckling and the adverse effects of residual stresses (section 2.2.7). Simply stated, this study intended to determine the elastic critical buckling moment of a beam. The limit on critical moment specified by SANS 10162-1 was used as a guide to ensure elastic buckling. SANS 10162-1 specify that when M_{cr} is greater than $0.67M_p$ (plastic moment used for Class 1 and 2 beams) or $0.67M_y$ (yield moment used for Class 3 beams), buckling is in the inelastic range. To avoid inelastic buckling, the beams were made slender enough to reduce the critical moment below the specified limit.

2.2.4   TORSIONAL PARAMETER

The torsional and warping rigidity of a beam greatly affects the buckling capacity of a beam. For an I-section, the torsional stiffness depends on the span length (segment), the dimensional properties of the cross-section, support conditions and the interface between the web and flanges (see Section 2.7 on Numerical modelling of overhang beams). Whereas, warping stiffness depends on the dimensional properties of the cross-section and the support conditions. The warping stiffness allows stress to be transferred from one beam segment to another. A support either allows warping (free to warp) or prevents warping (no warping).

Without support conditions considered, the torsional and warping stiffness of a beam segment may be combined and is quantified by Eq. 2.5. Eq. 2.5 is referred to as the torsional beam parameter and is applicable for each beam segment. The torsional parameter K is used extensively in the study of

lateral-torsional buckling and is a non-dimensional parameter. There are however slight variations of the formula and notations. The following were utilised as the standard for this study:

$$K = \sqrt{(\pi^2 EC_w)/(GJL^2)} \qquad \text{Eq. 2.5}$$

Where:

K = Torsional parameter of a segment.

EC_w = Warping rigidity.

GJ = Torsional rigidity.

L = Length of beam segment.

2.2.5 CONCEPT OF EFFECTIVE LENGTH

Pandey and Sherbourne (1990) defined the term effective length as the length of a similar cross-section simply supported beam, which has a uniform buckling moment that is equal to the buckling moment of the beam under the actual loading and boundary conditions. The effective length factor enables a general idea if the beam under consideration is either more or less stable than a simply supported beam. Also, effective length factors may act as a non-dimensional parameter, enabling comparisons of different cases to obtain trends or conclusions. In general, effective length factors modifies the critical buckling moment to be more representative of the actual buckling load under certain support conditions and loads.

Design codes, such as CAN/CSA-S16-01 does not use any effective length factors in determining the LTB capacity, whereas SANS 10162-1 (based on CAN/CSA-S16-01) have incorporated these effective length factors. SANS 10162-1 is a step forward from CAN/CSA-S16-01 in understanding LTB, but there is still scope for research. Using effective length factors is a possible method in refining the calculations for LTB. Before trying to refine calculations of LTB using effective length factors, it was first necessary to gain knowledge on current effective length factors and their limitations. In subsequent investigations, the summary of the research conducted was summarised in an effective length factor table or similar.

2.2.6 EFFECT OF LOAD HEIGHT AND SUPPORT CONDITIONS

The critical buckling load is influenced by the distance between the applied load and shear centre; the type of load applied; and the support conditions (restraints). Throughout the years, investigations were conducted on all three parameters, starting with simply supported beams. The effect of type of load

applied was discussed first, followed by the distance between the shear centre and the load applied (load height), thirdly the support conditions were discussed and finally the combination of the three parameters. This discussion was limited to only cantilevers and continuous overhang beams, as they were relevant to the investigations.

The type of load, i.e. point load, or a uniformly distributed load alters the bending moment within the beam. For a cantilever, a point load at the tip (free end) was the severest case of loading.

The height of application of a load could either increase (stabilise) or decrease (destabilise) the lateral-torsional buckling strength. Additional twisting moments arises when the load is applied to the top flange, causing a destabilising effect, because the point of load does not pass the centroid of the section. The opposite holds for bottom flange loading, the additional twisting moment becomes negative and reduces the overall twist, thus stabilising the beam. If the load is applied at the shear centre, no extra twist occurs in the beam. The buckling capacity of a beam varies with the vertical distance and direction between the shear centre and load applied. Therefore, the largest buckling capacity is obtained by bottom flange loading, with the minimum capacity by top flange loading.

To summarise the effect of the type of load used and the distance between the shear centre and load applied, Figure 2.4 demonstrates six different conditions: top flange, shear centre and bottom flange loading for either a point load or a uniformly distributed load. The weakest configuration is a beam with a point load at the free end applied at the top flange. Note also the effect the torsional parameter of a beam has on the buckling capacity. The shorter the beam (larger K), the larger the buckling capacity is.
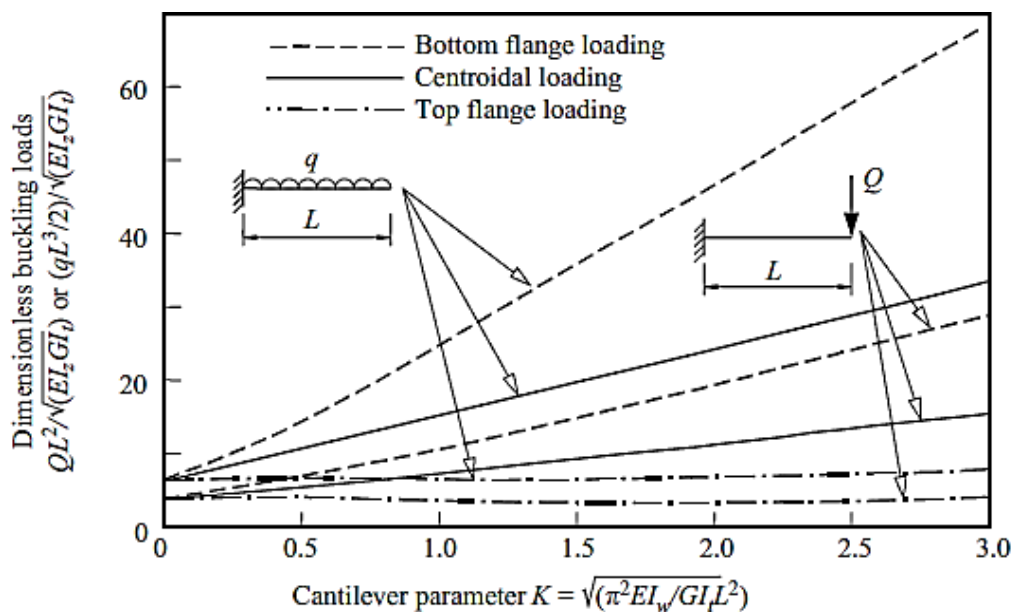
Figure 2.4: Effect of load height on buckling capacity for a cantilever (Trahair *et al*., 2008).

Where:

Q = Point load at free end.

q = Uniformly distributed load.

I_z = Moment of inertia about z-axis (European equivalent for I_y).

I_t = Torsional constant (European equivalent for J).

I_w = Warping torsional constant (European equivalent for C_w).

Essa and Kennedy (1994) formulated Eq. 2.6 for cantilevers to interpolate between the two extreme cases of shear centre loading, k_s and top flange loading, k_t to obtain an effective length factor for intermediate load height, h.
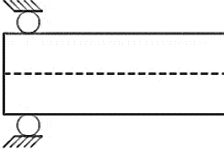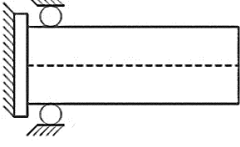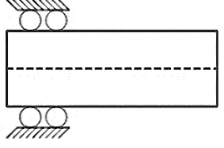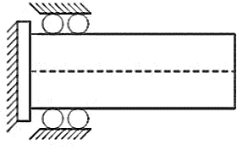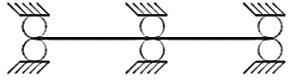
$$k = rk_t + (1 - r)k_s \qquad \text{Eq. 2.6}$$

Where:

k_s = 0.75

k_t = $0.57 + 0.71X - 0.1X^2$

X = Torsional parameter (Equivalent to K, but limited to $0 < X < 1.57$).

r = $\frac{h}{d}\left(1.5 + \frac{h}{d}\right)$

k = Effective length factor, taking into account distance between shear centre and load applied.

h = Distance between the shear centre and the load applied.

d = Depth of steel cross-section.

Restraints are either continuous along the span of the beam or concentrated at support points. At the supports (boundary conditions), the restraints are at either the top flange, bottom flange or both flanges. Various types of restraints exist, and they can vary throughout the full length of the beam. For a cantilever or overhang beam, no restraints were provided at the free end. This setup for the free end is common for cantilevers. Unlike a cantilever, a continuous beam can have various types of restraints. See Table 2.1 for a description of possible restraint conditions (cases) used throughout the study.

Table 2.1: Possible restraint conditions in a continuous beam (Ziemian (2010) from the work of Nethercot and Rockey, 1971).

Case	Restraint conditions	
I		$u = u'' = \phi = \phi'' = 0$ Simply supported
II		$u = u'' = \phi = \phi' = 0$ Warping prevented
III		$u = u' = \phi = \phi'' = 0$ Lateral bending prevented
IV		$u = u' = \phi = \phi' = 0$ Fixed end
V		Lateral support at centre. Restraints equal at both ends.

Where:

u = Lateral deflection.

ϕ = Longitudinal twist.

At the internal supports, the restraints can either allow or prevent warping, twist and lateral deflection of any flange. During this study, the investigation was limited to overhang beams with lateral and torsional restraints. This support condition is common in overhang beams. However, warping was allowed in the flanges to allow for interaction buckling occurring between beam segments.

The buckling strength of a beam may be improved by using bracing. The bracing must provide sufficient stiffness to prevent lateral movement and withstand any forces transmitted. Bracing is not always practical, or of sufficient strength, hence the determination of the lateral-torsional buckling capacity includes the conditions of the supports. Galambos (1968) proposed the effective length factors, K_y and K_z, which took into account the boundary conditions of a beam about two axis (Table 2.2). These factors effect Eq. 2.3, as shown in Eq. 2.7.

$$(M_0)_{cr} = \frac{\pi}{K_y L}\sqrt{EI_y GJ + \left(\frac{\pi E}{K_z L}\right)^2 I_y C_w}$$

Eq. 2.7

Where:

$(M_0)_{cr}$ = Effective elastic critical buckling moment of a simply supported beam.

K_y = Effective length factor about y-axis.

K_z = Effective length factor about z-axis.

Table 2.2: Effective length factors for simply supported beams (Galambos, 1968).
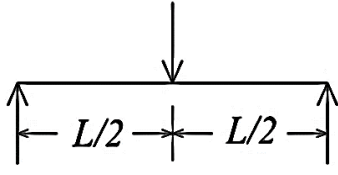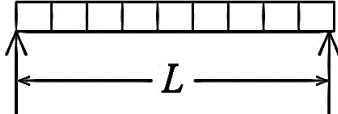
Boundary conditions (cases)		K_y	K_z
z = 0	z = L		
I	I	1.000	1.000
I	II	0.904	0.693
I	III	0.626	1.000
I	IV	0.693	0.693
II	II	0.883	0.492
III	IV	0.431	0.693
IV	IV	0.492	0.492
III	III	0.434	1.000
III	II	0.606	0.492

Salvadori (1955) demonstrated that when the applied moment between supports was non-uniform and laterally unsupported between supports, the buckling capacity could increase by an equivalent moment factor, known as ω_2 (C_b in American literature). The ω_2 factor allows determining the buckling capacity for various load cases between the supports. However, a uniform moment is the worst possible load case, with $\omega_2 = 1$. For cantilevers, these factors cannot be applied. Rather, taking the *actual* length of the cantilever as the effective length recognises the moment gradient, when determining the buckling capacity (Salmon *et al*., 2009).

To account for the various type of loadings, restraint conditions and the distance between the shear centre and the load applied, Nethercot and Rockey (1971) proposed equations for determining the equivalent moment factors: $\omega_2 = A$, $\omega_2 = AB$ and $\omega_2 = A/B$ for shear centre, bottom flange and top flange, respectively. The factors for A and B are summarised in Table 2.3, with X being equal to the
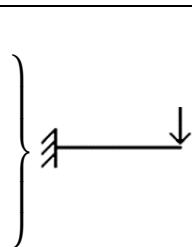
torsional parameter K. These equations are only applicable to simply supported beams and are only included to highlight the importance of support conditions and load height and the effect thereof.

Table 2.3: Determining ω_2 for beams with various boundary conditions (Ziemian (2010) from the work of Nethercot and Rockey (1971)).

Loading	Restraint	A	B
	I	1.35	$1 - 0.180X^2 + 0.649X$
	II	$1.43 + 0.485X^2 + 0.463X$	$1 - 0.317X^2 + 0.619X$
	III	$2.0 - 0.074X^2 + 0.304X$	$1 - 0.207X^2 + 1.047X$
	IV	$1.916 - 0.424X^2 + 1.851X$	$1 - 0.466X^2 + 0.923X$
	V	$2.95 - 1.143X^2 + 4.07X$	1
	I	1.13	$1 - 0.154X^2 + 0.535X$
	II	$1.2 + 0.416X^2 + 0.402X$	$1 - 0.225X^2 + 0.571X$
	III	$1.9 - 0.12X^2 + 0.006X$	$1 - 0.100X^2 + 0.806X$
	IV	$1.643 - 0.405X^2 + 1.771X$	$1 - 0.339X^2 + 0.625X$
	V	$2.093 - 0.947X^2 + 3.117X$	$1.073 + 0.044X$

As with simply supported beams, support conditions and load height has an effect on the buckling capacity of cantilevers and overhang beams. Nethercot (1973) suggested effective length factors for cantilevers and overhang beams, shown in Table 2.4. Note the use of effective length factors and not ω_2, as ω_2 is not applicable to cantilevers as previously mentioned. These factors, even though they were applied to cantilevers, were based on lateral-torsional buckling for simply supported beams. These factors are conservative.

Table 2.4: Effective length factors for cantilevers (Nethercot, 1973).

Support conditions (all have concentrated load at tip)		Shear centre loading	Top flange loading
Free at tip		0.75	1.4
Lateral deflection prevented at tip		0.65	1.4
Twist prevented at tip		0.55	0.55
Lateral deflection and twist prevented at tip		0.45	0.45
Built in laterally at tip		0.35	0.35
Overhang span not prevented from twisting at the fulcrum	Free at tip	2.5	7
Overhang span prevented from twisting at the fulcrum		1	2.6

The Structural Stability Research Council (SSRC) Guide (Ziemian, 2010) did a similar investigation though the effective length factors differed slightly from the results given by Nethercot (1973), shown in Table 2.5.

Table 2.5: Cantilever and overhang effective length factors (SSRC Guide (Ziemian, 2010)).
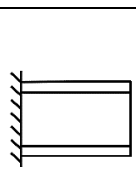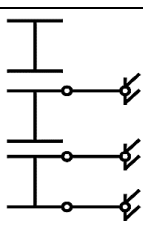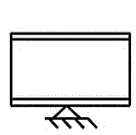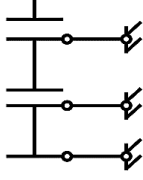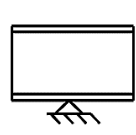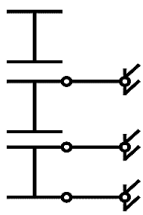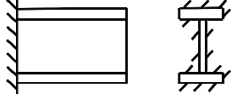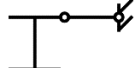
Restraint conditions		Effective length factor, k_b	
At root / fulcrum	At tip	Top flange loading	All other cases
		1.4	0.8
		1.4	0.7
		0.6	0.6
		2.5	1.0
		2.5	0.9
		1.5	0.8
		7.5	3.0
		7.5	2.7
		4.5	2.4

Table 2.6 shows alternative procedures for cantilevers that were proposed by Essa and Kennedy (1993). The effective length factors for top flange loading are a function of the torsional parameter K (X). In other words, the length of the cantilever beam also dictates the effective length factor for the beam when load is applied on the top flange.

Table 2.6: Alternative effective length factors (Essa and Kennedy, 1993).

Restraint conditions		Effective length factor, k_b	
At root	At tip	Top flange loading	Shear centre loading
	Free	$0.57 + 0.71X - 0.1X^2$	0.75
	Lateral	$1.2 - \dfrac{0.161}{X} - \dfrac{0.184}{X^2} \not< 0.85$	0.5
	Lateral and torsional	0.44	0.44
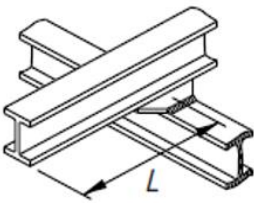
Kirby and Nethercot (1979) extended the factors given by Nethercot (1973) by including different restraint conditions at the fulcrum of an overhang (continuous) beam (Table 2.7). These extended factors are only applicable to continuous beams where the effective overhang length is at least as long as the adjacent span. Ideally, the factors apply only when the backspan and the overhanging segment has equal lengths. According to Kirby and Nethercot (1979), when the overhanging segment tip was prevented from twisting, the level of application of a point load at the tip made no difference to the lateral-torsional buckling capacity. Hence, uniformly distributed load were used for this particular case. The same values given below were adopted by the current SANS 10162-1: 2011 Code.

Table 2.7: Effective lengths for various restraint conditions (SANS 10162-1, 2011 (Kirby and Nethercot, 1979)).

Restraint conditions		Loading conditions	
At support	**At tip**	**Normal**	**Destabilising**
Built in laterally and torsionally	Free	0.8L	1.4L
	Lateral restraint only	0.7L	1.4L
	Torsional restraint only	0.6L	0.6L
	Lateral and torsional restraint	0.5L	0.5L
Continuous, with lateral and torsional restraint	Free	1.0L	2.5L
	Lateral restraint only	0.9L	2.5L
	Torsional restraint only	0.8L	1.5L
	Lateral and torsional restraint	0.7L	1.2L
Continuous, with lateral restraint only	Free	3.0L	7.5L
	Lateral restraint only	2.7L	7.5L
	Torsional restraint only	2.4L	4.5L
	Lateral and torsional restraint	2.1L	3.6L

From the table above, restraining the twist, either at the tip or fulcrum, were more efficient than restraining the lateral deflection, in particular for the destabilising load application. The BS 5950-1:2000 Code used the same values as above, except they added the case of a continuous beam with partial torsional restraint at the support, shown in Table 2.8.

Table 2.8: Effective lengths for continuous partial torsional restraints (BS 5950-1:2000, 2008).

Restraint conditions		Loading conditions	
At support	**At tip**	**Normal**	**Destabilising**
Continuous, with partial torsional restraint	Free	2.0L	5.0L
	Lateral restraint to top flange	1.8L	5.0L
	Torsional restraint	1.6L	3.0L
	Lateral and torsional restraint	1.4L	2.4L

The effective length factors by Nethercot (1973) are only applicable when $0 < K < 1.57$, restricting cantilevers to long members only. Nethercot (1973) only considered cantilevered beams that had an equal backspan segment. The effective length factors were therefore calibrated for a certain cantilever length and any deviation resulted in unreliable results. Kirby and Nethercot (1979) introduced the restriction that the backspan length should at least be equal to the effective cantilever length, to accommodate the limit specified by Nethercot (1973) on the cantilever length. This restriction was not specified by the SSRC guide provided by Ziemian (2010), which opens the scope for non-conservative results for short-cantilevered spans (Driver, 2014). To summarise, the SSRC Guide (Ziemian, 2010) used the same effective length factors as Kirby and Nethercot (1979), but without the limit on cantilever lengths. SANS 10162-1 adopted the effective length factors from Ziemian (2010), also without any limits. This limit was not used in the effective length method specified by Essa and Kennedy (1993); instead, they used effective length equations with K being a function, if loaded on the top flange.

Therefore, current design codes do not provide either effective length factors when the backspan is longer than the effective overhang length or, assumes that the effective length factors apply to any cantilever length. With any cantilever length, it is implied that the backspan to overhang ratio is not considered. This gap in the design codes forms the basis for this study. All of the investigations mentioned above gave similarly but different factors for the same boundary conditions and load heights. The variations prove the complexity of obtaining accurate and viable results when dealing with lateral-torsional buckling of cantilevers and overhang beams. Refinement of the current method of determining the LTB capacity was limited to cantilevers and overhang beams with concentrated point loads applied at the tip of the beam, with the tip being free from any supports.

2.2.7   RESIDUAL STRESSES IN REAL BEAMS

Unlike ideal beams, real beams may contain imperfections such as being initially crooked, twisted, eccentrically loaded or contain residual stresses. All of which reduces the buckling capacity of a beam. Residual stresses have a larger influence on the buckling capacity than dimensional imperfections of the beam. Residual stresses are caused by the fabrication process. The steel beams used in this study were hot-rolled; therefore contained residual stresses. Residual stresses affect the buckling capacity of a beam as lateral-torsional buckling is in part dependent on the web and flanges. Residual stresses and imperfections cannot be avoided, but care must be taken to prevent adding more defects or internal stresses. Illustrated in Figure 2.5 are the effects of imperfections and residual stresses on the buckling capacity for a specific slenderness. Curve C is a combination of both Curve A and Curve B.
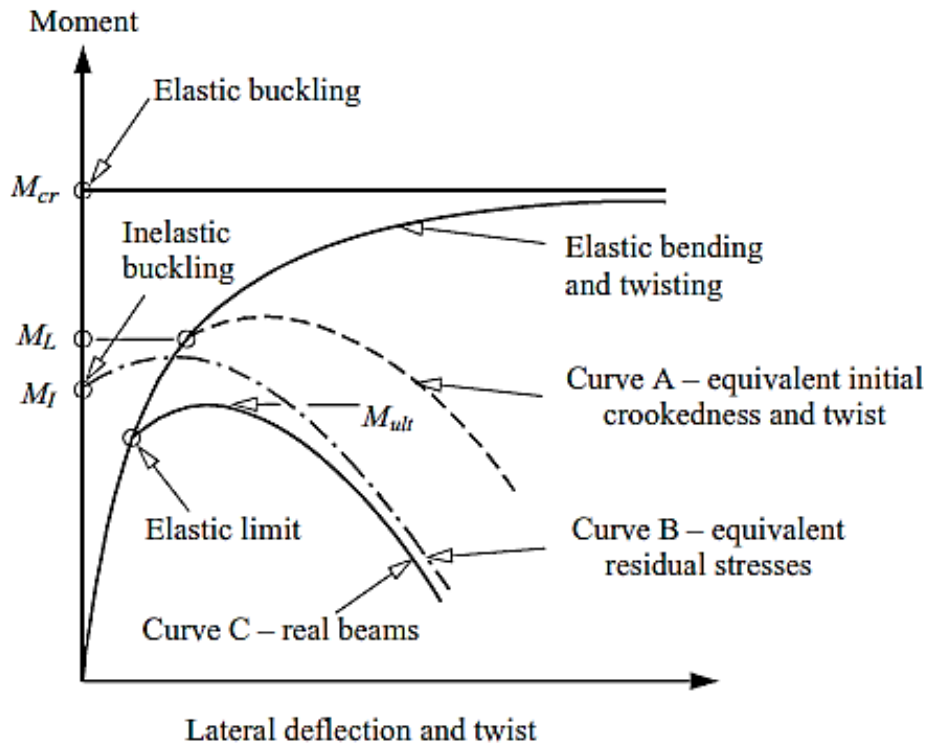
Figure 2.5: Effect of imperfections on ideal beams (Trahair *et al.*, 2008).

Where:

M_L = Limiting end moment on a crooked and twisted beam at first yield.

M_I = Inelastic beam buckling moment.

M_{ult} = Ultimate buckling moment.

Figure 2.6 (Trahair *et al.*, 2008) illustrates the effect of residual stresses on the buckling capacity of an I-beam with the slenderness being a variable. Note that the beam is simply supported, with a uniform moment. When $L/r_y < 150$, the buckling of the beam without residual stresses is no more elastic but becomes inelastic, hence the deviations from the ideal, fully elastic buckling curve. With residual stresses in the beam, buckling in the inelastic range occurs when $L/r_y < 240$, effectively reducing the buckling capacity. This study was interested in the elastic buckling range, which also reduced the adverse effect of residual stresses. Thus, the buckling capacity determined was closer to the true buckling capacity of an ideal beam.

Where:

r_y = Radius of gyration about y-axis.
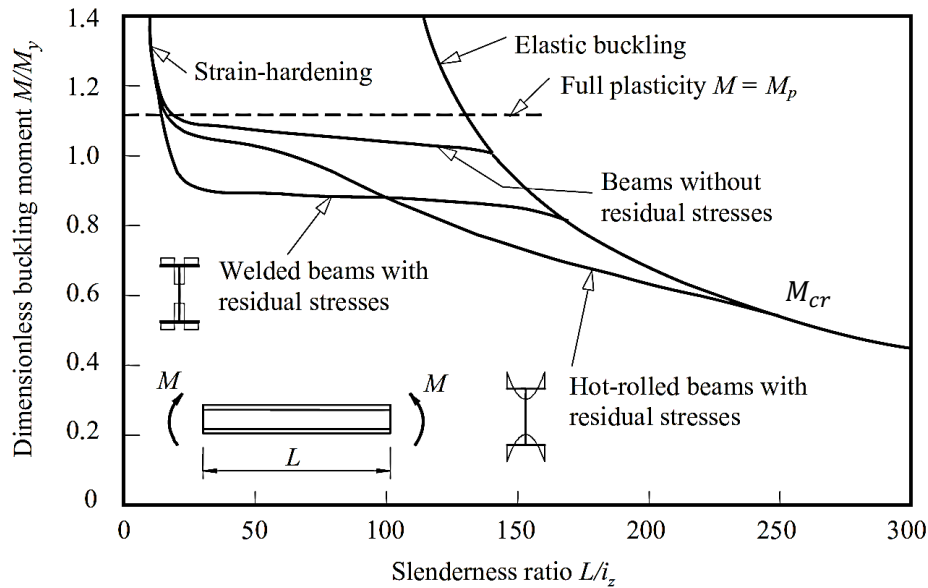
Figure 2.6: Effect of residual stresses on buckling capacity (Trahair *et al*., 2008).

Where:

M_y = Yield moment of cross-section.

M_{cr} = Critical moment.

i_z = Radius of gyration about z-axis (European equivalent for r_y).

2.3 LATERAL-TORSIONAL BUCKLING OF CANTILEVERS

When analysing the bending resistance of cantilevers or overhang beams, the buckling equations for simply supported beams are no longer valid. That is because the top tension flange at the free end is now the critical flange that deflects more. Lateral deflection, twist and warping are restrained at the support, while unrestrained at the free end. The following section presents a clearer understanding of the governing equations of buckling for cantilevers.

2.3.1 TIMOSHENKO AND GERE

As with a simply supported beam, Timoshenko and Gere (1961) also formulated Eq. 2.8 for an unbraced I-beam cantilever with full fixity (built-in) at the root and point load applied at the free end. The critical load was formulated using differential equations and solved using an infinite series. By taking into account support conditions, a transcendental equation was obtained.

$$P_{cr} = \gamma_2 \frac{\sqrt{EI_y C}}{L^2}$$

Eq. 2.8

Where:

P_{cr} = Elastic critical buckling load of a cantilever.

γ_2 = Dimensionless factor depending on the ratio of $L^2 C/C_1$.

C = GJ, Torsional rigidity.

C_1 = EC_w, Warping rigidity.

The γ_2 factors are tabulated in Timoshenko and Gere (1961). The formulae are only applicable for loads applied at the shear centre.

Since the formulation of the two equations by Timoshenko and Gere (1961), numerous investigations were conducted to improve and extend the application of these two solutions. These investigations are discussed further below. During these investigations, the symmetrical non-tapered I-beams were used, unless stated otherwise.

2.3.2 NETHERCOT

Nethercot (1973) used finite element theory to analyse beams and fitted polynomials to the results. This resulted in a more precise method by using the equation defined below by Eq. 2.9. The torsional parameter of the beam was limited to $0 < K < 1.57$. This limitation only allowed for long span overhang beams with no load or restraints between supports for the backspan and with equal backspan length (Driver, 2014). Nethercot's (1973) method included top and bottom flange loadings.

$$M_{cr} = \frac{\gamma_e}{L}\sqrt{EI_y GJ}$$
Eq. 2.9

Where:

M_{cr} = Critical buckling moment in the beam.

γ_e = $\alpha\gamma$, Effective buckling coefficient.

γ = $\pi\sqrt{1 + \frac{\pi^2}{R^2}}$

R = $\sqrt{\frac{L^2 GJ}{E\Gamma}}$, Torsional slenderness parameter.

Γ = Warping torsional constant (Equivalent to C_w).

α = Lateral buckling coefficient.

α = A for shear centre loading.

α = A/B_1 for top flange loading.

α = AB_2 for bottom flange loading.

For point load at cantilever free end:

$$A = 1.287 - 3.539/R^2 + 2.521/R$$
$$B_1 = 0.947 - 3.016/R^2 + 2.364/R$$
$$B_2 = 0.995 - 0.024/R^2 + 1.189/R$$

2.3.3 DOWSWELL

Dowswell (2004) proposed a design equation (Eq. 2.10) for the critical buckling moment of cantilevers. Dowswell (2004) used a special-purpose LTB program BASP to analyse cantilevers. These results were curve fitted to obtain non-dimensional coefficients.

$$M_{cr} = C_L C_H C_B \frac{\sqrt{EI_y GJ}}{L}$$ Eq. 2.10

Where:

C_L = Moment distribution coefficient.

C_H = Effect of load height coefficient.

C_B = Effect of bracing coefficient.

These coefficients depend on the bracing of the beam, the type of load and the distance between the shear centre and the load applied.

For C_L, the equations proposed by Trahair (1983, 1993) were used. Once again, a point load at the free end yielded a lower buckling capacity, as compared to a uniformly distributed load.

Point load at the free end, $C_L = 3.95 + 3.52X$

Uniformly distributed load, $C_L = 5.83 + 8.71X$

X = Torsional parameter (Equivalent to K)

For C_H and C_B, the following conservative equations were used:

Concentrated load at top flange at the free end: $C_H = 0.76 - 0.51X + 0.13X^2$

If the load is at shear centre or below: $C_H = 1.0$.

Bracing resists some of the twist and lateral deflection of a cantilever, thus increasing the buckling capacity. Therefore, it is safe and conservative to assume no bracing is present in a cantilever.

Load at the level of shear centre: $C_B = 1.42 + 0.88X - 0.26X^2$

Load at top flange, $C_B = 1.48 + 0.16X$

If no bracing is present, $C_B = 1.0$.

The equations above were curve-fitted from FE analyses, with the FE analysis verified by comparing the critical load to the Timoshenko and Gere equation (Eq. 2.8).

2.3.4   ANDRADE *et al.*

Andrade *et al*. (2007) conducted a rational approach, by extending the so-called 3-factor formula to include cantilevers. The three factors define the type of load applied, the distance between the shear centre and the load applied and the symmetry of flanges. The extended formula for a symmetrical beam is defined in Eq. 2.11.

$$M_{cr} = C_1 \frac{\pi^2 E I_z}{(k_z L)^2} \times \left[\sqrt{\left(\frac{k_z}{k_w} \right)^2 \frac{I_w}{I_z} + \frac{(k_z L)^2 G I_t}{\pi^2 E I_z} + \left(C_2 z_g \right)^2} - \left(C_2 z_g \right) \right] \qquad \text{Eq. 2.11}$$

Where:

C_1 & C_2 = Factors that depends on the warping restraint; the type of load; the distance between shear centre and the load applied; and on the modified torsional parameter.

z_g = Distance between shear centre and load applied (positive above the shear centre).

$\overline{K}$ = $\frac{\pi}{L} \sqrt{\frac{E I_z h_s^2}{4 G I_t}}$; Modified torsional parameter, $0.1 \leq \overline{K} \leq 2.5$, $\overline{K} = K$ for an equal flanged beam.

h_s = Distance between flange centroids.

k_z = Effective length factor for end reactions about the z-axis.

k_w = Effective length factor for end warping restraint.

When the load is applied at the shear centre, C_2 becomes non-applicable and Eq. 2.11 is reduced to Eq. 2.12 (given that there is no bracing). As C_1 and C_2 factors are dependent on the warping restraint, the formula above may be used for both cantilevers and overhang beams. The factors for C_1 and C_2 summarised in Table 2.9 are only for point loads.

$$M_{cr} = \frac{\gamma_{q\lambda_{cr}}}{L} \sqrt{E I_y G J} \qquad \text{Eq. 2.12}$$

Where:

$\gamma_{q\lambda_{cr}}$ = $\frac{\pi}{2} C_1 \sqrt{\overline{K}^2 + 1}$, Non-dimensional parameter.

Table 2.9: C_1 and C_2 factors for the 3-factor method (Cantilever) (Andrade *et al.*, 2007).

No warping		
C_1	C_2	
	Top flange	**Bottom flange**
$2.462/\sqrt{1 + \overline{K}^2} + 2.383\overline{K}/\sqrt{1 + \overline{K}^2}$	$0.38 + 2.092\overline{K} - 0.318\overline{K}^2$	$0.512 + 0.37\overline{K} - 0.033\overline{K}^2$

2.3.5 TRAHAIR *et al.*

Trahair *et al*. (2008) approximated using Eq. 2.13 the elastic critical buckling moment of a cantilever with a point load at the free end. This equation was adopted into Eurocode3 (EC3) 2008 edition. The equation does not rely on effective length factors or non-dimensional factors, except for K.

$$\frac{QL^2}{\sqrt{(EI_zGI_t)}} = 11\left\{1 + \frac{1.2\varepsilon}{\sqrt{1+1.2^2\varepsilon^2}}\right\} + 4(K - 2)\left\{1 + \frac{1.2(\varepsilon-0.1)}{\sqrt{(1+1.2^2(\varepsilon-0.1)^2)}}\right\}$$ Eq. 2.13

Where:

Q = Critical point load at free end.

I_z = Moment of inertia about z-axis (European equivalent for I_y).

I_t = Torsional constant (European equivalent for J).

ε = $\frac{y_Q}{L}\sqrt{\frac{EI_y}{GJ}} = \frac{2y_QK}{d\pi}$, Dimensionless load height parameter.

y_Q = Distance between the shear centre and the load applied (positive below the shear centre).

d = Distance between flange centroids.

K = Torsional parameter of a segment.

2.3.6 INTERPRETATION OF THESE METHODS

It should be noted from the two equations by Timoshenko and Gere (1961) that the buckling shape and load differ significantly between simply supported beams and cantilevers. A remark that was often overlooked in subsequent investigations, i.e. force-fitting the results from simply supported beams to cantilevers.

All five of the methods discussed above were related to each other by the factor $\frac{\sqrt{EI_yGJ}}{L}$, hence the only difference were the non-dimensional parameters given by each of them. It was therefore only necessary to compare these non-dimensional parameters. The governing buckling equation for a simply supported beam (Eq. 2.3) contained the same factor as mentioned above. Trahair (1963) showed that it was possible to relate Eq. 2.8 with Eq. 2.7 via a single effective length factor k. For instance, using Nethercot's (1973) equation, Eq. 2.14 relates k to the non-dimensional parameter y_e:

$$k = \frac{\pi}{\gamma_e\sqrt{2}}\sqrt{1 + \sqrt{1 + \frac{4\gamma_e{}^2}{R^2}}} \qquad\qquad \text{Eq. 2.14}$$

It was thus possible to relate all of the methods discussed above, to the simply supported beam equation given by Eq. 2.7 using an appropriate effective length factor k. If the effective length factors were known for the various methods, comparisons could be made between them. This was helpful later on when comparing FE analyses for cantilevers and overhang beams.

2.4 LATERAL-TORSIONAL BUCKLING OF OVERHANG BEAMS

2.4.1 NETHERCOT

Overhang beams are an intermediate step between simply supported beams and cantilevers. Moreover, overhang beams are continuous; hence, warping is unrestrained at the supports. Another parameter that is included in overhang beams is the ratio of backspan length to the overhang length. As with the case of simply supported beams, the restraint at the supports for overhang beams may vary. Once again, a point load was the severest case of loading. This study was based only on overhang beams with both supports laterally and torsionally restrained.

The procedure given by Nethercot (1973) is also valid for overhang beams with the internal (fulcrum) prevented from twisting. The external (root) support can either be fixed or simply supported. The factors A, B_1 and B_2 for these criteria becomes:

$A = 1.307 - 1.711/R^2 + 0.586/R$
$B_1 = 0.878 + 6.762/R^2 + 4.697/R$
$B_2 = 1.031 - 0.296/R^2 + 1.282/R$

2.4.2 ANDRADE *et al.*

As stated earlier, the method given by Andrade *et al.* (2007) can be used for continuous overhang beams as the formula allows for warping at the supports. C_1 & C_2 factors are shown in Table 2.10.

Table 2.10: C_1 and C_2 factors for the 3-factor method (Overhang beam) (Andrade *et al.*, 2007).

Free to warp		
C₁	**C₂**	
	Top flange	**Bottom flange**
$2.437/\sqrt{1+\bar{K}^2} + 0.613\bar{K}/\sqrt{1+\bar{K}^2} - 0.105\bar{K}^2/\sqrt{1+\bar{K}^2}$	$0.409 + 1.444\bar{K} - 0.07\bar{K}^2$	$0.529 + 0.234\bar{K} - 0.149\bar{K}^2$

2.4.3 TRAHAIR *et al.*

Trahair *et al.* (2008) also approximated the buckling capacity of an overhang beam, as shown in Eq. 2.15.

$$\frac{QL^2}{\sqrt{(EI_z GI_t)}} = 6\left\{1 + \frac{1.5(\varepsilon-0.1)}{\sqrt{1+1.5^2(\varepsilon-0.1)^2}}\right\} + 1.5(K-2)\left\{1 + \frac{3(\varepsilon-0.3)}{\sqrt{(1+3^2(\varepsilon-0.3)^2)}}\right\} \qquad \text{Eq. 2.15}$$

2.4.4 INTERPRETATION OF THESE METHODS

For the three methods discussed above, the length was taken as the overhang length. There were no backspan to overhang ratios involved, implying that the length of the backspan had no influence on the LTB capacity of the overhanging segment. The method by Nethercot (1973) was only applicable to continuous beams with equal spans, which is not always the case in beam design. Andrade *et al.* (2007) did not analyse overhang beams as such, but free to warp cantilevers. These two cases were similar, except that the warping resistance at the support is also dependent on the length (stiffness) of the adjacent span. Trahair *et al.* (2008) assumed no lateral rotation at the internal support; in addition, the internal support had no warping restraint. In each of the three methods explained above, the non-dimensional factor included the torsional parameter of the beam. Currently, without taking interaction buckling into account, there is no method of calculating the buckling capacity of an overhang beam with different backspan to overhang lengths. Therefore, interaction buckling was considered in this study.

2.5   INTERACTION BUCKLING

2.5.1   CONTINUOUS BEAMS

Interaction buckling is the effect where the lateral-torsional buckling capacity of a continuous beam is increased by the stiffness of adjacent spans. In continuous beams, the end conditions are never completely fixed or pinned. Thus, the unbraced beam segment at the ends is influenced by stiffness's of adjacent segments (Driver, 2014). In continuous beams, it is unusual for all segments to buckle simultaneously; rather, the segment that buckles first tends to be restrained by the adjacent unbuckled segments (Driver, 2014). The behaviour of all unbraced segments determines the critical load that a continuous lateral and torsional beam can withstand (Driver, 2014). Continuous beams consist of two segments: "restrained" and "restraining". The restrained segment is the segment that buckled first, and its effective length is shorter due to the adjoining restraining segments. Conversely, the restrained segments increase the effective length of the restraining segments. The illustration of this concept with a three-span continuous beam on the left side and a single-span beam on the right side is in Figure 2.7.
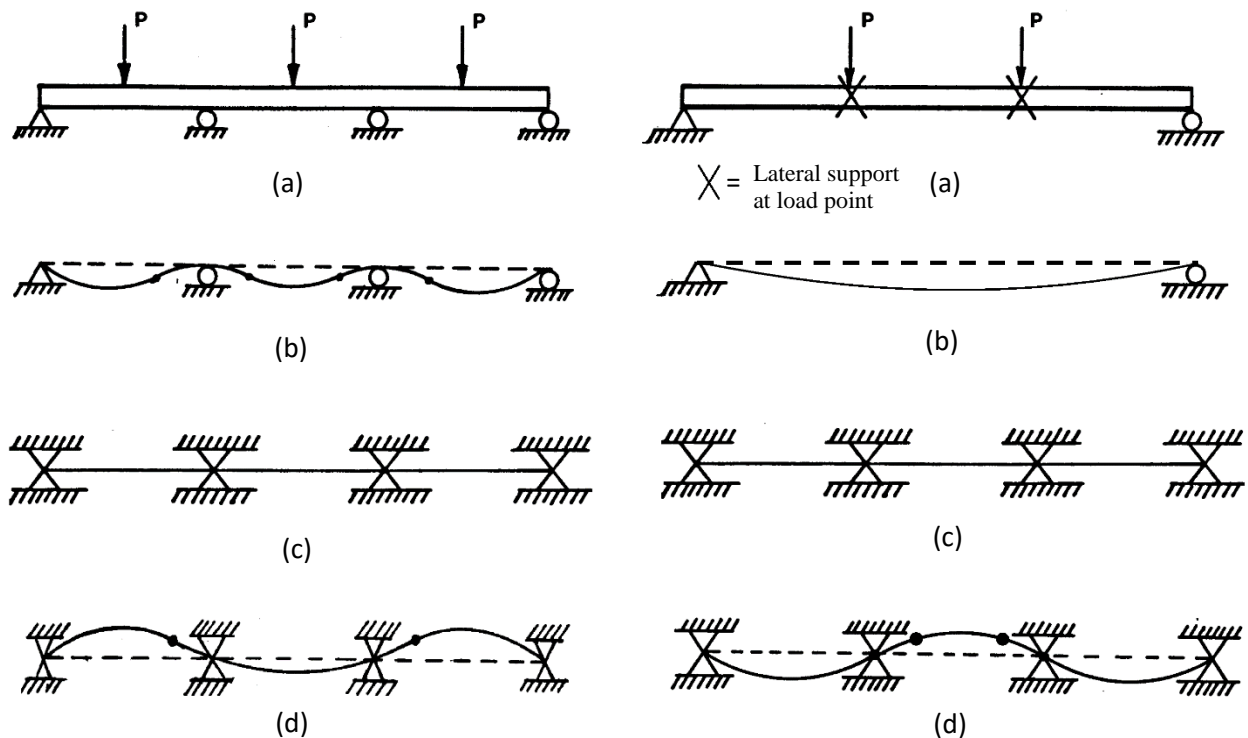
Figure 2.7: (a) Vertical loading, (b) Deflection, (c) Lateral support, (d) Laterally buckled shape (Schmitke and Kennedy, 1984).

To determine the elastic interaction buckling capacity of a laterally and torsionally continuous beam, the method as presented by Nethercot and Trahair (1976) can be used. This method takes into account known loading conditions and uses the concept of effective length. This method requires an out-of-plane stiffness that takes into account the end supports. The internal supports must be lateral and torsionally restrained.

2.5.2   OVERHANG BEAMS

In an overhang beam with at least one cantilevered segment, there is no end support at the far end (i.e. free). Currently, the method by Nethercot and Trahair (1976) cannot effectively be used when there is, at least, one cantilever in the continuous beam, as was the case for this study. The different segments of a continuous beam do interact and affect each other; hence, the principle remains applicable for this study. Under the same type of loading, that of a uniform moment, a cantilever is more susceptible to buckling than a simply supported beam (smaller moment modification factor α_m in Figure 2.8). That is to say, that the overhanging segment of a continuous beam should be the most critical segment, i.e. the first to buckle if under the same moment pattern and length.
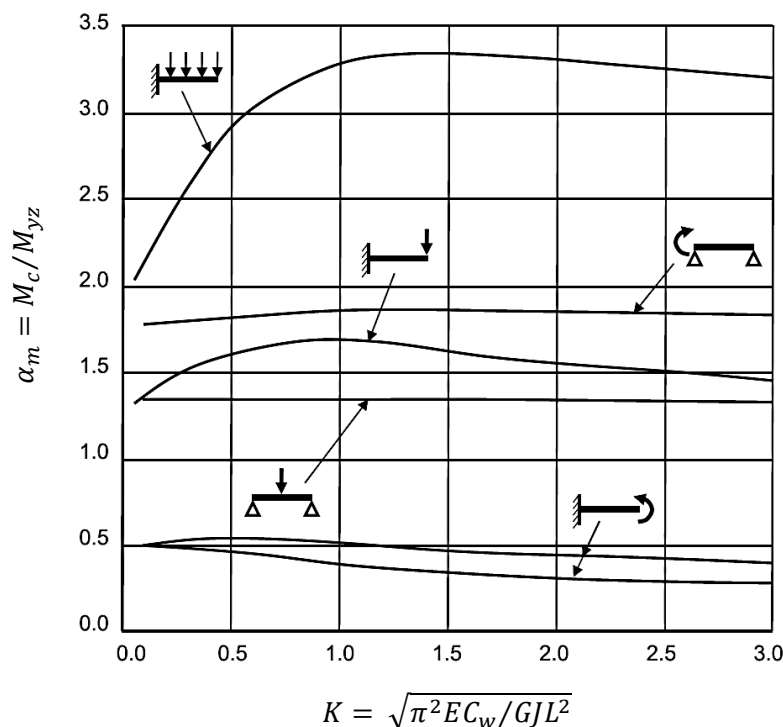
Figure 2.8: Elastic buckling of beams (Trahair, 2010).

α_m = Moment modification factor.

M_c = Maximum moment.

M_{yz} = Elastic lateral buckling moment of a simply supported beam in uniform bending.

Essa and Kennedy (1994) included an interaction factor when the overhanging segment was the critical segment. The interaction factor is part of the determination of the elastic critical buckling moment, Eq. 2.16. The interaction factor was curve fitted from FE analyses. The FE models were compared to full-scale tests. The FE model consisted of two-node line elements for the flanges and four-node plate elements for the web.

$$M_{cr} = M_c + I(M_b - M_c)$$ Eq. 2.16

Where:

M_c = Critical moment of cantilever segment that is free to warp.

Top flange loading: $M_c = 1.5 \frac{GJ}{d}$

Shear centre loading: $M_c = \frac{4}{L_c} \sqrt{EI_y GJ}$

$M_b = \frac{\omega_2 \pi}{L_b} \sqrt{EI_y GJ + \left(\frac{\pi E}{L_b}\right)^2 I_y C_w}$

M_b = Critical moment of backspan segment that is free to warp (simply supported beam).

L_c = Length of cantilever (overhang) segment.

L_b = Length of backspan segment.

d = Distance between flange centroids.

ω_2 = 1.75, as both supports are rollers and the end moment ratio becomes zero.

I = Interaction factor, a function of the ratio of backspan to the overhang span.

$I = -0.08 + 0.18 \frac{L_b}{L_c} - 0.009 \left(\frac{L_b}{L_c}\right)^2$ (Overhang with a free tip).

2.5.3 INTERPRETATION OF INTERACTION BUCKLING

When analysing overhang beams with intermediate lateral and torsional restraints, interaction buckling is not considered when determining the elastic buckling of each segment between intermediate restraints, as stated by Trahair *et al*. (2008). According to Trahair *et al*. (2008), in a continuous beam with lateral and torsional restraints, the elastic buckling of each segment should be calculated taking into account interaction buckling. As both of the two cases above have the same lateral and torsional restraints, and both are divided into segments, both cases should have interaction buckling involved in the analysis, meaning that the two cases above contradict each other. Therefore, in this study, interaction buckling was assumed to occur in both overhang and backspan segments.

Increasing the LTB capacity of a continuous beam is partly dependent on the magnitude of warping resistance by the adjacent span at the internal supports. The magnitude of warping resistance increases

as the adjacent span length increases until a maximum warping resistance is reached. The advantageous effect of warping resistance is surpassed by the adverse effect of decreased lateral stiffness of the adjacent span if the adjacent span gets longer, therefore, decreasing the LTB capacity of a continuous beam.

In the method described by Essa and Kennedy (1994), the interaction factor I was based on top flange loading. The study indicated that this interaction factor could be used for both shear centre and top flange loading. In terms of shear centre loading, this can result in inaccurate buckling capacities, as the interaction factor was formulated using top flange loadings. Thus, during this study, individual interaction factors were formulated for both shear centre and top flange loading.

Their method considered only interaction buckling in the cantilevered segment; neglecting interaction buckling in the backspan. Hence, it was not a true interaction buckling system of the entire continuous beam. At a certain ratio of backspan to overhang, interaction buckling could occur in the backspan.

The FE software that Essa and Kennedy (1994) used was capable of modelling lateral-distortional buckling. Hence the interaction factors might include web distortion and not just LTB. Nonetheless, Essa and Kennedy (1994)'s method could result in highly conservative buckling capacities if the backspan is considerably shorter than the overhanging segment.

Essa and Kennedy (1994) also stated that for top flange loading, the buckling capacity was independent of the overhang length. This statement has resulted in a large difference in critical moments compared to initial FE analyses (Chapter 3) and other methods (with $L_b/L_c = 1$), whereas for, shear centre loading, the differences were small. Because of their statement regarding top flange loading being independent on the cantilever length, the buckling capacity of the overhang beam for top flange loading was considerably higher than that for shear centre loading for any L_b/L_c ratio. This was the opposite of what was expected, as top flange loading reduces the buckling capacity due to the destabilising effect (as explained in section 2.2.6). For this study, the buckling capacity was assumed dependent on the overhang length.

Not only do these irregularities lead to inaccuracy in determining the buckling capacity, but also becomes tentative when applying these factors taking into account L_b/L_c as there are no other methods for comparison. The use of an interaction factor combines the torsional parameter of several different beams into a single equation using curve-fitting techniques. The same approach as Essa and Kennedy (1994) was used in this study as a method of determining the buckling capacities and interaction factors, with some key differences, as explained in the paragraphs above.

2.6   LATERAL DEFLECTION OF FLANGES

According to Bradford (1994), during buckling, either the top or bottom flange (or both) undergoes lateral deflection. Based on Figure 2.9 (Bradford, 1994), for overhang beams with shear centre loading, the bottom compression flange displaced significantly in the internal span. For top flange loading, the reverse holds for the internal span, with small displacement for the bottom flange. While at the tip, the top tension flange displaced more than the bottom flange for both top and shear centre loading (Bradford, 1994). It was unclear, for shear centre loading at least, at what point between the internal support and free end the crossover point is for top or bottom flange being the largest displaced flange. Regarding distortional buckling, the top flange was the largest displaced flange (as the bottom flange was fixed at the internal support). The discussions above are depicted in Figure 2.9 for the flange-width-to-beam-depth ratio of 0.2 and a flange-thickness-to-web-thickness ratio of 0.25.
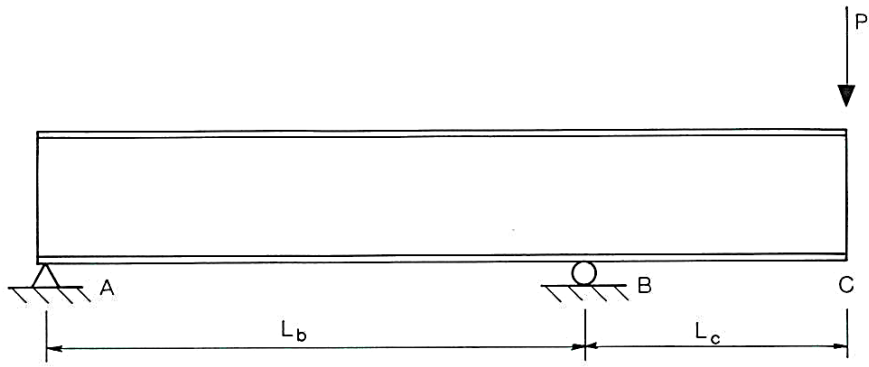
a) Beam elevation
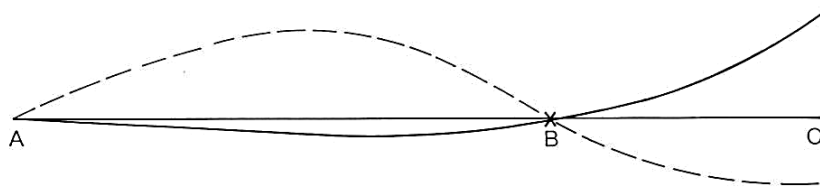
(a)   LATERAL s.c.
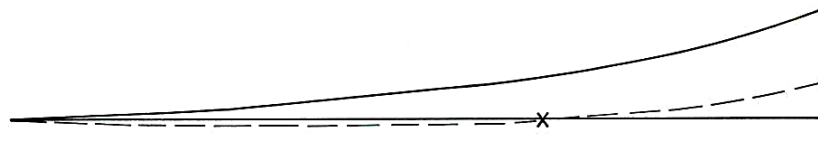
(b)   DISTORTIONAL s.c.
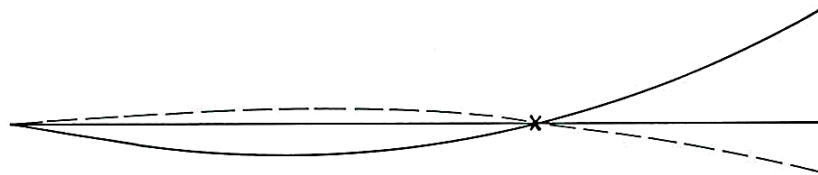
(c)   LATERAL t.f.
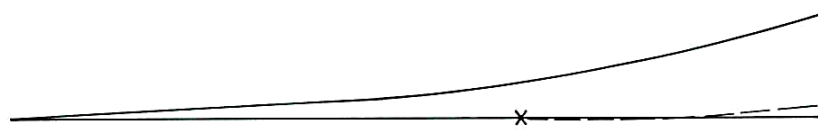
(d)   DISTORTIONAL t.f.

———————   TOP FLANGE
— — — — —   BOTTOM FLANGE

$b_f / d_w = 0.2$
$t_w / t_f = 0.25$

b) Buckling modes

Figure 2.9: Deflection of flanges for various cases (Bradford, 1994).

2.7   NUMERICAL MODELLING OF OVERHANG BEAMS

In the last couple of decades, the improvement in computing power saw the rise of numerical modelling. One of the methods of numerical modelling is finite element analysis (FEA). The method of FEA was considerably improved over the years and is now commercially available. Today, FEA theory is not only used to find numerical solutions but to extend the scope of testing. Various parameters for the same model could be altered without spending too much time and resources (when compared to physical experiments), enabling a greater understanding of the current problem and deriving better conclusions. Therefore, this study incorporated FEA theory along with the physical experiments.

Finite element analysis is a numerical method for solving the equation [K] {U} = {F}, where K is the global stiffness matrix, [U] the global displacement vector and {F} the global load vector. The finite element method splits a complex problem into finite simpler problems (elements) and then uses variation concepts to approximate the solution to the complex problem (Mac Donald, 2013). Finite element analysis is a preferred method to be used when the problem is too complex to solve using conventional methods, such as hand calculations. Finite element analysis can readily be used by computer software, allowing large models to be analysed. The key part to remember is that finite element analysis is only an approximation to a practical problem. The accuracy and validity of FEA depend on the assumptions made in the finite element model, material properties and analysis results.

When doing finite element analyses, it is crucial that the FE model is representative of the 'real' model. Representation is ensured by correct assumptions of the problem, loading conditions, boundary conditions, material properties, linearity vs. non-linearity and the effects of the environment. The effect of the environment refers to the inclusion of relevant factors to the model, but not making the model too complex by adding unnecessary elements, i.e. it is not necessary to model the wall to which the cantilever is attached if the wall is considered as rigid.

For any finite element model to be of value, calibration of the model is required. Most often, the models are calibrated to physical experiments, hand calculations or previous FE models. All three methods mentioned above were used to calibrate and verify the finite element models in this study.

For the same purposes as physical experimental setups, research was conducted on previous investigations that included FE modelling. Below three such investigations are discussed that highlight some of the important aspects and shortcomings of finite element modelling. All three investigations were for coped simply supported beams, but it was the designs of the models that were of interest. A coped beam refers to a beam with the flange partially cut to allow fixing that beam to the web of another beam.

2.7.1 INELASTIC LATERAL BUCKLING BEHAVIOUR OF COPED I-BEAMS

Before conducting a numerical parametric study, Dessouki *et al*. (2015) modelled six test specimens. The experimental tests were replicated using ANSYS V.11 commercial software, with a difference in results of 7%. "Thin shell 93" elements that contain six degrees of freedom per node were utilised for the models. These elements allowed X, Y and Z translations, as well as rotation about the X, Y and Z-axis. Quadratic shape functions for both in-plane and out-of-plane directions were used. The element properties included plasticity (non-linear material), stress-stiffening, non-linear geometry, large deflection and large strain capabilities. In total, the model consisted of 7188 elements with 21989 nodes. The flange width was eight elements wide and web height 30 elements. Imperfections were added to the model in the out-of-plane direction at the point of load application, with a value of 1/ 1000 span length. Residual stresses were not part of the model. The FE model is illustrated in Figure 2.10.
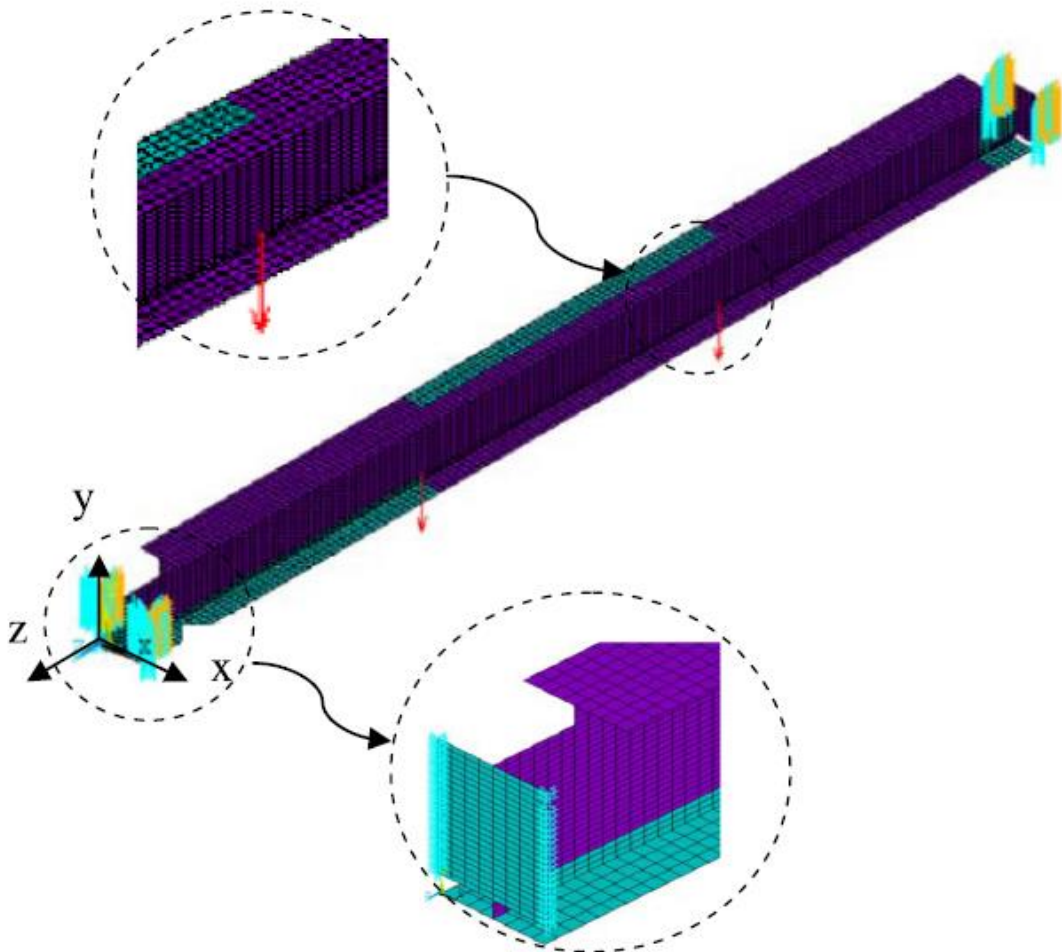
Figure 2.10: FE model of a coped beam (Dessouki *et al*., 2015).

2.7.2   CAPACITY OF COPED BEAM ENDS

The second investigation, by Aalberg (2015), used Abaqus to model and verify experimental tests. Either solid or shell elements were used (Figure 2.11). Good results were obtained from shell models with 7 x 7 mm S4R elements and five integration points through the thickness. Again, the element properties included non-linear material and geometry. Isotropic hardening was applied along with von Mises yield criterion. Force was applied by displacing the elements beneath the point of application in small increments. The first elastic buckling mode, with amplitudes varying from 0.0 – 1.0 mm was used to model imperfections. If no imperfection were present, the buckling did not trigger correctly (Aalberg, 2015). The web element thickness at the web-flange interface was increased for shell elements.
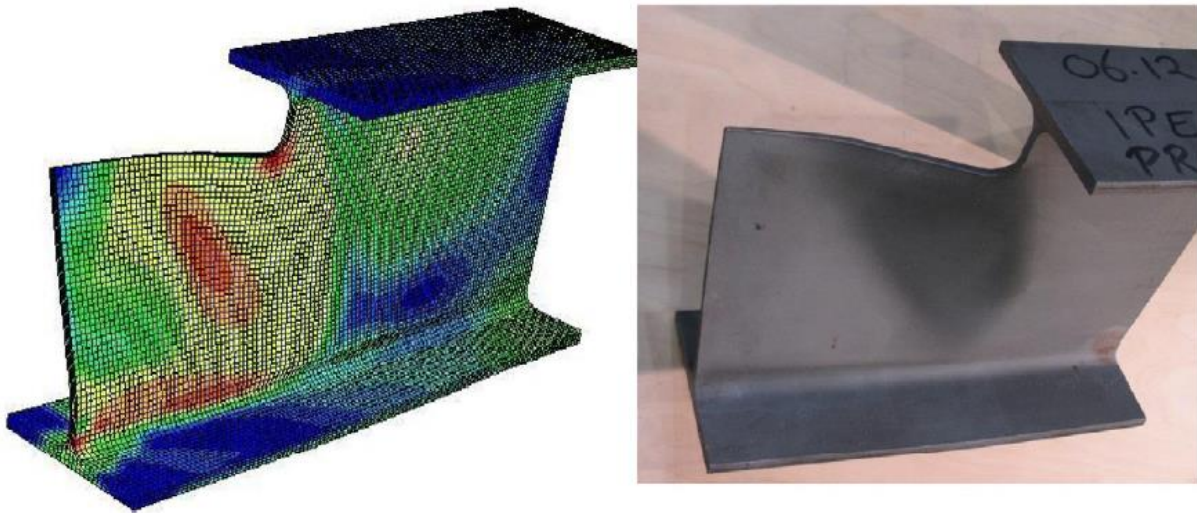
Figure 2.11: Solid elements used for modelling vs. real beam (Aalberg, 2015).

2.7.3   BUCKLING OF COPED STEEL BEAMS

The last study, which was modelled using the DIANA software, was investigated by Maljaars *et al.* (2004). The model consisted of curved shell elements with eight nodes each, four elements per flange and the web. No volume can be assigned to a shell element. Therefore, discrepancies in geometrical properties arose between the model and the real cross-section, most notably the torsional constant I_t (see Table 2.11). Using shell element, the circular stresses at the web-flange junction was not adequately simulated, illustrated by Figure 2.12, resulting in an underestimated torsional constant. The lateral-torsional buckling capacity is greatly affected by the torsional constant. Hence, provisions were made to minimise the difference. Beam elements and torsional springs were added at the web-flange junction to increase the area and torsional constant of the model to equal the real beam,

respectively (Figure 2.13). Computation time was reduced by modelling only half of the beam, with symmetry supports at midspan.

Table 2.11: Model and real geometric properties of an IPE 160 section (Maljaars *et al*., 2004).

Property	Model consisting of shells	Real section	Difference
A	1977 [mm^2]	2009 [mm^2]	1.62 %
I_y	8551391 [mm^4]	8692929 [mm^4]	1.63 %
I_z	681610 [mm^4]	681748 [mm^4]	0.02 %
I_w	3959x10^6 [mm^6]	3959x10^6 [mm^6]	0.00 %
I_t	28511 [mm^4]	35406 [mm^4]	19.48 %
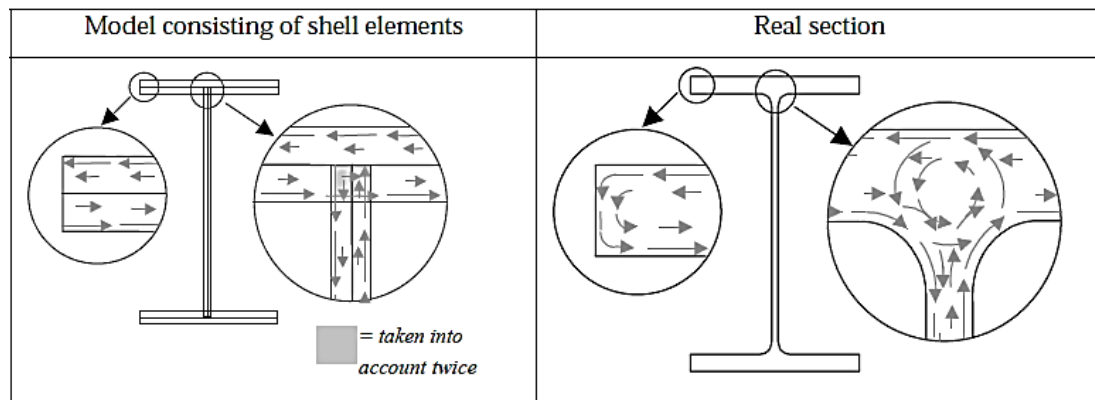
Figure 2.12: Difference in torsional stress paths (Maljaars *et al*., 2004).
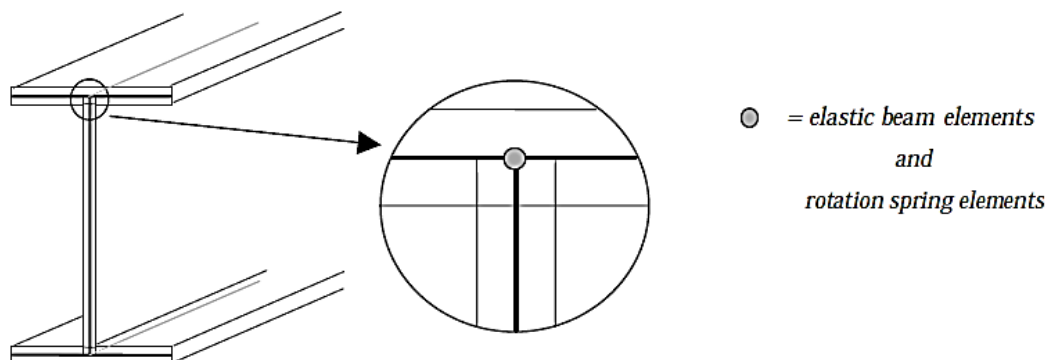
Figure 2.13: FE model consisting of shell, beam and torsional spring elements (Maljaars *et al*., 2004).

The extra torsional stiffness required per flange-web junction is calculated using Eq. 2.17.

$$k_{spring} = \frac{GI_{t,spring}}{l}$$ Eq. 2.17

Where:

k_{spring} = Rotation spring stiffness.

$I_{t,spring}$ = Converted torsional constant of a spring element.

l = Length of the element.

From the above investigations, it became apparent that there were shortcuts and shortcomings when using FE modelling to solve a real problem. Before any numerical parametric study was undertaken, it was crucial to ensure that the models were calibrated correctly, to avoid any inaccuracies or setbacks later in the FE modelling process. To obtain an estimate of the experimental setup, simple FE shell element models were constructed to gain insight on how to setup a physical test. FE modelling was therefore used to improve and extend any test conducted.

2.8   EXPERIMENTAL STUDY

Experimental studies contributed significantly to this study as it allowed a better understanding of the physical setup of the experiment. It also brought to light any possible shortcomings, areas that require attention and methods that could improve the accuracy and consistency of testing. Results obtained from physical experiments allowed calibration of the numerical modelling. The discussions of two experimental studies were as follow:

2.8.1   DISTORTION IN SIMPLE SUPPORTED BEAMS

The first investigation, performed by Zirakian and Showkati (2007), entails full-scale testing for the distortion in doubly symmetric I-section beams. Both local and lateral-torsional buckling were investigated and measured. The effect of restrained distortion buckling was also investigated. The relevance of including this research is that experimental work was conducted that included the testing setup, and results were obtained that could be compared to theory or numerical models.

In total, six I-beams were tested, either with IPE 12 or IPE 14 hot-rolled profiles. The specimens had three different lengths: 3.6 m, 4.4 m and 5.2 m and two different heights: 180 mm and 210 mm. Lateral and torsional restraints were provided at the end supports.

The standard, nominal and measured dimensions of the beam were tabulated and showed a slight variance. The height of the beams was averaged over quarter lengths (i.e. three measurements). The average method eliminates errors in the fabrication process.

The load was applied gradually at the top flange at midspan via a hydraulic jack. Between the jack and beam was a 100 mm x 100 mm x 100 mm steel cube, fixed between two restriction plates and greased to prevent frictional restraint. The steel cube allowed a point load to be applied at midspan and prevented lateral deflection and twist of the top flange.

Lateral deflection of the top flange, mid-height and bottom flange were recorded using displacement transducers and the vertical web strains with strain gauges. The measured data was then stored using a data logger.

The two vertical strain gauges showed diversion in values (negative and positive strain) at mid-height of the web, verifying flexural deformation in the web. Figure 2.14 shows the lateral movement and distortion of the web with and without torsional restraint at the top flange, respectively.

Critical loads obtained from load-deflection plots determined from experiments are usually inaccurate due to excessive deflection (Attard, 1983; Bradford and Wee, 1994). Extrapolation techniques were therefore used to determine the critical load of the test beams.
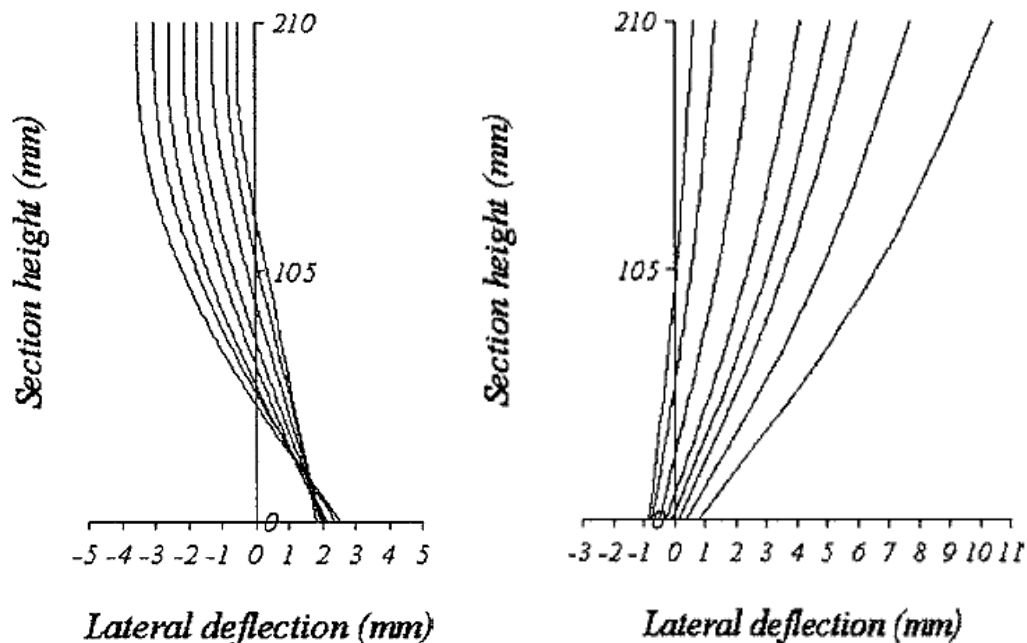
Figure 2.14: Distortion behaviour of the web at midspan a) restrained, b) unrestrained (Zirakian and Showkati, 2007).

2.8.2 LATERAL-TORSIONAL BUCKLING OF A CANTILEVER

To determine an alternative design procedure for lateral-torsional buckling of cantilevers, Ozbasaran *et al*. (2015) used physical experiments. The experiment discussed below is more relevant but was limited regarding specifications.

The test rig consisted of a large steel loading frame, hydraulic jack, data acquisition system, inclinometers, Linear Variable Differential Transformers (LVDT) and strain gauges. A circular bolt hole was drilled, with the bottom tangent on the shear centre line, for shear centre loading. For the top and bottom flange loading, a plate with a bolthole was welded to the flange (Figure 2.15). At the free end, deflection and rotation were measured during the experiment.
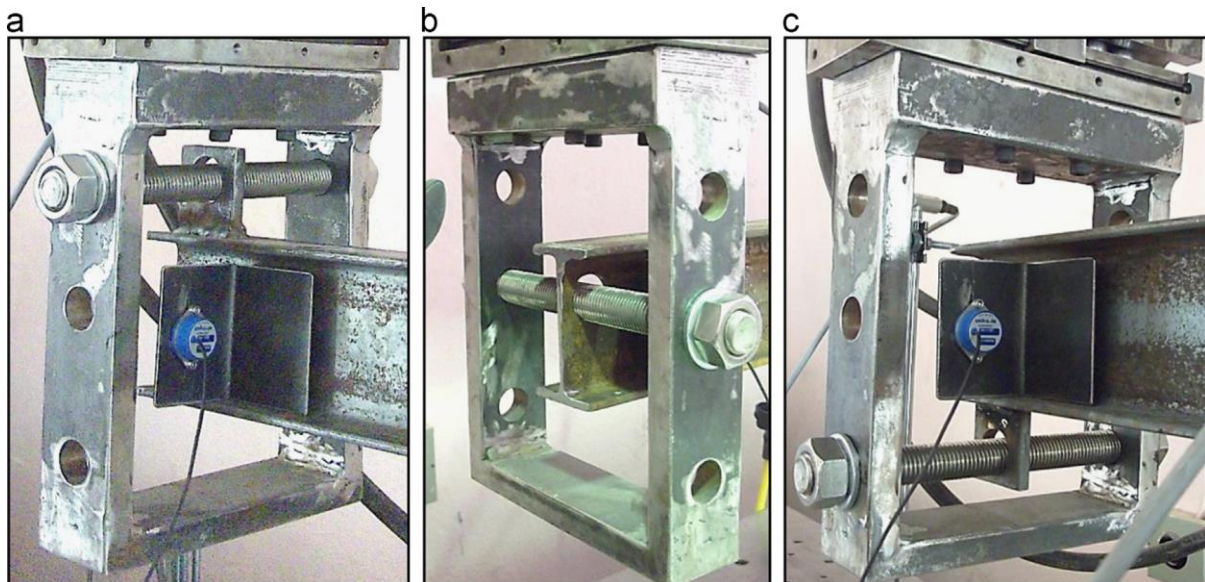
Figure 2.15: Loading positions of a) top flange, b) shear centre and c) bottom flange (Ozbasaran *et al*., 2015).

The testing of mechanical properties of the specimens was conducted before the physical test. The samples were extracted according to the TS EN ISO 6892-1 code.

The LTB capacity can be taken as the load that causes excessive displacement and rotation of the free end. However, this is difficult to control as buckling tends to be sudden. For this study, the beams were loaded until buckling occurred, with provisions made for large deflections and twist.

From the studies above, a clearer insight in the setup of lateral-torsional buckling was gained, along with methods to measure the effects and to capture the results.

2.9   CONCLUSION

Lateral-torsional buckling is a stability failure of the beam that occurs before the yield strength of the beam was reached.   Unlike yielding, lateral-torsional buckling may occur suddenly and without warning.

Comparing the different methods to determine the buckling capacity has revealed substantial differences in techniques, assumptions and effective length factors. Therefore, doubt arises as to which method to use to obtain accurate results that are consistent with any beam size or length. Merely comparing the effective length factors, SANS 10162-1 is very general for overhang beams (refer to Table 2.7). Also, SANS 10162-1 have only two set of effective length factors for both shear centre and top flange loading, regardless of the length of the overhang or the backspan to overhang ratio. A designer has at least two options: assume that the critical buckling moment of an overhang beam is independent of the length of the backspan, or rely on constructing FE models for specialised high-risk beams to determine the buckling capacity, a costly, tedious and time-consuming venture.

The buckling capacity of a beam relies on the shape of the beam, length, size of the cross-section, application of load, support conditions and imperfections. Essa and Kennedy (1994) showed that it was possible to use FE to model and analyse cantilevers and overhang beams, although they used a rudimentary FE software. From the analyses, they were able to, by using curve-fitting techniques, to refine the effective length factors. Maljaars *et al.* (2004) proposed a method to improve the accuracy of FE shell element models by adding rotational springs at the interfaces to increase the torsional stiffness of the beam to the required value.

The purpose of this study was, therefore, to see if it was possible to refine the method of determining the critical moment M_{cr} of overhang beams. The backspan length to overhang length was varied to investigate the effect the backspan has on the buckling capacity of an overhang beam. This was left out in previous studies or was partially investigated. The analysis methodology done by Essa and Kennedy (1994) was used with primary differences in assumptions. Interaction buckling was considered for overhang beams, as these beams were continuous, with warping unrestrained in the flanges. Interaction buckling of both segments was investigated with either shear centre or top flange loading. Both physical experiments and FE analyses (shell and solid elements) were conducted to determine the effect of the adjacent span on overhang beams. To gain a better understanding of the mechanisms of lateral-torsional buckling of cantilevers and overhang beams, a set of basic preliminary FE models were analysed first, using shell elements.

3. FINITE SHELL ELEMENT ANALYSES

Preliminary shell finite element (FE) models were analysed to gain insight into the behaviour of lateral-torsional buckling (LTB) and the factors that affect the buckling capacity. The aim of this chapter was to enhance the accuracy of experimental tests and to avoid potential setbacks in the setup of the experiments. In short, a broad but simple set of FE models were analysed, varying certain parameters and gaining confidence in the models and results. A method of refining the determination of the critical moment was proposed, which were extended upon in Chapter 6. In this chapter, the effective length approach of Kirby and Nethercot (1979) (see Table 2.7) was used as a method of refining. The FE shell element models were compared to SANS 10162-1 (see Appendix B) and Essa and Kennedy (1994). The following discussions and results were only preliminary and served as a reference point for experimental testing and future FE solid element analyses.

3.1   FINITE ELEMENT MODELLING

Finite element modelling approximates a practical problem. FE modelling takes advantage of the computational power of a computer to solve large, complex equations. These equations encapsulate the entire problem: geometry, material, boundary conditions and loading conditions. FE modelling solves complex problems by dividing the model into a finite amount of simpler problems (Mac Donald, 2013). The simpler problems, or elements, are then added to form a global matrix containing the properties of the elements. Matrix manipulation is conducted to determine the displacement, strain and stress of the model from the global matrix.

3.2   FINITE ELEMENT PROPERTIES

Various types of FE analyses were possible, but only the Buckling Analysis solver was used. In a Buckling Analysis solver, eigenvalues were determined using the bifurcation method. An eigenvalue is a load factor based on the load applied to the model that causes buckling of the model. For each eigenvalue is an associated eigenmode. The eigenmode is the deflection of the model. The first eigenmode is generally the buckling mode, i.e. the lowest eigenvalue obtained.

All of the FE models consisted of shell elements to predict the critical buckling moment. Shell elements, unlike beam elements, could predict the out-of-plane buckling capacity. Although, a shortcoming of shell elements was that the torsional stiffness J of the beam was underestimated, as discussed by

Maljaars *et al.* (2004) (Figure 3.1). The underestimation was due to the fillets not being modelled. Additionally, shell elements cannot reproduce the effect of St. Venant torsion shear stresses at the roots and tips of the flanges. Torsional spring supports at the interfaces between the web and the flanges at the tip only were added to the models, similar to Maljaars *et al.* (2004). Unlike Maljaars *et al.* (2004), the difference in cross-sectional area was not modelled, as these differences were negligible for the small beams investigated.
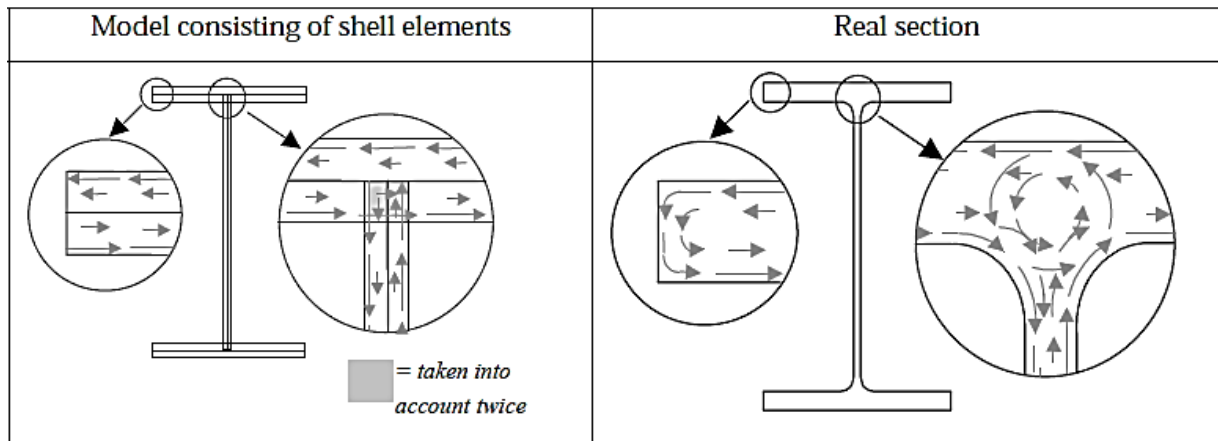
Figure 3.1: Difference in torsional stress paths (Maljaars *et al.*, 2004).

The material properties of the models were taken as 350W steel ($f_y = 350$ MPa), with $E = 200$ GPa and $G = 77$ GPa. The material used for the buckling analysis was elastic. $IPE_{AA}100$ beams with varying lengths were modelled in Strand7 using quadratic quadrilateral shell elements (8 nodes per element, with 6 degrees of freedom per node).

All beams analysed were not Class 4 (no local buckling) and satisfied the web crippling and yielding checks for both end and interior loads. The FE shell element analyses were limited to small I-sections, as they required short overhang lengths to undergo lateral-torsional buckling. Thus, it was possible to test these beams experimentally. It was also impractical to test experimentally large beams with large backspan to overhang ratios, as the beams were then very long before lateral-torsional buckling occurred in the elastic range. With practicality a factor, small I-sections required a small load to initiate LTB.

The aspect ratio between the longest and shortest side of the element was kept below 3:1 to ensure quality solutions (Mac Donald, 2013). The web height was divided into eight elements and the two flanges width into six elements. For example, an $IPE_{AA}100$ section at 2.5 m long, the length of the elements was 20 mm or 125 elements long per beam. In total, 2500 elements were constructed for an

IPE$_{AA}$100 section that was 2.5 m long. Figure 3.2 is a sketch of an IPE$_{AA}$100 cantilever, displaying the relative size of the shell elements.
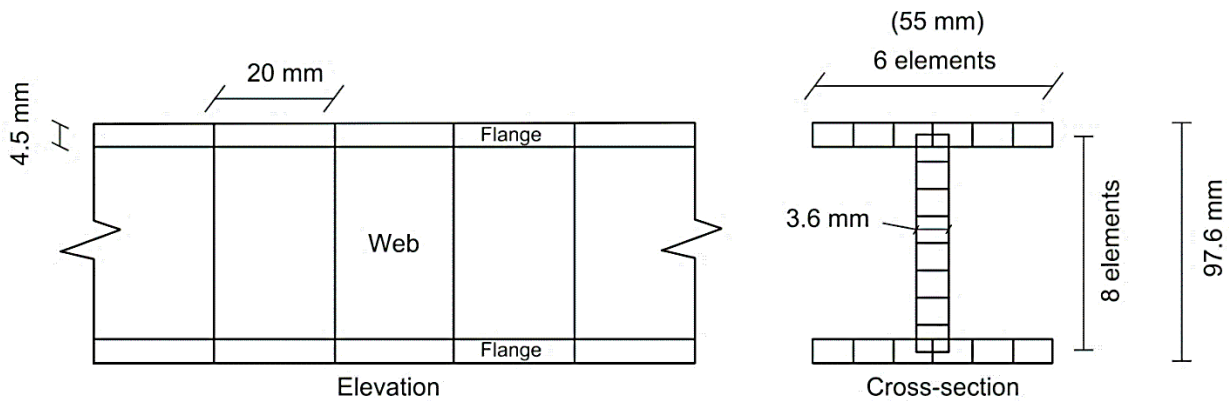
Figure 3.2: IPE$_{AA}$100 model with shell elements.

The analyses of the models were performed using the Buckling Analyses solver with a tolerance of less than 1%. Only the first eigenvalue and eigenmode were required.

All loads applied were 1 kN, thus the resulting critical buckling load (P_{cr}) was simply the value of the first eigenvalue, known as the buckling load factor. As explained earlier, the eigenvalue is a load factor that depends on the magnitude of the load applied. In this case, the eigenvalue was multiplied with 1; therefore, the buckling load factor was equal to the first eigenvalue. The critical buckling moment M_{cr} was calculated by multiplying P_{cr} with the cantilever (overhang) length L_c.

3.3 ANALYSING BUILT-IN CANTILEVERS

As a control, built-in cantilevers were modelled and analysed first. These analyses were compared to existing design equations. Full fixity was applied at the root support. A point load of 1000 N (1.0 kN) was applied at the free end, with the load either at the shear centre or on the top flange. The load applied acted at the longitudinal centre line, to avoid any eccentricities. Figure 3.3 shows the free end and fixed end of a built-in cantilever beam model.
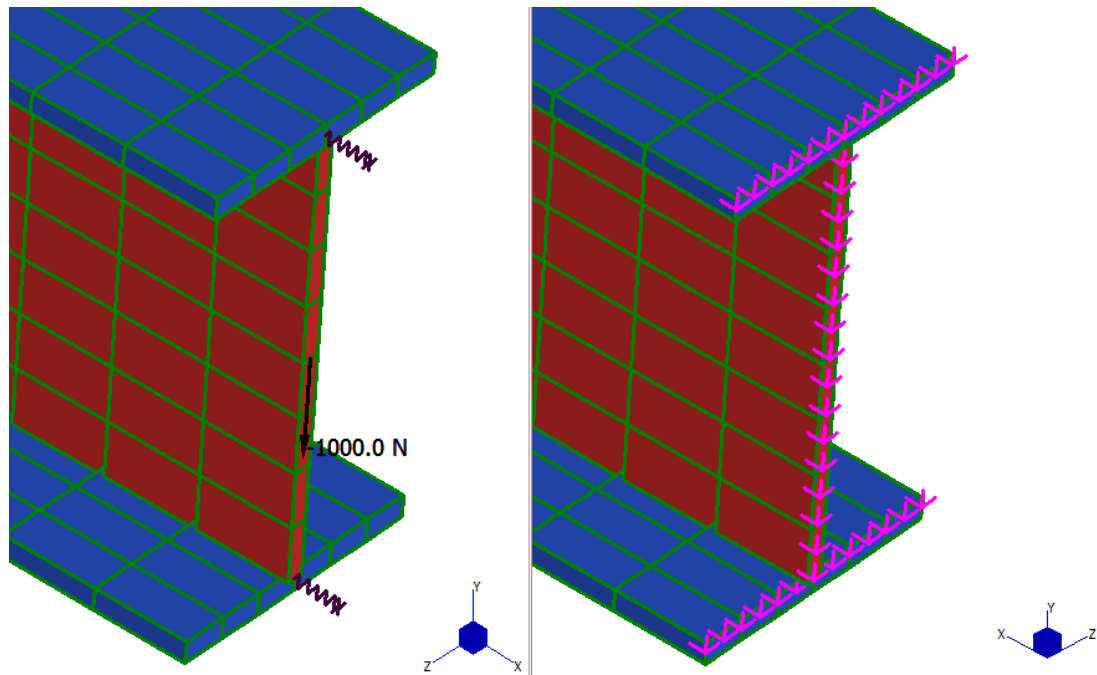
Figure 3.3: Load at shear centre (left) and full fixity at support (right) for cantilever beams.

The length at which a beam was deemed elastic depended on the effective length $k_c L_c$ (to satisfy $M_{cr} < 0.67 M_p$). The constant values of k_c used by SANS 10162-1 for fixed cantilevers (0.8 and 1.4) were used to determine the inelastic and elastic range, with the yield stress $f_y = 350$ MPa. The plastic moment M_p for an IPE$_{AA}$100 beam was 11.2 kN.m or $k_c L_c = 1.3$ m and the inelastic moment $0.67 M_p$ was 7.48 kN.m or $k_c L_c = 1.8$ m. For example, for an IPE$_{AA}$100 beam, this equated to a torsional parameter (Eq. 2.5) of $K = 0.6$ (plastic) and 0.43 (inelastic) for shear centre loading. However, due to residual stresses, the critical moment of a beam does not reach the theoretical elastic buckling moment. This reduction in critical moment reduces as the slenderness of the beam increases.

Table 3.1 is a summary of the cantilever lengths that were analysed. The plastic and inelastic range for shear centre loading for an IPE$_{AA}$100 included the 1 m and 2 m cantilever, respectively. Therefore, the shortest beam that buckled in the elastic range for both shear centre and top flange loading was 2.5 m.

Table 3.1: Cantilever lengths analysed for IPE$_{AA}$100 I-section.

L_c (m)	K	Failure mode	
		Shear centre	**Top flange**
0.4	2.44	Plastic	Plastic
0.5	1.95	Plastic	Plastic
0.65	1.5	Plastic	Plastic
1	0.98	Plastic	Inelastic
2	0.49	Inelastic	Elastic
2.5	0.39	Elastic	Elastic
3	0.33	Elastic	Elastic
3.5	0.28	Elastic	Elastic

Figures 3.4 and 3.5 illustrate the effective length factors k_c obtained for various torsional parameters K using different methods to solve for the critical buckling moment. $K = \sqrt{\pi^2 E C_w / GJL^2}$ and was varied by changing the cantilever (overhang) length L_c. The effective length factors k_c were determined by numerically solving Eq. 3.1 using the new critical buckling moment M_{cr}.

$$M_{cr} = \frac{\pi}{k_c L_c} \sqrt{EI_y GJ + \left(\frac{\pi E}{k_c L_c}\right)^2 I_y C_w} \qquad \text{Eq. 3.1}$$

The torsional parameter K was decreased by increasing the length of the cantilever L_c. For an IPE$_{AA}$100 section, if the torsional parameter K became too large, web crippling occurred and the beam had reduced capacity (increased k_c). This was observed by the results of the FE shell element analyses (Strand7). To model the capacity of the beam itself, web stiffeners were *not* added to models. The FE shell element analyses included beams in the inelastic and plastic ranges but only the results for the elastic range were used for further investigations. Using a method similar as proposed by Maljaars *et al*. (2004) increased the torsional stiffness of the beam and therefore the critical moment. Various methods of employing the torsional springs were analysed: a single large spring at the flange root at the end of the beam using the beam length or using smaller springs at each element using the element lengths. None of these various methods of adding torsional springs increased the torsional stiffness of the beam sufficiently to match the ideal beam, resulting in larger effective length factors.

The finite element models were in close agreement with existing literature in the *elastic* range for both shear centre and top flange loading. The finite element process was now used with more confidence

when analysing overhang beams. It should also be noted that the effective length factor k_c was in fact dependant on the length of the cantilever (overhang) segment, especially for top flange loading. This phenomenon was not stated in the SANS 10162-1 method.
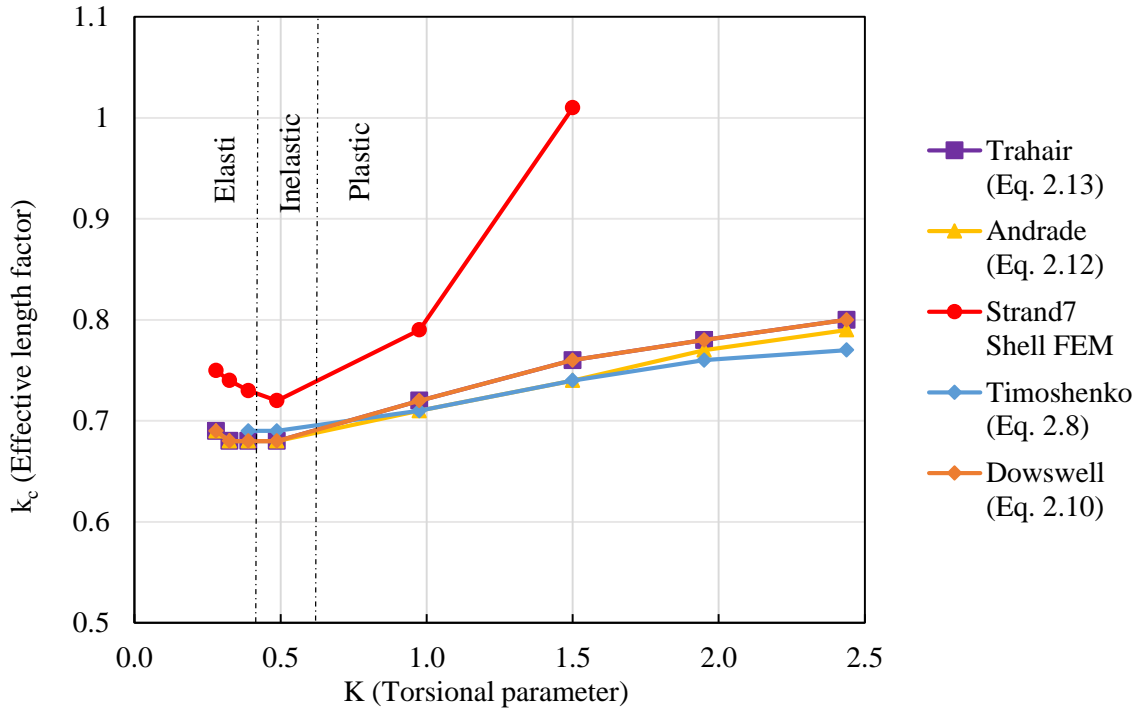
Figure 3.4: Effective length factors for IPE$_{AA}$100 cantilever with shear centre loading.
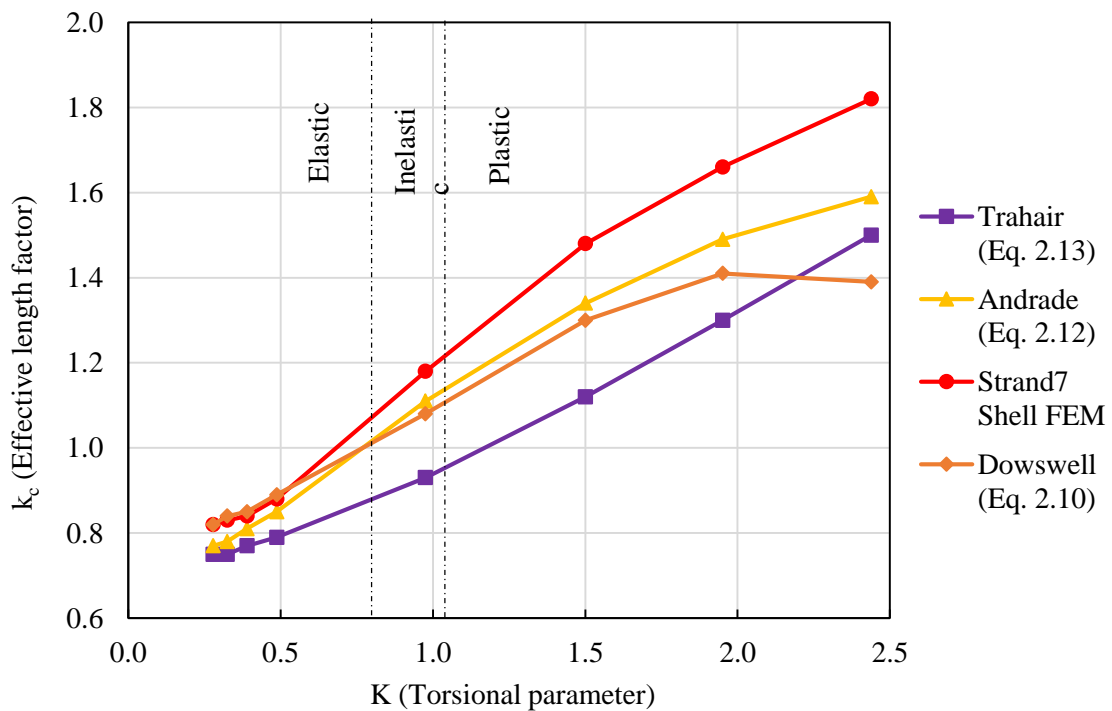
Figure 3.5: Effective length factors for IPE$_{AA}$100 cantilever with top flange loading.

3.4 ANALYSING OVERHANG BEAMS

Overhang beams were modelled with the same procedure as with a cantilever, except that at the root and fulcrum, the supports were modelled as a roller connection. At both supports, lateral and torsional restraints were provided by restraining the lateral deflection at both top and bottom flanges. Warping was thus allowed at both the root and fulcrum supports. Figure 3.6 illustrate the boundary conditions for an overhang beam.
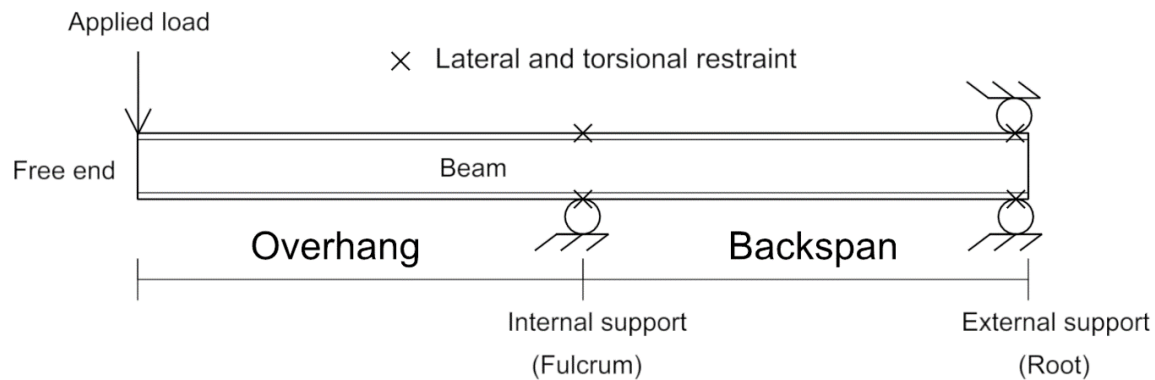
Figure 3.6: Boundary conditions of an overhang beam.

Figures 3.7 and 3.8 illustrate the effective overhang length factors k_c obtained for various torsional parameters K using different methods. As with cantilevers, the torsional parameter K was varied by increasing the length of the overhang L_c. For FE shell element analyses, the backspan length L_b was taken arbitrarily as equal to the overhang length L_c. The effective length factors for overhang beams, as given by SANS 10162 were 1.0 and 2.5 for shear centre and top flange loading, respectively. The span lengths for elastic buckling were chosen as 2 m, 2.5 m, 3 m and 3.5 m.

Once again, the results from the finite elements were in close agreement with existing literature. After sufficient accuracy had been obtained by analysing cantilevers and continuous beams (with equal backspan to overhang lengths), the analyses continued to overhang beams with variable backspan lengths. In short, ratio of the backspan to overhang length was defined as L_b/L_c.

Table 3.2 is a summary of the different overhang beams that were analysed using finite element method. The variable L_c referred to the length of the overhanging segment. With $L_b/L_c = 0$ the overhang beam became a free-to-warp cantilever. The 2 m overhang beam with backspan to overhang ratios of 0.5 and 1.0 were in the inelastic range for shear centre loading. Once again, the shortest overhang beam that buckled in the elastic range for any L_b/L_c was $L_c = 2.0$ m. The results were discussed in the next section.
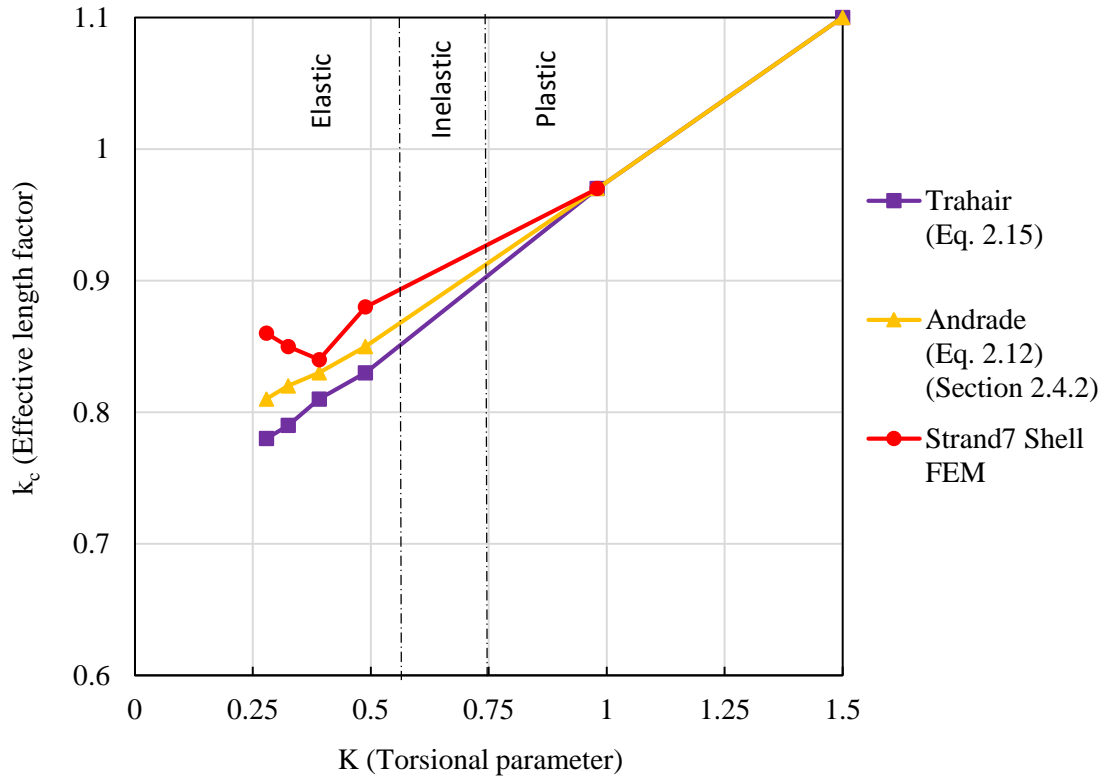
Figure 3.7: Effective length factors for IPE$_{AA}$100 overhang beams with shear centre loading.
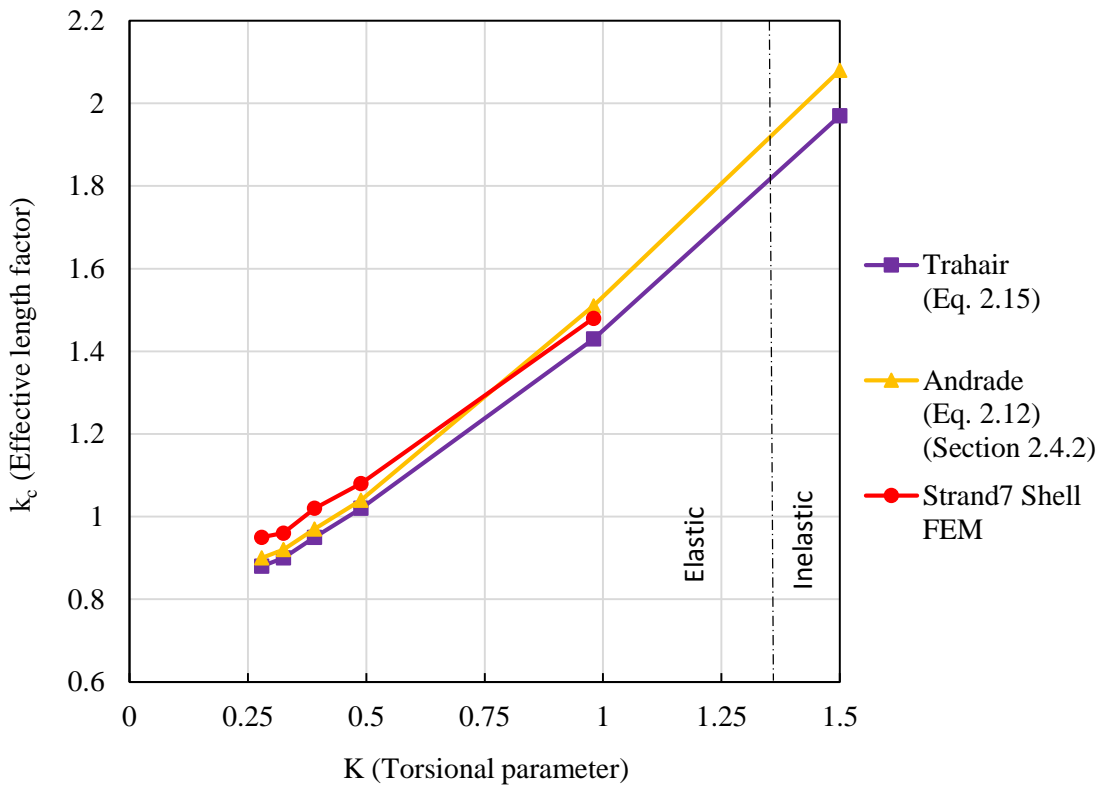
Figure 3.8: Effective length factors for IPE$_{AA}$100 overhang beams with top flange loading.

Table 3.2: Overhang lengths and ratios analysed for IPE$_{AA}$100 I-section.

L_c (m)	Backspan to overhang ratio, L_b/L_c
2.0	0, 0.5, 1.0, 1.5, 2.0, 2.5, 3.0, 4.0, 5.0
2.5	0, 0.5, 1.0, 1.5, 2.0, 2.5, 3.0, 4.0, 5.0
3.0	0, 0.5, 1.0, 1.5, 2.0, 2.5
3.5	0, 0.5, 1.0, 1.5, 2.0

3.5   ANALYSIS OF FINITE ELEMENTS RESULTS

The buckling capacity of an overhang beam was affected by factors such as:

- Interaction buckling.
- The distance between the shear centre and the load applied.
- The length of the backspan.
- The size of the beam.

The factors mentioned above also affected in which segment buckling occurred. By determining the buckling capacity of each segment, it was then possible to determine which value of L_b/L_c the critical segment changed from overhang to backspan.

Continuous beams were analysed using the method proposed by Essa and Kennedy (1994) that divided the overhang beam into an overhanging and backspan segment. The critical cantilever moments was obtained from finite element analysis on cantilevers that were free to warp. The backspan critical moments were calculated using the unfactored elastic critical moment for a simply supported beam (Eq. 3.2), in this case $\omega_2 = 1.75$. Finite element analyses were not performed on simply supported beams, as the given equation was derived from first principles and was deemed accurate.

$$M_b = \frac{\omega_2 \pi}{L_b} \sqrt{EI_y GJ + \left(\frac{\pi E}{L_b}\right)^2 I_y C_w}$$
                                                                             Eq. 3.2

Where:

ω_2 = Equivalent moment factor.

Unlike Essa and Kennedy (1994), if the backspan was the critical segment, the overhang beam's critical moment was not taken as that of the backspan segment, unless $L_b/L_c > 2$ (justified on p. 3-16, par. 1). With $L_b/L_c < 2$, interaction buckling occurred between the overhang and backspan segment. Not only did interaction buckling affect the capacity of both segments, but also both segments could buckle simultaneously.

The capacity of a cantilever that was restrained from warping at the support was taken as the upper-bound capacity. The upper-bound capacity could never be reached in an overhang beam as the warping at the internal support in an overhang beam could never reach full restraint. For large backspan to overhang ratios L_b/L_c, the capacity of a simply supported beam was used as the upper-bound capacity. The boundaries are given with the results obtained from finite element analyses in Figures 3.9 and 3.10, with $L_c = 2.5$ m.

The two cantilever capacities were from finite shell element analyses and were plotted for all values of L_b/L_c for illustrative purposes (should only be for $L_b/L_c = 0$). The 'backspan' line referred to the capacities obtained from Eq. 3.2.

Without taking interaction buckling into account, the capacity of the overhanging segment (both free to warp and no warping) was independent of the backspan length, i.e. remained constant over L_b/L_c. The capacity of the backspan, assuming simply supported, was highly dependent on the backspan length.

The backspan partially restricted the warping in the flanges, especially when the backspan was short; hence, the critical overhanging segment had increased capacity compared to a free to warp cantilever. The increase in capacity in the overhanging segment was a maximum of 15%, proving that the adjacent span affected the lateral-torsional buckling of an overhang beam. With the backspan at intermediate lengths, the backspan was the critical segment, with slightly reduced capacity. Between the two cases above, a small range of L_b/L_c exist where the overhanging segment remained the critical segment, but with reduced capacity. The abovementioned is illustrated in Figures 3.9

When the backspan segment is long relative to the overhanging segment, the capacity of the overhang beam could be taken as the capacity of a simply supported beam, with the backspan length taken as the segment length.

Top flange loading had similar effects on the capacity of the overhang beam. Except, the range for the reduced capacity of the overhanging segment was now larger. The increase in the capacity of the overhanging segment was less than 10%.
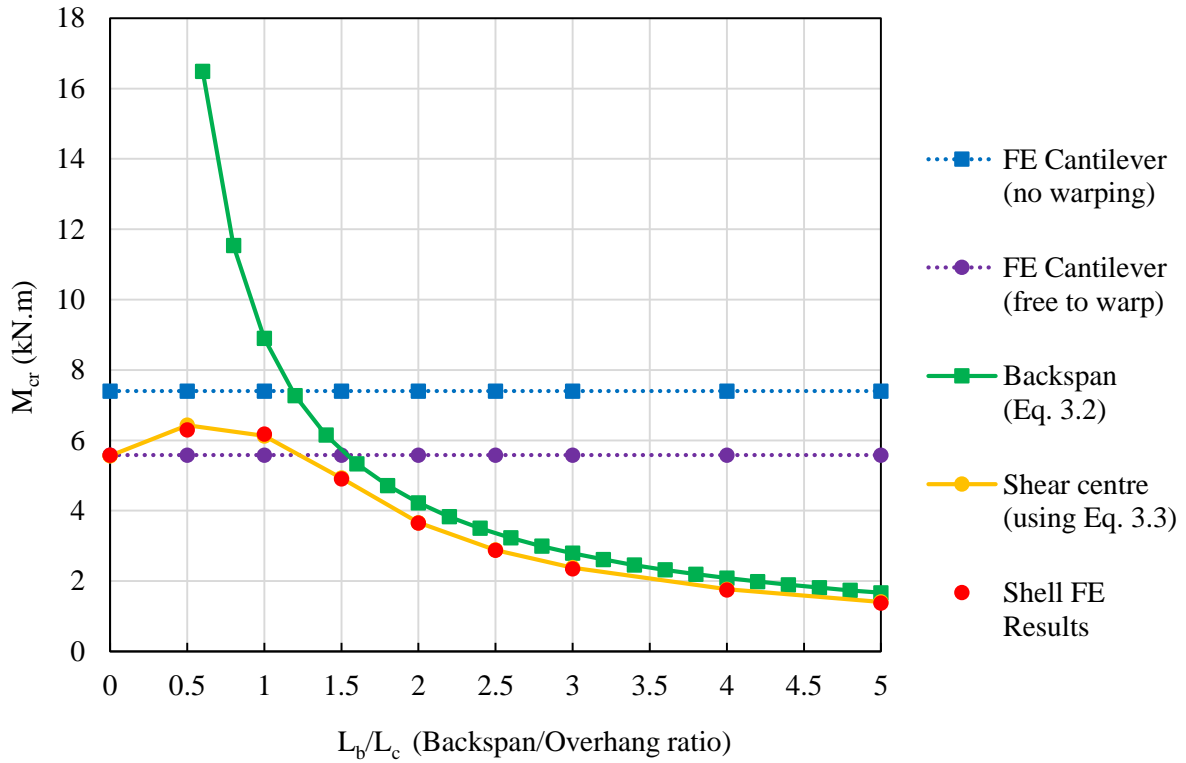
Figure 3.9: Critical moments for IPE$_{AA}$100 with 2.5 m overhanging segment and with shear centre loading.
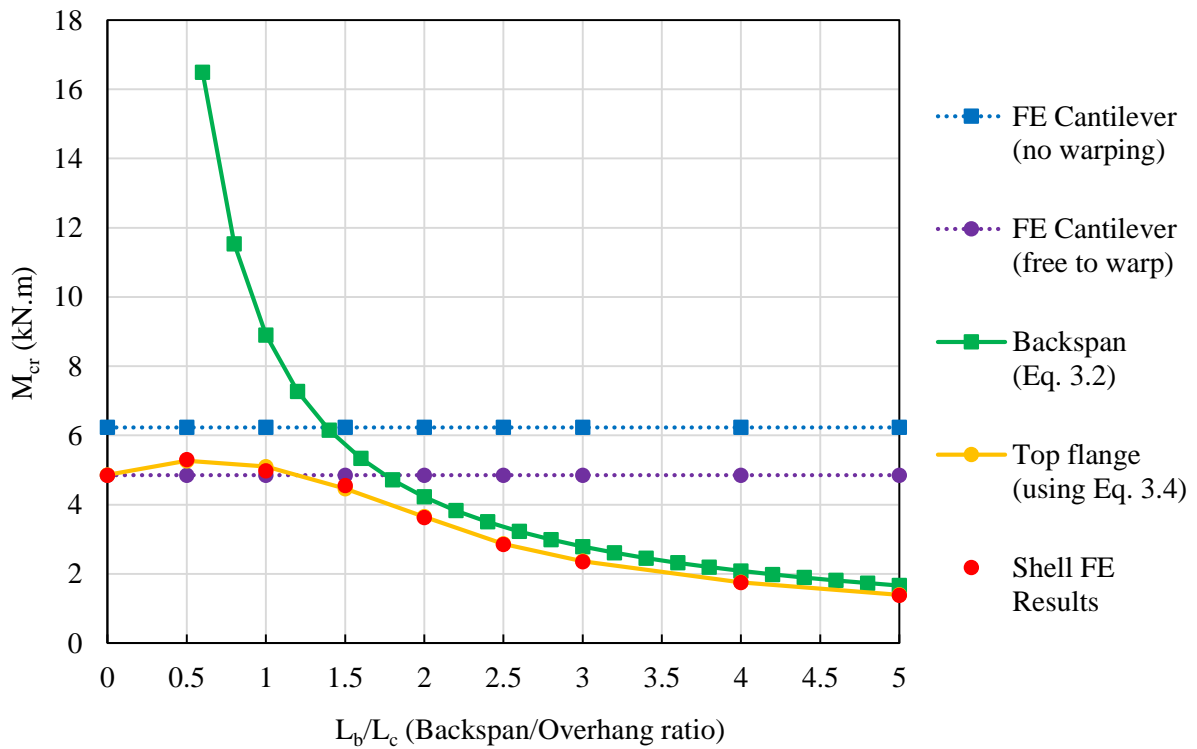
Figure 3.10: Critical moments for IPE$_{AA}$100 with 2.5 m overhanging segment and with top flange loading.

To determine the value of L_b/L_c at which these ranges occurred, it was first necessary to curve-fit the finite element results to obtain a formula relating effective overhang length factor k_c to L_b/L_c (Figure 3.11). The factor k_c was chosen, because the length of the overhang may vary whilst keeping L_b/L_c constant (but in effect varying the backspan length in relation). If k_c was known, the critical elastic buckling moment could be calculated using Eq. 3.1.

The range of L_b/L_c was from 0.0 to 5.0 and L_c was chosen as 2.5 m as the beam was in the elastic range, regardless of the backspan length. Similarly to Essa and Kennedy (1994), a second-order polynomial was used to curve-fit the finite shell element results. It was noted for both shear centre and top flange loading that for $L_b/L_c > 2$, the effective overhang length factors k_c was linear in terms of L_b/L_c, hence were excluded in the curve-fitting procedure.
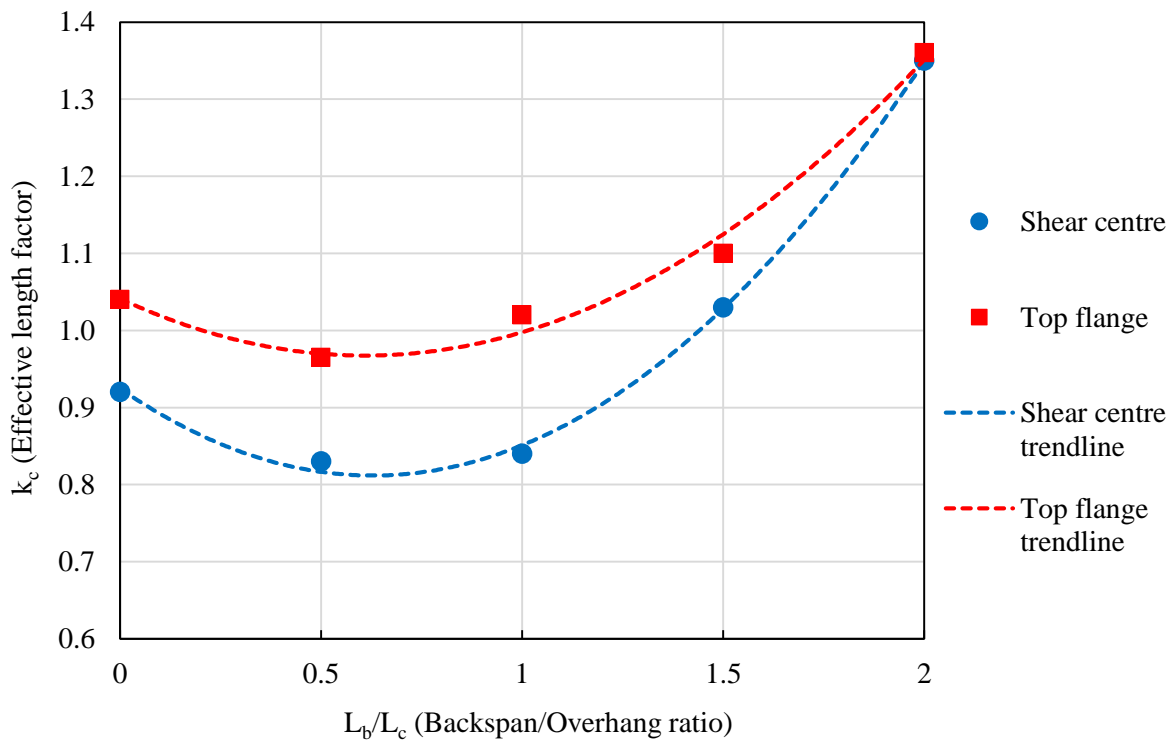
Figure 3.11: Curve fitting effective length factors using an IPE$_{AA}$100 beam with 2.5 m overhang length.

Different formulae were obtained for the shear centre and top flange loading. The formulae had an R-squared value of 0.9982 and 0.9873 for the shear centre and top flange loading, respectively. The second-order formulae, for the shear centre and top flange loading, respectively, are:

Shear centre: $k_c = 0.2857(L_b/L_c)^2 - 0.3594\,(L_b/L_c) + 0.9249$ Eq. 3.3

Top flange: $k_c = 0.1986(L_b/L_c)^2 - 0.2421(L_b/L_c) + 1.0413$ Eq. 3.4

With L_b/L_c between 0.0 and 2.0.

Unlike the interaction formula as given by Essa and Kennedy (1994) (Eq. 3.5) which applied to both shear centre and top flange loading, the equations obtained had different constants for the shear centre and top flange loading. Also, the critical moment M_{cr} could be calculated directly from the factor k_c using Eq. 3.1. Whereas the interaction formula given by Essa and Kennedy (1994) must first be added to Eq. 3.6 before the critical moment M_{cr} could be calculated.

Essa and Kennedy: $I = -0.08 + 0.18\frac{L_b}{L_c} - 0.009\left(\frac{L_b}{L_c}\right)^2$ — Eq. 3.5

$M_{cr} = M_c + I(M_b - M_c)$ — Eq. 3.6

Eqs. 3.3 and 3.4 (based on 2.5 m overhang) were compared to 2 m, 3 m and 3.5 m overhang lengths to illustrate the accuracy and validity of these formulae for an IPE$_{AA}$100 section (Figures 3.12 and 3.13). With the load applied at the shear centre, a good correlation existed between k_c and L_b/L_c, regardless of the length of the overhang. The k_c values in terms of L_b/L_c were slightly dependent on the length of the overhang with short backspan and top flange loading. However, by using the k_c values of a short overhang beam, a lower bound (conservative) capacity was obtained for that specific size of beam.
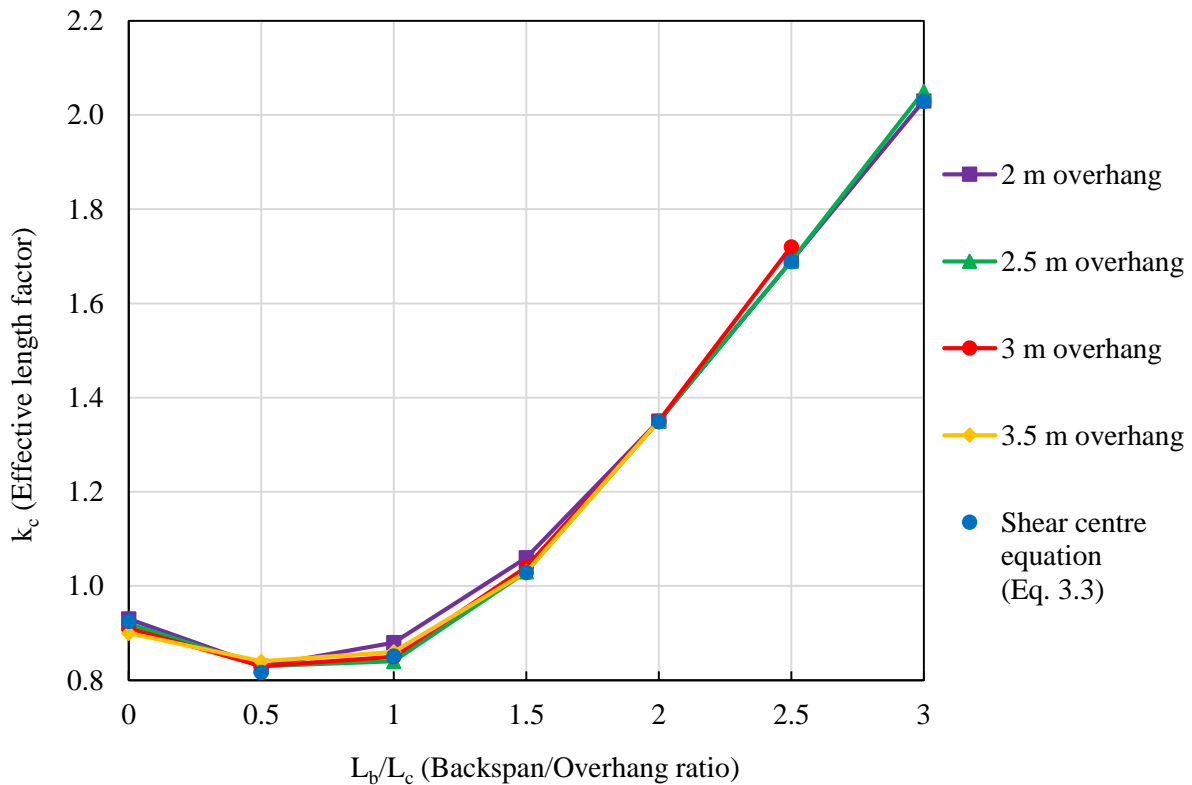
Figure 3.12: Finite element results vs. equation for IPE$_{AA}$100 with shear centre loading.
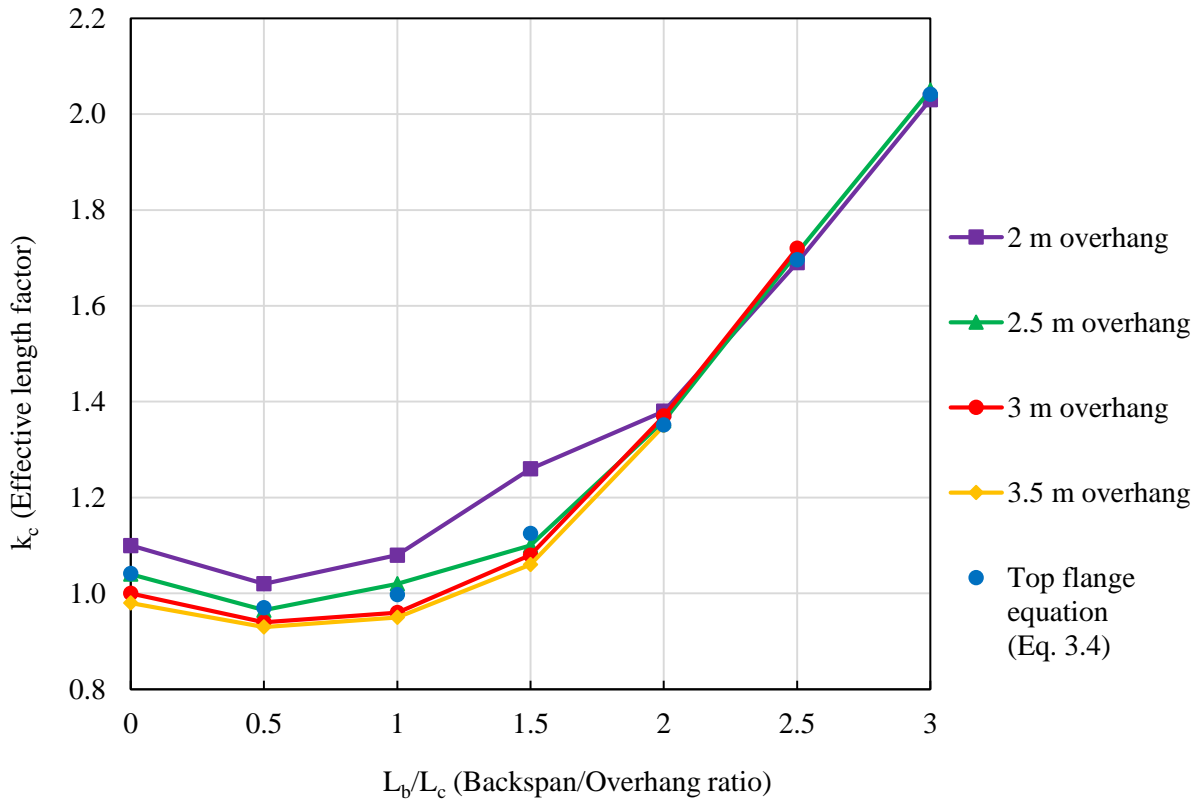
Figure 3.13: Finite element results vs. equation for IPE$_{AA}$100 with top flange loading.

By curve fitting, the precise L_b/L_c values for the different critical ranges were determined using Eq. 3.1 with the effective length factors obtained by Eqs. 3.3 and 3.4. The following discussion was based on an IPE$_{AA}$100 section with shear centre loading and the contents of Figure 3.9.

At $L_b/L_c < 1.53$, the *overhang* was the critical segment (free to warp cantilever had a smaller buckling capacity than the backspan). Between $L_b/L_c = 1.25$ and $L_b/L_c = 1.53$, the capacity of the overhanging segment was *reduced* (weaker than a free to warp cantilever) and below $L_b/L_c = 1.25$, the capacity of the overhanging segment was *increasing* (stronger than a free to warp cantilever). For $L_b/L_c > 1.53$ the *backspan* was the critical segment (smaller buckling capacity than a free to warp cantilever), but the capacity was reduced compared to a simply supported beam. At $L_b/L_c = 2$ and above, interaction was negligible, and the capacity of the beam was slightly less than a simply supported beam.

Similarly, for top flange loading (Figure 3.10), the overhanging segment was critical when $L_b/L_c < 1.75$. When $1.23 < L_b/L_c < 1.75$, the overhanging segment had reduced capacity. For $L_b/L_c > 1.75$, the backspan was critical, with buckling capacity less than a simply supported beam.

The decreased capacity of the backspan was not limited by L_b/L_c (Figures 3.12 and 3.13). Instead, k_c increased linearly regarding L_b/L_c when $L_b/L_c > 2$. When $L_b/L_c > 2$, Eqs. 3.3 and 3.4 were slightly modified to include the following linear term:

$$k_c = k_c(L_b/L_c = 2) + 0.68(L_b/L_c - 2)$$

<div align="right">Eq. 3.7</div>

A simpler approach for $L_b/L_c > 2$ is to assume a simply supported beam and to analyse it as such.

With the ranges known, it was not necessary to first distinguish which segment was critical or what was the capacity of that critical segment. Eqs 3.3 and 3.4 calculates the effective length factor based on the overhanging segment length, by taking into account the backspan segment length. These two equations took into account interaction buckling and hence only one calculation is required to determine the effective length of the continuous overhang beam and then subsequently the capacity.

With $L_b/L_c > 2$, the k_c values for the shear centre and top flanges converged to the same value. Thus, for large backspan to overhang ratios, the capacity of the backspan was independent on the height of the load applied at the free tip of the overhanging segment.

3.6   COMPARING RESULTS TO ESSA AND KENNEDY

The results obtained from the finite shell element analyses were compared to Essa and Kennedy (1994) and the current SANS 10162-1 design code in Figures 3.14 and 3.15. The current SANS 10162-1 design code (Appendix B) did not take into account the length of the backspan segment. Hence only one point was plotted. In all of the cases, SANS 10162-1 was over-conservative if $L_b/L_c = 1$. With the approach of Essa and Kennedy (1994), there was no smooth transition from the overhanging segment being critical to the backspan segment being critical, as they neglected interaction buckling in the backspan. According to Essa and Kennedy's (1994) method, if the overhanging segment was critical, the backspan segment always increased the capacity of the overhanging segment.

Between $L_b/L_c = 0.5$ and $L_b/L_c = 1$, the buckling capacities were similar for shear centre loading. For top flange loading, due to no interaction buckling in the backspan, Essa and Kennedy's (1994) method resulted in a higher buckling capacity (up to 74% difference compared to FE shell element results). The large difference in top flange loading was also due to their statement that the capacity for top flange loading was independent on the overhanging segment length (Essa and Kennedy, 1994). Thus, the buckling capacity remained fixed for top flange loading, regardless of the length of the overhanging segment.
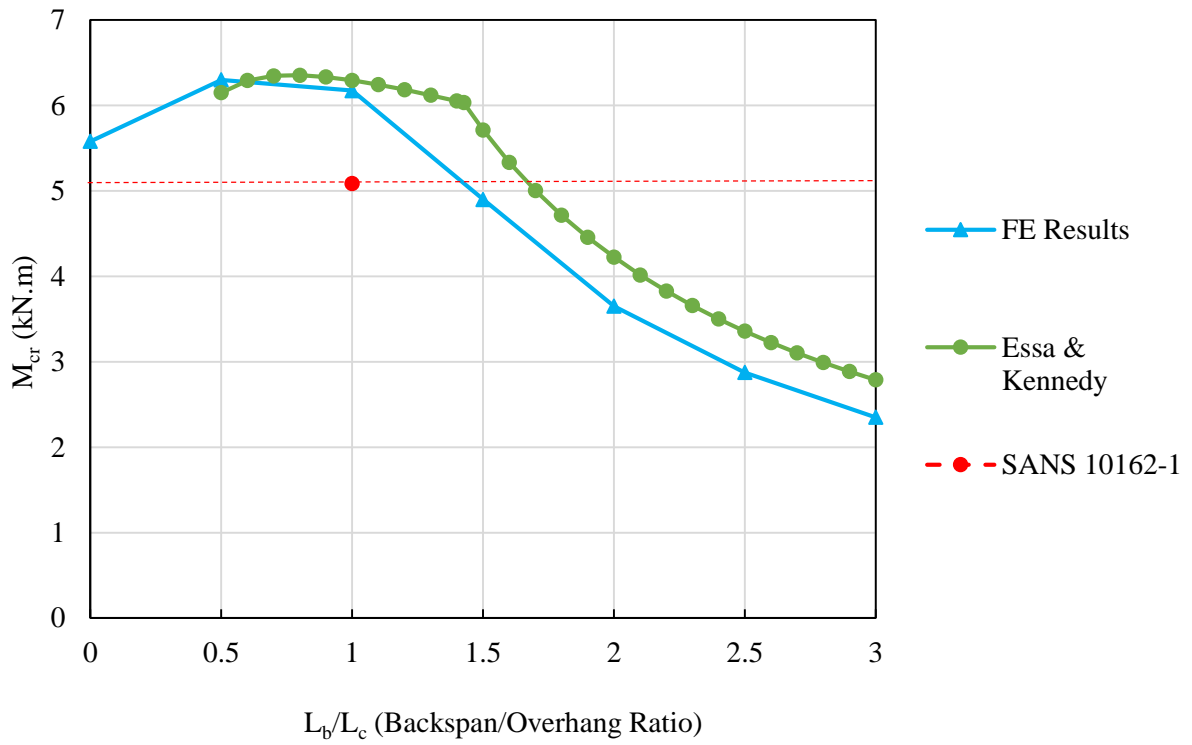
Figure 3.14: IPE$_{AA}$100 with 2.5 m overhang and shear centre loading.
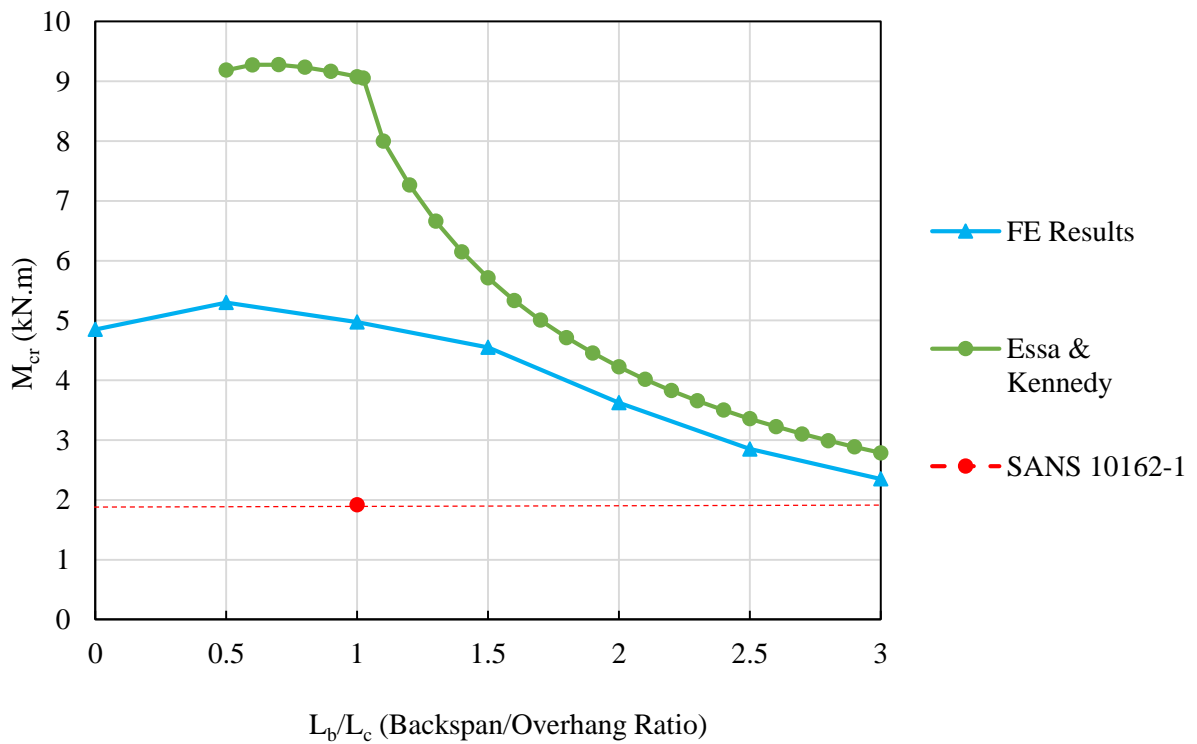
Figure 3.15: IPE$_{AA}$100 with 2.5 m overhang and top flange loading.

3.7   SUMMARY OF OBSERVATIONS

Interaction buckling was defined as the increase in capacity in a critical segment, due to another segment. It was observed that this was not always the case. For a certain range of backspan to overhang length, both segments became, in part, the critical segment. When this occurred, both segments had reduced capacities.

Similar to cantilevers, the effective length factor of overhang beams were dependent on the overhanging segment length L_c. However, it was also dependent on the distance between shear centre and load applied; and the ratio of the backspan to overhang. The buckling capacity of the backspan (when critical) was independent of the distance between the shear centre and height of load applied at the overhanging tip.

Based on the consideration of an $IPE_{AA}100$ beam: With equal backspan to overhang lengths, the SANS 10162-1 was over-conservative when the load was applied at the shear centre or on the top flange. Essa and Kennedy (1994) also showed significant variance in results when compared to FE shell element analyses, even though the same methodology was used in calculating the critical moment, but with differences in assumptions.

If the overhanging segment was the critical segment, the top flange became critical (deflected laterally the most), similar to Bradford (1994). Only the overhanging segment experienced LTB, with the backspan relatively unchanged. When the backspan was the critical segment, the bottom flange in the backspan became critical, while the overhanging segment experienced lateral deflection only (no twist), due to the warping of the backspan at the support.

A new method was formulated to determine the buckling capacity of an overhang beam. Instead of determining which segment was critical, the proposed method took interaction buckling into account in both segments. Hence, a single formula was obtained to determine the effective length factor for the overhang beam. With this factor known, the critical elastic buckling moment could be determined using the length of the overhanging segment.

Note that this chapter provided a technique to refine the determination of the critical moment of overhang beams. This technique was investigated thoroughly in Chapter 6 using calibrated FE solid element models. Therefore, the equations formulated in this chapter served only as a reference for Chapter 6. Additionally, this chapter aided the understanding of LTB of overhang beams necessary for physical experimenting.

4. EXPERIMENTAL SETUP

To test the cantilever and overhang beams, it was first necessary to construct an apparatus capable of supporting, loading and measuring the beams. The instruments that were used were calibrated in advance to ensure accurate and valid measurements. This chapter explains the setup of the experiments.

4.1 CANTILEVER EXPERIMENTAL SETUP

The cantilever beams were built-in beams, meaning that there were only one support and one span. The 'built-in' refers to full fixity of the beam at the support. No translations or rotations were allowed at this specific support. The load was applied at the free end of the beam, the far end of the fixed support. Measurements were taken at the free end, as at this end, the beam deflects and twist. Figure 4.1 is a sketch of a 2.5 m IPE$_{AA}$100 cantilever setup. Detailed discussions on the support and loading were provided in the next two sections.
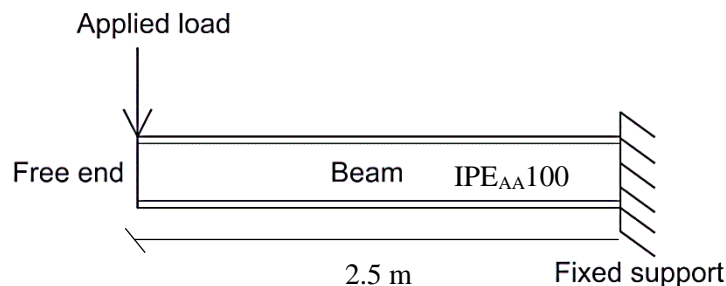
Figure 4.1: Basic sketch of the cantilever setup.

4.2 OVERHANG EXPERIMENTAL SETUP

The setup of the overhang experiments was more complex than the cantilever setup. An overhang beam consists of two supports and two spans. The overhanging segment was the span that consisted of one support, with the load applied at the other end. The backspan segment had supports on either end but had no load applied in the span. The internal support was the support between the overhanging and backspan segments. The internal support was a single roller allowing longitudinal movement of the beam and warping in the flanges. The external support refers to the support on the far end of the backspan segment. The external support comprised of two rollers, above and below the beam. Measurements were taken at the free end of the overhanging segment and midspan of the backspan

segment. Figure 4.2 is a sketch of an IPE$_{AA}$100 overhang beam setup with 2.5 m spans, as explained above. Once again, detailed discussions of the supports and loading to follow in the next two sections.
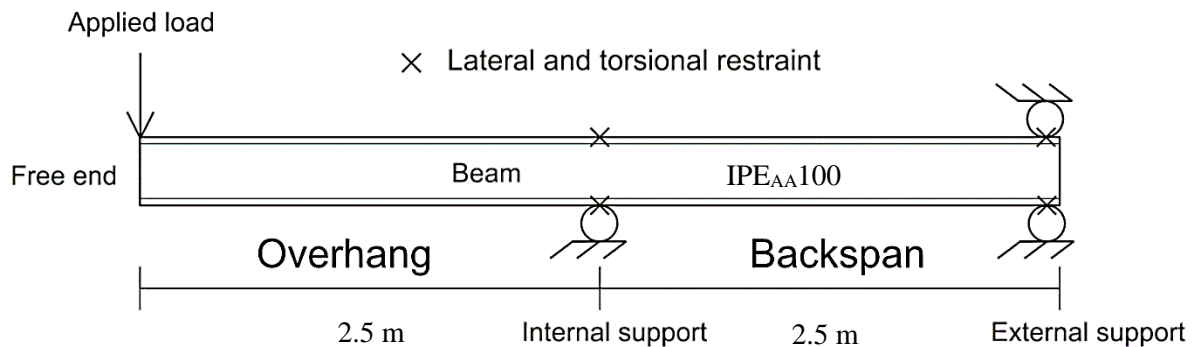
Figure 4.2: Basic sketch of the overhang beam setup.

4.3   SUPPORT CONDITIONS

Two different support conditions were used for the experimental tests: fixed support for the cantilevers and roller supports for the overhang beams.

4.3.1   FIXED SUPPORT FOR CANTILEVER BEAM

The cross-section of the cantilever beam was welded onto a 10 mm thick plate, with the 10 mm plate bolted and welded to a larger 15 mm thick plate. The extra weld prevented the 10 mm plate from prying off the 15 mm plate. The 15 mm plate was welded onto a large steel frame. The frame was then considered as rigid. At the back end of the frame was another 15 mm plate, connected via two channels and welded to the frame. The channels and the 15 mm plates strengthened the fixed support and reduced the risk of movement when loaded. Two M12 nuts were provided for the top two M12 bolts, to prevent shearing of the thread as these two bolts were loaded in tension. All bolts, nuts and threads were Grade 8.8 to allow yielding but withstood the forces applied. Figure 4.3 shows the design of the fixed support. The 15 mm plate was connected to the existing frame.
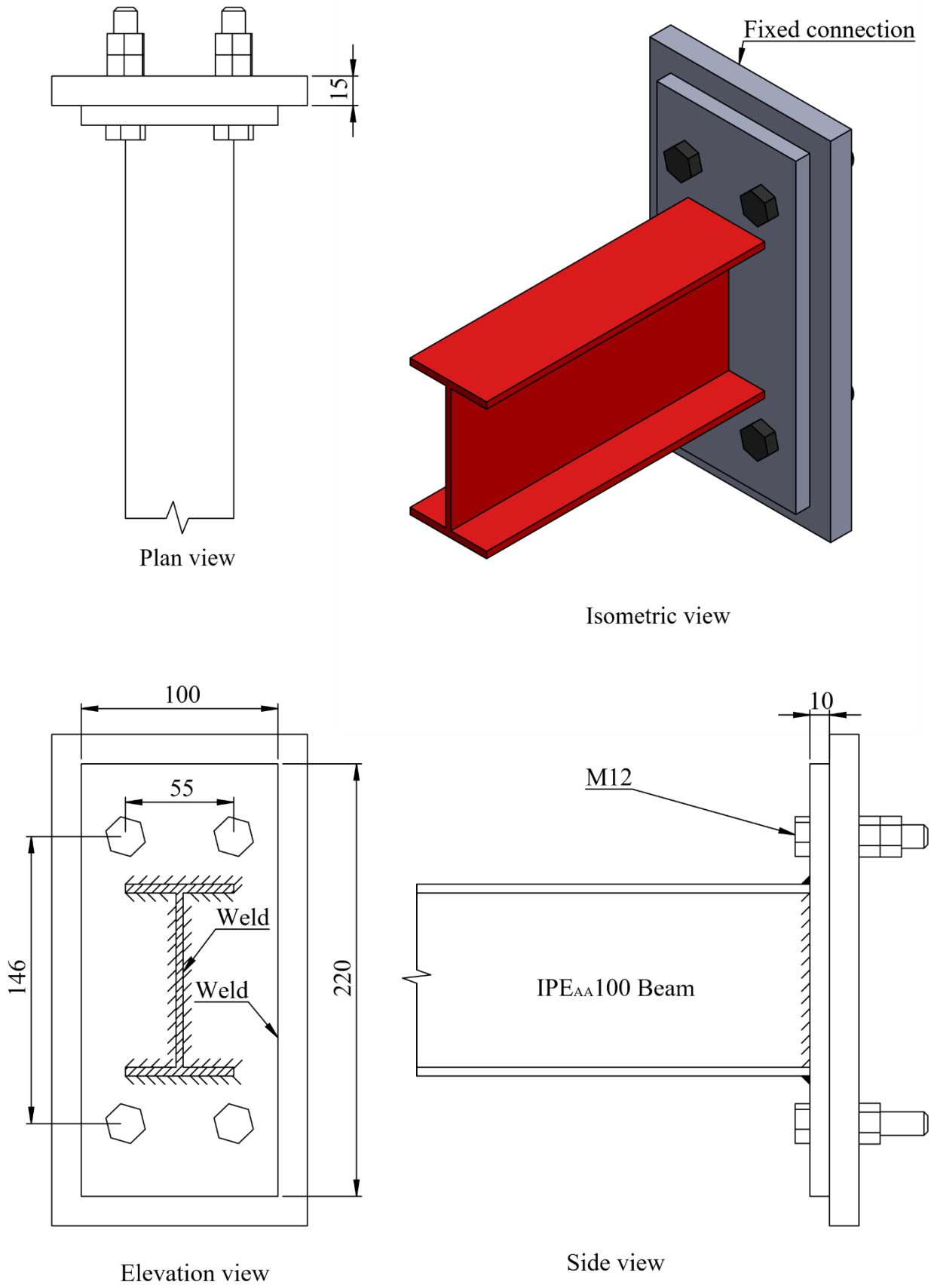
Figure 4.3: Design of fixed support for the cantilever.

4.3.2   OVERHANG BEAM SUPPORTS

The supports for the overhang beams were very different from the cantilever. Also, the internal support was different in design to the external support. Due to the load being applied downwards at the overhanging segment end, the internal support acted as a fulcrum point. Thus the resultant load at the external support was upwards. The external support, therefore, required to resist vertical forces in both directions: downwards during the setup and upwards during loading.

Two movable rollers and a fixed roller were used for the two supports. The internal support had one roller beneath the beam allowing longitudinal movement of the beam. The external support had a movable roller above the beam and a fixed roller beneath the beam. The bottom roller was fixed preventing rigid body motion of the beam in the longitudinal direction. Due to the roller being round and the beam pushing upwards away from the roller, the roller did not prevent warping in the bottom flange. The fixed roller was therefore not a pin support. Thus, warping was allowed in both top and bottom flanges at both supports.

The vertical restraints were adjusted to fit snuggly against the beam providing lateral support and preventing twist at the supports. Adjustable vertical restraints ensured that small errors in beam widths and vertical alignment were compensated. The beams were therefore in its natural shape over the supports, and extra internal stresses were mitigated. The height of the movable roller at the external support was also adjustable accounting for differences in beam heights. Figures 4.4 and 4.5 are the design for the interior and exterior supports, respectively.
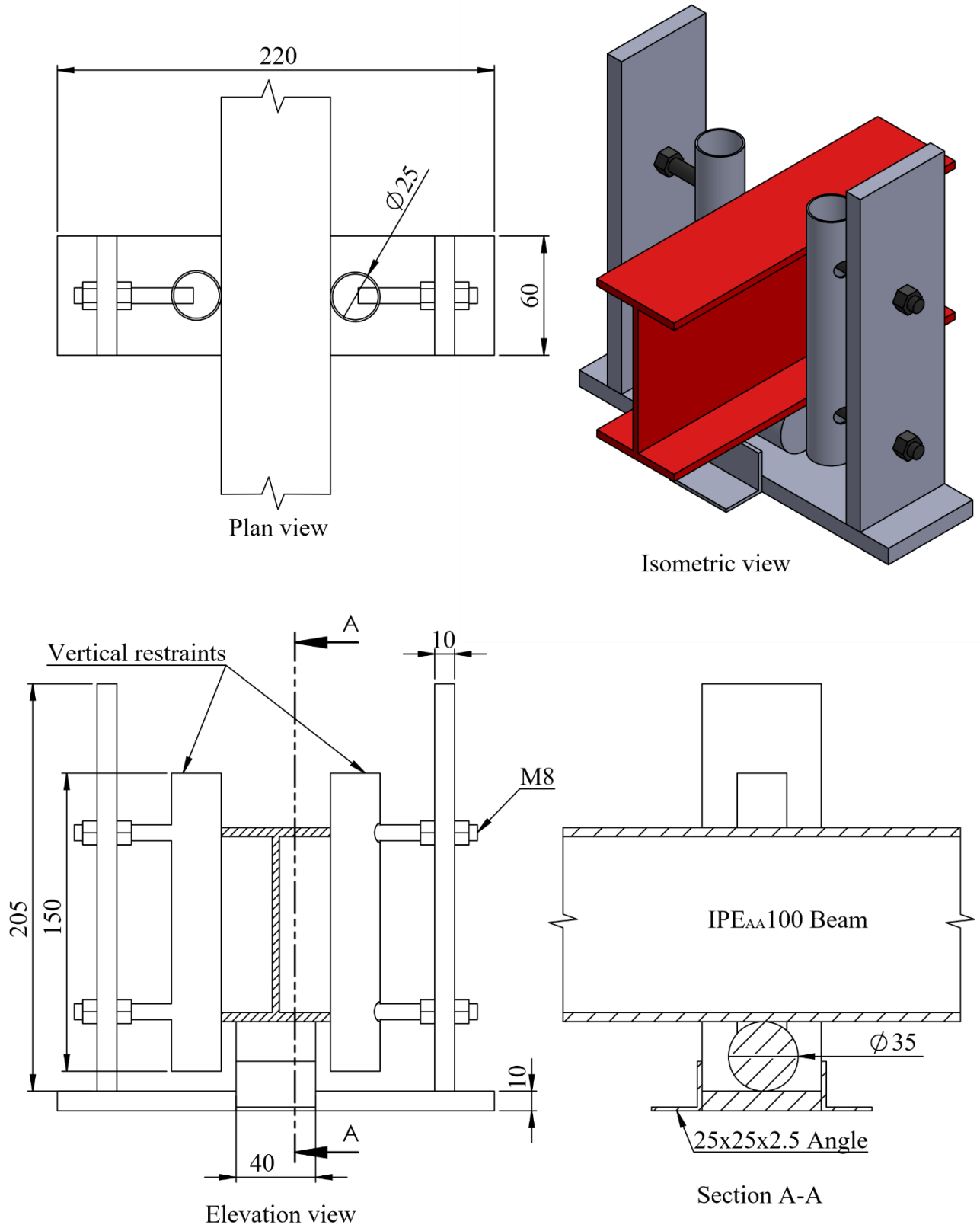
Figure 4.4: Design of internal support for the overhang beam.

180

70

100

M12

Plan view

Isometric view

A

40

10

A

Elevation view

Ø 35

Fixed roller

Section A-A
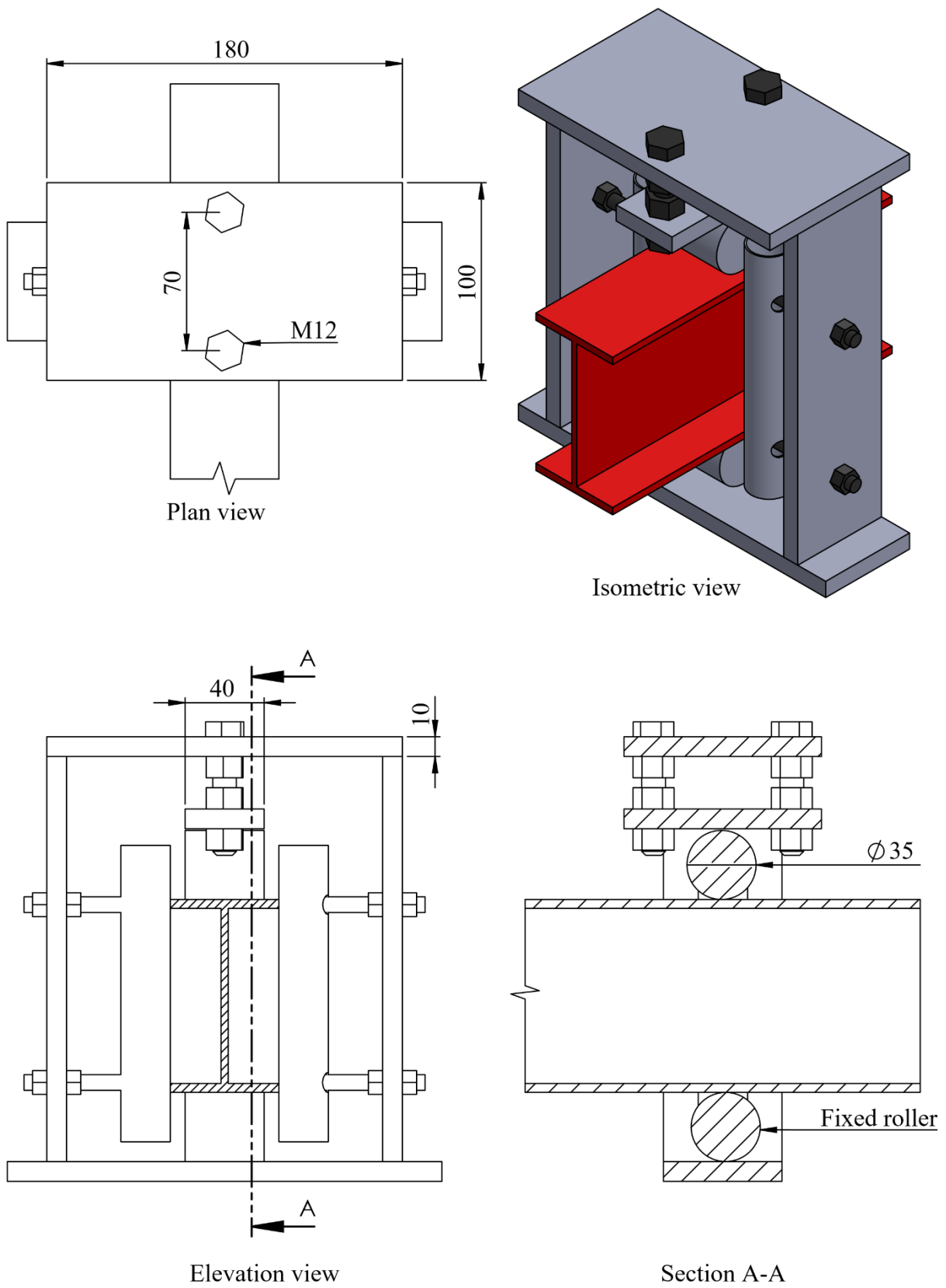
Figure 4.5: Design of external support for the overhang beam.

4.4   LOADING OF BEAMS

The load at the overhanging segment end was applied either at the shear centre or on the top flange. A single, simple design was used for both shear centre and top flange loading, albeit with minor differences. The simple design allowed the process of setting up the test easier, quicker and consistently.

A single Ø14 mm hole was drilled through the web to apply the load at shear centre. The hole was drilled 30 mm from the end of the overhang beam to prevent tearing. In the case of cantilevers, the hole was drilled 2.5 m from the fixed support. The bottom tangent of the hole was on the shear centre line of the beam. An M12 thread was then fitted through the drilled hole and bolted to prevent movement. A 10 mm thick plate was then bolted to either side of the M12 thread. The M12 thread allowed rotation of the 10 mm plates as the beam deflects downwards. Thus the force applied remained vertical. Another M12 thread was attached to the two 10 mm plates below the beam. The load cell was then suspended from the bottom M12 thread via a shackle (Figure 4.6). Two M12 nuts were placed on either side of the shackle allowing some movement and a twist of the shackle but prevented significant horizontal movement. Restricting the horizontal movement of the shackle (and thus the load cell) to about 20 mm ensured that the force applied remained directly below the beam. The entire setup prevented eccentricities about the vertical centre line during loading, thus no artificial twist in the beam.

The top flange loading structure was slightly different, but the mechanics remained the same. Instead of a hole through the web, two Ø10 mm holes were drilled in the top flange, 30 mm from the end of the overhang beam. An upside-down PC 100x50 channel was then fixed to the top flange with two M8 bolts. The two 10 mm plates were then attached to the sides of the channel via M12 bolts. The rest of the setup remained the same as for shear centre loading. The channel ensured that the load was applied $h/2$ above the shear centre, i.e. at the surface of the top flange. Figures 4.7 and 4.8 are the designs for the shear centre and top flange loading setup for an overhang beam, respectively.

Cantilevers were 100 mm longer so that the load applied was not at the very tip of the cantilever. The load was still applied 2.5 m away from the support. To prevent the overhang beams from falling off the frame, the back end of the beam extended 170 mm beyond the rollers. Therefore, taking into account the distance between the tip and the load applied and the part extending over the support, the beams were 200 mm longer. However, the span between supports remained a factor of 2.5 m, and the distance between the load and the internal support remained 2.5 m

Figure 4.6: Shackle to attach load cell to the beam.

140

Plan view

Isometric view

M12 Thread

10

Shear centre

40

30

170

110

Applied load

Elevation view

Side view
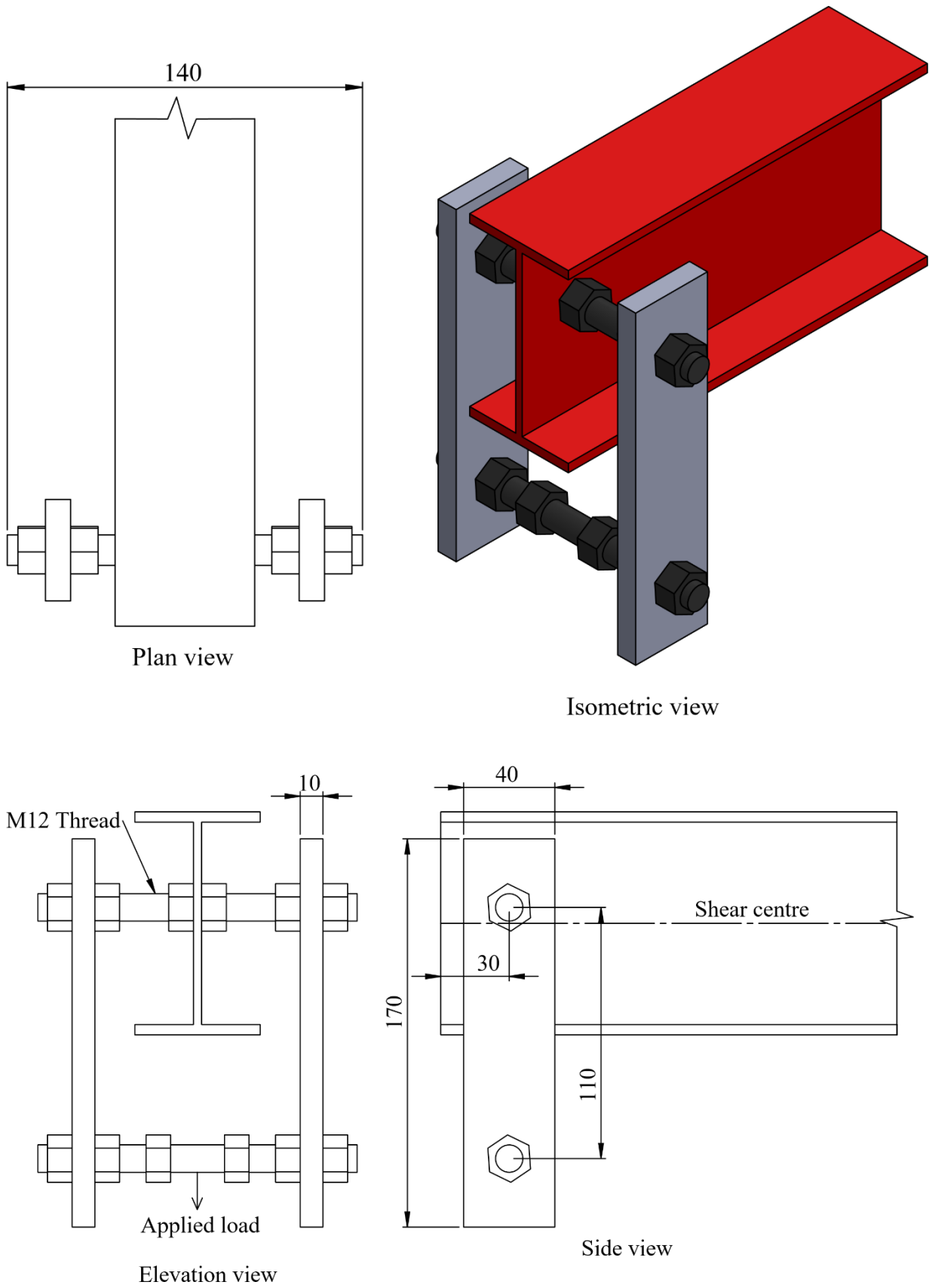
Figure 4.7: Design for shear centre loading.

PC 100x50

Plan view

Isometric view

M8

M12

Applied load

Elevation view

Side view
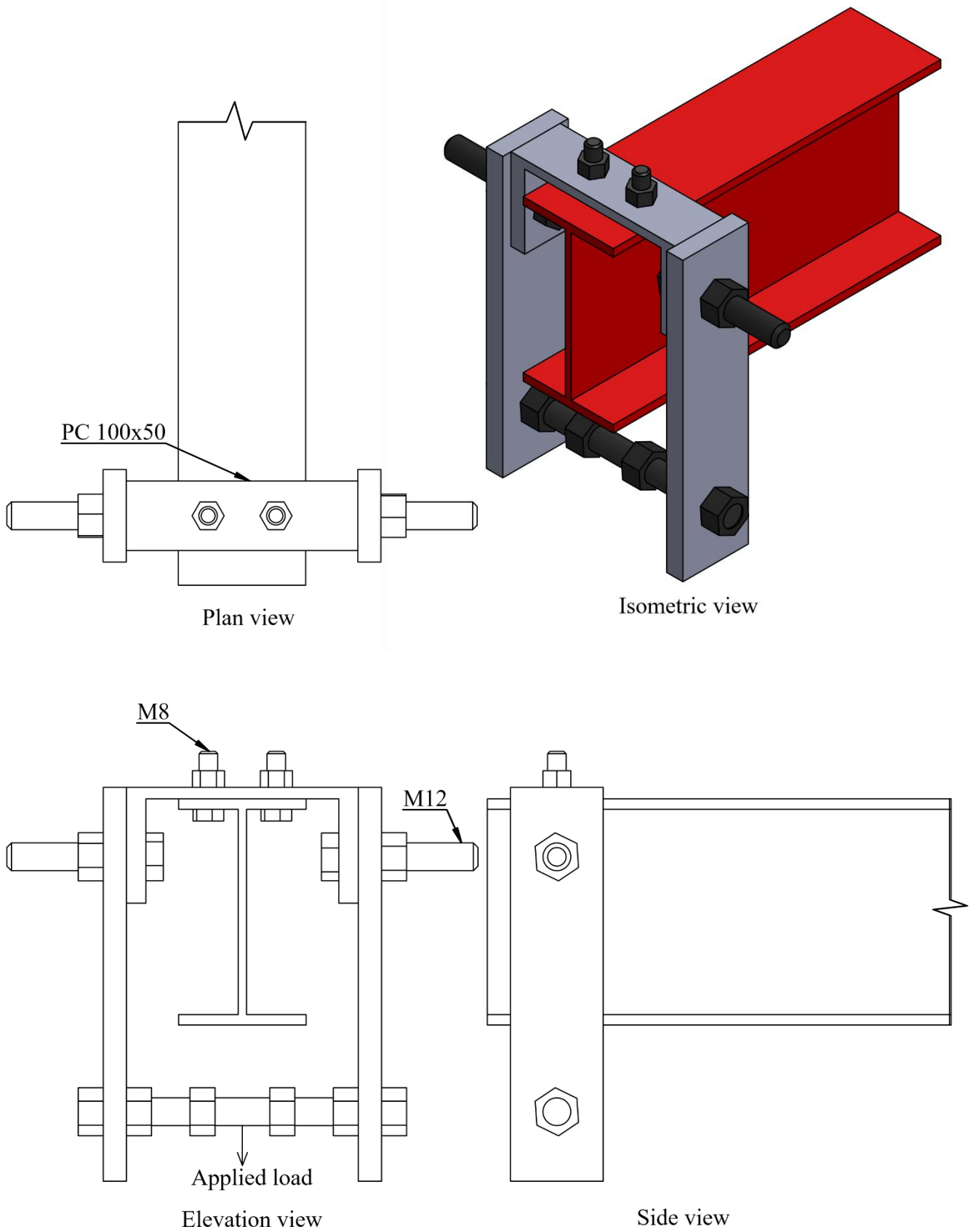
Figure 4.8: Design for top flange loading.

4.5 MEASUREMENTS

4.5.1 STRING LVDTS

String Linear Variable Differential Transformers (String LVDTs) (Figure 4.9) were used to measure beam deflection in the vertical and horizontal direction. Lateral deflection of the beam was measured to assist in the determination of the buckling load. Two String LVDTs were placed horizontally at different heights allowing for computation of the longitudinal twist of the beam. In total, five String LVDTs were used throughout the test programme. Four of the String LVDTs measured the vertical and horizontal deflection (at top flange) of the overhanging segment tip and the midspan of the backspan segment. The last String LVDT measured the lateral deflection of the bottom flange. The location of the String LVDT that measured the lateral deflection of the bottom flange varied depending on the L_b/L_c ratio of the beam. If $L_b/L_c \leq 1.0$ the lateral deflection of the bottom flange was measured at the overhanging segment tip; otherwise, the measurements were taken at the midspan of the backspan segment. The reason for the change in location of the last String LVDT was to allow computation of twist in the segment that twisted the most.

Two different lengths of String LVDTs were used: string range of 250 mm and 1000 mm lengths. Once again, the String LVDTs were interchanged depending on which segment was critical. The changes allowed the longer range String LVDTs to measure the segment that displaced the most, as the displacements could be larger than the range of the shorter, 250 mm String LVDTs. The ends of the strings were attached to hooks that were placed securely on the beam (Figure 4.10). Care was taken to ensure that the string remained parallel with the String LVDT casing. The String LVDT used voltage as its output. The output is discussed in Section 4.6.

Figure 4.9: A String LVDT that is measuring in the horizontal direction.

Figure 4.10: String LVDT end attached to a hook to measure displacement.

4.5.2 LOAD CELL

To measure the load applied at the tip of the overhanging segment, a load cell was used. The load cell was capable of measuring accurately up to 1 tonne. The load cell was connected to shackles allowing for rotation and twist as the beam was loaded. Therefore, the load always acted vertically downwards and thus avoided eccentricities or moments that could affect the beam buckling capacity. The load cell also used voltage as its output.

4.5.3 LOGGING

The five String LVDTs and the load cell were all connected to a graphical logger (Graphtec Model GL220). The graphical logger converted the output voltage from the String LVDTs and the load cell, after calibration, to millimetres and kilogrammes, respectively.   The logger provided immediate feedback via a Graphical User Interface (GUI), as seen in Figure 4.11, while also recording the data to a CSV (text) file format. The logger was also used to calibrate the String LVDTs.

Figure 4.11: Data logger.

4.6   CALIBRATION

Calibration of instruments ensured that the data acquired were accurate, valid and consistent. Upon calibrating the instruments, the output voltage was immediately converted to the respective units. The conversion made it easier to determine the change in load or deflection as the beam was loaded. Also, the recorded data were then already in the correct format, speeding up the data analysis period.

The load cell was calibrated using a Budenberg 3/500 dead-weight system (Figure 4.12). Weights, with increasing load, were added onto a piston, see Figure 4.13, the weights applied pressure onto the Budenberg dead-weight tester.   The pressure obtained was then transferred to the Budenberg dead-weight system onto the load cell. The difference was the area onto which the pressure acted. The readings obtained from the Hottinger Baldwin Messtechnik (Figure 4.14) output display were then compared to the weights added to verify the accuracy and linearity of the load cell. Upon calibration, the load cell was deemed fit for use. Even though the output display was accurate to 100 grammes, the data logger could capture data with an accuracy of 10 grammes.

Figure 4.12: Budenberg dead-weight system to calibrate the load cell.

Figure 4.13: Budenberg dead-weight tester that converts the weights to pressure.

Figure 4.14: Hottinger Baldwin Messtechnik output display.

The String LVDTs were calibrated using the data logger and an absolute 1 m ruler. At 0.0 mm, the voltage should be 0.0 V, but due to wear and tear, the values varied. The same problem occurred when the String LVDTs were fully extended, i.e. either 250 mm or 1000 mm. At the maximum extended range, the voltage should be 10 V. As an example: if the String LVDT was in a perfect working conditions, then at 0.0 mm, the voltage should be 0.0 V; and at 1000 mm, the voltage should be 10 V. Therefore, for every 1 V, the displacement is 100 mm. However, for a used String LVDT, at 0.0 mm, the voltage could be 0.05 V, and at the maximum range, it could be 9.95 V. The maximum range could also be above or below 1000 mm.

To overcome these inaccuracies, the voltage of the String LVDTs were shifted until 0.0 V was measured at 0.0 mm displacement, i.e. the String LVDTs were zeroed. The maximum ranges of the String LVDTs were then measured, along with the associated voltage (not always exactly 10 V). The voltages of the upper range of the String LVDTs were then multiplied by a factor to get to 10 V.

- Firstly; the measured range was divided by 1000 mm (or 250 mm depending on the String LVDT), say X.
- The measured voltage was then divided by the factor X, say Y.
- Finally, the factor required to adjust the voltage to 10 V at 1000 mm (or 250 mm) was then 10 V divided by Y, say Z.

Example, if the maximum range of the String LVDT was 1050 mm with the voltage being 9.8 V, then $X = \frac{1050\,mm}{1000\,mm} = 1.05$, $Y = \frac{9.8\,V}{1.05} = 9.333$ and then finally the factor becomes $Z = \frac{10\,V}{9.333} = 1.071$. Thus, at 1050 mm, the voltage is $9.8\,V \times 1.071 = 10.5\,V$ and at 1000 mm, the voltage is 10 V. Therefore, the String LVDT remained linear at 100 mm/V (or 25 mm/V for the shorter String LVDT).

The ranges of the String LVDTs were programmed into the data logger and the results were immediately displayed in millimetres. Measurements were taken at 0 mm, 5, 10, 15, 25, 35, 50, 75, 100, 150, 200, 250, 300, 400, 500 and 1000 mm and were compared to the data logger output to verify the accuracy and linearity of the String LVDTs. All the String LVDTs were deemed linear and in good working conditions.

4.7 SETUP OF INSTRUMENTS

A requirement of String LVDTs was that the strings should remain parallel to the String LVDT housing. That is to say, if the String LVDT measured the lateral deflection of the beam, the string must remain level during the test. Knowing that the beams buckled and deflected along two axes, merely attaching the String LVDT to something immovable were not the correct technique to follow. Fixing the String LVDT to an immovable object meant that the String LVDT was sensitive to both lateral and vertical beam deflection. Therefore, inaccurate measurements were then taken.

The solution for the horizontal measurements was to allow the String LVDT to move vertically with the beam as the beam deflected. Thus the string remained level. The horizontal measuring String LVDTs were attached to a 35x35x3.5 angle that rested on top of the beam. As the beam deflected vertically, the angle and thus the String LVDTs moved vertically with the beam.

To measure the vertical deflection accurately, the String LVDT was fixed to a frame that was independent of the beam. However, the string was not attached to the beam, but to the 35x35x3.5 angle that rested on top of the beam. Horizontal movement of the 35x35x3.5 angle was prevented using a vertical shaft and bush. The bush allowed the shaft, which was attached to the steel angle, to move vertically only. A smooth shaft and bush were used to reduce friction, allowing the steel angle to move vertically under its weight and without any disruptions.

A 'rocker' was attached on top of the beam, below the 35x35x3.5 angle. The steel angle, therefore, rested on top of the rocker, which was fixed to the beam. The purpose of the rocker was to reduce the measurement of the vertical component of twist of the beam. The shape of the rocker was designed such that regardless of the twist of the beam, the steel angle remained $h/2$ above the shear centre. Care was taken to ensure that friction was reduced as much as possible between the rocker and the steel angle, allowing the beam to deflect horizontally without interference. The beam could deflect laterally and twist without affecting the height of the steel angle.

The design of the frame holding the String LVDTs at midspan of the backspan segment is shown in Figure 4.15. The frame holding the String LVDTs at the tip of the overhanging segment was the same design, except that the frame was 2000 mm wide and not 750 mm, to provide space for the water tank that fitted between the frame supports. Similarly, the steel angle holding the String LVDTs was 1500 mm wide at the overhanging segment and not 650 mm, as these String LVDTs had a range of 1000 mm. The vertical String LVDT at the backspan segment was fully extended before the test, as the beam deflected upwards. The horizontal String LVDTs were extended halfway (125 mm) as the beam could deflect in either direction. At the overhanging segment, the vertical String LVDT was at 0 mm before the test, and the horizontal String LVDTs was extended halfway (500 mm).

Elevation view

250 mm String LVDT

String

250 mm String LVDT

Hook

Rocker

750

650

Plan view

35x35x3.5 Angle

Side view

Ø 25

Shaft

Bush

Isometric view
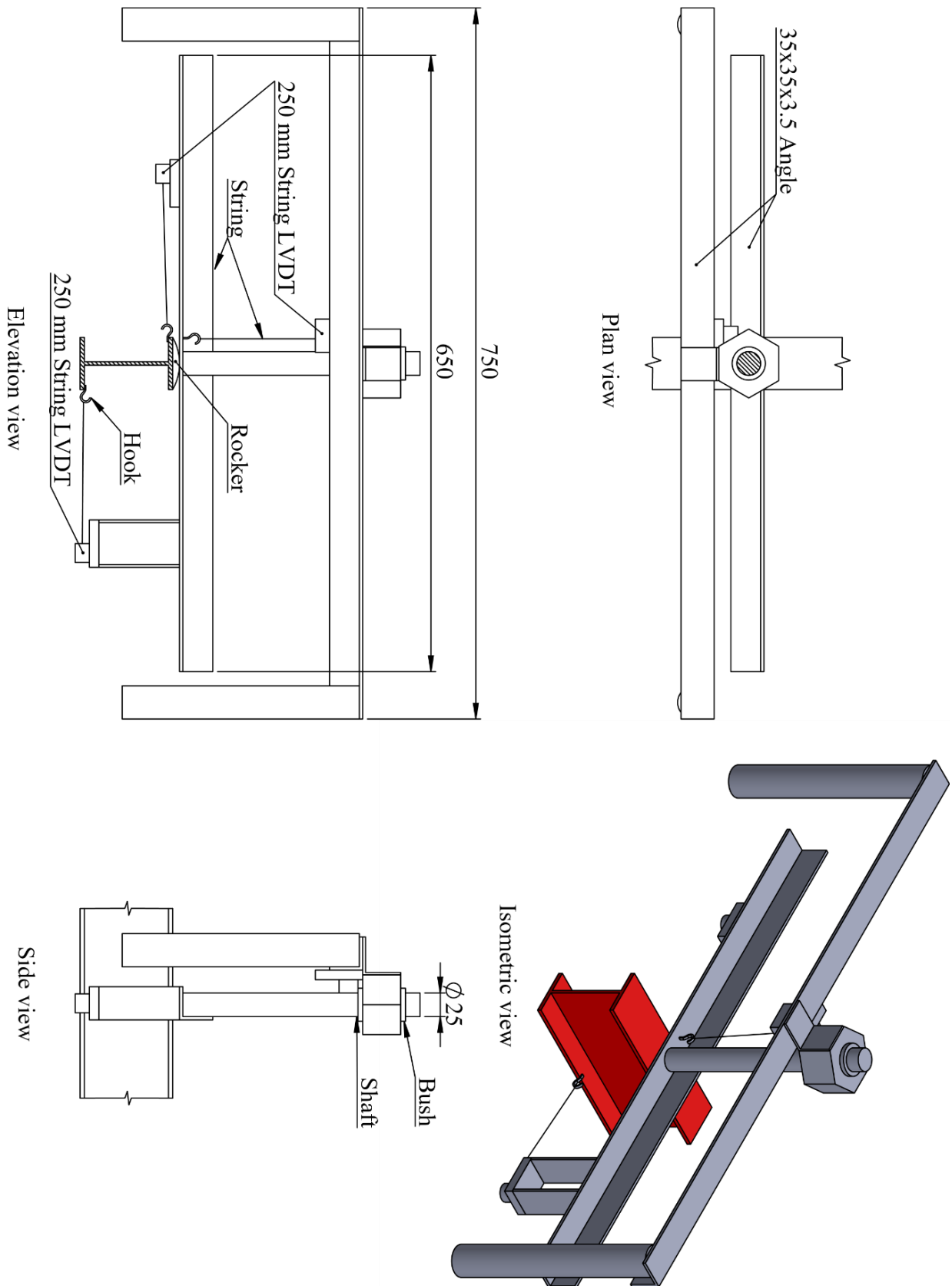
Figure 4.15: Design of instrument setup for the backspan segment.

4.8   BEAM DIMENSIONS AND PROPERTIES

Before the commencement of the testing programme, the following dimensions were measured for all 24 beams and compared to the nominal dimensions: thickness of the web and flanges, the width of the flanges, height of the beam and the length of the beam.

4.8.1   WEB THICKNESS

The web thickness is a beam parameter that might have a noticeable influence on the buckling capacity of a certain beam. Where possible, the web thicknesses at both ends of the beam were measured and were tabulated in Table 4.1 (which can be viewed at the end of this chapter). Difficulty in measuring the web thickness at an end arose when the beams were not properly cut, resulting in metal obstructing the Vernier calliper to measure at that point. The average web thicknesses of both ends for all 24 beams were 3.58 mm. The average was only 0.02 mm smaller than the nominal thickness specified by SASCH (2013). The thinnest web was 0.1 mm smaller than the specified 3.6 mm and the thickest 0.3 mm larger. Therefore, this particular beam dimension was consistent and accurate.

4.8.2   FLANGE THICKNESS

The flange thickness referred to both the top and bottom flange. The flange thicknesses were measured at the front end of the beam, at midspan (of the full length of the beam) and the back end and were tabulated in Table 4.2. The measurements were taken approximately 100 mm from each end to avoid beam deformations due to the fabrication process. The average top and bottom flange thicknesses were 4.55 mm and 4.57 mm, respectively. The top flange was 0.05 mm thicker than specified and the bottom flange 0.07 mm thicker. The thinnest flange was 0.4 mm smaller and the thickest 0.8 mm larger than the specified 4.5 mm.

4.8.3   FLANGE WIDTH

Once again, the flange width referred to both top and bottom flanges. The average top and bottom flange widths were 54.95 mm and 54.72 mm, respectively. The specified width was 55 mm. The narrowest flange was 2.3 mm smaller and the widest 1.9 mm larger. The measurements are presented in Table 4.3.

4.8.4   BEAM HEIGHT

The heights of the beams were grouped in Table 4.4. The beam height was the only beam dimension that differed from the specified value of 97.6 mm. The average beam height was 99.24 mm. The smallest beam was 0.1 mm larger than the specified value and the largest 3.7 mm larger. All of the beams were thus taller than the nominal beam. The difference in height should not affect the beams subjected to top flange loading, as the distance between the load and shear centre had increased on average by only 0.75 mm.

4.8.5   BEAM LENGTH

Most of the 24 beams were within 15 mm of the lengths specified (Table 4.5). Due to a small typo, the beam lengths for the case of $L_b/L_c = 1.5$ were 200 mm shorter. To overcome this deficit, the ratio L_b/L_c was reduced to 1.45, without influencing the buckling capacity considerably. The four beams for this case should therefore have slightly larger buckling capacity.

4.9   IMPERFECTIONS IN BEAMS

An observation regarding the widths of the flanges was that the top flange did not always coincide with the bottom flange. Either the top flange was not the same width as the bottom flange or the centroid of the top flange was not directly above the centroid of the bottom flange; see Figure 4.16. The beams were therefore not perfectly symmetrical about the vertical or horizontal axes. These types of imperfection were not measured, and its effect on buckling capacity was outside the scope of the study. However, these imperfections could be a contributing factor regarding the difference between experimental tests and FE analyses. Most of the beams had flanges that were slightly tapered. The slightest taper dramatically increases the torsional stiffness of the beam. The increase in width of the flange at the web was on average 1 mm.
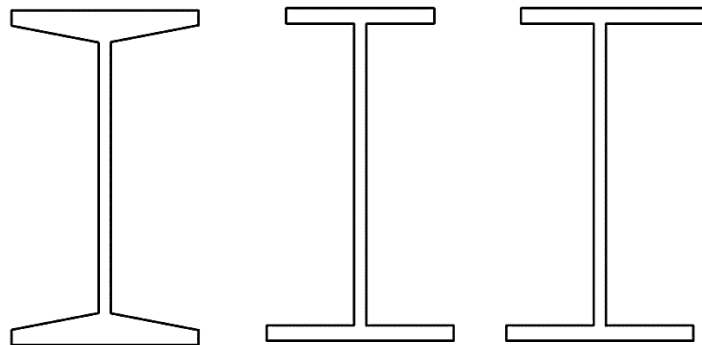
Figure 4.16: Possible imperfections in cross-section of an I-beam.

An imperfection that was measured and its effects on buckling capacity discussed was the curvature of the beam (the difference between the working line and the theoretical centre line, see Figure 4.17). The two ends of the beam were situated on a straight line, the largest offset along the beam between the beam and the theoretical centre line was then measured. These imperfections were not measured for the first five test. For the longest beams, measuring the curvature became impractical, as the beam was slender and bent laterally with ease, thus not possible to the find the original longitudinal profile of the beam. The curvature of the beams ranged from 3 mm to 21 mm.

Perfectly straight beam
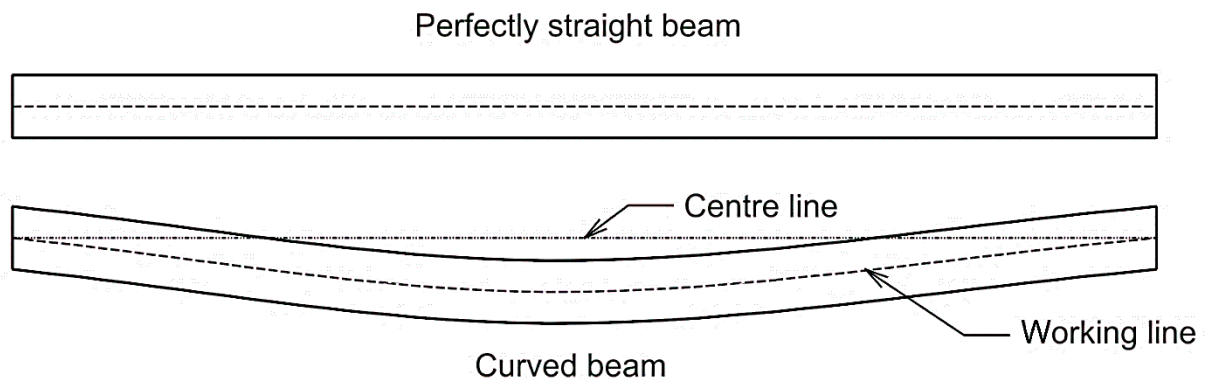
Figure 4.17: Curvature of a beam (top view).

Another imperfection noted in some beams was the skewness of the cross-section of a beam: the two flanges not being parallel or the web not being vertical, see Figure 4.18. Once again, these imperfections were outside the scope of the study. The initial twist in the beam could cause the beam to buckle gradually as the beam was loaded.
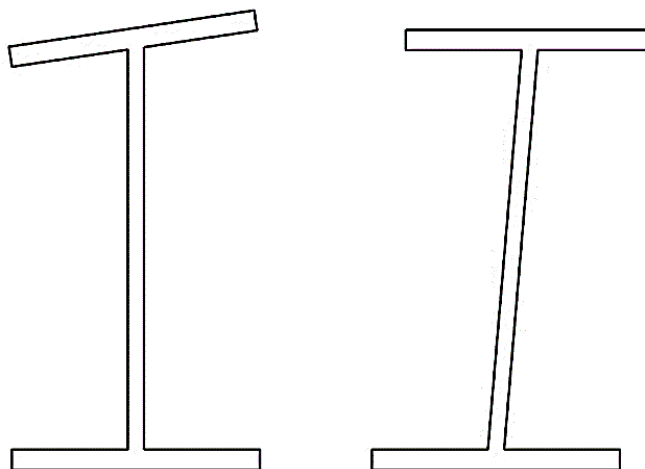
Figure 4.18: Possible skewness of flanges in an I-beam.

4.10   TESTING PROCEDURE

The following section describes the procedure that was used throughout the experimental tests firstly for cantilevers followed by overhang beams.

First, the cantilever, which was welded to a 10 mm thick plate, was bolted to the 15 mm plate that was attached to the frame. After the cantilever had been bolted into place, the 10 mm plate was then welded to the 15 mm plate. The apparatus, which the load hanged from, was then connected to the beam (Figures 4.19 and 4.20). The frame supporting the String LVDTs was placed into position such that the shaft and bush were directly above the rocker. The strings of the String LVDT were connected to the hooks on the beam, and the load cell was shackled to the M12 thread. For every test, a load smaller than 10 kg was applied to the beam, to check if all the instruments were working. After the verification process, the instruments started recording every 250 ms. A drum weighing 35 kg was attached to the bottom shackle of the load cell to load the cantilever. The drum was used to hold weights ranging from 1 kg to 20 kg. The weights were added until the load applied to the beam was close to the predicted buckling load; afterwards, water was added to the drum until the beam had buckled. During loading, a video was taken to record the process of buckling for verification when analysing the results. Photos were also taken after the beam had buckled. The beam was then unloaded and removed and the process was repeated.

For the overhang beams, upon placing the beam on the frames, the vertical restraints were tightened to fit snugly against the sides of the top and bottom flanges. The top roller at the backspan was then added and tightened to fit snuggly against the top flange (Figure 4.21). The roller was still able to roll and allowed warping at the support. Both frames holding the String LVDTs were then placed in the correct position, and the strings were connected to the hooks on the beam. The rest of the procedures were the same as for the cantilever. Except, a 1000 ℓ water tank was attached to the load cell (which on its own weighed 80 kg) to load the beam. Water was then fed to the tank until the beam had buckled. The water tank allowed the load to be applied to the beam gradually and uniformly. Figure 4.22 is the final setup of an overhang beam.

Figure 4.19: Cantilever with shear centre loading (side view).

Figure 4.20: Cantilever with shear centre loading (view from the front end).

Figure 4.21: Exterior support on top of the existing frame.

Figure 4.22: Overhang beam with equal backspan and overhang length.

4.11   BEAM DIMENSIONS DATA

The 24 beams were divided into six groups, each with a unique short label. The label ensured easy identification of each beam and took up less space in the report. The first digit referred to the L_b/L_c ratio of the beam. Cantilevers were denoted by 1, whereas 2, 3, 4, 5 and 6 referred to overhang beams with $L_b/L_c = 0.5$, 1, 1.5, 2 and 2.5, respectively. 'S' was the notation used to indicate shear centre loading and 'T' for top flange loading. The second number was to distinguish which beam was tested first, as each test was duplicated. The unique label was used for the rest of the report. The measured dimensions of the beams are tabulated in Tables 4.1, 4.2, 4.3, 4.4 and 4.5.

Table 4.1: Web thicknesses at the front and back end of the beam (mm).

Cantilever		
Test no.	**Front**	**Back**
1S1		3.6
1S2	3.8	
1T1		3.5
1T2	3.5	3.6
Overhang		
2S1	3.5	3.5
2S2	3.5	3.5
2T1	3.4	3.6
2T2	3.8	3.8
3S1	3.5	3.7
3S2	3.4	3.6
3T1	3.5	3.8
3T2	3.5	3.6
4S1	3.6	3.6
4S2	3.5	3.6
4T1	3.5	3.7
4T2	3.5	3.6
5S1	3.4	3.5
5S2	3.5	3.9
5T1	3.4	3.7
5T2	3.5	3.7

Test no.	Top	Bottom
6S1	3.6	3.7
6S2	3.6	3.7
6T1	3.5	3.6
6T2	3.6	3.6

Table 4.2: Flange thicknesses at the front, middle and back end of the beam (mm).

Cantilever						
Test no.	Top flange			Bottom flange		
	Front	Middle	Back	Front	Middle	Back
1S1	4.5	4.5	4.5	4.5	4.5	4.4
1S2	4.6	4.6	4.6	4.6	4.6	4.5
1T1	4.5	4.5	4.5	4.4	4.4	4.5
1T2	4.6	4.5	4.6	4.6	4.5	4.3
Overhang						
2S1	4.4	4.5	4.5	5	5.1	4.9
2S2	4.5	4.4	4.6	5	5.3	4.8
2T1	4.5	4.5	4.5	4.5	4.5	4.5
2T2	4.5	4.5	4.4	4.6	4.5	4.4
3S1	4.6	5.1	4.9	4.3	4.4	4.7
3S2	4.2	4.1	4.2	4.8	4.6	4.8
3T1	4.5	4.9	4.7	4.5	4.6	4.4
3T2	4.5	4.8	4.6	4.6	4.7	4.7
4S1	4.6	4.7	4.7	4.6	4.7	4.6
4S2	4.4	4.6	4.3	4.3	4.6	4.5
4T1	4.6	4.4	4.6	4.7	4.6	4.6
4T2	4.5	4.4	4.3	4.3	4.6	4.4
5S1	4.6	4.6	4.4	4.8	4.6	4.8
5S2	4.7	4.5	4.7	4.5	4.8	4.8
5T1	4.7	4.7	4.8	4.4	4.3	4.4
5T2	4.7	4.7	4.7	4.5	4.6	4.5
6S1	4.5	4.3	4.3	4.7	4.3	4.3
6S2	4.4	4.6	4.6	4.4	4.4	4.6
6T1	4.6	4.5	4.4	4.7	4.6	4.3
6T2	4.6	4.5	4.7	4.3	4.6	4.6

Table 4.3: Flange widths at the front, middle and back end of the beam (mm).

Cantilever						
Test no.	**Top flange**			**Bottom flange**		
	Front	**Middle**	**Back**	**Front**	**Middle**	**Back**
1S1	55.1	55.1	55	55.4	55.2	55.6
1S2	54.9	54.9	54.9	55	55.1	54.9
1T1	55	55.1	54.9	55.3	55.4	55.2
1T2	56	55.6	55.2	54.6	54.7	55
Overhang						
2S1	56.6	56.3	56.3	53.2	53.4	53.4
2S2	54.6	54.1	54.4	53.1	53.2	53.2
2T1	55	55.3	55.3	55.9	55.4	55.4
2T2	55.7	54.7	54.5	53.8	54.7	55.2
3S1	53.5	53.4	54	55.6	55.7	55.8
3S2	55.6	54.8	54.8	52.9	52.7	53.3
3T1	55.2	54.7	54.3	55	54.9	55.7
3T2	54.5	55.2	55.4	55.7	54.6	54.7
4S1	55.1	55	55.8	55.1	54.3	54.8
4S2	55	54.4	54.3	55	55	55.2
4T1	55.3	55.5	55.6	54.7	54.8	54.9
4T2	54.9	54.3	54	55.2	55.2	55.7
5S1	55	54.6	55.1	52.8	53	53.3
5S2	55.7	55.4	55.7	54.8	54.5	55.1
5T1	53.7	53.9	53.6	56.3	56	56.1
5T2	55	54.4	55	55.5	55.7	55.7
6S1	56	55.6	55.5	55.3	55.1	55.4
6S2	54.6	54.3	54.9	55.1	55.5	54.5
6T1	56.9	56.3	56.5	53.2	53.6	53.1
6T2	53.1	53	53.7	54.1	54.2	54.1

Table 4.4: Beam heights at front, middle and back end of the beam (mm).

Cantilever			
Test no.	**Front**	**Middle**	**Back**
1S1	99.2	98.8	99.4
1S2	99.2	99.4	99.2
1T1	98.9	98.6	98.8
1T2	99.3	98.9	99.1
Overhang			
2S1	100.9	101	101
2S2	98.9	98.5	98.5
2T1	100.2	100.4	100
2T2	98.7	99	99
3S1	100.4	100.4	100.6
3S2	98.9	98.5	98.2
3T1	98.4	99	99
3T2	99.3	99.1	99.1
4S1	99.4	99.3	99.7
4S2	98.4	98.7	98.9
4T1	99.1	99	98.9
4T2	98.5	98.7	99.4
5S1	100.3	101.3	100.1
5S2	99.1	98.7	99.2
5T1	99.3	98.4	99.6
5T2	99	99.1	99.4
6S1	99.1	99.8	99.3
6S2	99.5	100	99.4
6T1	97.7	98.3	98.2
6T2	98.9	98.9	98.9

Table 4.5: Beam lengths and curvature of beams.

Cantilever			
Test no.	**Length (mm)**	**Curvature (mm)**	**Deflection per length (mm/m)**
1S1	2630		
1S2	2600		
1T1	2593	-	
1T2	2593		
Overhang			
2S1	3957	-	-
2S2	3959	6	1.52
2T1	3959	15	3.79
2T2	3955	6	1.52
3S1	5210	-13	2.5
3S2	5210	-8	1.54
3T1	5209	-11	2.11
3T2	5210	5	0.96
4S1	6255	21	3.36
4S2	6255	-15	2.4
4T1	6261	-4	0.64
4T2	6266	4	0.64
5S1	7707	-11	1.43
5S2	7708	-4	0.52
5T1	7713	-12	1.56
5T2	7708	-3	0.39
6S1	8960	-20	2.23
6S2	8962	-	-
6T1	8956	-19	2.12
6T2	8955	-	-

5. ANALYSIS OF RESULTS

5.1   INTRODUCTION

The analyses of the experiments conducted are grouped into various sections:

- The procedure and results of the tensile tests performed on the samples that were cut from the web of the steel were discussed.
- Analyses of the tests conducted, where buckling loads, deflection and twist were examined and compared to initial FE analyses.
- Finally, conclusions based on the results throughout this chapter were provided.

During testing, six variables were measured for each beam: the load applied at the tip of the beam (P), the vertical deflection, lateral deflection and twist of the overhanging segment (δ_{V_C}, δ_{L_C} and ϕ_C) and the backspan segment (δ_{V_B}, δ_{L_B} and ϕ_B). The initial position of the beam before the water tank was attached to the beam was taken as the reference point for the measurements. Figure 5.1 illustrates the measurements for the cantilevered (overhanging) segment.   The backspan was similar, with measurements taken at midspan of the segment.
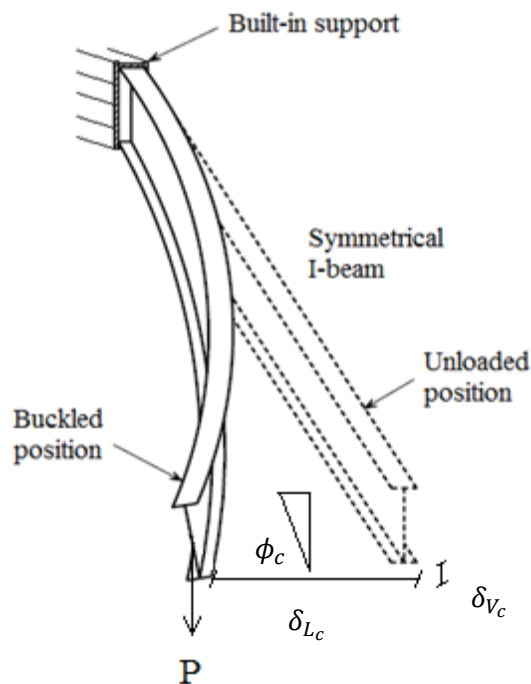

Figure 5.1: Measurements for cantilevered segment.

5.2   BEAM MATERIAL PROPERTIES

The Young's modulus of the steel beams was determined by conducting tensile tests. In total, nine samples known as 'dog bones' were cut from the steel beams (Figure 5.2). The cut-outs were performed using water-jet technique to avoid changing any material properties of the samples. The web sections of the I-beams were used as the sampling material. These samples were not loaded previously.

The samples were measured using a Vernier calliper (Table 5.1) and tested using a SANS universal testing machine (Figure 5.3). The elongation of the samples during testing was measured using a 50 mm clip gauge (Figure 5.4). The rate of loading was 800 N/s until the sample had fractured, thus loaded beyond the elastic range. Figure 5.5 is a graph comparing the stress vs. strain for all the samples. From the data acquired, the yield stress, ultimate stress and Young's modulus were determined. On average of the nine samples, the lower yield strength f_{y_l} was calculated as 362.8 MPa, the upper yield strength $f_{y_u} = 377.8$ MPa, the ultimate strength $f_u = 480.8$ MPa and Young's modulus was calculated as 204.3 GPa. Figure 5.6 shows graphically that all the samples had a slight drop in strength as the sample yielded, therefore according to the ISO 6892-1 (2009) standard, both the upper and lower yield strength was required. For FE analysis purposes, the lower yielding strength was used to obtain conservative results. The Young's modulus was calculated using the slope between 50 MPa and 300 MPa; all nine samples elongated linearly over this range.
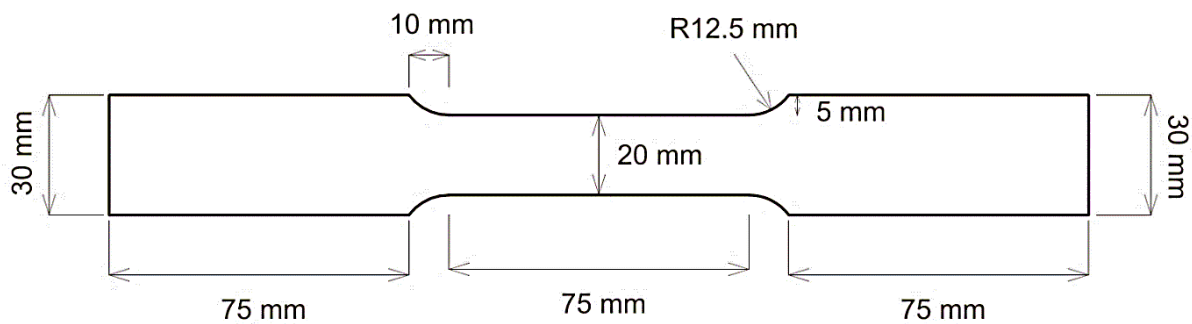

Figure 5.2: Dimensions of a 'dog bone' sample.

Table 5.1: Measured dimensions and strength of samples.

Sample no.	Width (mm)	Thickness (mm)	Lower yield (MPa)	Upper yield (MPa)	Ultimate strength (MPa)	Young's Modulus (GPa)
1	20.19	3.26	340.8	362.0	461.3	214.6
2	20.3	3.28	363.9	369.0	482.3	198.5
3	20.24	3.25	348.9	368.3	487.1	184.0
4	20.38	3.27	368.2	378.1	479.8	188.9
5	20.32	3.29	364.6	382.0	480.7	218.3
6	20.49	3.25	368.3	392.7	484.2	201.7
7	20.42	3.28	366.9	385.9	480.1	208.8
8	20.24	3.24	375.3	385.5	485.7	214.7
9	20.35	3.24	367.8	376.6	487.2	209.6
Average			362.8	377.8	480.8	204.3

Figure 5.3: SANS universal testing machine.

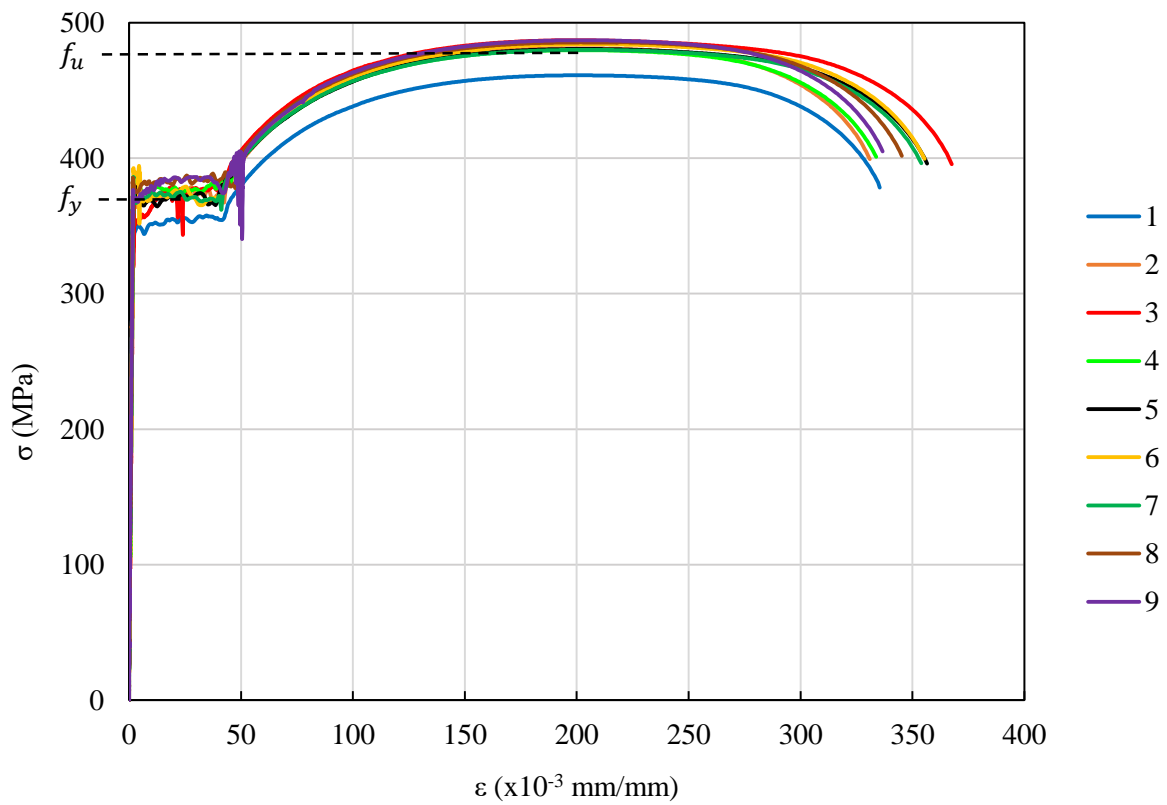**Figure 5.4: Position of clip gauge before testing.**

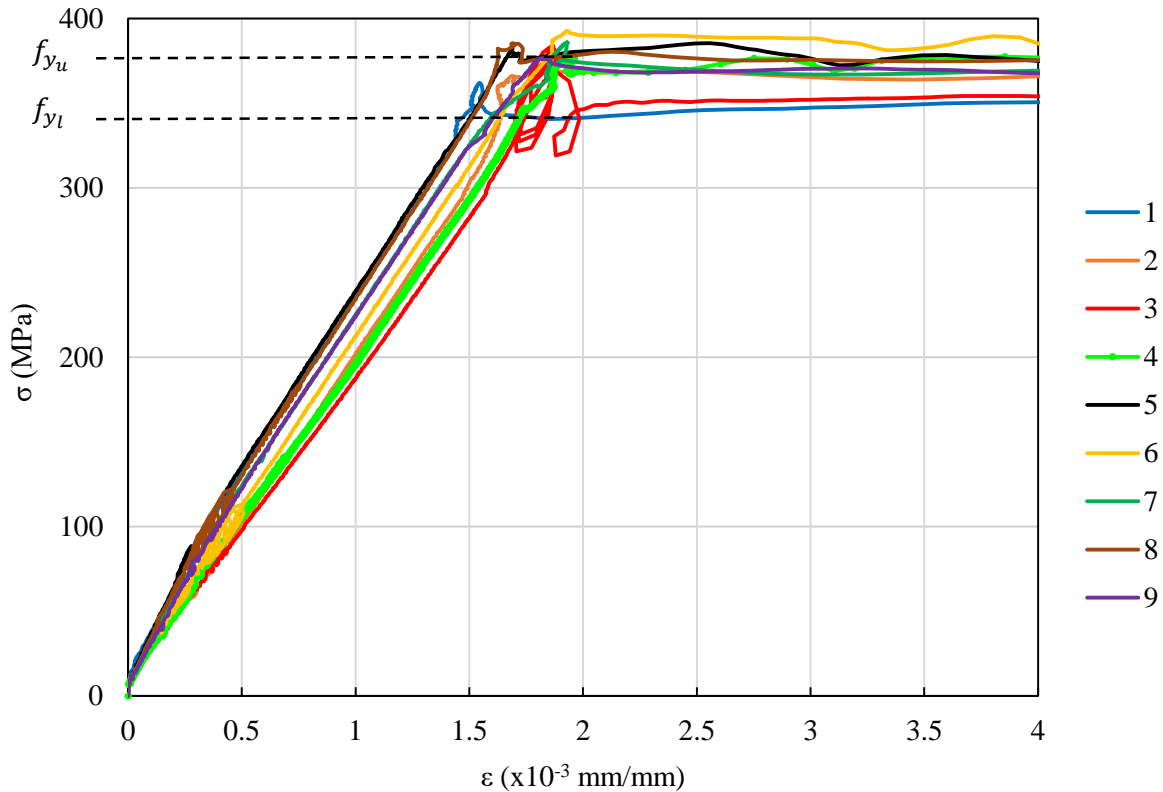**Figure 5.5: Stress vs. strain for all the samples.**

Figure 5.6: Elastic range and yield of all samples.

5.3   LATERAL-TORSIONAL BUCKLING TESTS

5.3.1   EXTENT OF BEAM DEFLECTION AFTER BUCKLING

The height of the water tank above the ground was a factor that influenced the amount of load that could be applied to the beam and the extent of the deflection or twist of the beam. The height of the water tank, i.e. the clearance between the water tank and the ground, determined the extent of buckling. Larger clearance resulted in larger available space for the beam to deflect. With larger vertical deflection, larger lateral deflection and twist were possible as well. Therefore, the deflection up to the point of buckling was of interest, because it was not dictated by the height of the water tank (as long as the beam had buckled).

If the clearance was too small, the water tank grounded before the beam had buckled. If the clearance were too large, the beam displaced beyond the working range of the String LVDTs. It was, therefore, essential to place the water tank at the correct height to ensure buckling of the beam without excessive beam deformation.

The first overhang beam test, with $L_b/L_c = 0.5$ (test 2S1) the water tank had a clearance of approximately 120 mm. At the time, it seemed that the beam had not buckled before the water tank touched the ground (later justified that the beam had not buckled). Hence, the data for test 2S1 were not used in the analyses of results. For the subsequent tests, the water tank had a clearance between 150 mm and 230 mm. Afterwards, all the beams buckled before the water tank had touched the ground.

5.3.2   BUCKLING LOADS

The critical buckling load P_{cr} was determined by plotting the applied load to the lateral deflection of the flanges δ_{L_C}. The point of buckling coincided with the maximum load that was applied. At the buckling point, the change in lateral deflection was still small (pre-buckling). After the critical buckling load was reached, the change in lateral deflection became large (post buckling) and the load resisted reduced.

Figure 5.7 illustrates how the critical buckling load P_{cr} can be determined from a load vs. lateral deflection graph. Figure 5.7 is based on the lateral deflection of the top flange at the overhanging segment. The critical buckling load P_{cr} can be determined in a similar method using the lateral deflection of the bottom flange or the backspan segment. To clarify, the lateral and vertical deflection continued after the beam had buckled, depending on the height of the water tank, but this had no relevance for this study. Therefore, for this chapter, only deflections and twist up to the critical buckling load were used. Noise was generated below 700 N for each experiment, as the chains in the water tank were still slacked while the water tank was attached. Upon attaching the water tank, the water tank was allowed to settle in and the cables stiffening to reduce noise when adding additional load.
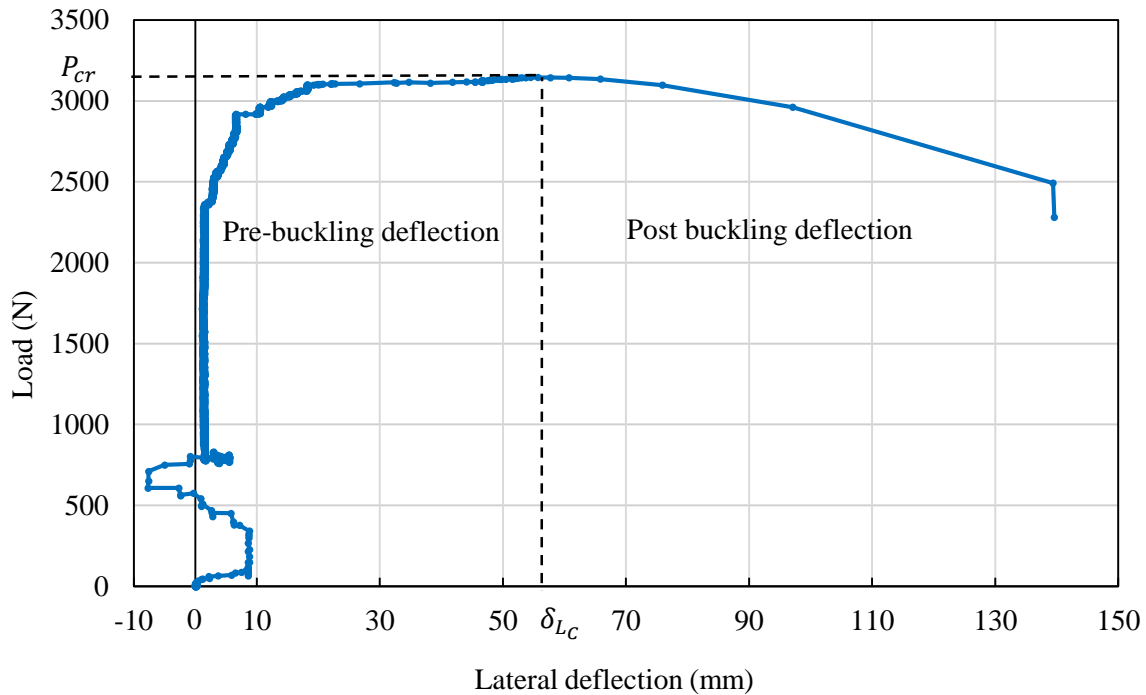
Figure 5.7: Buckling load determined from lateral deflection of the top flange.

The results from all 24 tests are shown in Table 5.2. The load, which was measured in kg, was converted to a force in Newton (N) by multiplying the load with the gravitational constant $g = 9.81 \ m/s^2$. Note that $L_b/L_c = 1.45$ was used, as the beams for these test were 200 mm to short, thus was not able to test at $L_b/L_c = 1.5$.

Table 5.2: Experimental buckling loads (N), with $L_c = 2.5$ m.

L_b/L_c	Shear centre #1	Shear centre #2	Top flange #1	Top flange #2
Fixed cantilever	2620.7	3477.2	2714.9	2763
0.5	2383.3*	2676.2	2507.4	3141.2
1	2777.7	3052.9	3144.6	3179.4
1.45	2568.3	2479.5	2816	2935.6
2	2042.4	2110.6	1974.3	2035.1
2.5	1989	1863.4	1663.8	1702
* Note: Test was concluded before the beam had buckled.				

Figures 5.8 and 5.9 illustrate the critical moments calculated from the buckling load, along with the FE shell element results (Strand7 software); and Essa and Kennedy (1994) for the shear centre and top flange loading, respectively.
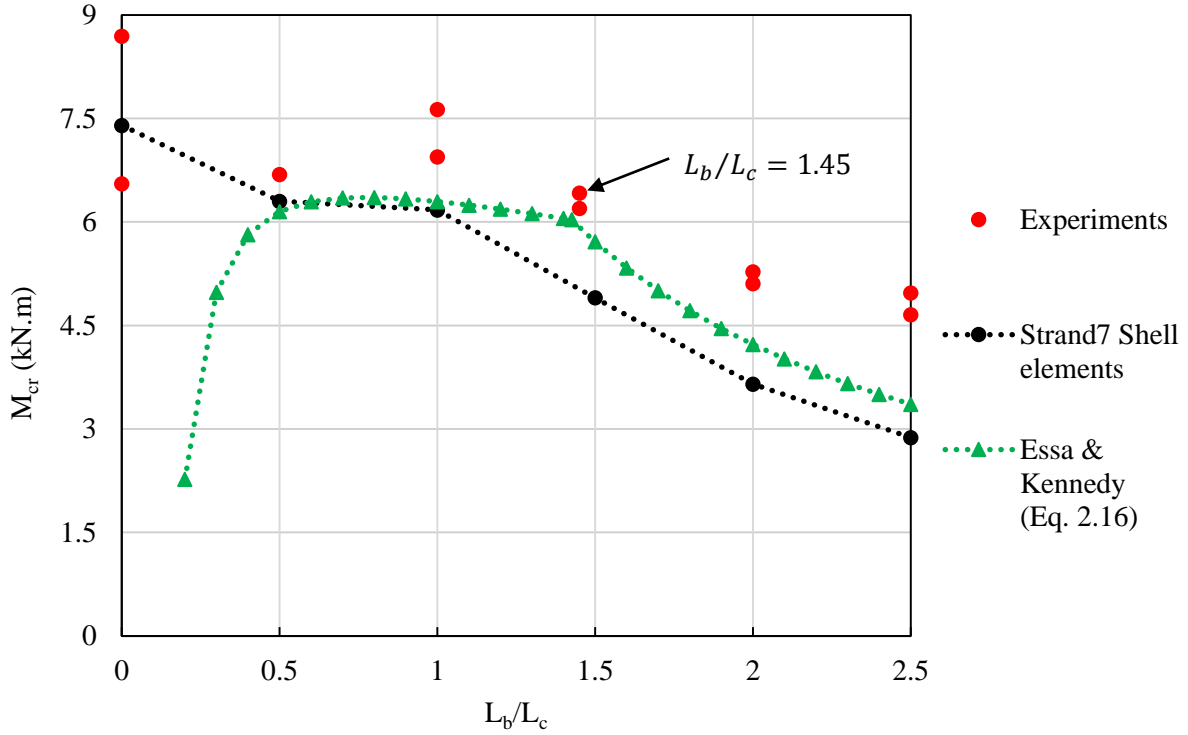

Figure 5.8: Critical moments vs. backspan to overhang ratio for shear centre loading.
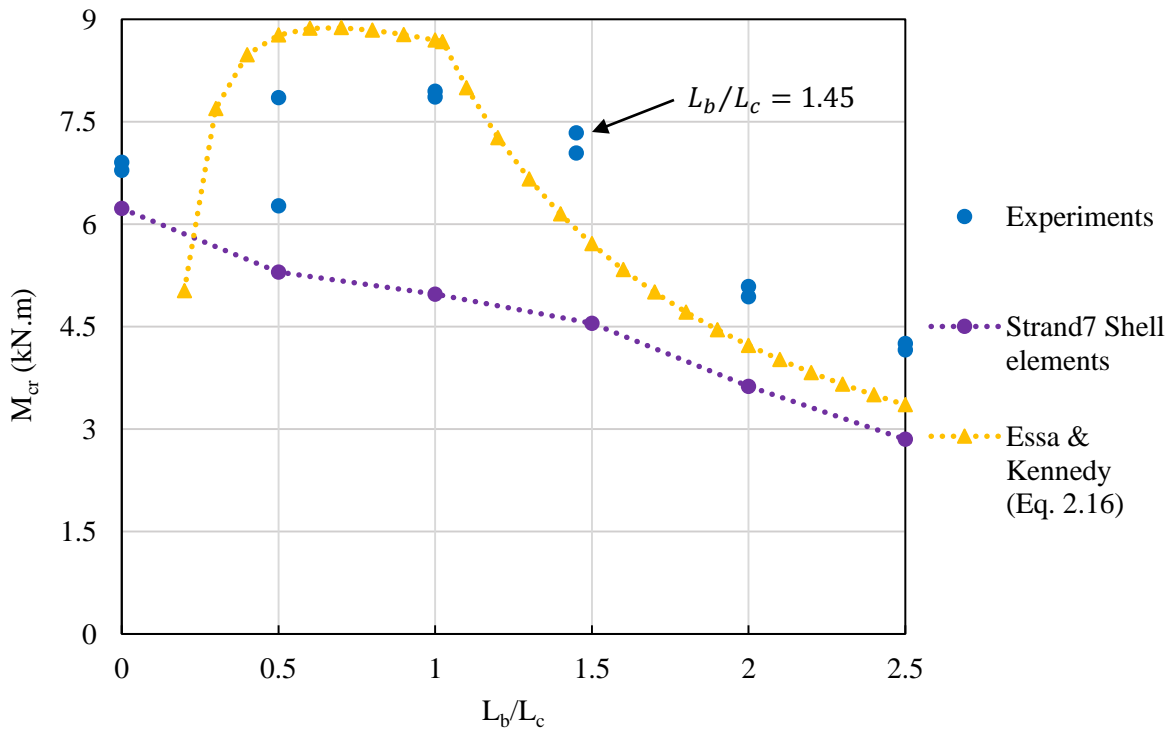

Figure 5.9: Critical moments vs. backspan to overhang ratio for top flange loading.

Table 5.3 compares the percentage difference between the experiments and the critical moments of Strand7 shell elements and Essa and Kennedy (1994). Both experiments for each shear centre (SC) and top flange (TF) loading were used (#1 and #2) for $L_b/L_c = 0.5$, 1 and 2. A negative value referred to the experiment having a larger critical moment than the comparison.

Table 5.3: Experiments compared to Strand7 shell elements and Essa and Kennedy (%).

| | $L_b/L_c = 0.5$ | | $L_b/L_c = 1$ | | $L_b/L_c = 2$ | |
	SC	TF	SC	TF	SC	TF
Strand7 #1	-	-15.5	-11.0	-36.6	-28.6	-26.5
Strand7 #2	-5.8	-32.5	-19.0	-37.4	-30.9	-28.7
Essa & Kennedy #1	-	+38.6	-9.2	+10.7	-17.4	-14.6
Essa & Kennedy #2	-8.1	+10.8	-17.4	+9.4	-20.1	-17.1

A summary of observations made during the experimental work is given below.

- As L_b/L_c increased, the difference in critical moments for shear centre and top flange loading decreased, as predicted by the FE shell element analyses.
- According to the FE shell element analyses, the critical moment for both shear centre and top flange loading decreased as L_b/L_c increased; the experimental data had a similar trend. Except for top flange loading, the critical moment increased between the cantilevers and $L_b/L_c = 1.0$, then decreased as L_b/L_c increased past 1.0.
- For $L_b/L_c \geq 1.45$ the critical moment for both shear centre and top flange loading followed the same trend as the FE shell element analyses and the method by Essa and Kennedy (1994).
- In general, the difference between experimental results and FE shell element analyses were larger for top flange loading than for shear centre loading. Top flange loading was more susceptible than shear centre loading regarding twist, therefore increased resistance of twist in the beam had a larger influence when loaded on the top flange.
- The region of $L_b/L_c < 1.45$ required further FEA investigation, because the buckling loads for the critical overhanging segment had a large variance between the different methods.
- Top flange loading reduced the buckling capacity of the cantilever.

In theory, the results obtained from the experiments should be similar to the FE shell element analyses. In reality, various factors influenced the experiments. A notable difference exists between the experimental data and the initial FE analyses. The reason for the differences was that the FE shell

element beams were perfectly straight, symmetrical about both axes and had no initial twist. By considering these imperfections, the experimental beams should have reduced buckling capacities compared to the initial FE analyses; however, this was not the case. All of the beams had buckling capacities higher than predicted. The exception being the first cantilever test, the buckling capacity was much lower than expected, though this beam was noted as being initially bent along the length.

A possibility explaining the buckling capacity being higher than anticipated could be larger than expected cross-sections, especially if the torsional stiffness J was increased. The warping torsion and torsional stiffness depends on the shape and size of the cross-section. The majority of the beams measured had flange thicknesses, flange widths and web thickness larger than the specified nominal values, including containing tapered flanges.

In the FE analyses, the models had perfect boundary and loading conditions. The boundary and loading conditions of the beam setup were designed as close to the FE models to minimise minor axis rotation restrictions and warping restrictions. However, some restrictions remained in the experimental setup. Surface contact between the beam and the supports (rollers and vertical restraints) induced friction, especially when the beam was loaded. The additional friction in the flanges of the beam increased the warping resistance, causing the beam to resist a larger load before buckling occurred. Additionally, for the experimental setup, the distance between the supports and the load applied (load application points) was not perfect, as was the case for FE analyses. A reduction in span length, even minor, increased the stiffness of the beam, therefore increased the critical moment of the beams.

Therefore, the critical moment is influenced by the beneficial stiffening effect of the boundary and loading conditions and the adverse section geometric imperfections.

5.4   MEASURED DEFLECTION AND TWIST

A discussion based on the observations made during testing regarding deflection and twist were added to determine which factors, if any, had an influence on the buckling capacity of a beam. The deflection and twist could increase rapidly before and after the beam buckled, making it difficult to obtain the deflection and twist of the beam when it buckled. Only deflection and twist up to the buckling load were used, as explained earlier.

During the 20 overhang beam tests, the deflection and twist were measured at various predetermined locations, depending on the length of the beam. The changes were necessary to facilitate the constraints of the String LVDTs. For example, the twist of the beam was measured in the overhanging segment

for the shorter beams but was measured in the backspan segment for the longer beams. For short beams, there was almost no twist in the backspan (due to high stiffness), similarly, for a long span; the twist was negligible in the overhanging segment. Therefore, it was only necessary to measure twist in the critical segment. The critical segment was the segment that was predicted to buckle.

The twist of the beam was not measured directly but was calculated from the measured lateral deflection of both the top and bottom flange using Eq. 5.1. The distance between the flanges was used to calculate the twist, as the String LVDTs were situated at these locations (Figure 5.10). Figure 5.11 shows the original position and the buckled position of the same beam. The vertical and lateral deflections, as well as the relevant twist of all the experiments at the buckling load, are tabulated in Tables 5.4 and 5.5. All deflections that were measured are presented in millimetres (mm) and the twist in degrees (°).

$$\phi = \tan^{-1}\left(\frac{\delta_{L_t} - \delta_{L_b}}{h - t_{tf} - t_{bf}}\right) \qquad\qquad \text{Eq. 5.1}$$

Where:

ϕ = Twist of beam (°).

δ_{L_t} = Lateral deflection of top flange.

δ_{L_b} = Lateral deflection of bottom flange.

h = Measured height of the beam.

t_{tf} = Thickness of top flange.
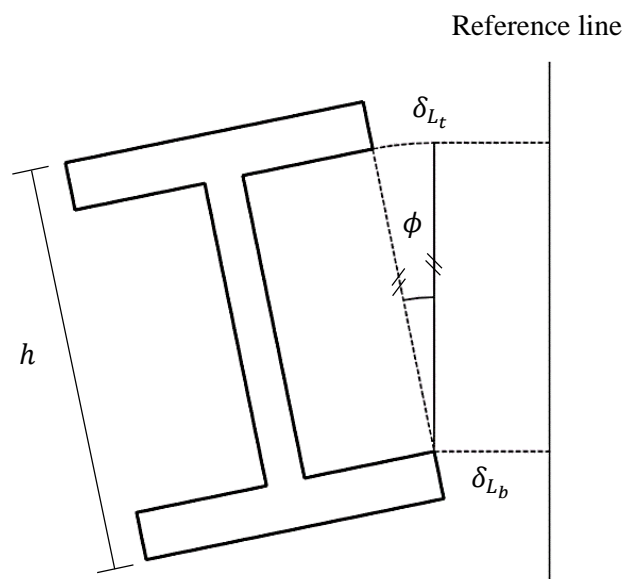
t_{bf} = Thickness of bottom flange.

Figure 5.10: Calculation of twist of the beam.

Figure 5.11: Original position (left) and the buckled position (right).

Table 5.4: Deflection (mm) and twist (°) at buckling load for shear centre loading.

L_b/L_c	Type	Overhanging segment				Backspan segment			
		Lateral deflection		Vertical	Twist	Lateral deflection		Vertical	Twist
		Top	Bottom			Top	Bottom		
Cantilever	SC #1	131.7	-	122.09	9.59	N/A			
	SC #2	32.8	24.1	90.57	5.52				
0.5	SC #1	-	-	-	-	-	-	-	-
	SC #2	135.5	113.8	98.53	13.64	0.1	0.76	1.43	-
1	SC #1	96.5	84.8	120.42	7.29	0.06	-	8.06	-
	SC #2	62.7	51.5	111.39	7.1	0.09	-	8.81	-
1.45	SC #1	56.7	60.9	129.18	2.67	2.36	-	27.11	-
	SC #2	117.7	-	145.8	-	16.11	31.84	25.22	9.97
2	SC #1	177.2	-	168.2	-	35.32	65.42	47.62	18.1
	SC #2	180.7	-	181.3	-	49.11	75.42	52.06	16.4
2.5	SC #1	4.5	-	119.32	-	1.28	6.9	38.49	3.53
	SC #2	166.2	-	155.43	-	57.51	79.3	54.35	13.47

Table 5.5: Deflection (mm) and twist (°) at buckling load for top flange loading.

L_b/L_c	Type	Overhanging segment				Backspan segment			
		Lateral deflection		Vertical	Twist	Lateral deflection		Vertical	Twist
		Top	Bottom			Top	Bottom		
Cantilever	TF #1	106.4	89	83.12	10.94	N/A			
	TF #2	131.2	110	102.3	13.27				
0.5	TF #1	106	81.7	92.8	14.92	0.13	-	1.13	-
	TF #2	45.9	32.1	86.15	8.76	0.02	-	2.27	-
1	TF #1	60.7	46.2	116.46	9.21	0.13	-	9.84	-
	TF #2	13.5	2.2	121.67	7.14	1.14	-	9.43	-
1.45	TF #1	54	-	128.1	-	12.26	22.77	19.76	6.66
	TF #2	55.5	-	130.6	-	6.65	16.47	11.3	6.25
2	TF #1	166.5	-	152.4	-	46.93	67.97	47.62	13.24
	TF #2	177.7	-	157	-	41.68	57.93	40.59	10.26
2.5	TF #1	140.9	-	152.91	-	58.08	80.7	54.66	14.23
	TF #2	204.6	-	170.29	-	59.18	83.7	54.77	15.27

The first overhang beam, 2S1, did not buckle. Therefore, it was difficult to make an accurate conclusion based on this test and was thus left out from the subsequent graphs and discussions.

5.4.1 VERTICAL DEFLECTION OF BOTH SEGMENTS

Figures 5.12 and 5.13 illustrate graphically the downwards vertical deflection (negative) of the tip of the overhanging segment for the shear centre and top flange loading, respectively. The results were grouped according to the L_b/L_c ratio and load height for clarity. As L_b/L_c increased, the slope of vertical deflection vs. load applied decreased. That is to say, the vertical deflection became more sensitive to the applied load. Increasing L_b/L_c therefore decreased the stiffness, N/mm. There was no distinct difference in the stiffness between shear centre and top flange loading.
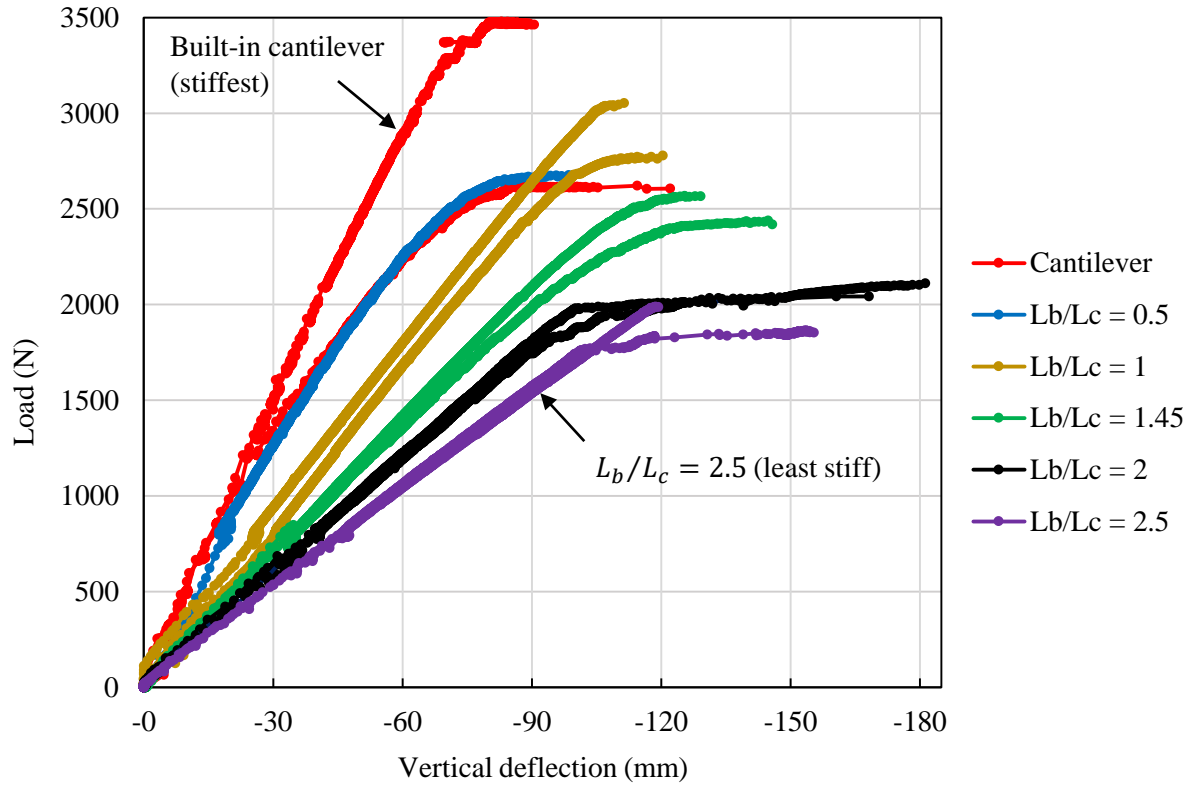
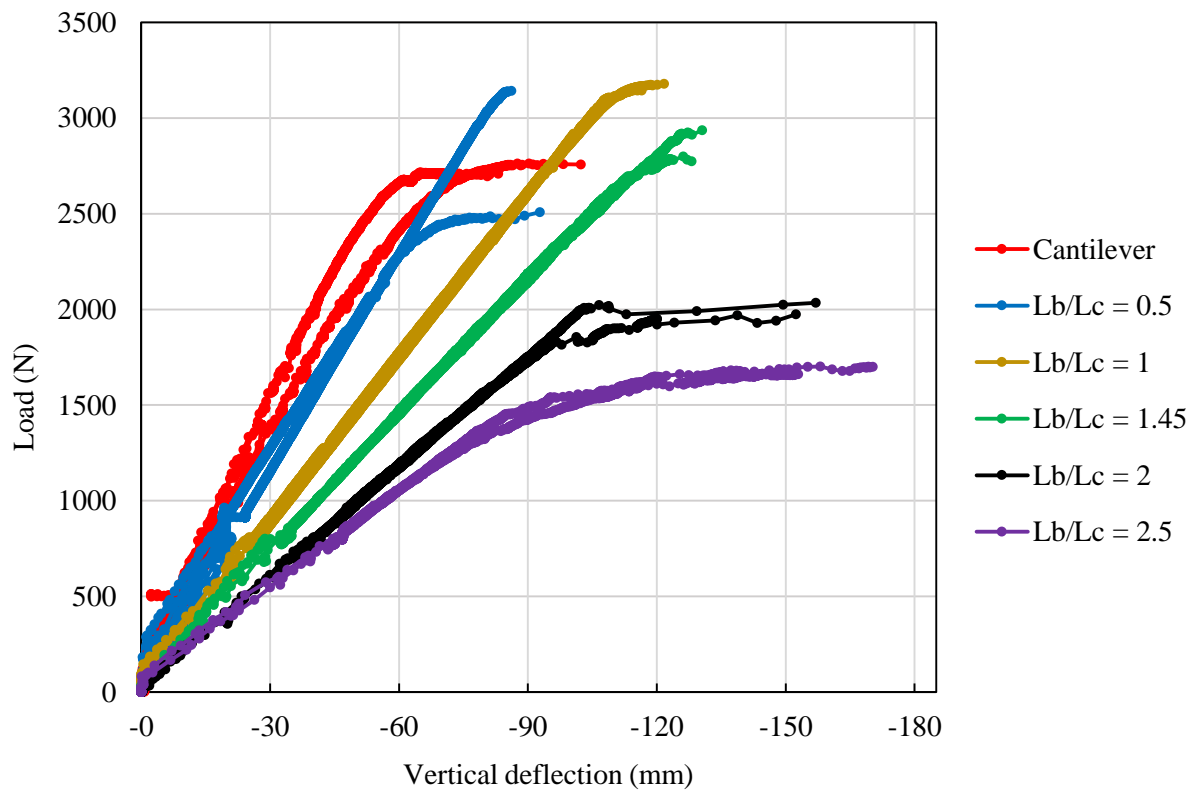**Figure 5.12: Vertical deflection of the overhanging segment for shear centre loading.**

Figure 5.13: Vertical deflection of the overhanging segment for top flange loading.

Figures 5.14 and 5.15 displays the vertical deflection at midspan of the backspan segment. Upwards deflection is illustrated in Figure 5.16. The variance in the rate of vertical deflection as L_b/L_c increased was more profound at the backspan segment than at the overhanging segment. The general shapes of the curves were similar to the overhanging segment above. Once again, the height of the load applied had no significant impact on the stiffness.
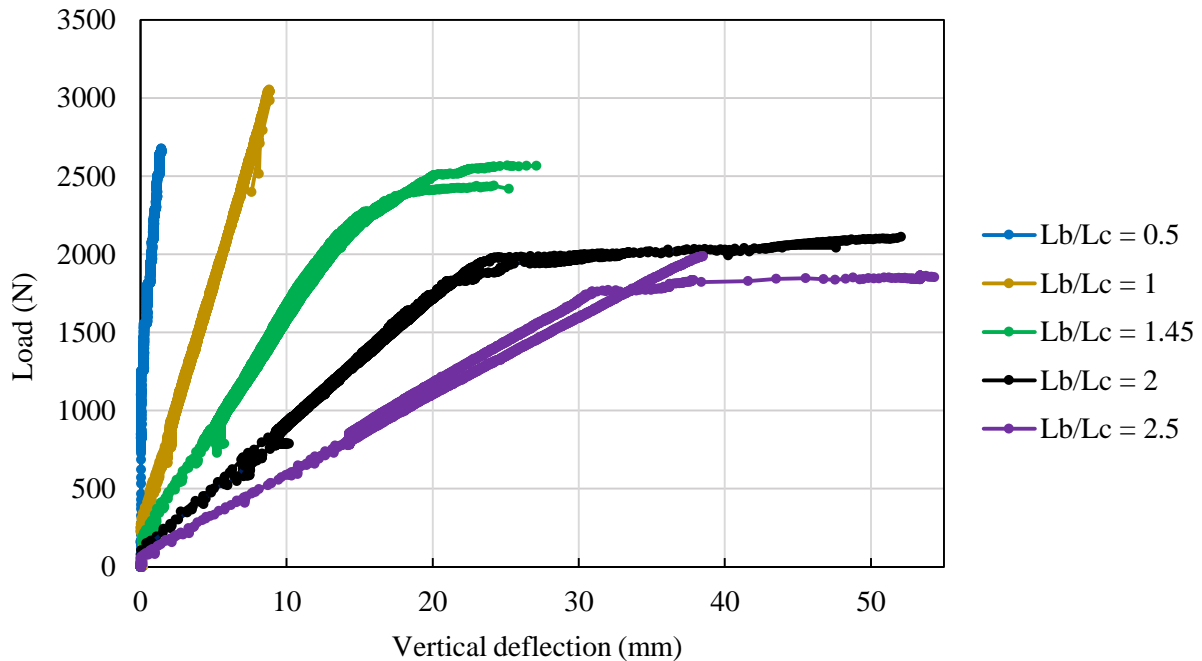
Figure 5.14: Vertical deflection of the backspan segment for shear centre loading.
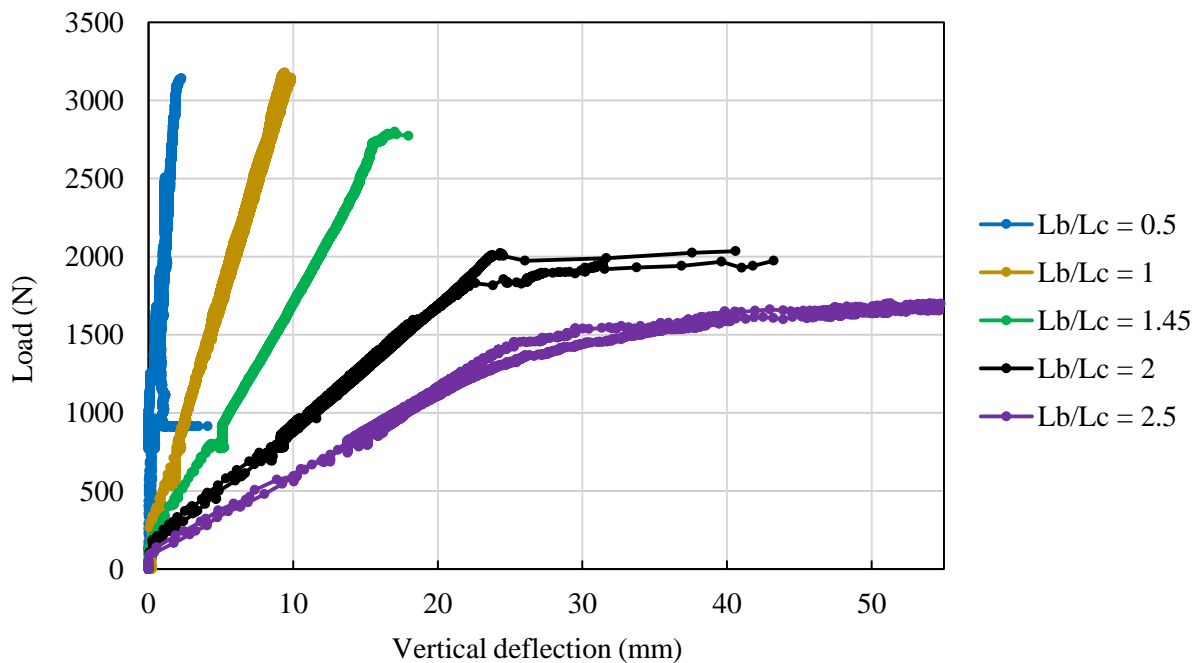
Figure 5.15: Vertical deflection of the backspan segment for top flange loading.

Figure 5.16: Upward deflection of the backspan segment.

The absolute vertical deflection of the tip of the overhang and at midspan of the backspan at the buckling load is displayed in Figure 5.17.

- The graph clearly illustrates the increased vertical deflection of both segments at the buckling load as L_b/L_c increased.
- Vertical deflection at the buckling load increased as the backspan length increased, due to the reduction in stiffness of the beam segment, which in effect, increased the maximum vertical deflection of the overhanging segment.
- Either shear centre or top flange loading caused the larger vertical deflection at either segment as L_b/L_c increased. Vertical deflection was primarily dependent on the magnitude of the load applied.
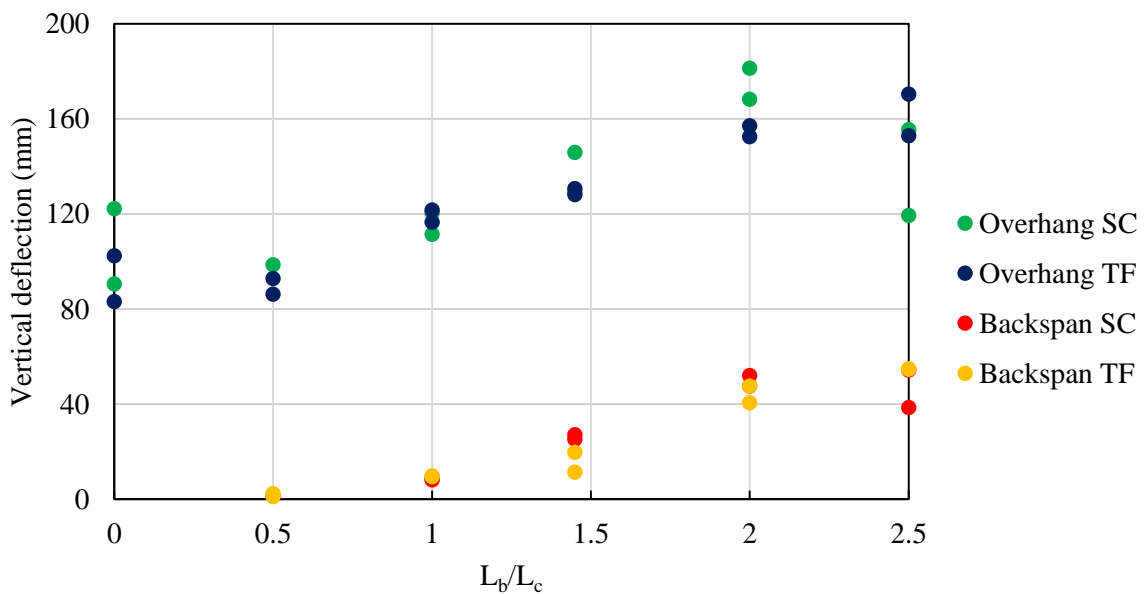

Figure 5.17: Vertical deflection at buckling of both segments.

5.4.2 LATERAL DEFLECTION OF OVERHANGING SEGMENT

The lateral deflection at midspan of the overhanging segment was divided into the deflection of the top flange (Figures 5.18 and 5.19) and the bottom flange (Figures 5.20 and 5.21). Lateral deflection of the top flange was measured for every test. The bottom flange of the overhanging segment was only measured from test 1S2 up to 4S1.

- The four graphs show that as L_b/L_c increased, the overhanging segment deflected laterally progressively. This was due to increased warping in the flanges as the backspan got longer.
- The lateral deflection of the overhang was dependent on the length and lateral deflection of the backspan segment.
- The lateral deflection of the top flange of the overhanging segment was also dependent on the amount of twist in the overhanging segment, as explained in Figure 5.10.
- The top flange was the critical flange in the overhanging segment, with the critical flange being the flange that deflected laterally the most.
- The noise below 700 N in the subsequent graphs was the same as that explained in Figure 5.7.
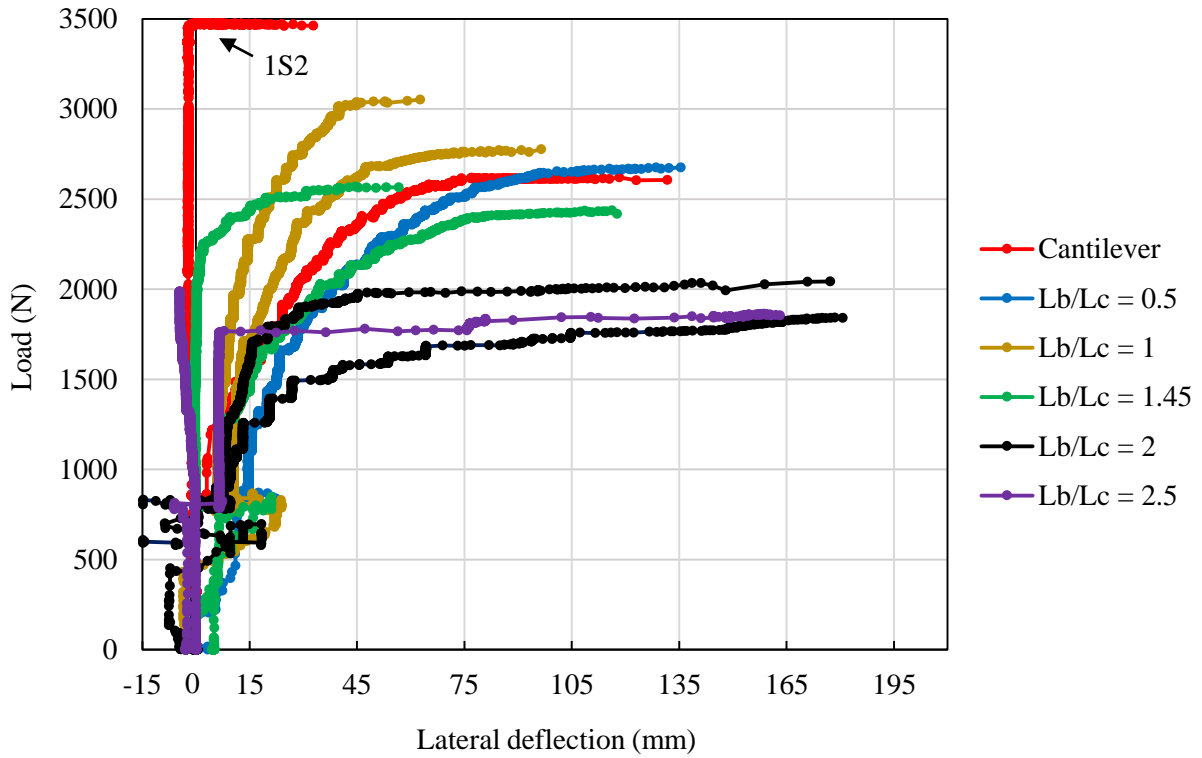
Figure 5.18: Lateral deflection of the top flange at the overhanging segment for shear centre loading.
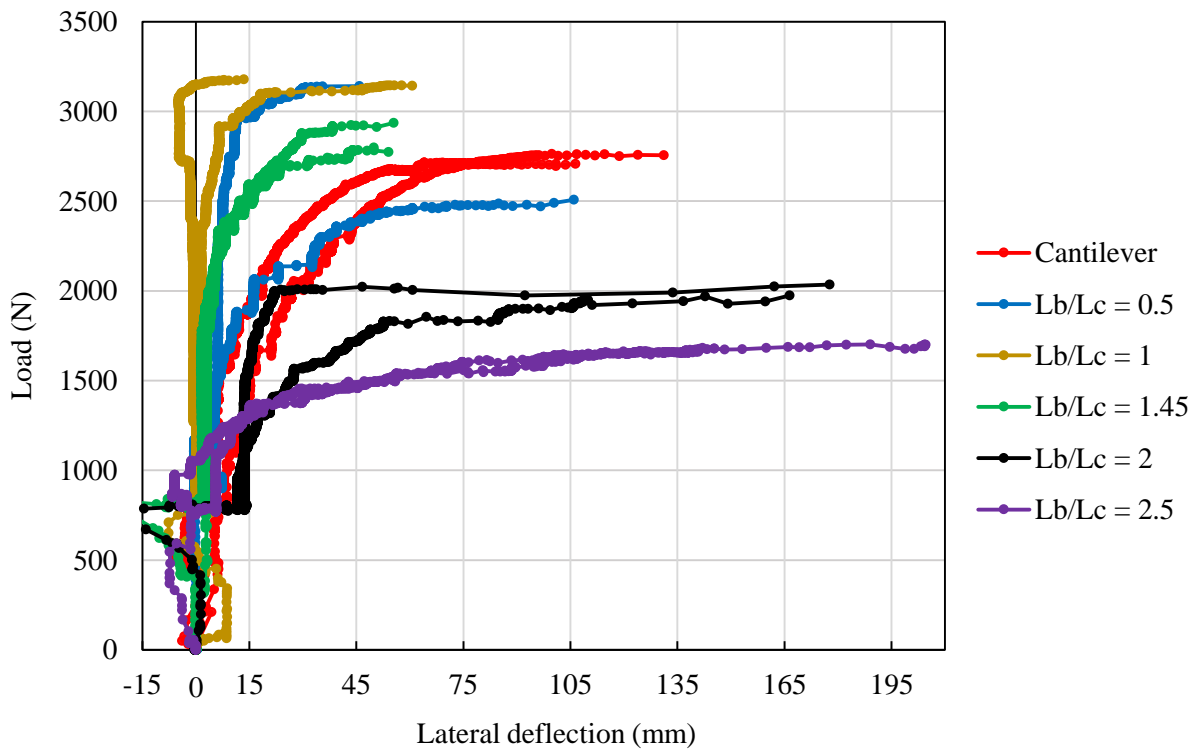

Figure 5.19: Lateral deflection of the top flange at the overhanging segment for top flange loading.
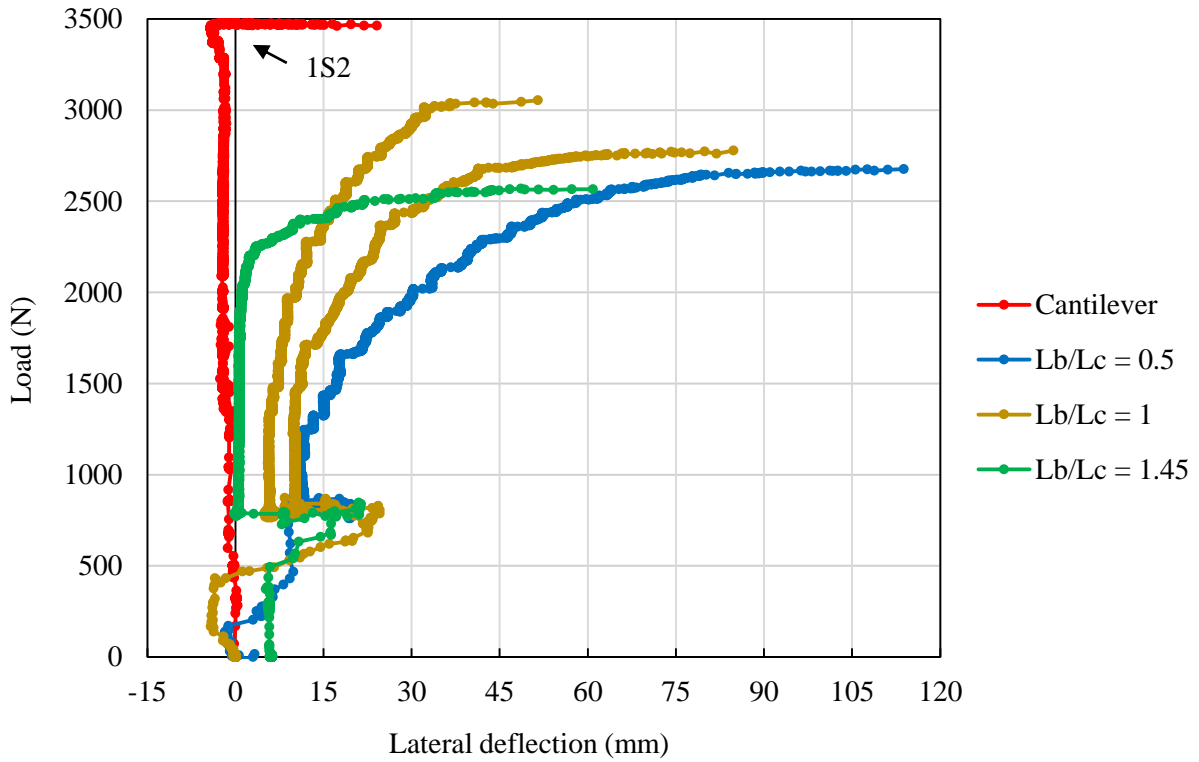
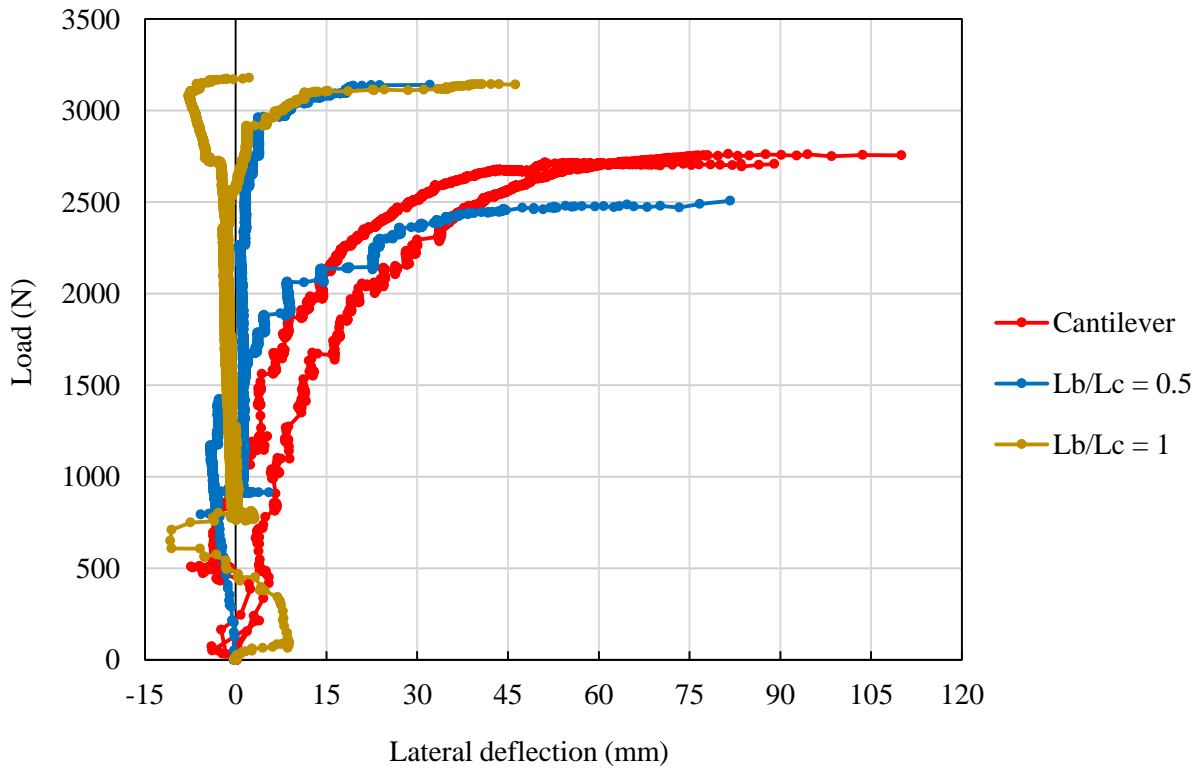**Figure 5.20: Lateral deflection of the bottom flange at the overhanging segment for shear centre loading.**

Figure 5.21: Lateral deflection of the bottom flange at the overhanging segment for top flange loading.

5.4.3 LATERAL DEFLECTION OF BACKSPAN SEGMENT

For larger ratios of L_b/L_c, significant lateral deflection occurred in the backspan segments as depicted in Figure 5.22. A few observations noted regarding lateral deflection of the backspan were as follows:

- The lateral deflection of the top and bottom flanges at the backspan segment (Figures 5.23, 5.24, 5.25 and 5.26) remained small initially but then increased considerably as the load approached the buckling capacity.
- The lateral deflection of the flanges was negligible when $L_b/L_c \leq 1$.
- The bottom flange was the critical flange in the backspan segment, with the critical flange being the flange that deflected laterally the most.
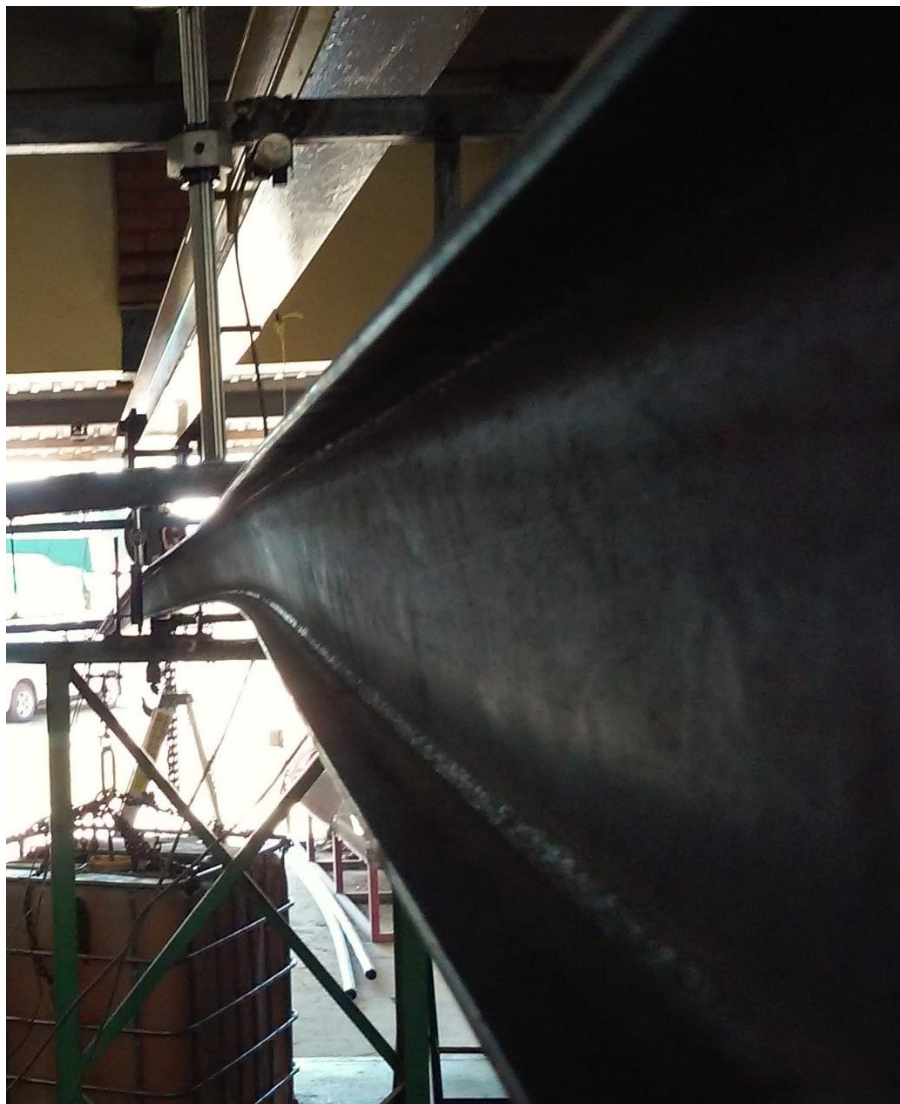

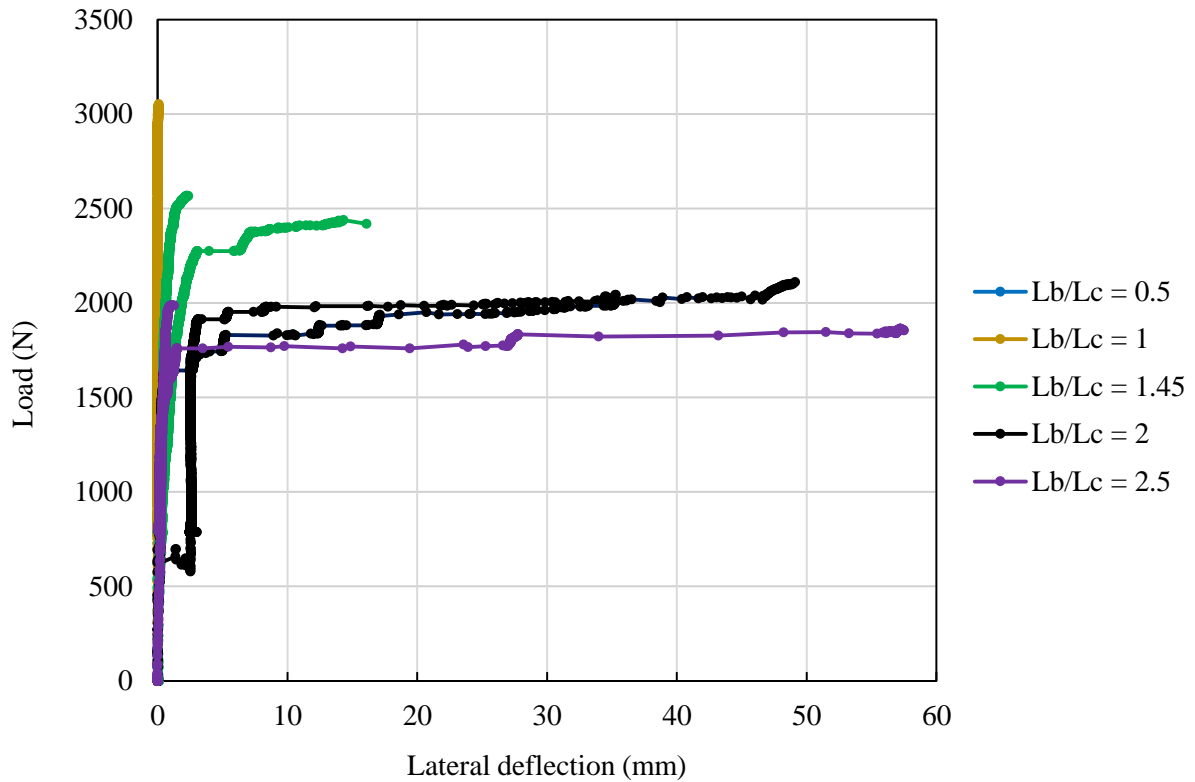**Figure 5.22: Lateral deflection of backspan during an experiment.**

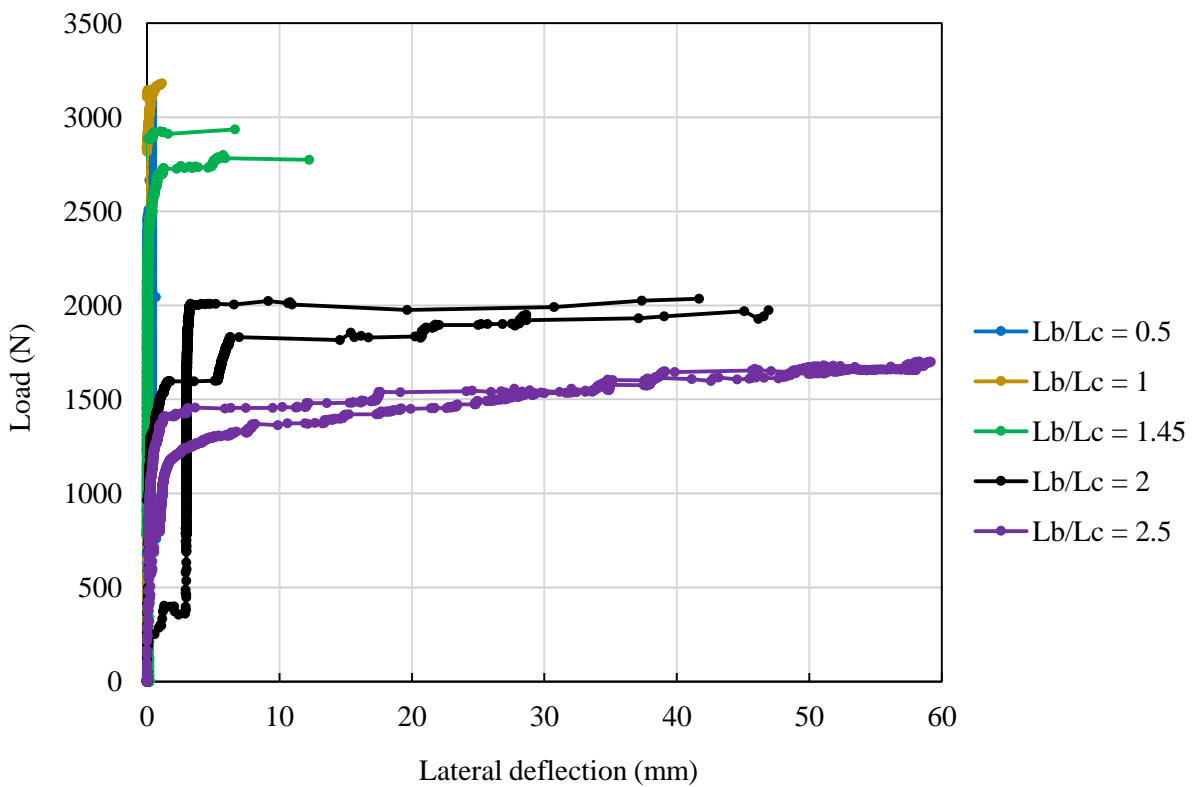**Figure 5.23: Lateral deflection of the top flange at the backspan segment for shear centre loading.**

Figure 5.24: Lateral deflection of the top flange at the backspan segment for top flange loading.
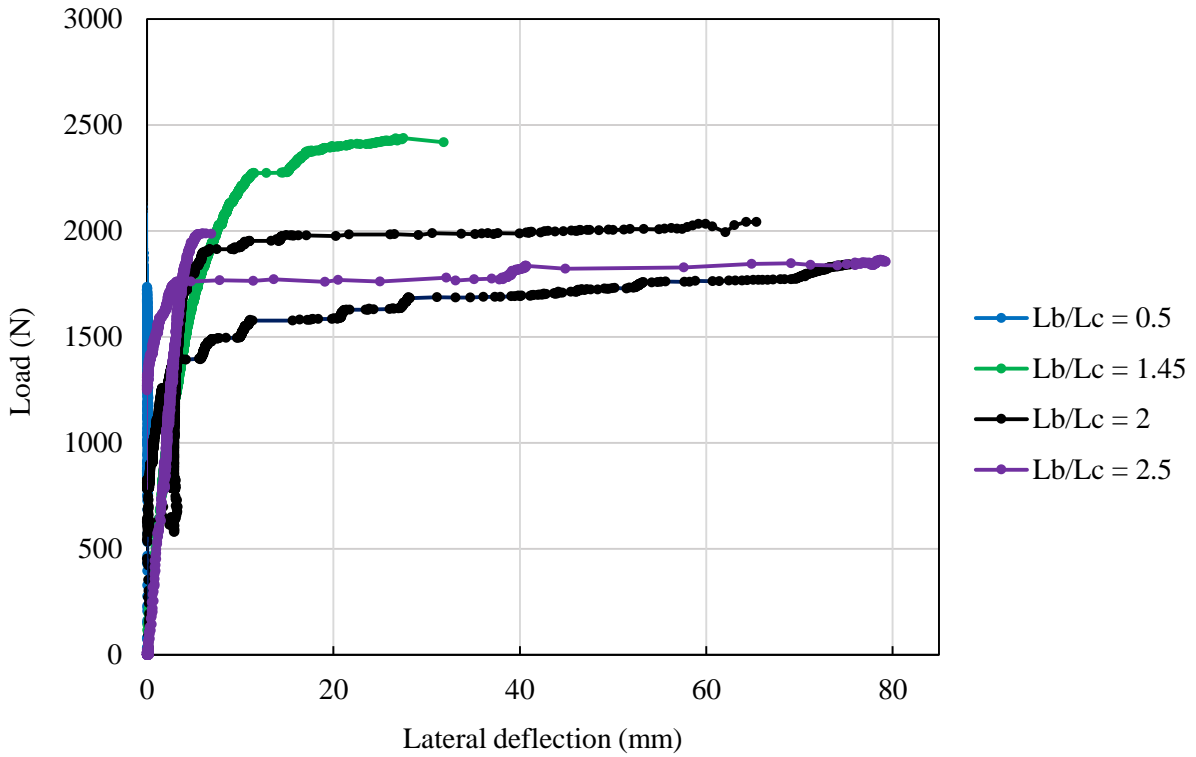
Figure 5.25: Lateral deflection of the bottom flange at the backspan segment for shear centre loading.
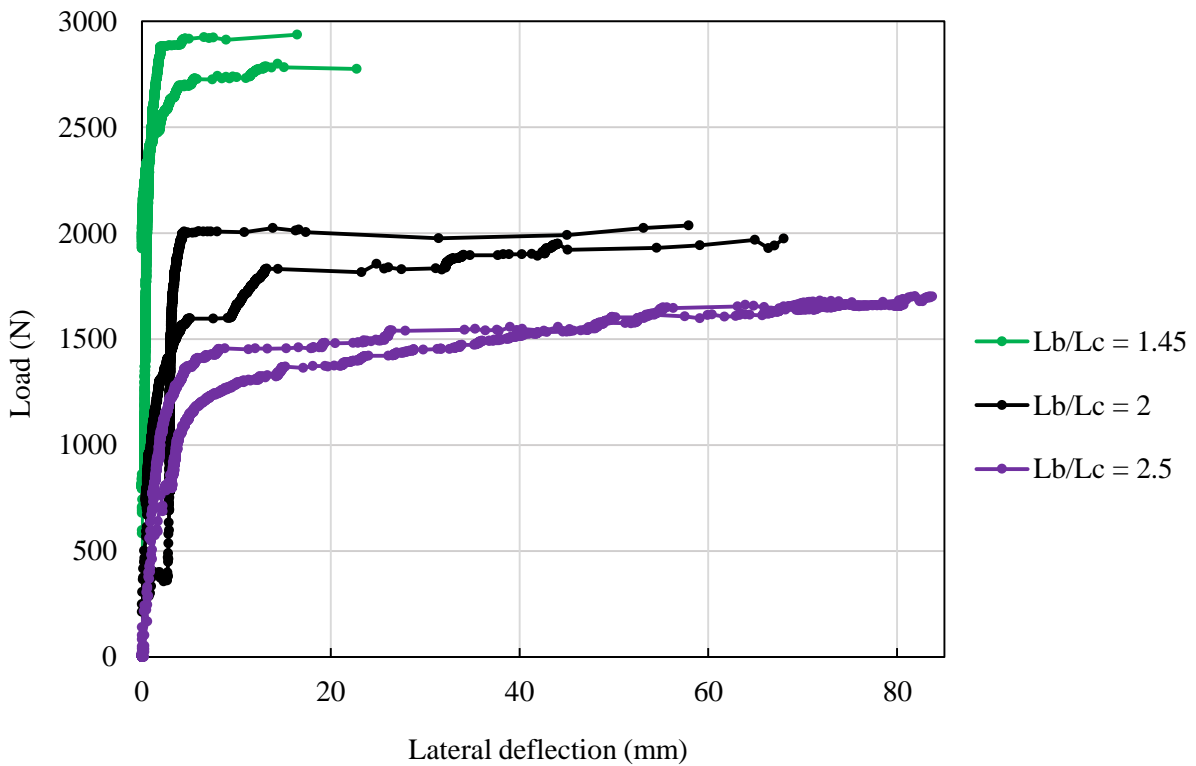

Figure 5.26: Lateral deflection of the bottom flange at the backspan segment for top flange loading.

5.4.4 TWIST OF BOTH SEGMENTS

The twist was observed and measured in both segments. Figure 5.27 illustrates the twist of the beam in the backspan segment. The twist in the overhang and backspan segment (Figures 5.28, 5.29, 5.30 and 5.31) was partly affected by the initial twist in the beam; nonetheless, it was still possible to make a few conclusions.

- As the backspan segment became longer, the rotational stiffness of the beam reduced. Thus the tendency of the beam to twist under the applied load increased.
- The twist in the backspan segment under top flange loading increased as L_b/L_c increased.
- The twist in the overhanging segment reduced as L_b/L_c increased; eventually the twist became negligible (Figure 5.32).
- There was a high variability in the twist of either segment, regardless if the load was applied at the shear centre or on the top flange. The variance was due to the initial out-of-straightness in the beams.
- Initial twist of the beams (imperfections) affected the amount of twist at the buckling load.

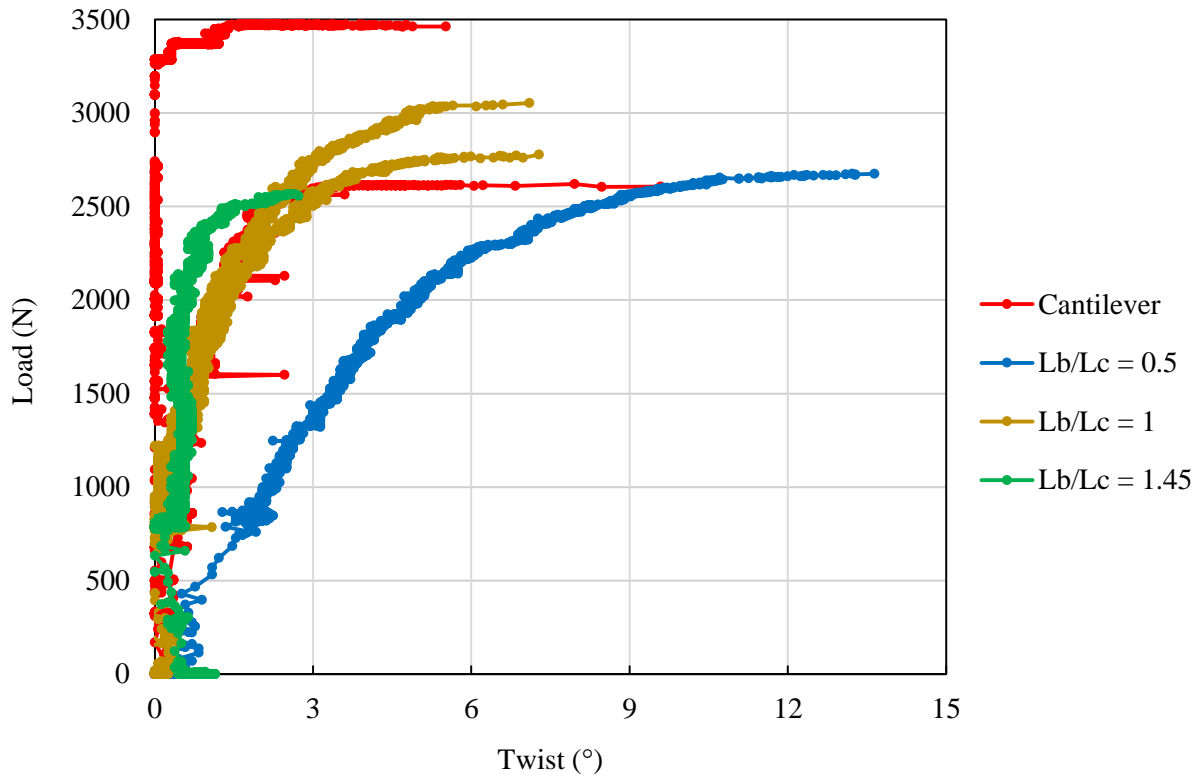**Figure 5.27: Twist in the backspan segment during the experiment.**

Figure 5.28: Twist of the overhanging segment for shear centre loading.
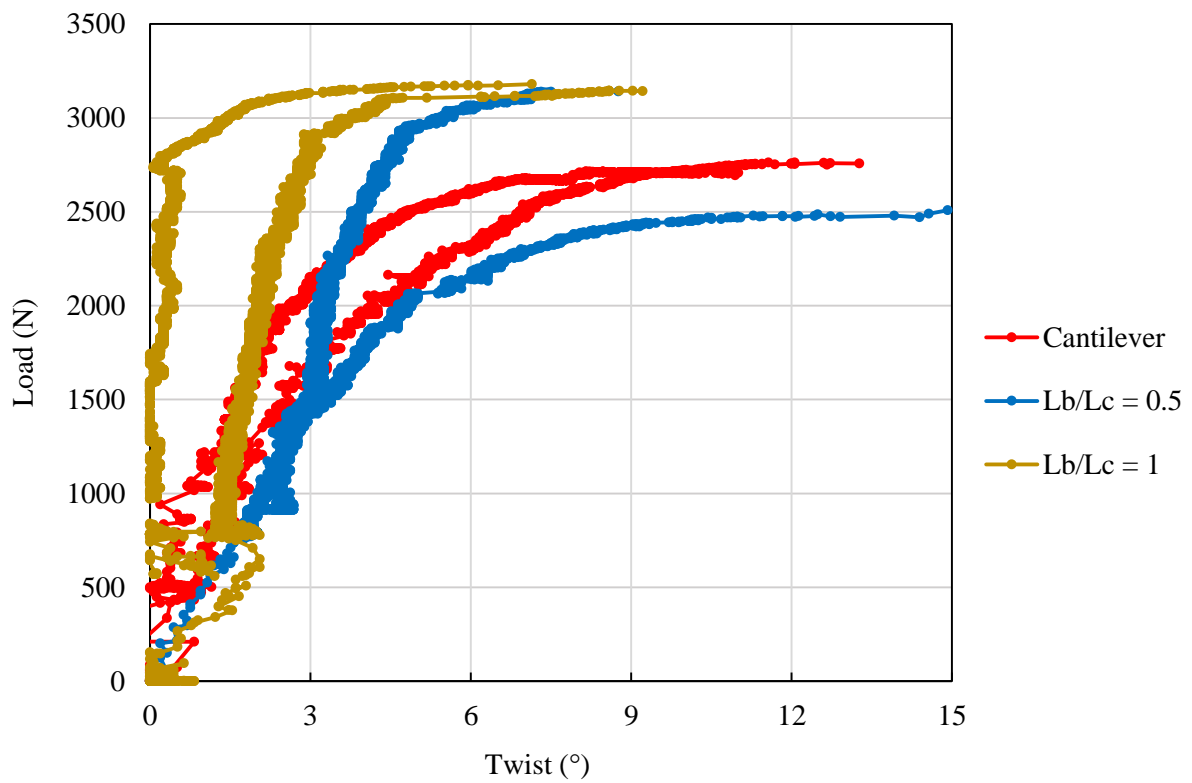

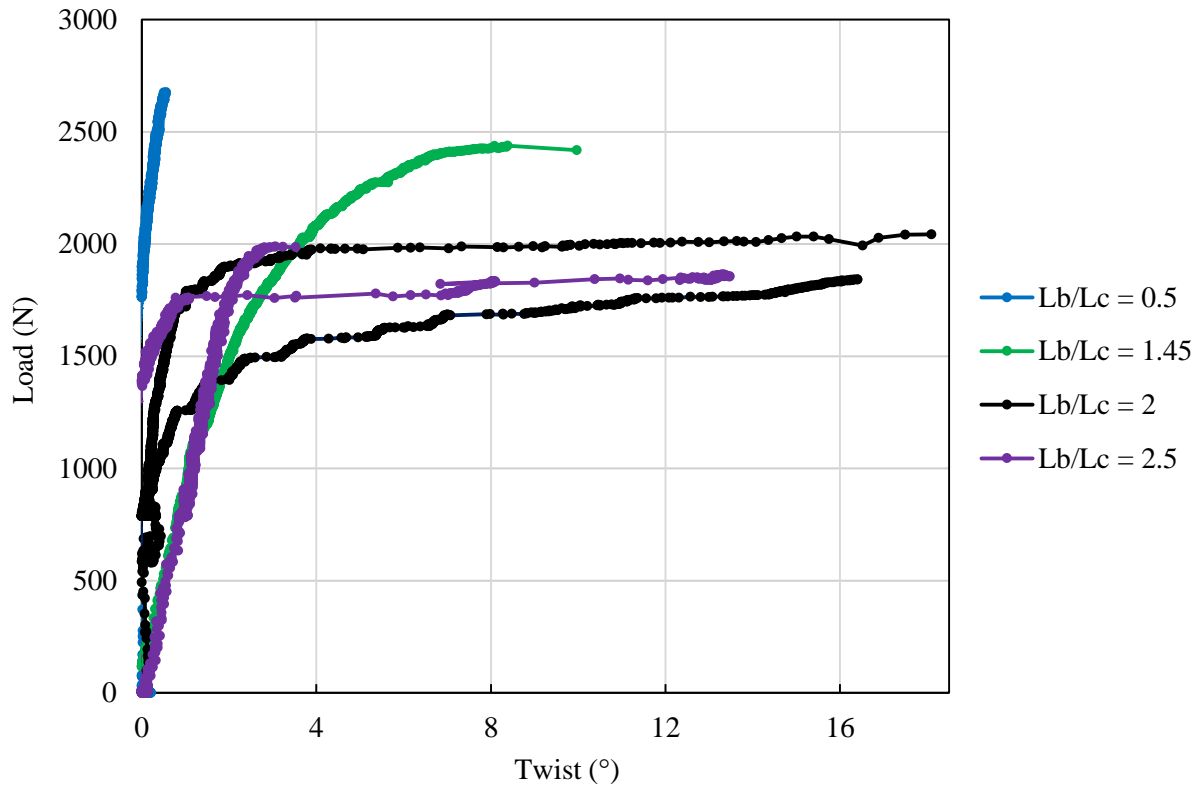**Figure 5.29: Twist of the overhanging segment for top flange loading.**

Figure 5.30: Twist of the backspan segment for shear centre loading.
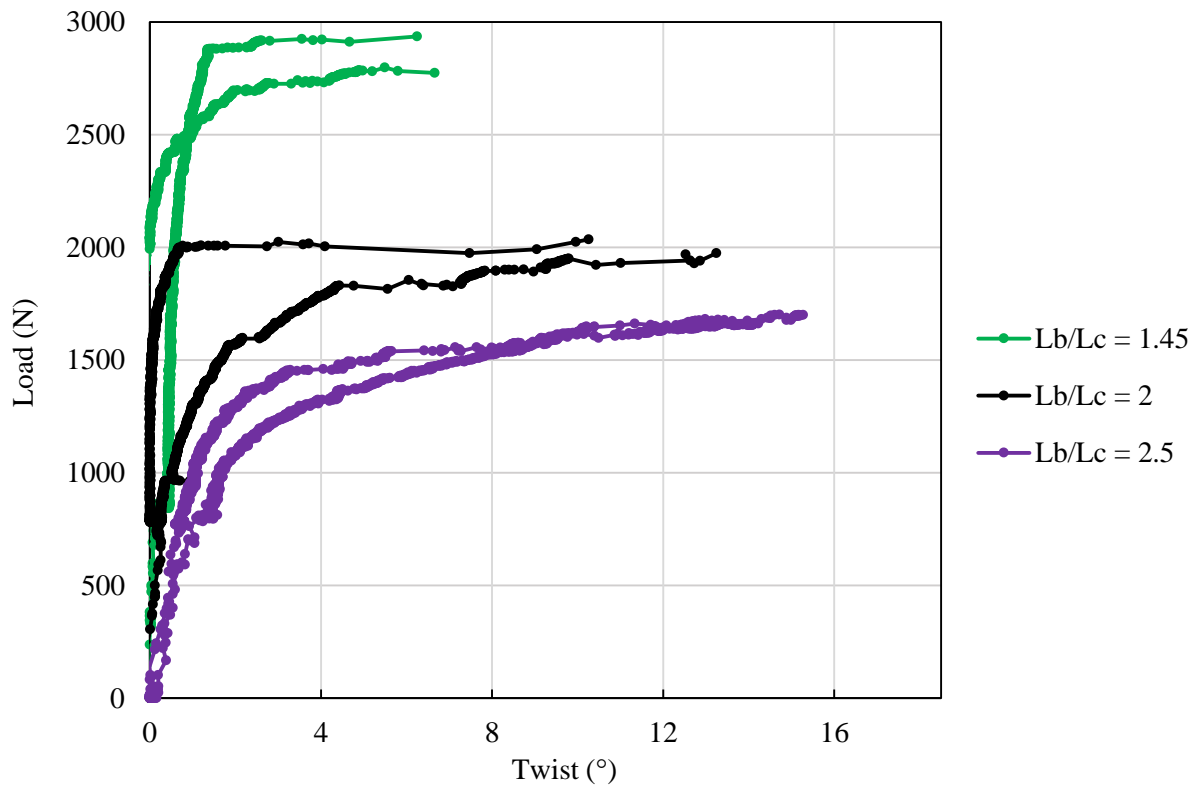

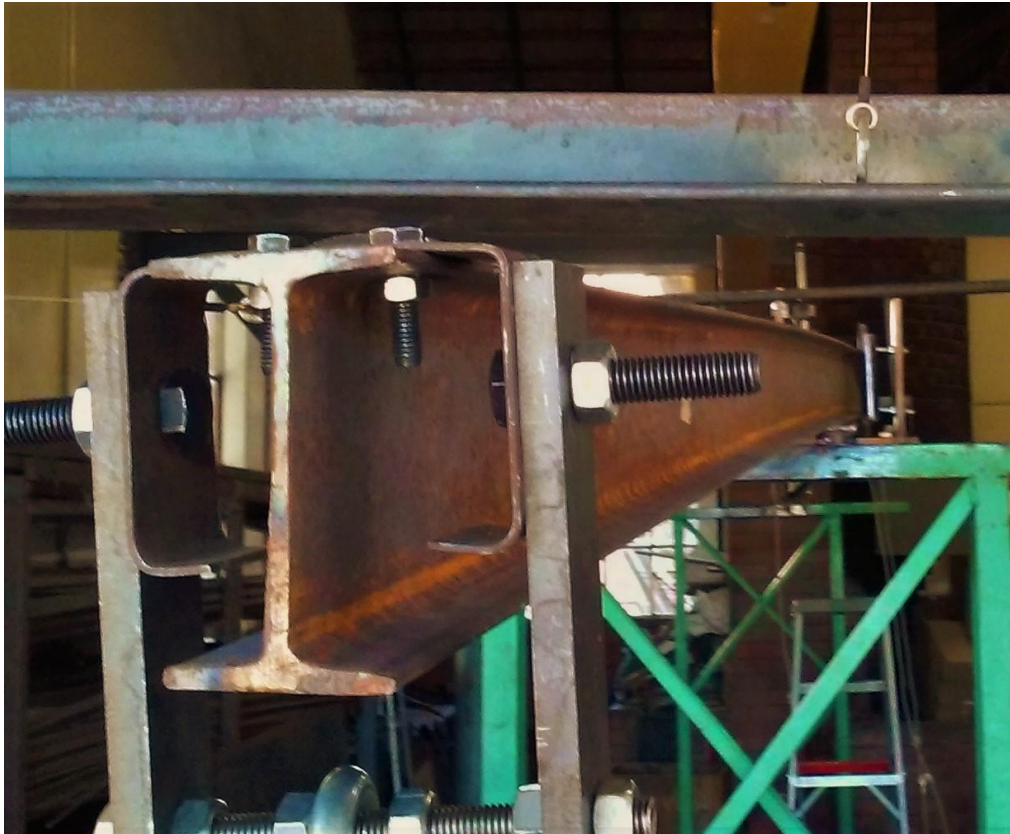**Figure 5.31: Twist of the backspan segment for top flange loading.**

Figure 5.32: No twist in overhanging segment for large L_b/L_c when backspan had buckled.

5.4.5 INITIAL TWIST IN CANTILEVERS

The two cantilevers with shear centre loading had a large difference in buckling capacity. The first cantilever beam had significant initial out-of-straightness (not measured but noted) rendering the beam more susceptible to buckle gradually as the load was applied. The second cantilever beam was initially straight, and buckling was sudden. The 'speed' of buckling (gradual vs. sudden) was verified by the rate of twist in the beam. For the first cantilever beam, the twist increased as the load increased and had a small buckling capacity (blue line in Figure 5.33). The second cantilever beam, the twist was negligible up to the point of buckling and had a significantly larger buckling capacity (red line in Figure 5.33).

The case of top flange loading, the two tests had a similar increase in a twist as the load increased and had similar buckling capacities (Figure 5.34). The rate of twist was, therefore, consistent with the buckling capacity, also, was a contributing factor in the buckling capacity of a beam. Restricting or delaying the twist in the beam, therefore, increased the buckling capacity of the cantilever beam. Figure 5.35 shows the twist of a cantilever during an experiment.
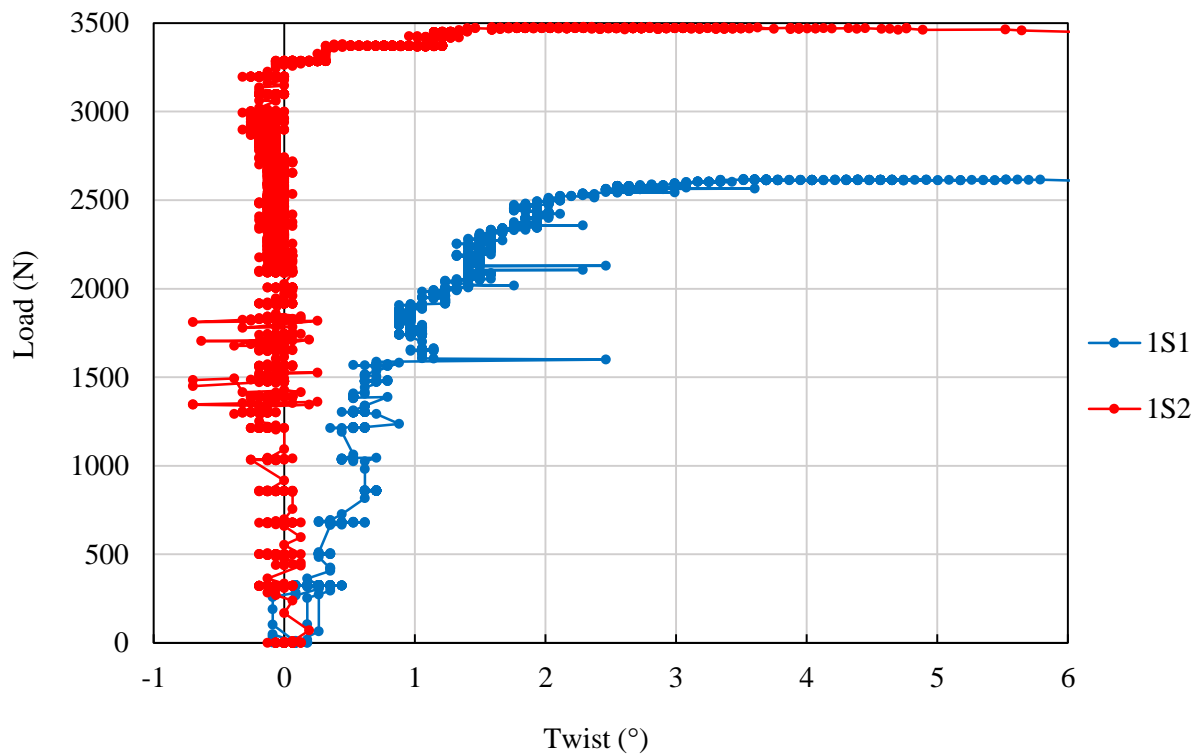
Figure 5.33: Twist of the cantilever with shear centre loading.
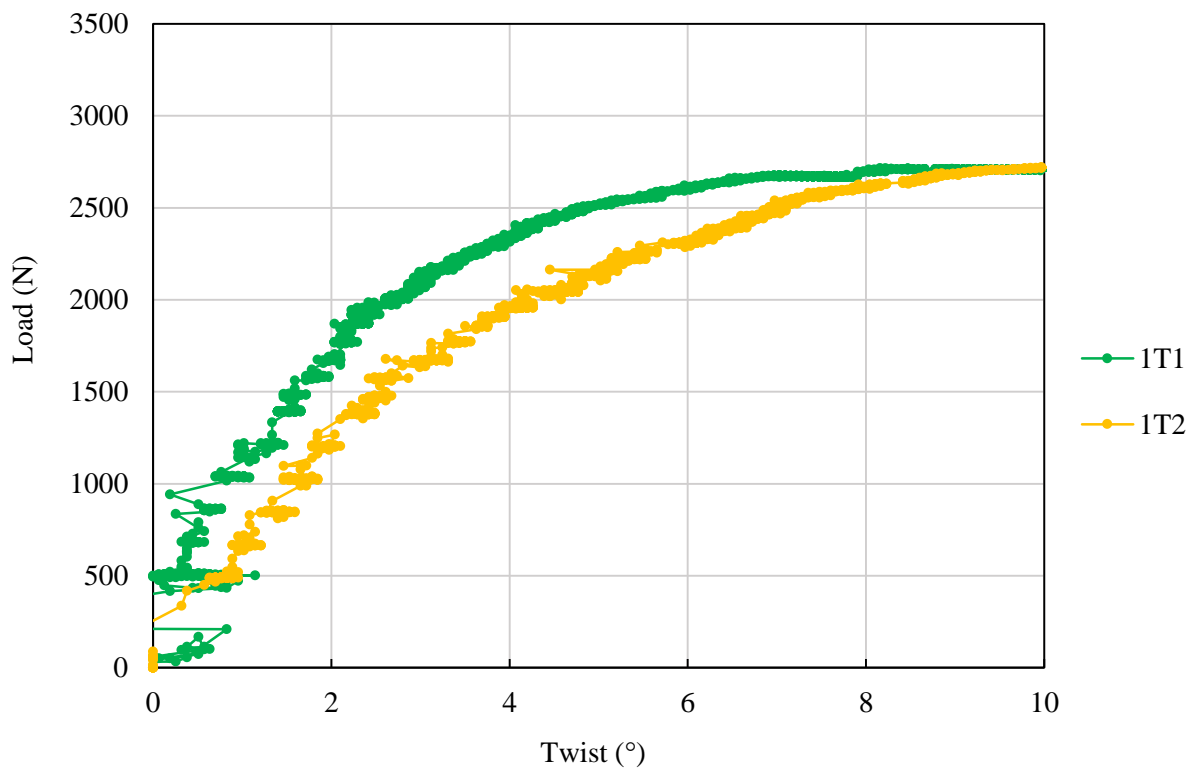
Figure 5.34: Twist of the cantilever with top flange loading.

Figure 5.35: Twist of the cantilever during an experiment.

5.4.6   TWIST IN OVERHANG BEAMS

The overhang beams of 5S1, 5S2, 6T1 and 6T2 showed the same phenomena as that explained above where a similar rate of twist led to similar buckling loads, confirming that twist could affect the buckling capacity of overhang beams too.

Most of the overhang beams with a larger rate of twist, as the load increased, had smaller buckling capacities. With Figure 5.36 as an example, test 2T1 had a smaller change in twist and a noticeable larger buckling capacity than test 2T2. It is concluded that the amount of twist in a beam was a contributing factor to the buckling capacity.

Figure 5.36: Twist of beam with $L_b/L_c = 0.5$ for top flange loading.

5.5 BEAM BEHAVIOUR

A straight beam could buckle in any direction by either twisting or deflecting. In reality, no beam was perfectly straight, and inherent imperfections existed within the beams that predetermined the buckling direction. The curvature of the beam was one of these imperfections that predetermined the direction of buckling.

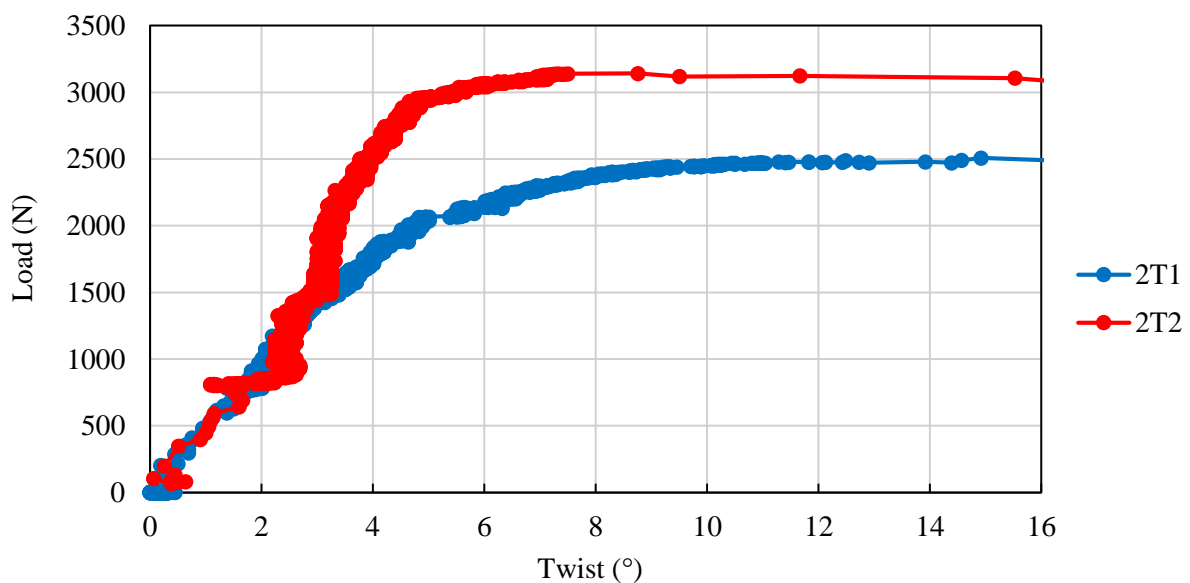Another beam behaviour noted was the change in the direction of buckling during the test. Some beams tended to displace laterally under the load applied in a certain direction, but as the beam began to buckle, the direction changed. The reason for this phenomenon could be dependent on the curvature and the initial twist of the beam. For example, a beam could be initially skew to the left and initially twisted in the opposite direction, causing the beam to buckle to the right.

In theory, the overhang and backspan segment should buckle in different directions. If the backspan buckled to the left, then the overhang should have displaced to the right. Table 5.6 shows the direction of buckling and any changes of direction during the test. 'L' is short for 'Left' and 'R' for 'Right' if viewing from the overhang end. 'L, R' simply meant that the beam deflected to the left, but ultimately buckled to the right. The measured data was validated with photos taken before and after each test.

Table 5.6: Direction of buckling.

L_b/L_c	Type	Overhang	Backspan	L_b/L_c	Type	Overhang	Backspan
Cantilever	SC #1	L		1.45	SC #1	R	L
	SC #2	R, L	N/A		SC #2	L	R
	TF #1	L			TF #1	L	L, R
	TF #2	L			TF #2	L	R
0.5	SC #1	-	-	2	SC #1	R	L
	SC #2	R	L, R, L		SC #2	L	R
	TF #1	R	L		TF #1	L	R
	TF #2	R	L		TF #2	L	R
1	SC #1	L	R, L	2.5	SC #1	R, L	R
	SC #2	R	R		SC #2	L	R
	TF #1	L	R, L		TF #1	R, L	R
	TF #2	L, R	R		TF #2	L	R

- The backspan segments buckled in the opposite direction of the overhanging segment, except for the case of $L_b/L_c = 1$. For all four tests with $L_b/L_c = 1$ did both segments deflect in the same direction; that is to say, both segments had buckled simultaneously. The shape of the buckled beam was therefore similar to a Sine function.
- Where both top and bottom flanges were measured, both flanges had displaced in the same direction.

5.6   SUMMARY OF OBSERVATIONS

The following conclusions were based on the results obtained from the 24 experimental tests:

The buckling load was taken as the maximum load achieved during the test. The deflection and twist varied significantly either before or after the buckling load. Thus, deflection and twist were measured up to the point where δ_H.and ϕ coincided with the buckling load. By investigating the direction of buckling of both flanges in both segments, it was observed that both flanges buckled in the same direction. This was the opposite of the observations made by Bradford (1994).

Increasing L_b/L_c beyond 1.0 decreased the buckling capacity, similar to the FE shell element analyses. Additionally, when $L_b/L_c \geq 1.45$, the critical moment followed the same trend as the FE shell element analyses and the method by Essa and Kennedy (1994). As predicted by FE shell elements, the difference between critical moments for shear centre and top flange loading decreased as L_b/L_c increased.

The twist at the tip of the overhang beam became negligible when $L_b/L_c \geq 2$. This was because at $L_b/L_c \geq 2$, the backspan was the critical segment; hence, twist occurred in this segment and not in the overhanging segment. The rate of twist, which was dependent on the initial twist of the beams, influenced the buckling capacities of the overhang beams.

The curvature of the beam; the thicknesses of the flanges and the web; the flange widths and Young's modulus had an influence on the buckling capacity of a beam. Therefore, sensitivity analyses were performed in Chapter 6 to investigate the impact of these imperfections.

6. FINITE ELEMENT ANALYSIS

6.1 CALIBRATION OF FE SOLID ELEMENT MODELS

The Abaqus software was utilised to conduct detailed FE solid element analyses for a parametric study. Being a research orientated FE program, it was ideal for varying beam parameters to study the impact on buckling capacity. Before commencing the parametric study, it was necessary to calibrate the Abaqus model. The Abaqus models were calibrated against the physical experiments conducted previously. Calibrating the models ensured that the results obtained were accurate and viable. It was then possible to compare results and draw conclusions based on observations. Henceforth, FE refers to the Abaqus solid element models and not the Strand7 shell element models.

6.1.1 SENSITIVITY ANALYSES

Sensitivity analyses were conducted before the calibration process started. The purpose was to understand which factors had an influence on the buckling capacity of a beam. Therefore the correct factors in the FE models were altered to calibrate the models.

The sensitivity analyses were conducted on $IPE_{AA}100$ cantilever beams. Determining the buckling capacity of cantilevers was readily available, such as using Eq. 3.1. Hence, beam parameters could be varied and the resulting critical moments could be calculated. Table 6.1 presents the results from sensitivity analyses, based on Eq. 3.1 and the effective length factors provided by SANS 10162:1. The results obtained were compared to the elastic critical buckling moment of an ideal (nominal) cantilever (reference values) with capacities of 6.59 kN.m and 3.51 kN.m for the shear centre and top flange loading, respectively. The changes in dimensions used in the sensitivity analyses were consistent with the differences measured in the beams that were tested experimentally.

Table 6.1: Sensitivity analyses for a 2.5 m long IPE$_{AA}$100 built-in cantilever.

Dimension / property	Change in dimension / property	Change in M_{cr} (kN.m)		Change in M_{cr} (%)	
		Shear centre	Top flange	Shear centre	Top flange
Web thickness	+ 0.2 mm	+ 0.14	+ 0.12	+ 2.1	+ 3.4
Flange thickness	+ 0.2 mm	+ 0.32	+ 0.18	+ 4.9	+ 5.1
Flange width	- 3 mm	- 0.7	- 0.18	- 10.6	- 5.1
Beam height	+ 1.3 mm	+ 0.03	+ 0.01	+ 0.45	+ 0.28
Young's modulus	+ 10 GPa	+ 0.33	+ 0.18	+ 5.0	+ 5.1
Flange profile	+ 0.1 mm (at web)	+ 1.55	+ 0.94	+ 23.5	+ 26.8

The parameters that had a noticeable influence on the buckling capacity of a beam included the thickness of the flanges; web thickness; the width of the flanges; Young's modulus and the curvature of the beam. The most prominent parameter was the flange profile, i.e. the taper of the flange. The taper caused the flange to become thicker near the web, as a result, significantly increased the torsional stiffness J. A small taper, in the order of + 0.1 mm effectively doubled the torsional stiffness of the beam. Tapered flanges, even small, were noted in all the beams tested. The tapered flanges explain why the experiments had higher buckling capacities than the FE analyses, even though they contained imperfections that should have reduced the buckling capacity. The small difference in the height of the beams had a negligible effect on the buckling capacity.

6.1.2   FE MODEL CHARACTERISTICS

Unlike the Strand7 models, which used shell elements, the Abaqus models consisted of solid elements. The solid elements can accurately reproduce the St. Venant torsion shear stresses at the roots and tips of flanges. Also, Abaqus software allowed profiling of the cross-section of the beam. Modelling curved areas were thus possible if fine meshing were used; therefore, the fillets of the beam were modelled accurately without providing rotational springs. The solid elements were divided into hexahedral and wedge elements. Once again, the shape functions of the elements were quadratic, i.e. 20 nodes per hexahedral (brick) element and 15 nodes per wedge (triangular) elements. The elements were either 25 mm or 50 mm long, depending on the size of the beam. Due to shear centre loading, it was necessary to divide the thickness of the web into two elements; this had resulted in a maximum aspect ratio of 6.5 for the wedge elements and 13.89 for the hexahedral elements. The aspect ratio was less than 10.0

when omitting the thickness of the element. These aspect ratios did not negatively influence the results. Separate analyses, with the thicknesses and widths of the flanges and web divided into multiple layers (mesh refinement), resulted in a negligible difference in the critical moment of the beam. Refinement of the mesh did not improve the results. Therefore, to reduce computation time and the aspect ratio, only the web thickness was divided into two layers, with the flanges remaining one element thick (see Figure 6.1).

The dimensions of the beams were according to the Southern African Steel Construction Handbook (SAISC, 2013), thus contained no deformities in the cross-section of the beam. Similarly, the beams were perfectly straight with Young's Modulus of 200 GPa and a Poisson's ratio of 0.3 (SAISC, 2013). The internal and external supports prevented lateral and torsional deflection but allowed warping. Only the bottom flange at the external support was fixed in the longitudinal direction; this was to avoid rigid body movement of the beam and to simulate the experiments. Figure 6.1 illustrates the mesh and boundary conditions that were used in the models. Note that the figure on the right in Figure 6.1 is a section-view of the model.

The FE models were analysed using the Buckling Analysis solver, which calculated the eigenvalue for a given mode. The Lanczos method was used to solve the Buckling Analysis. For these models, the buckling mode was the first mode, with the eigenvalue being the buckling load.
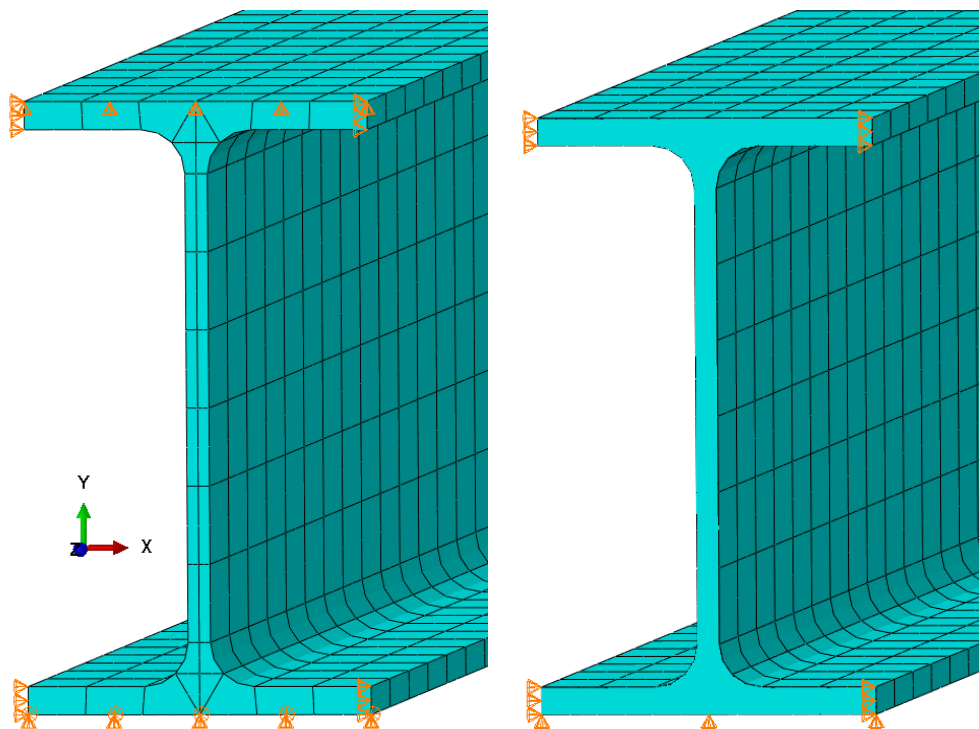

Figure 6.1: Restraint conditions at external (left) and internal supports (right).

6.1.3 CALIBRATING FE MODELS

These new FE model characteristics as discussed above were for the ideal beams that were used in the parametric study. However, to calibrate the Abaqus models, the beams were modelled as measured before the physical experiments. Calibrating the FE models consisted of changing the beam's cross-sections and curvature to match the measured dimensions. In addition to changing the cross-section dimensions, the elastic modulus was also altered. The elastic modulus used for all three analyses was 204.3 GPa, as calculated from the tensile tests.

The results obtained from the FE analyses (Abaqus software) were then compared to the experimental data. Initial twist and tapered flanges of the beam were not measured; therefore, differences remained between the FE analyses and the experimental results. Three experimental beams were used to calibrate the FE models: the cantilever 1T1 (top flange loading, with $L_c = 2.5$ m) and the overhang beams of 3S1 (shear centre loading, with $L_b = L_c = 2.5$ m) and 5T1 (top flange loading, with $L_b = 5$ m and $L_c = 2.5$ m.

The results obtained from the FE models was consistent with the results obtained from the experimental data, with an over-estimate of 3.2% for the cantilever 1T1 and 2.4% for overhang beams 3S1 and 5T1, see Table 6.2.

Table 6.2: Comparing FE models to experimental results.

Beam setup	Experimental result (kN.m)	FE solid element model (kN.m)	Difference (%)
1T1	6.79	7.01	+ 3.2
3S1	6.94	7.11	+ 2.4
5T1	4.94	5.06	+ 2.4

Figures 6.2, 6.3 and 6.4 illustrate the buckling shape of the three beams that were modelled. It was noted that the deflection values were not the actual deflection, but a factor from the largest deflected node. The 3S1 model clearly showed the beam buckling in both overhang and backspan segment (see also Figure 6.5), whereas the 5T1 model buckled in the backspan segment only; this was consistent with the observations of the experiments. A reference line is provided in Figures 6.3 and 6.4 to illustrate the buckling direction and magnitude of the overhang beams effectively. Figure 6.5 illustrates the top view of the lateral deflection of the beams based on the FE solid element models. It was noted that the

buckled shape for both shear centre and top flange loading were similar to Bradford (1994) (Figure 2.9). In all three beams analysed, the top flange in the overhanging segment had the largest lateral deflection, as was stated by Bradford (1994). Similar to Bradford (1994), in the backspan, for the shear centre and top flange loading, the bottom flange and the top flange had the largest lateral deflection, respectively. The only difference compared to Bradford (1994) was the direction of buckling of both flanges in both segments. Both flanges in each segment of the FE solid element models deflected in the same direction. However, the difference in the backspan to overhang ratios analysed could be the difference in the buckling directions.
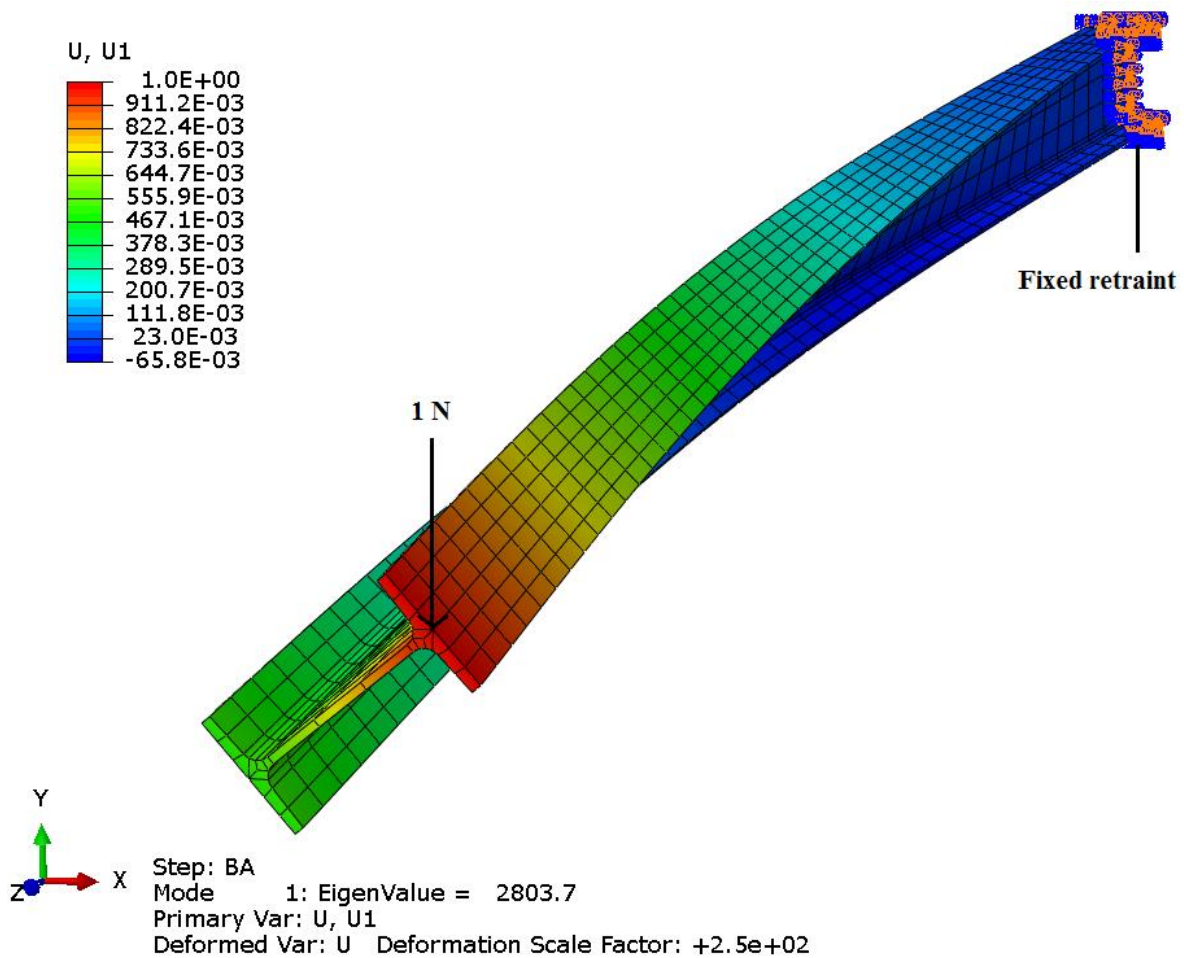
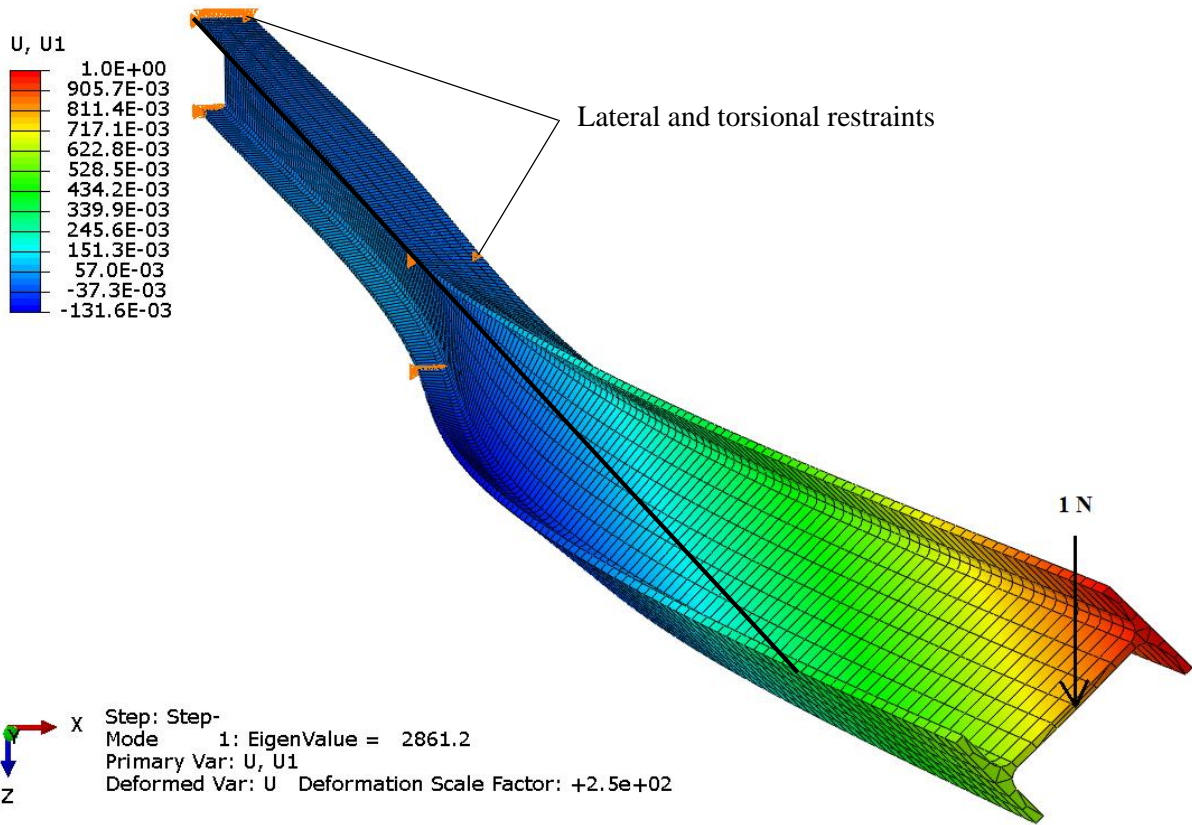**Figure 6.2: Buckling shape of cantilever 1T1 FE model.**
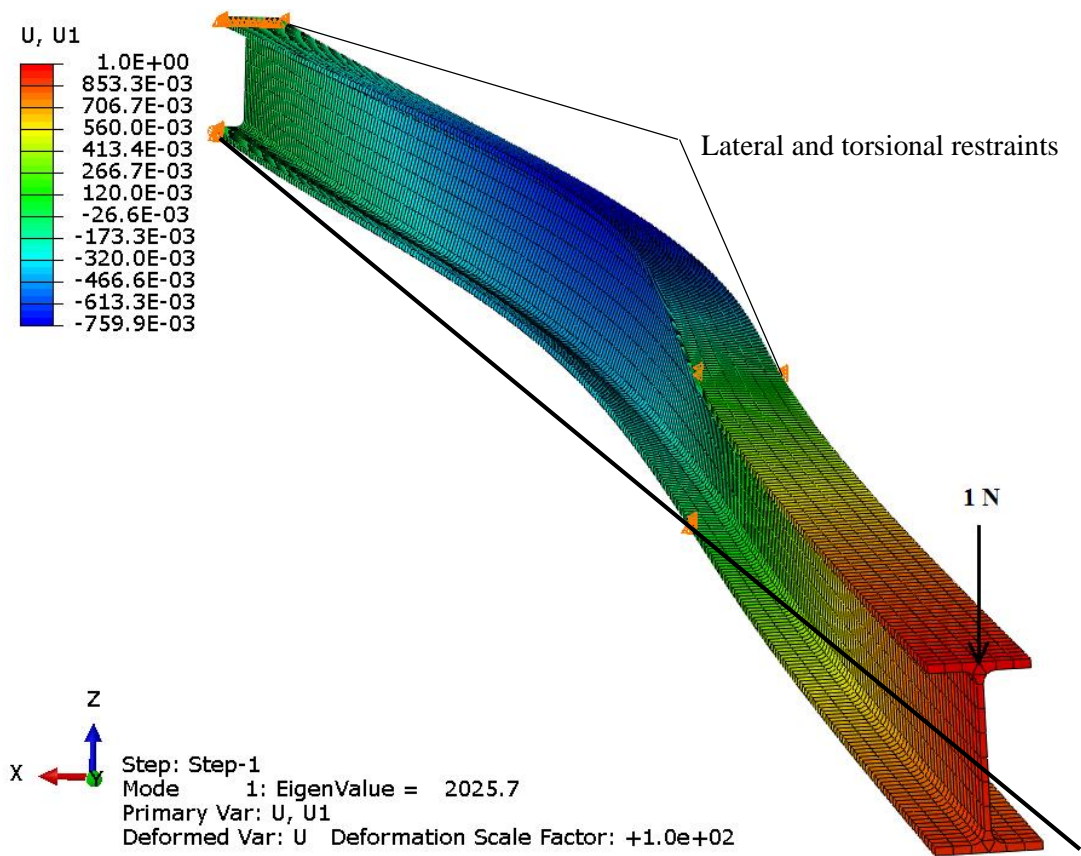
Figure 6.3: Buckling shape of overhang beam 3S1 FE model.

Figure 6.4: Buckling shape of overhang beam 5T1 FE model.

a)

b)

——— Top flange
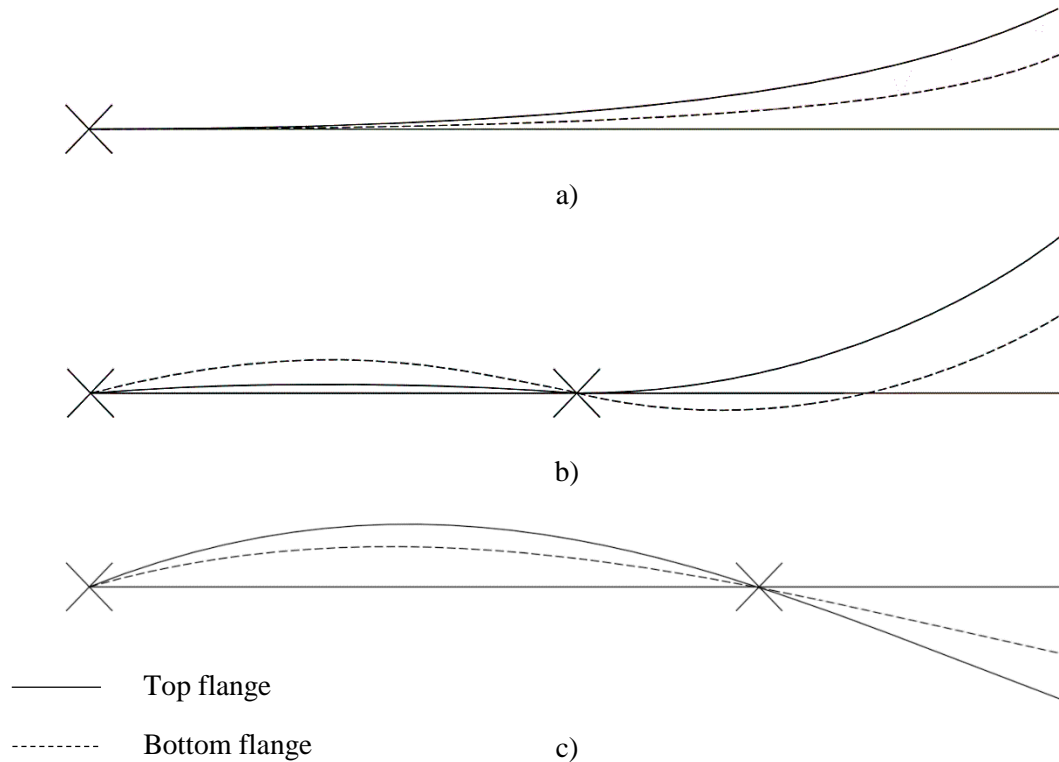
---------- Bottom flange

c)

Figure 6.5: Top view of lateral deflection of a) cantilever 1T1, b) overhang beams 3S1 and c) 5T1.

6.2   FE MODEL SETUP

Calibration of the Abaqus models had ensured that the FE models were a reliable and accurate method of determining the buckling capacities of beams. Therefore, a parametric study was achieved using a numerical method. The parameters that were analysed are the length of the overhanging segment L_c; the backspan to overhang ratio L_b/L_c; and the size of the beam. The forces were still applied at the unbraced free end of the overhanging segment and were either at the shear centre or on the top flange. From the data acquired, a relationship between the critical moment M_{cr} and the parameters analysed were obtained from curve fitting the FE results.

The beams modelled ranged from the smallest IPE$_{AA}$ beam to the largest 533x210 beam (see Appendix C for the geometrical properties of the beams). The backspan to overhang ratio ranged from 0.25 to 2.0, with increments of 0.25. The ratio of L_b/L_c was limited to 2.0, because larger ratios could have resulted in the backspan segment buckling. Eq. 3.2 is used to determine the elastic critical moment of the backspan of the beam. The lengths of the overhanging segments were long enough to be in the elastic buckling range, i.e. $M_{cr} < 0.67M_p$. Due to elastic buckling limiting overhang beams to large overhang lengths, a minimum length was required for the overhang length L_c, depending on the beam size. Thus, to obtain a relationship between buckling capacities and overhang lengths, various overhang

lengths were analysed. Currently, the maximum beam lengths used in South Africa are limited to 13 m (for transport considerations), thus some of the analyses were for academic purposes only (to obtain relationships). The overhang lengths used in the analyses are tabulated in Table 6.3. The values in brackets refer to top flange loading only, as these beams were still in the elastic range.

Table 6.3: Size and lengths of beams analysed.

Beam designation	Length of overhang, L_c
IPE$_{AA}$100	2, 2.5, 3 and 3.5 m
IPE 200	3, 3.5 and 4 m
203x133x25	(2, 2.5, 3, 3.5), 4, 4.5, 5, 5.5 and 6 m
305x165x40	(2, 3, 4), 4.5, 5, 5.5, 6, 7 and 8 m
406x178x54	4.5, 5.5 and 6.5 m
406x178x74	(2, 3, 4), 5, 5.5, 6, 6.5, 7 and 7.5 m
533x210x82	(5), 6 and 7 m
533x210x122	(3, 4, 5), 6, 6.5, 7 and 9 m

6.3 BUCKLING CAPACITY

The buckling capacity for all the analyses, which was in Newton, was converted to kN.m (critical moment) by multiplying the buckling load with the length of the overhang. For simplicity, only graphs for the results of the 203x133x25 I-beam were added in this chapter for explanation purposes. The complete results of M_{cr} from the analyses are attached in Appendix A. The discussions and conclusions that follow were based on all the analyses conducted, which apply to all beam sizes and lengths.

- The critical moment, for either shear centre or top flange loading, decreased as the ratio of L_b/L_c increased. However, for top flange loading, this observation was less profound.
- When the load applied was at the shear centre of the beam, the buckling capacity became less sensitive to the overhang length L_c as the ratio L_b/L_c increased.
- Loading the beam on the top flange decreased the buckling capacity of the beam significantly.
- However, as the overhang length L_c increased, the reduction in capacity when the beam was loaded on the top flange became less.
- All beams failed by LTB and not lateral-distortional buckling (visually verified by models).
- These observations were consistent with all the beam sizes analysed.

With various overhang lengths L_c, Figures 6.6 and 6.7 illustrate the observations made above for a 203x133x25 I-beam with shear centre and top flange loading, respectively.
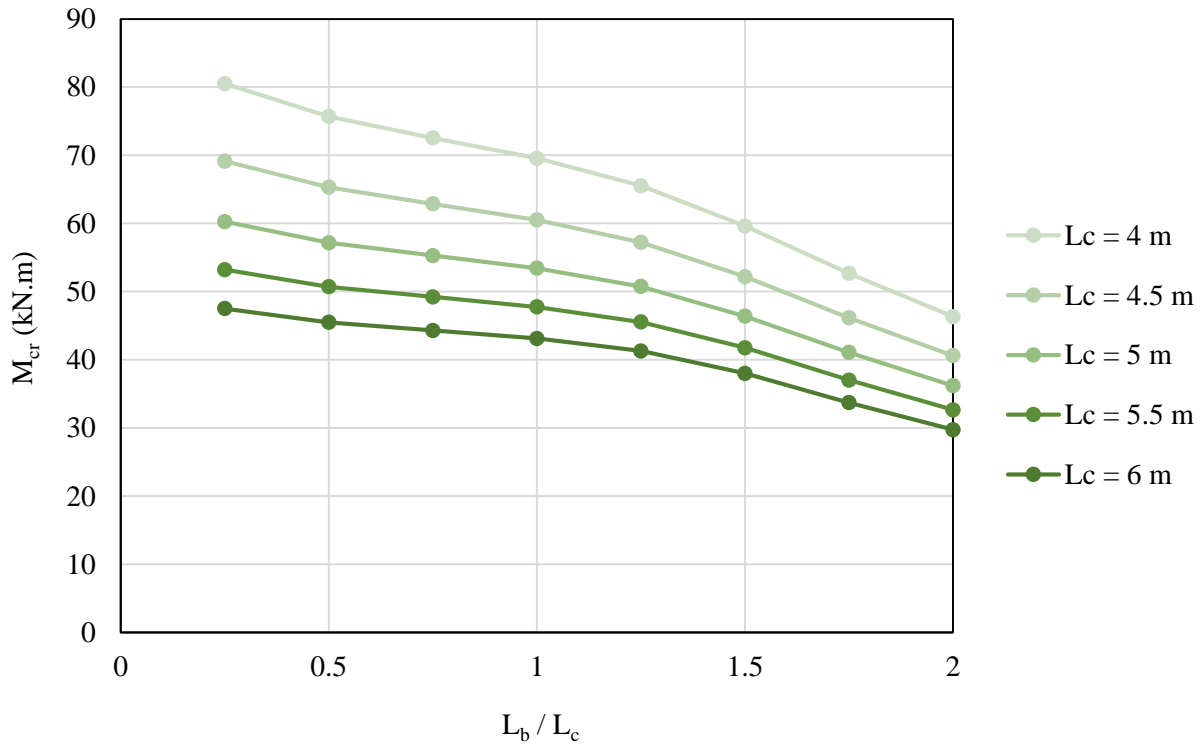

Figure 6.6: Critical buckling moments for a 203x133x25 beam with shear centre loading.
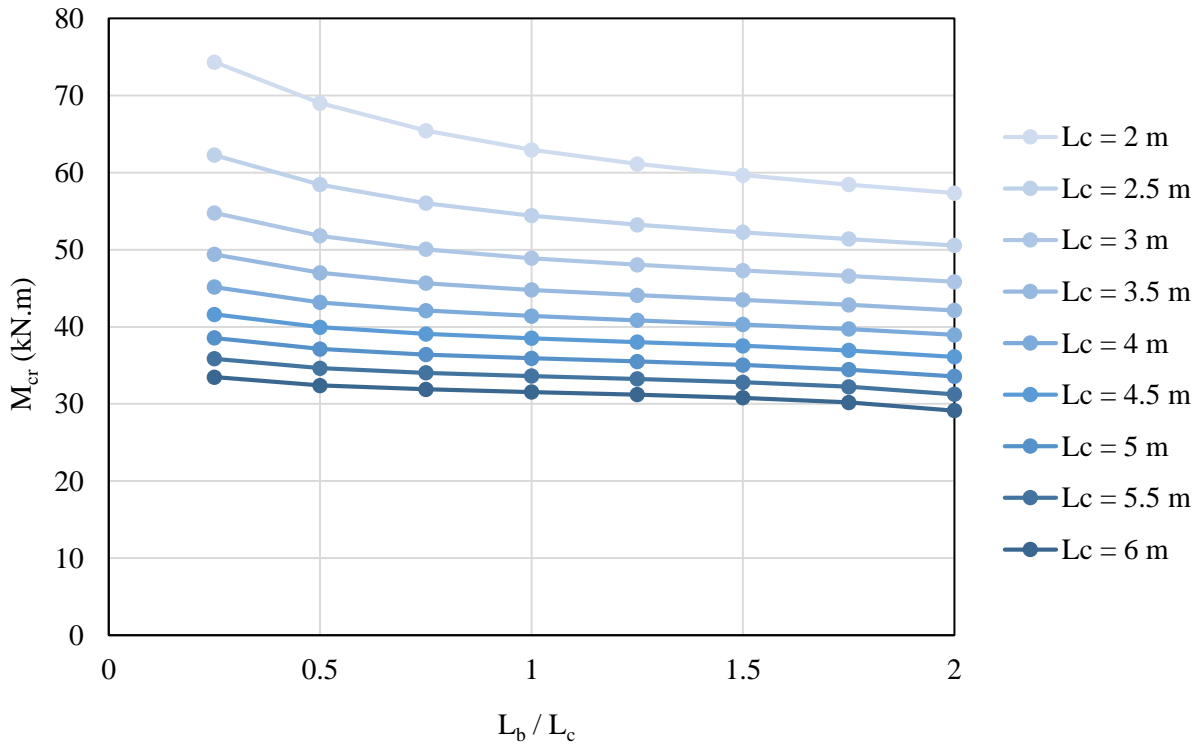

Figure 6.7: Critical buckling moments for a 203x133x25 beam with top flange loading.

6.4 NON-DIMENSIONAL BUCKLING PARAMETER

Comparing the critical buckling moments for different beams with different overhang lengths was difficult as many parameters were influencing the buckling capacity. Instead, the non-dimensional part of the buckling equation was used. The beam size ($\sqrt{EI_yGJ}$) and overhang length (L_c), was therefore, already taken into account, resulting in better comparisons and conclusions. Timoshenko and Gere (1961) formulated Eq. 6.1, which was specifically derived for cantilever beams and not simply supported beam. This equation was then rewritten in Eq. 6.2, with γ_2 replaced with S, which is also a non-dimensional parameter, but is specifically for overhang beams. The parameter S is very similar to the effective length factor k. The length of the backspan L_b was incorporated in the parameter S via the ratio L_b/L_c (discussed later on). The value/function of S at this point was still unknown and was later formulated using the FE results. It was first necessary to understand how S varies for different beam sizes and lengths, before it was broken down to take into account the backspan to overhang length. The same procedure as in Chapter 3 was used to formulate the design equations to determine the critical moments.

$$P_{cr} = \gamma_2 \frac{\sqrt{EI_yC}}{L^2}$$
Eq. 6.1

Where:

γ_2 = Dimensionless factor depending on the ratio of $L^2\,C/C_1$.

C = GJ, Torsional rigidity.

C_1 = EC_w, Warping rigidity.

$$M_{cr} = S\frac{\pi\sqrt{EI_yGJ}}{L_c}$$
Eq. 6.2

$$S = \frac{M_{cr}L_c}{\pi\sqrt{EI_yGJ}}$$ Non-dimensional buckling parameter.
Eq. 6.3

Increasing S therefore increased the critical moment. The constant π, being a constant, was added to the dimensioned part of the equation, thus simplifying the formulation of S. Using the critical moments (M_{cr}) obtained from FE results, S was determined and plotted against the backspan to overhang ratio. The relationship is illustrated in Figures 6.8 and 6.9 for a 203x133x25 I-beam, for shear centre and top flange loading, respectively. The non-dimensional buckling parameter is not a constant. SANS-10162-1 and BS 5950-1 provide a single set of effective length factors. Instead, the

non-dimensional part of the equation depended on the length of the overhanging segment, the ratio of L_b/L_c and the size of the beam.

- Figures 6.8 and 6.9 illustrate that the buckling parameter S decreased when L_b/L_c or the overhang length increased.
- The buckling parameter was less sensitive to the overhang length when the load was applied at the shear centre.
- The buckling parameter was less sensitive to the ratio of L_b/L_c when the load was applied on the top flange.
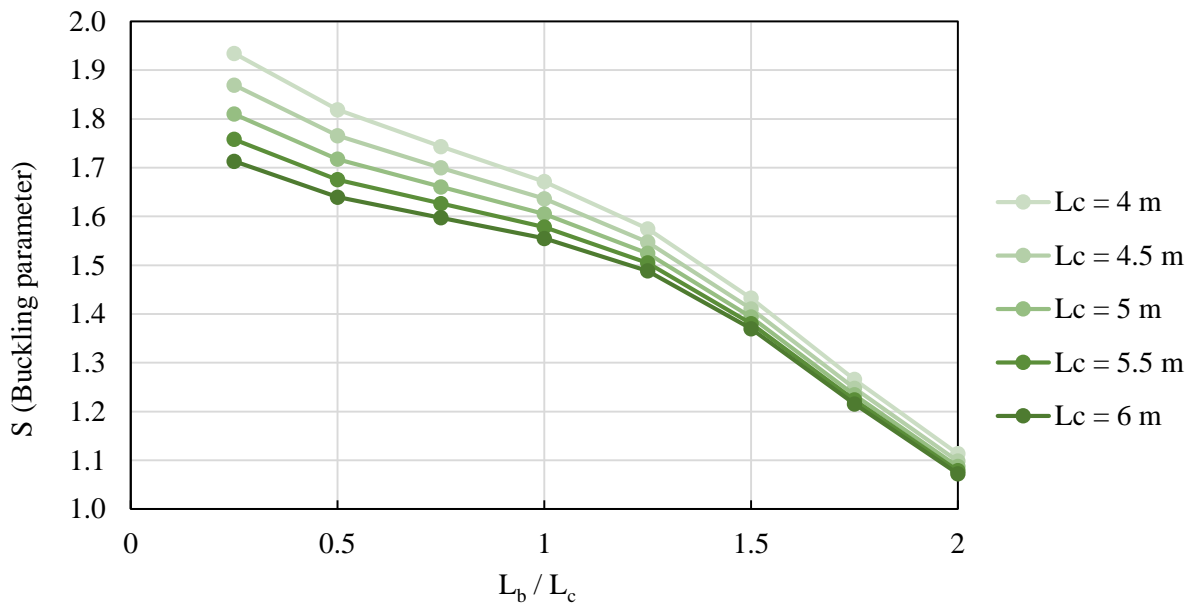

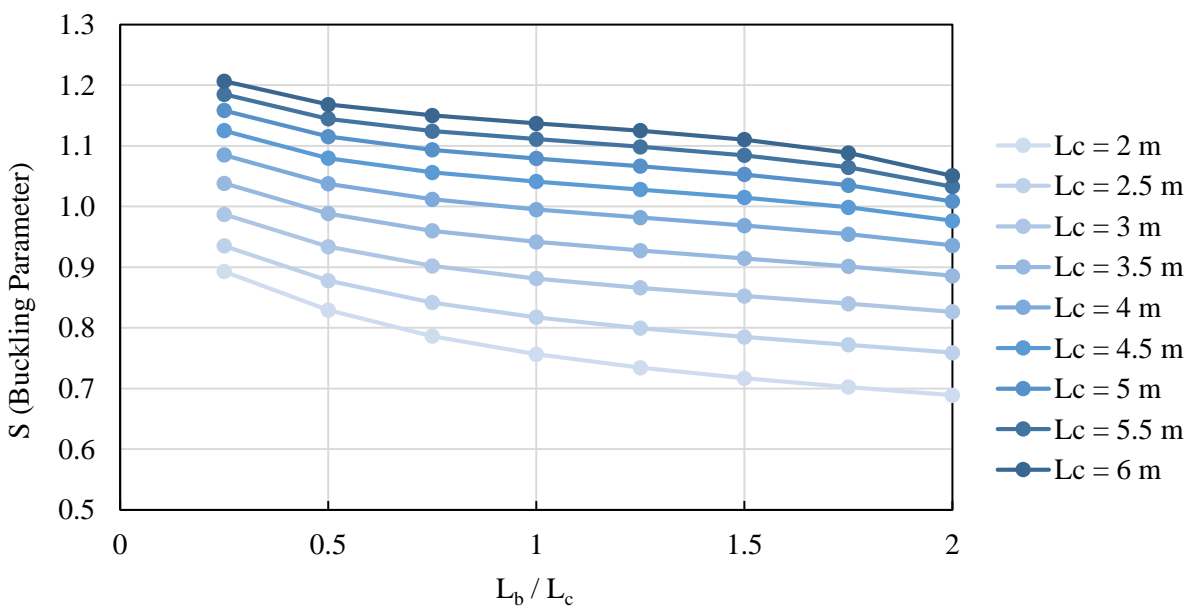**Figure 6.8: Buckling parameter for 203x133x25 I-beam with shear centre loading.**

Figure 6.9: Buckling parameter for 203x133x25 I-beam with top flange loading.

6.5 COMBINING THE BUCKLING AND TORSIONAL PARAMETERS

Instead of comparing the dimensionless parameter to both the overhang length and the size the beam independently, the comparisons were made concerning the torsional parameter K. The torsional parameter K ($K = \gamma^2$, which was used by Timoshenko and Gere's (1961) for a simply supported beams) includes both the torsional properties as well as the length of the overhangs, making it unique for any beam size and length. As a reminder, the torsional parameter K was formulated as $K = \sqrt{(\pi^2 E C_w)/(G J L_c^2)}$, using the length of the overhang and *not* the length of the entire beam. The buckling parameter S therefore, is only influenced by the ratio of L_b/L_c and the torsional parameter K.

The comparisons of S vs. K are illustrated in Figures 6.10 and 6.11 for various backspan to overhang ratios. Figures 6.10 and 6.11 combines all the beams analysed by using the torsional parameter K, for shear centre and top flange loading, respectively. The torsional parameter consists of three beam parameters that may vary: C_w, J and L_c^2. Thus, a long 533x210x122 I-beam could have the same torsional parameter as a short IPE$_{AA}$100 I-beam. However, the curves were not smooth lines and did not consist of a clear relationship between the three variables.

Instead of comparing S vs. K, the buckling parameter S was divided by the torsional parameter K (also dimensionless). Eq. 6.3 then became Eq. 6.4. The 'normalised' non-dimensional buckling parameter S/K was computed for all the beams analysed (any beam size or length) as done previously. The comparisons of S/K against K and L_b/L_c are illustrated in Figures 6.12 and 6.13. Definitive relationships between the three variables (S/K, K and L_b/L_c) exists, hence, conclusions were possible.

$$\frac{S}{K} = \frac{M_{cr} L_c}{\pi K \sqrt{EI_y GJ}}$$

Eq. 6.4

- Increasing the torsional parameter of the beam decreased S/K, especially when the load was applied on the top flange.
- The non-dimensional parameter S/K was less sensitive to the ratio L_b/L_c when the load was applied on the top flange. This statement deemed true for the entire range of the torsional parameter K analysed.
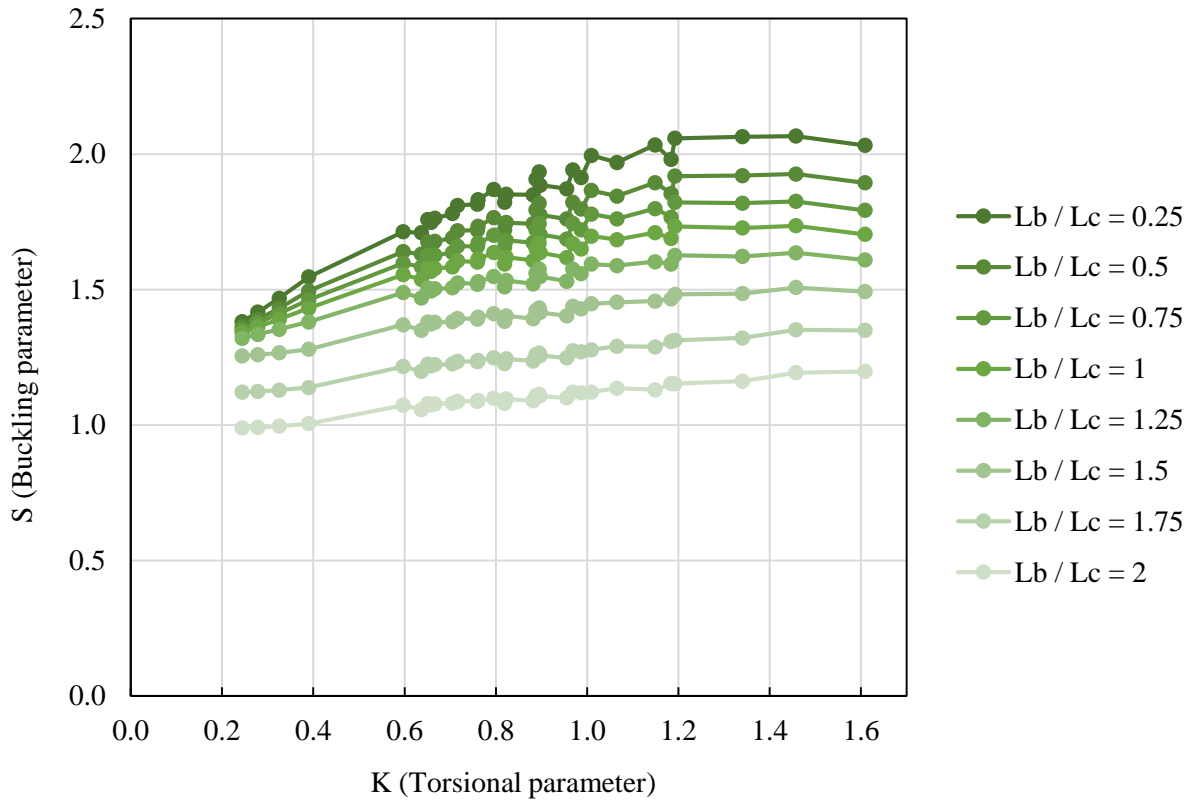
Figure 6.10: Buckling parameter vs. the torsional parameter with shear centre loading.
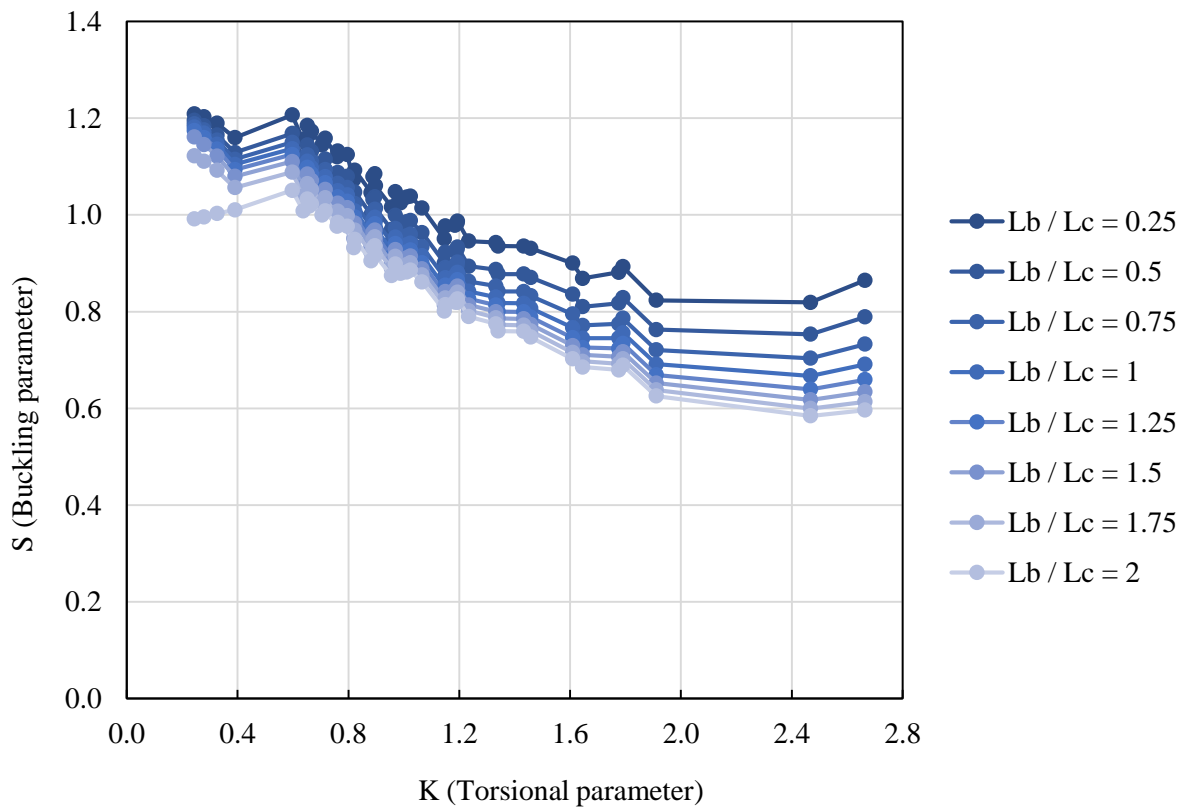

Figure 6.11: Buckling parameter vs. the torsional parameter with top flange loading.
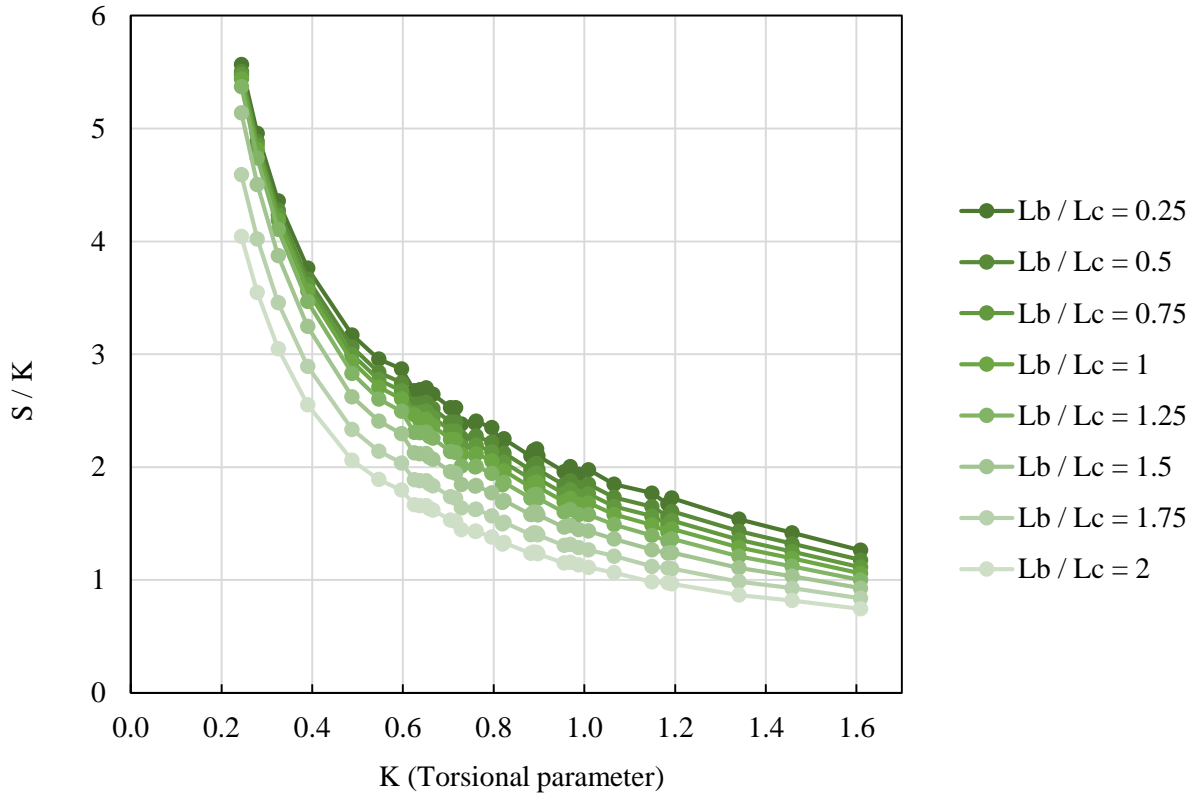
Figure 6.12: Normalised non-dimensional buckling parameter with shear centre loading.
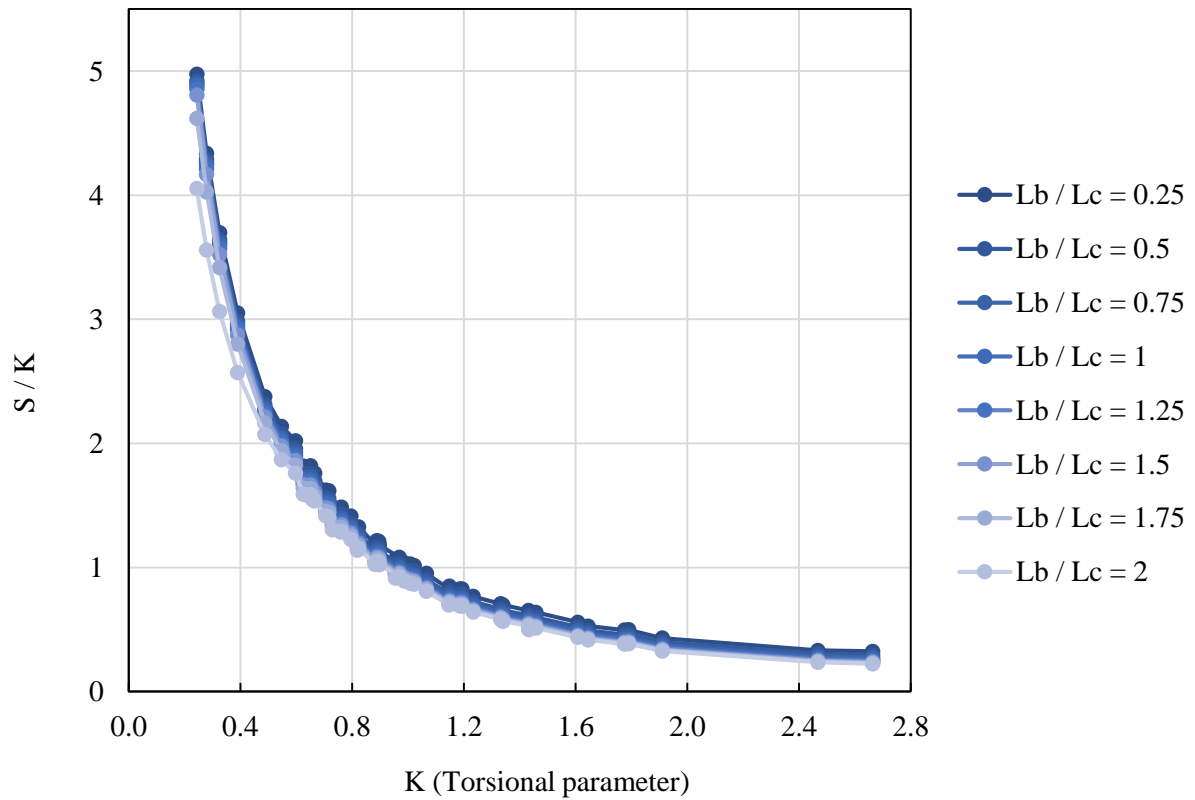

Figure 6.13: Normalised non-dimensional buckling parameter with top flange loading.

The torsional parameter was another useful parameter when comparing the difference in critical moments between the shear centre and top flange loading (Figure 6.14). Increasing the torsional parameter K increased the difference in critical moments between the shear centre and top flange loading. Increasing the backspan to overhang ratio reduced the difference, up to a point where the difference became negligible. Thus, the buckling capacity was independent on the distance between shear centre and load applied for large L_b/L_c and small K.
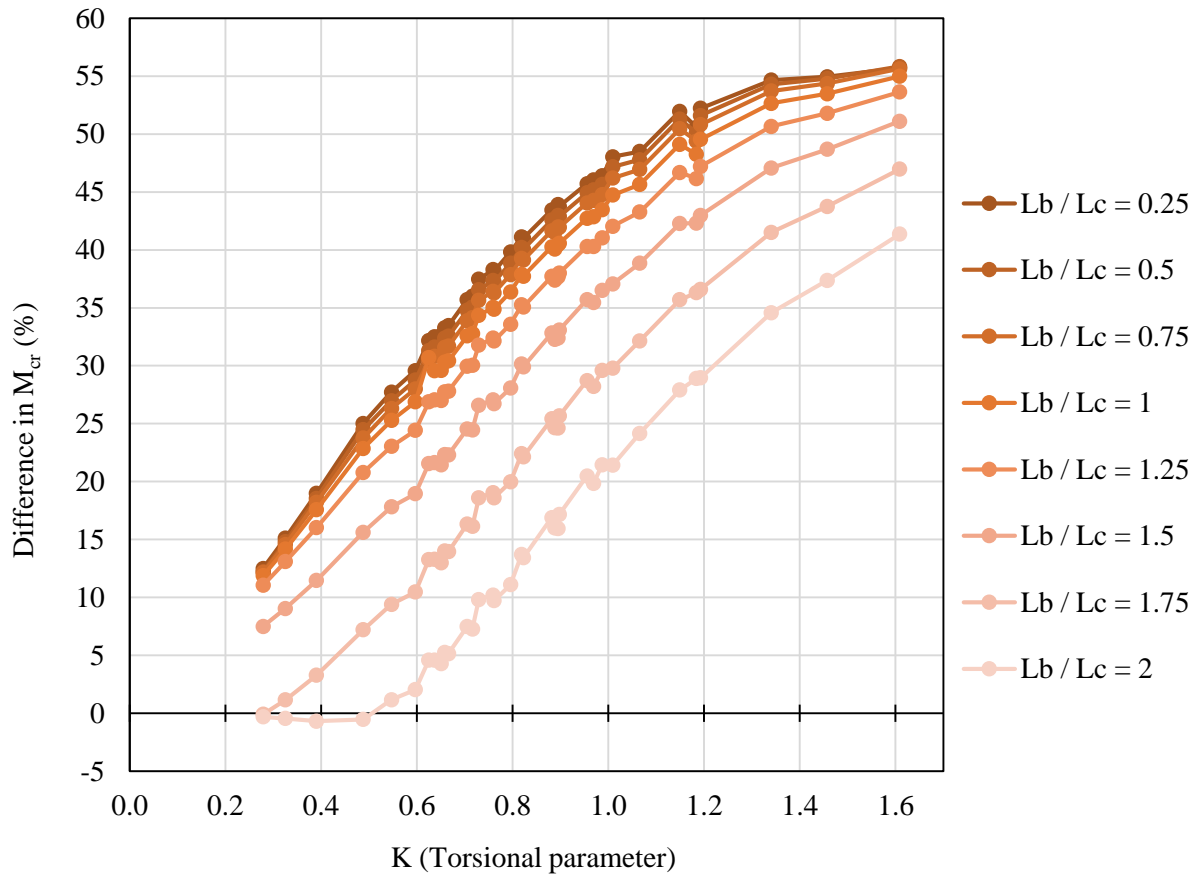

Figure 6.14: Difference in critical moments between the shear centre and top flange loading.

6.6 DESIGN EQUATION FOR NON-DIMENSIONAL BUCKLING PARAMETER

The normalised non-dimensional buckling parameter S/K was related to the torsional parameter K via power function curves (Eq. 6.5). The factors A and B were not constants but depended on the backspan to overhang ratios and the load height.

$$S/K = AK^B \hspace{5cm} \text{Eq. 6.5}$$

Rewriting the equation Eq. 6.5, the buckling parameter S became Eq. 6.6. A factor C was added to adjust the equation to ensure conservative results while reducing over-estimation of the buckling capacity to less than 1 % (see Section 6.7).

$$S = AK^{(B+1)} + C \hspace{4.5cm} \text{Eq. 6.6}$$

For each value of the ratio L_b/L_c, the factors A and B were determined via power function trendlines. To obtain a smaller difference between design equations and FE results, the two 'IPE' beams were separated from the 'universal' beams (universal beams referring to the 203x133x25 beams etc.). Therefore, for the two different types of beams, two different sets of factors were obtained. These values for A and B were plotted against L_b/L_c, as shown in Figures 6.15 and 6.16 (universal beams). The factors A and B were quadratic functions (Eqs. 6.7, 6.8, 6.9 and 6.10). The design equations, which were also plotted in Figures 6.15 and 6.16, were conservative. These equations were calibrated for the range of $0.25 \leq L_b/L_c \leq 2.0$. For the IPE beams the factors A and B ensured conservative results without the need of adjustments, hence $C = 0$.

Universal beams:

Shear centre:	$A = -0.121(L_b/L_c)^2 - 0.2(L_b/L_c) + 1.89$	Eq. 6.7
	$B = +0.044(L_b/L_c)^2 - 0.205(L_b/L_c) - 0.7$	Eq. 6.8
	$C = +0.033(L_b/L_c) + 0.016$	Eq. 6.9
Top flange:	$A = +0.023(L_b/L_c)^2 - 0.162(L_b/L_c) + 0.91$	Eq. 6.10
	$B = +0.03(L_b/L_c)^2 - 0.2(L_b/L_c) - 1.206$	Eq. 6.11
	$C = +0.016(L_b/L_c) + 0.07$	Eq. 6.12

IPE beams:

Shear centre: $A = -0.136(L_b/L_c)^2 - 0.11(L_b/L_c) + 1.8$ Eq. 6.13

$B = +0.023(L_b/L_c)^2 - 0.15(L_b/L_c) - 0.75$ Eq. 6.14

Top flange: $A = +0.069(L_b/L_c)^2 - 0.225(L_b/L_c) + 1.12$ Eq. 6.15

$B = +0.121(L_b/L_c)^2 - 0.266(L_b/L_c) - 0.99$ Eq. 6.16

The equations above were used in conjunction with Eq. 6.6 to obtain the non-dimensional buckling parameter for any overhang length, beam size and backspan to overhang ratio, for either shear centre or top flange loading. Eq. 6.6 was then used with Eq. 6.2 to determine the critical moment of an overhang beam. Thus, the critical moment for any overhang I-beam is:

$$M_{cr} = (AK^{(B+1)} + C)\left(\frac{\pi\sqrt{EI_yGJ}}{L_c}\right)$$ Eq. 6.17

Where:

A, B & C = Factors as defined in Eqs. 6.7 - 6.16, depending on distance between shear centre and load applied and the type of beam.
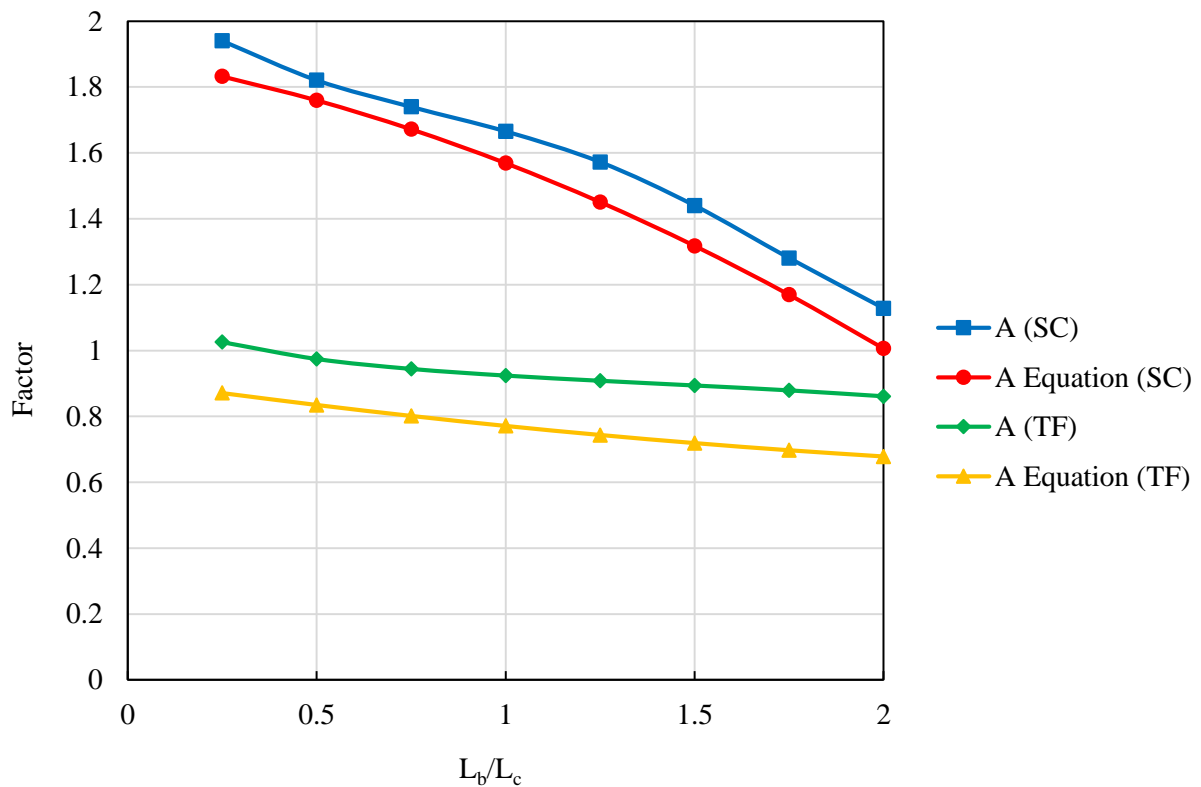

Figure 6.15: Comparing factor A against L_b/L_c for universal beams.
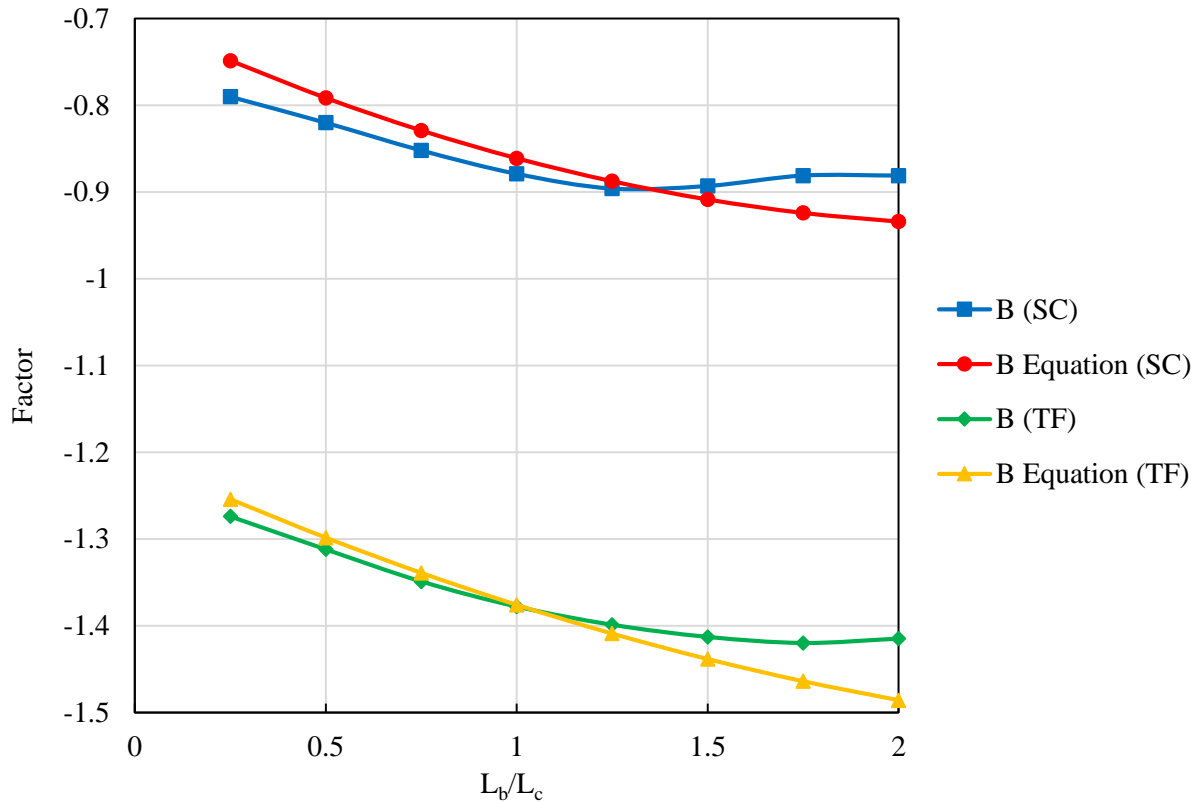
Figure 6.16: Comparing factor B against L_b/L_c for universal beams.

See Appendix D for a worked out example using the proposed design method. In addition, the proposed method is compared to the current SANS 10162-1 method using an equal spanned overhang beam.

6.7   RESULTS OF EMPLOYING THE PROPOSED EQUATION

The proposed equations in Section 6.6 were compared to the FE solid element results and showed good correlation. The maximum and minimum difference between the design equations and FE analyses are tabulated in Table 6.4. For each backspan to overhang ratio considered, the maxima and minima obtained were for all overhang lengths analysed. The results from the design equations were conservative, meaning the buckling capacity was slightly less than observed from FE analyses, denoted with a minus sign. With the aid of the adjustment factor C, the equations were conservative up to 6.7% and 12.9% for the shear centre and top flange loading, respectively. The maximum over-estimate was less than 1% (the largest positive difference between FE results and design equation). As an example, Figure 6.17 illustrates the comparison for a 203x133x25 I-beam, with an overhang length of 5 m. The buckling capacity for both shear centre and top flange loading were plotted.

Table 6.4: Difference between equations and FE analyses.

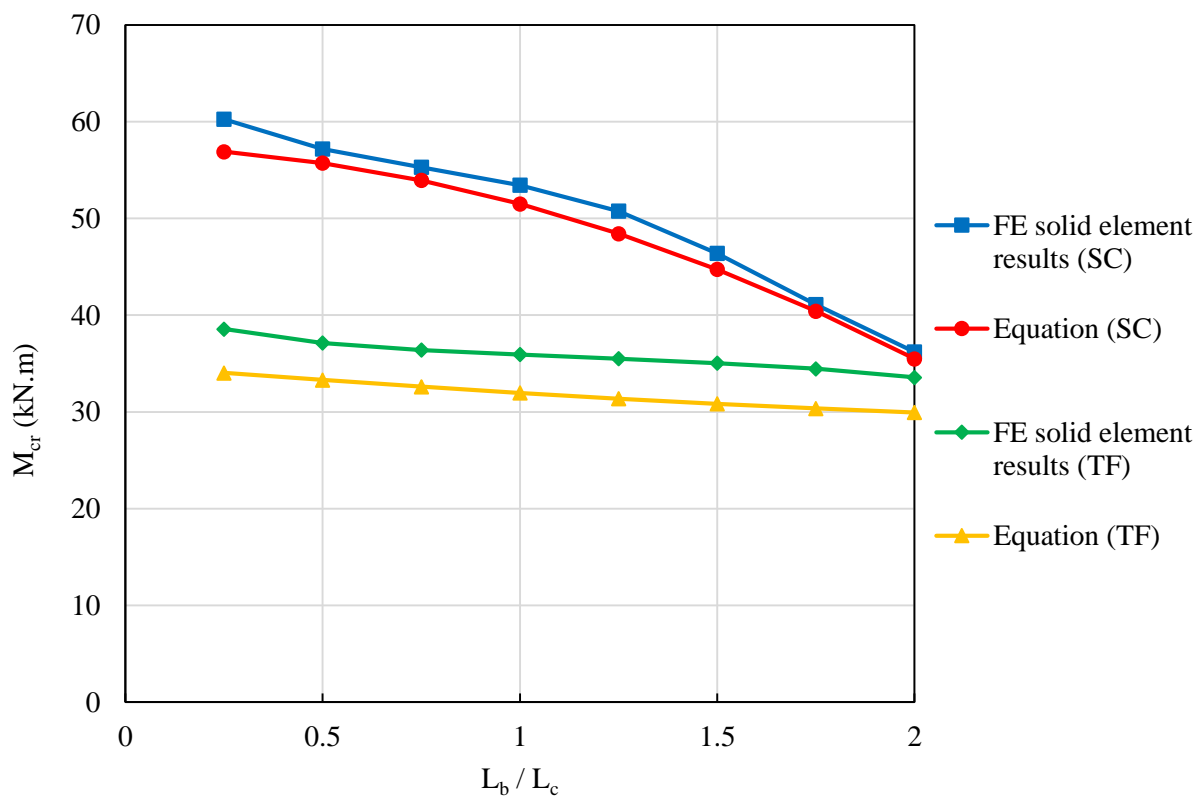| Beam designation	Maximum (%)		Minimum (%)	
	Shear centre	Top flange	Shear centre	Top flange
IPE$_{AA}$100	- 4.8	- 7.1	+ 0.9	+ 0.97
IPE 200	- 5.1	- 7.0	- 1.2	+ 0.88
203x133x25	- 6.6	- 12.8	- 1.4	- 5.7
305x165x40	- 5.5	- 12.9	+ 0.1	- 4.3
406x178x54	- 6.7	- 11.8	+ 0.5	- 5.4
406x178x74	- 4.5	- 11.1	- 0.9	- 1.5
533x210x82	- 5.5	- 9.7	- 0.9	- 3.9
533x210x122	- 3.1	- 9.3	+ 0.5	+ 0.6

Figure 6.17: Comparing design equation to FE solid element results for 203x133x25 I-beam with L_c = 5 m.

6.8   COMPARING FE RESULTS TO EXPERIMENTS

Both the FE solid element results from the Abaqus software and the design equations were compared to the FE shell element results noted from the Strand7 software and the physical experiments conducted. The comparisons were applicable only to the IPE$_{AA}$100 beam with an overhang length of 2.5 m, as these were the only beams tested experimentally. The design equation and FE solid element results showed good correlation compared to the experimental data for shear centre loading. However, for top flange loading, the design equation and FE shell element results for M_{cr} were significantly less than obtained by experimental tests. Imperfections such as tapered flanges could be a contributing factor for the significant difference. Therefore, the Abaqus models were modified to include tapered flanges. The flanges were given a taper of 1 mm at the interface with the web. As can be seen in Figures 6.18 and 6.19, the effect of the taper had a large impact on the critical moment of the beam. With the load applied at the shear centre, a 1 mm tapered flange increased the critical moment of the beam by 19% when $L_b/L_c = 1$. Similarly, the critical moment was increased by 22% when the load was applied on the top flange. Therefore, large differences in critical moments between experimental data and FE analyses were explained by possible imperfections in the cross-section of the beam.

The Strand7 shell element models were modelled using two torsional springs at the end of the beam. These torsional springs overcame the deficit in torsional stiffness due to the fillets of the beam not being modelled. However, these two torsional springs were concentrated at the free end of the beam. The Abaqus solid element model, which used the exact shape and size of a beam, as specified by the SASCH (SAISC, 2013), already contained the exact torsional stiffness. The difference between the two models (programs) was the 'spread' of the torsional stiffness. In Abaqus, the exact torsional stiffness was spread out along the beam, whereas in the Strand7 models, the exact torsional stiffness was concentrated at two points at the end of the beam. This slight difference in torsional stiffness modelling partly explained the difference between the results from the FE models, as illustrated in Figures 6.18 and 6.19.

To prevent rigid body movement of the model and to obtain a model that simulates the experiments performed, the bottom flanges in the external support of the Abaqus solid element models were restricted in the longitudinal direction. The preliminary FE shell element models in Strand7 had slightly different restraints at the external support, in which a single point along the web of the beam was restrained against longitudinal movement (this method of restraint was not practical for experiments). The difference in restraining the external support resulted in a slight difference in warping stiffness and consequently, the critical buckling moment of the beams.
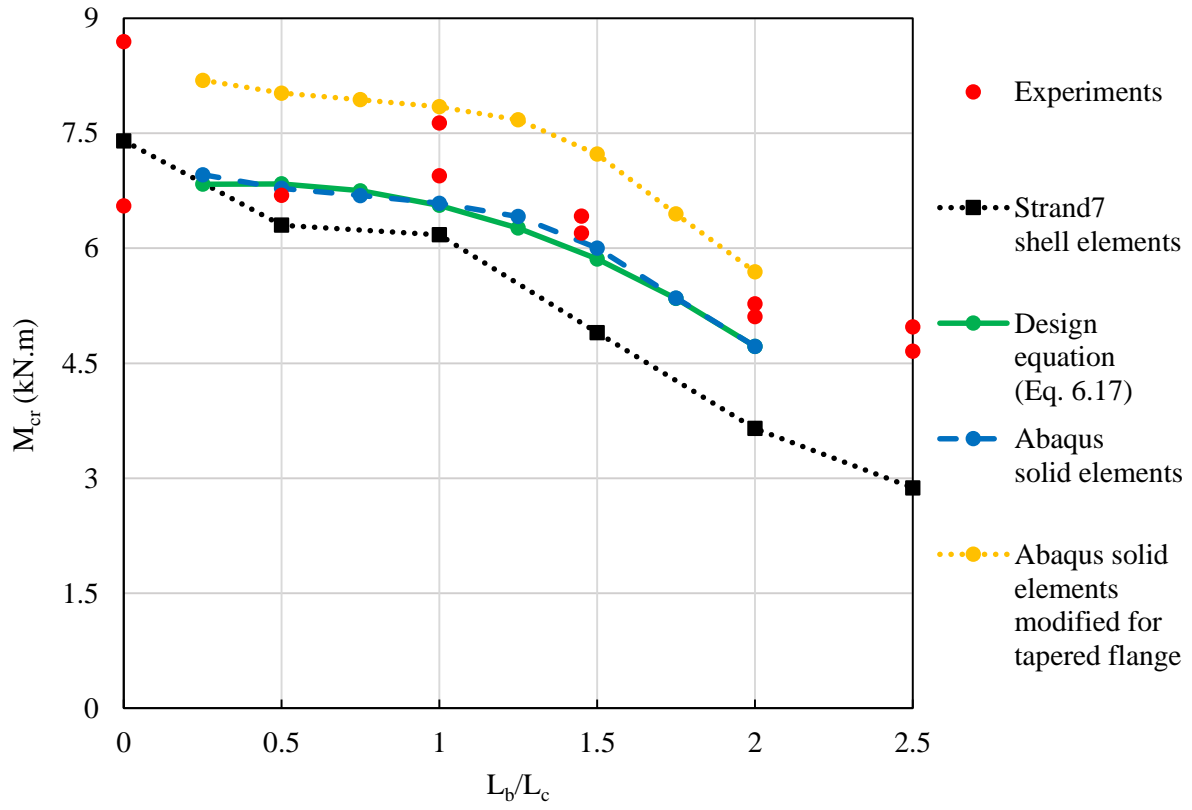
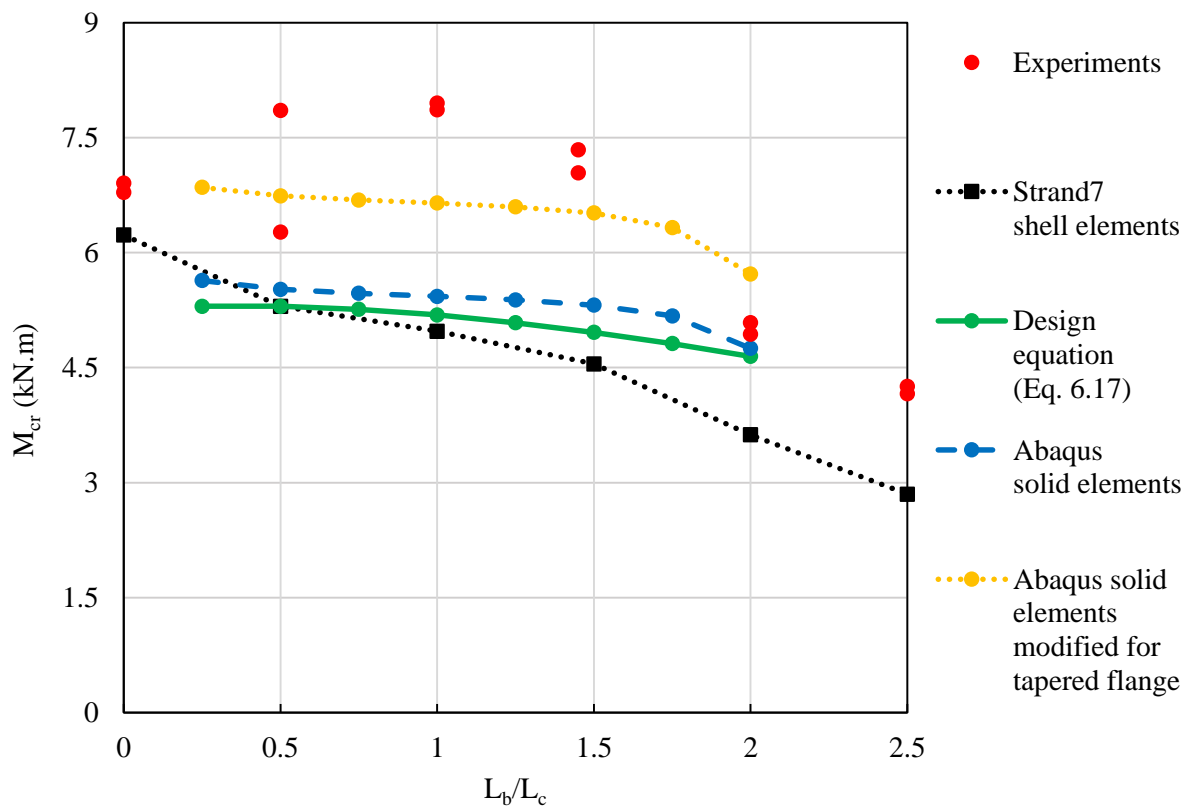**Figure 6.18: Comparing FE results and design equation to experiments for shear centre loading.**

Figure 6.19: Comparing FE results and design equation to experiments for top flange loading.

6.9   COMPARING RESULTS TO ESSA AND KENNEDY

Essa and Kennedy (1994) was the only previous investigation that included the backspan to overhang ratio. The design equations as discussed in Section 6.6 were therefore also compared to the equations given by Essa and Kennedy (1994). Table 6.5 shows the difference between the equations provided by Essa and Kennedy (1994) and the design equations for equal backspan and overhang lengths. When the load was applied at the shear centre, the critical moment given by Essa and Kennedy (1994) was less than the design equation. With top flange loading, the critical moment was higher, especially for long overhanging segments. In Table 6.5, a negative value denotes that the design equation had a smaller buckling capacity compared to Essa and Kennedy (1994).

Table 6.5: Comparing the design equation to Essa and Kennedy.

Beam designation	Shear centre	Top flange
IPE$_{AA}$100, L_c = 2.5 m	+ 4.1%	- 40.3%
203x133x25, L_c = 4 m	+ 16.3%	- 6.0%
203x133x25, L_c = 5 m	+ 14.3%	- 13.6%

Figure 6.20 illustrates the difference between the two equations for an IPE$_{AA}$100 beam with a 2.5 m overhang length. Whereas Figures 6.21 and 6.22 compares the two equations for a 203x133x25 I-beam with an overhang length of 4 m and 5 m, respectively. All three figures compared shear centre and top flange loading. The top flange loading equation given by Essa and Kennedy (1994) did not take into account the length of the overhang. Therefore, the critical moment could be higher or less compared to shear centre loading, depending on the length of the overhang.
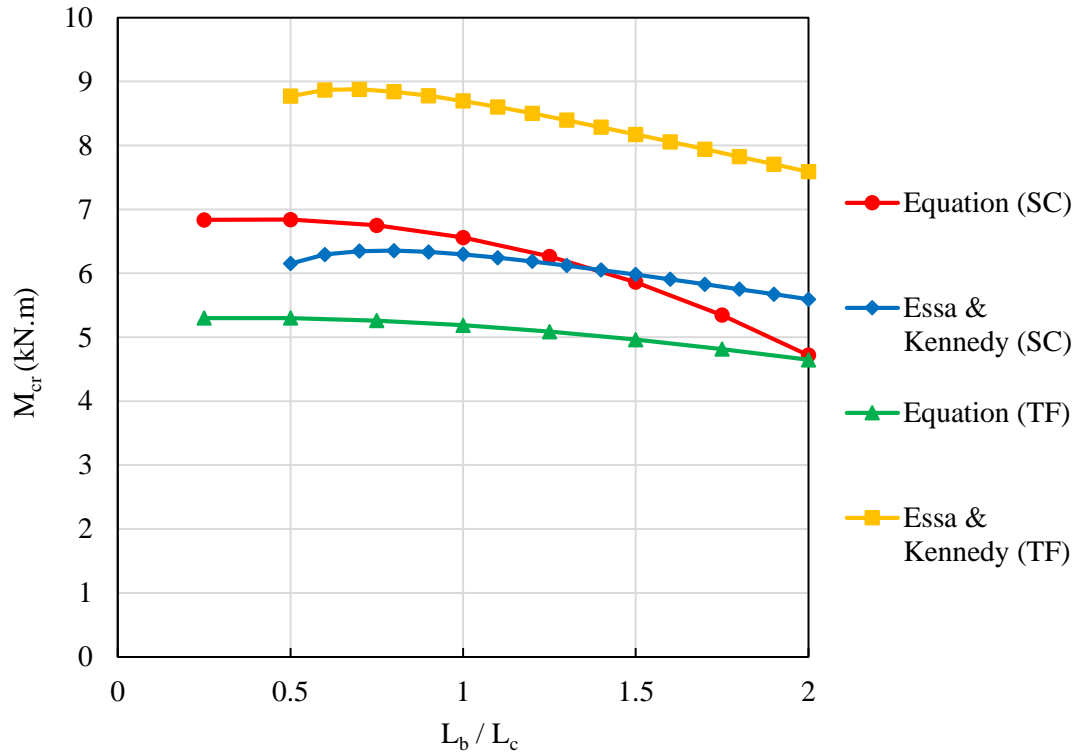
Figure 6.20: Comparing equations to Essa and Kennedy for IPE$_{AA}$100 with 2.5 m overhang length.
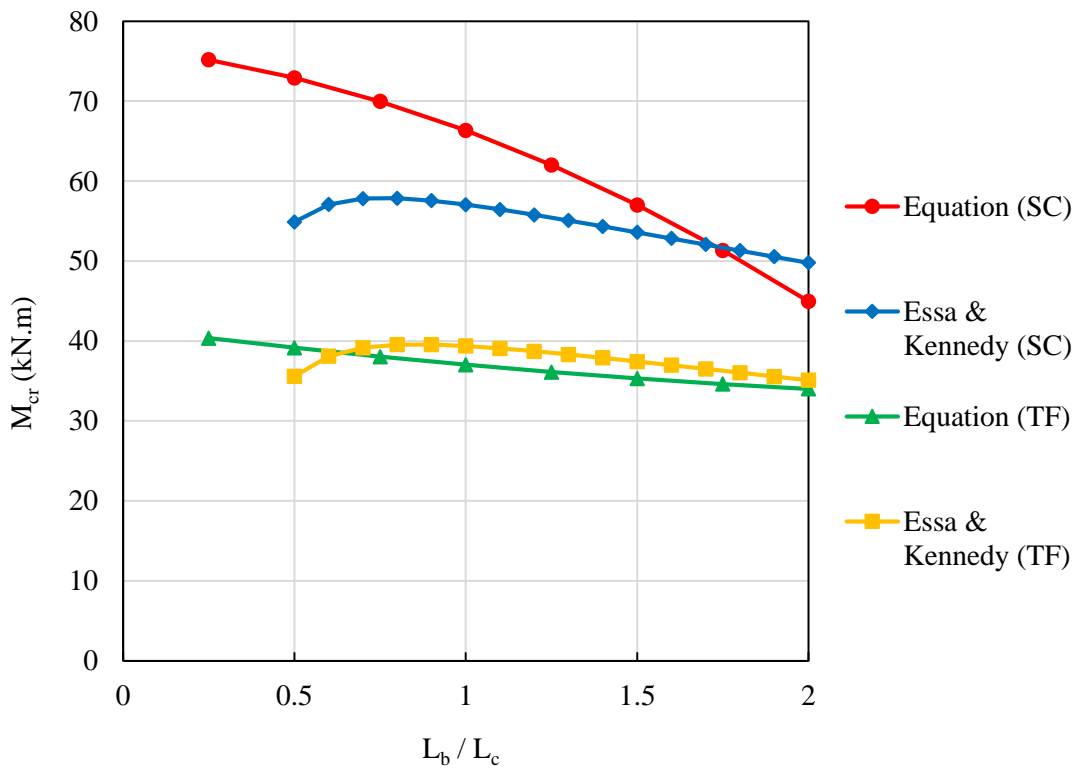

Figure 6.21: Comparing equations to Essa and Kennedy for 203x133x25 I-beam with 4 m overhang length.
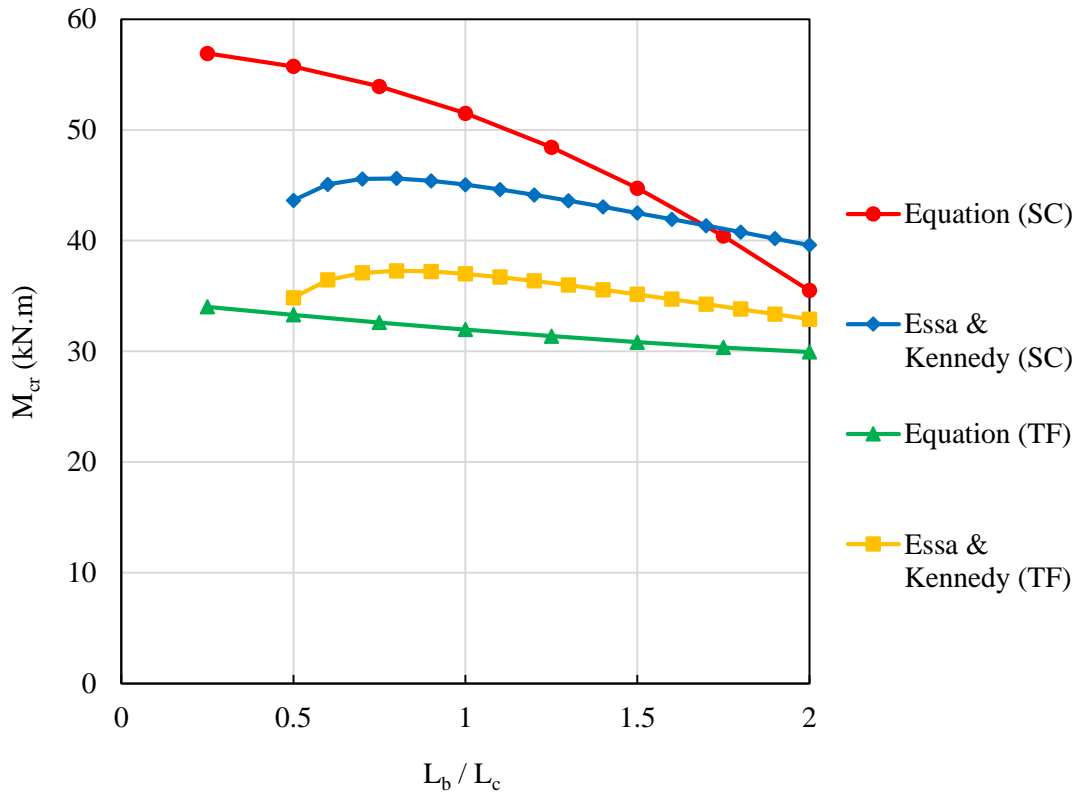
Figure 6.22: Comparing equations to Essa and Kennedy for 203x133x25 I-beam with 5 m overhang length.

7. CONCLUSIONS AND RECOMMENDATIONS

7.1   CONCLUSIONS

The observations and conclusions made throughout this report are summarised within this chapter. The results of the objectives, as outlined in Chapter 1, are also presented.

7.1.1   OBSERVATIONS BASED ON CURRENT METHODS

The literature study provided knowledge in the field of lateral-torsional buckling of beams. It was noted that CAN/CSA-S16-01 uses no effective length factors in determining the critical buckling moment of a beam. BS 5950-1 and SANS 10162-1 have two effective length factors for overhang beams which are laterally and torsionally restrained. Thus neither BS 5950-1 nor SANS 10162-1 takes into account the effect of the backspan.

Nethercot (1973), Andrade (2007) and Trahair (2008) each have formulated equations for both cantilevers and overhang beams. Andrade (2007) and Trahair (2008) took into account the effect of warping at the restraints but not the length of the backspan. The method by Nethercot (1973) is only valid for beams with equal overhang and backspan lengths. Kirby and Nethercot (1979) stated that the effective overhang length must be at least as long as the backspan. These literatures above provide different methods for determining the critical buckling capacity of an overhang beam, but interaction buckling was neglected in each of those methods.

Essa and Kennedy (1994) investigated the effect of interaction buckling in the overhanging segment of overhang beams. However, their equation is non-conservative for top flange loading as it neglects the overhang length. This study assumed interaction buckling in both segments and investigated different overhang lengths for both shear centre and top flange loading. The equation formulated is also applicable to small ratios of L_b/L_c.

All of the methods investigated had the dimensional term $\frac{\sqrt{EI_yGJ}}{L}$ in the equation. The difference between the equations for the different methods was the non-dimensional term of the equation. In SANS 10162-1, the non-dimensional parameter is the effective length factor k. It is concluded that the method of determining the LTB capacity could be refined by adjusting the non-dimensional parameter. For this study, it proved beneficial to use a non-dimensional buckling parameter instead of effective length factors.

7.1.2   CONCLUSIONS BASED ON EXPERIMENTS AND FE ANALYSES

Essa and Kennedy (1994), amongst others, proved that FEA is a viable option in determining the LTB capacity of an overhang beam. One setback using FE models with shell elements was the lack of torsional stiffness. The technique described by Maljaars *et al.* (2004) in which torsional springs are added to simulate the required torsional stiffness, were used. This method improved the modelling of the torsional stiffness of the beam, *but* the buckling capacity was still underestimated (when compared to Abaqus solid element models and existing methods). Instead, solid elements were used for the parametric study. The FE solid element models (Abaqus) were calibrated to the physical experiments with a maximum difference in critical moment of 3.2 %. It is concluded that the best technique to model FE problems for LTB is to use solid element models.

The results of the physical experiments were slightly larger than predicted by the FE shell element analyses; due to the underestimation of FE shell elements; the additional stiffness in the beam setup; and the imperfections in the beams. Stiffening effects (increased warping resistance) from the supports in the physical setup increased the critical moment of the beams. Additionally, most of the beams had slightly larger cross-section than the nominal dimensions given in SASCH.

It is concluded, based on FE solid element results, that the buckling capacity is reduced when the load is applied to the top flange; the ratio of L_b/L_c is increased; and the overhang length L_c is increased. Regarding top flange loading, it is observed that the reduction in buckling capacity diminishes as L_b/L_c increases. The adjacent span therefore has an effect on the LTB capacity of overhang beams.

The segment in which buckling occurs depends on the ratio of L_b/L_c. Buckling occurs in the overhanging and backspan segment for $L_b/L_c < 1$ and $L_b/L_c \geq 1.5$, respectively. With the two spans being equal in length, buckling occurs in both segments. When $L_b/L_c > 2.0$, the capacity of the backspan can be calculated using the simply supported formula presented by SANS 10162-1 (Eq. 3.2).

7.1.3   PROPOSED DESIGN METHOD

The closed form solution of an I-section beam with lateral and torsional restraints and under uniform bending can be written as follow:

$$M_{cr} = \frac{\pi}{L} \sqrt{EI_y} \sqrt{GJ + \frac{\pi^2 EC_w}{L^2}}$$

The solution can be transformed to take the following term:

$$M_{cr} = \gamma \frac{\pi}{L} \sqrt{EI_y GJ}$$

Where:

M_{cr} = Critical moment of the overhang beam (N.m).

γ = $\sqrt{1+K}$, Buckling parameter

K = $\pi^2 E C_w / L^2 GJ$, Torsional parameter

Current methods have extended the above solution for single and double span beams of different boundary and loading conditions by applying different structure of the γ factor being a function of more than the K parameter only. The extended solutions do not include the backspan to overhang ratio L_b/L_c. A renamed and extended form of the factor γ is proposed, specifically formulated for overhang beams:

$$S = AK^{(B+1)} + C$$

Where:

A, B & C = Second degree polynomial functions of L_b/L_c and is defined in Tables 7.1 and 7.2.

The proposed design method was validated using experimental investigations and verified by FE analysis. The length of the beam L is replaced by the overhang length L_c when determining M_{cr}.

Table 7.1: Design equation factors for universal beams.

Factor	Universal beams	
	Shear centre	**Top flange**
A	$-0.121(L_b/L_c)^2 - 0.2(L_b/L_c) + 1.89$	$+0.023(L_b/L_c)^2 - 0.162(L_b/L_c) + 0.91$
B	$+0.044(L_b/L_c)^2 - 0.205(L_b/L_c) - 0.7$	$+0.03(L_b/L_c)^2 - 0.2(L_b/L_c) - 1.206$
C	$+0.033(L_b/L_c) + 0.016$	$+0.016(L_b/L_c) + 0.07$

Table 7.2: Design equation factors for IPE beams.

Factor	IPE beams	
	Shear centre	**Top flange**
A	$-0.136(L_b/L_c)^2 - 0.11(L_b/L_c) + 1.8$	$+0.069(L_b/L_c)^2 - 0.225(L_b/L_c) + 1.12$
B	$+0.023(L_b/L_c)^2 - 0.15(L_b/L_c) - 0.75$	$+0.121(L_b/L_c)^2 - 0.266(L_b/L_c) - 0.99$

The design equation eliminates the need for a designer to use FE modelling to determine the buckling capacity of a specialised high-risk overhang beam, thus simplifying the procedure. In addition, having a single equation that encapsulates the load height; the overhang length; the backspan to overhang ratio; and the beam size standardises the method in calculating the critical moment of an overhang beam.

The design equation is valid for IPE and Universal I-beams in the elastic range. The design equation was calibrated for beams having a torsional parameter between $0.2 \leq K \leq 2.7$. In addition, the design equation and its factors are applicable only to overhang beams with lateral and torsional supports and loaded with a point force at the free end. The design equation provides the critical buckling moment of the beam. The critical buckling moment is subjected to partial load or material factors to obtain the design buckling capacity.

To conclude, the design equation allows for the determination of the buckling capacity of overhang beams with various overhanging and backspan lengths via fairly simple calculations. Thus, the need for FE modelling for uniform, symmetrical, laterally unbraced overhang beams not prone to distortional buckling is reduced.

7.2   RECOMMENDATIONS FOR FUTURE WORK

This investigation focused on the effect the adjacent span has on the buckling capacity of an overhang beam by using a concentrated point load at the free end and lateral and torsional supports. The scope of work can be expanded by changing the support and loading conditions. It will be beneficial to compare the buckling capacity for different support and loading conditions.

Another aspect of loading that was not considered is bottom flange loading. In theory, this should increase the buckling capacity of the overhang beam, but this is a special case, which is mostly used in overhead trolleys (pulleys). For the manufacturing sector, this could be of importance and remains a scope for a study.

As was observed during experimental testing, an initial twist of the beam had an influence on the buckling capacity of the beam. In future work, the equations obtained by this study could be modified to incorporate an initial twist.

As observed in this study, a tapered beam increased the buckling capacity. It will be beneficial to determine the buckling capacity of tapered overhang beams.

Finally, the FE models were calibrated to the experimental results using $IPE_{AA}100$ beams. It will be beneficial to test larger beams experimentally and compare these results to the FE models and the equations to verify the accuracy when using larger beams.

The beams in this study were all unbraced. A scope of study includes the determination of the buckling capacity for various backspan to overhang ratios of braced overhang beams.

8. REFERENCES

Aalberg, A. 2015. Experimental and numerical parametric study on the capacity of coped beam ends. *Journal of Constructional Steel Research,* Vo 113, October, pp 146-155.

Andrade, A. Camotim, D. and Costa, P.P. 2007. On the evaluation of elastic critical moments in doubly and singly symmetric I-section cantilevers. *Journal of Constructional Steel Research,* Vol 63, No 7, July, pp 894-908.

Attard, M.M. 1983. Extrapolation techniques for buckling loads. *Journal of Structural Engineering,* Vol 109, No 4, pp 926-935.

Bradford, M.A. 1992. Lateral-distortional buckling of steel I-section members. *Journal of Constructional Steel Research.,* Vol 23, No 1-3, pp 97-116.

Bradford, M.A. 1994. *Elastic distortional buckling of overhanging beams.* The University of New South Wales. UNICIV Report No R-337. Sydney.

Bradford, M.A. and Wee, A. 1994. Analysis of buckling tests on beams on seat supports. *Journal of Constructional Steel Research,* Vol 28, No 3, pp 227-242.

BS 5950-1:2000. 2008. *Structural use of steelwork in building - Part 1.* London: British Standards.

CAN/CSA-S16-01. 2004. *Handbook of Steel Construction.* 8th ed. Canadian Institute of Steel Construction, Toronto.

Dessouki, A.K. Ibrahim, S.A. and El-Sa'eed, S.A. 2015. Experimental and finite element study on the inelastic lateral buckling behavior of coped I-beams. *HBRC Journal,* Vol 11, No 3, pp 339-352.

Dowswell, B.O. 2004. Lateral-torsional buckling of wide flange cantilever beams. *Engineering Journal*, No 3, pp 135-147.

Driver, R.G. 2014. Beams. In R.G. Driver *Steel Design Course*. July. Edmonton, Canada: University of Alberta.

Essa, H.S. and Kennedy, D.J.L. 1993. *Distortional buckling of steel beams.* University of Alberta. Edmonton.

Essa, H.S. and Kennedy, D.J.L. 1994. Design of cantilever steel beams: Refined approach. *Journal of Structural Engineering,* Vol 120, No 9, September, pp 2623-2636.

Galambos, T.V. 1968. *Structural members and frames.* Prentice Hall, Englewood Cliffs.

ISO 6892-1. 2009. *Metallic materials – Tensile testing – Part 1: Method of test at room temperature.* European Committee for Standardization, Brussels.

Kirby, P.A. and Nethercot, D.A. 1979. *Design for Structural Stability.* Halsted Press, New York.

Mac Donald, B.J. 2013. *Practical Stress Analysis with Finite Elements.* 2nd ed. Glasnevin Publishing, Dublin.

Mahachi, J. 2013. *Design of structural steelwork to SANS 10162.* 3rd ed. Xsi-tek, Randburg.

Maljaars, J. Stark, J.W.B. and Steenbergen, H.M.G.M. 2004. Buckling of coped steel beams and steel beams with partial endplates. *HERON,* Vol 49, No 3, pp 233-271.

Nethercot, D.A. 1973. The effective lengths of cantilevers as governed by lateral buckling. *The Structural Engineer,* Vol 51, No 5, pp 161-168.

Nethercot, D. and Rockey, K.C. 1971. A Unified Approach to the Elastic Lateral Buckling of Beams. *The Structural Engineer,* Vol 49, No 7, July, pp 945-949.

Nethercot, D.A. and Trahair, N.S. 1976. Lateral Buckling Approximations for Elastic Beams. *The Structural Engineer,* Vol 54, No 6, pp 197-204.

Ozbasaran, H. Aydin, R. and Dogan, M. 2015. An alternative design procedure for lateral-torsional buckling of cantilever I-beams. *Thin-Walled Structures,* Vol 90, May, pp 235-242.

Pandey, M.D. and Sherbourne, A.N. 1990. Elastic, lateral-torsional stability of beams: general considerations. *Journal of Structural Engineering,* Vol 116, No 2, February, pp 317-335.

Papangelis, J.P. Trahair, N.S. and Hancock, G.J. 1998. Elastic flexural-torsional buckling of structures by computer. *Computers and Structures,* Vol 68, No 1-3, July, pp 125-137.

Salmon, C.G. Johnson, J.E. and Malhas, F.A. 2009. *Steel structures design and behaviour.* 5th ed. Pearson Prentice Hall, Upper Sadle River.

Salvadori, M.G. 1955. Lateral buckling of I-beams. *ASCE Transaction,* Vol 120, pp 1165-1177.

SAISC. 2013. Southern African Steel Construction Handbook. 8th ed. SAISC, Johannesburg.

SANS 10162-1. 2011. *The structural use of steel – Part 1: Limit-states design of hot-rolled steelwork.* South African Bureau of Standards, Pretoria.

Schmitke, C.D. and Kennedy, D.J.L. 1984. *Effective Lengths of Laterally Unsupported Steel Beams.* University of Alberta. Structural Engineering Report No. 118. Edmonton.

Timoshenko, S.P. and Gere, J.M. 1961. *Theory of Elastic Stability.* McGraw-Hill, New York.

Trahair, N.S. 1963. The effective lengths of simply supported rolled steel joists. *Journal of the Institution of Engineers. Australia,* Vol 36, No 6, pp 121.

Trahair, N.S. 1983. Lateral Buckling of Overhanging Beams. *Instability and Plastic Collapse of Steel Structures.* Ed L. J. Morris. Granada Publishing, London, pp 503-515.

Trahair, N.S. 1993. *Flexural-Torsional Buckling of Structures.* CRC Press, Boca Raton.

Trahair, N.S. 2010. Steel cantilever strength by inelastic lateral buckling. *Journal of Constructional Steel Research,* Vol 66, No 8-9, August-September, pp 993-999.

Trahair, N.S. Bradford, M.A. Nethercot, D.A. and Gardner, L. 2008. *The behaviour and design of steel structures to EC3.* 4th ed. Taylor & Francis, New York.

Ziemian, R. 2010. *Guide to Stability Design Criteria for Metal Structures.* 6th ed. John Wiley & Sons. Hoboken.

Zirakian, T. and Showkati, H. 2007. Experiments on Distorional Buckling of I-beams. *Journal of Structural Engineering,* Vol 133, No 7, July, pp 1009-1017.
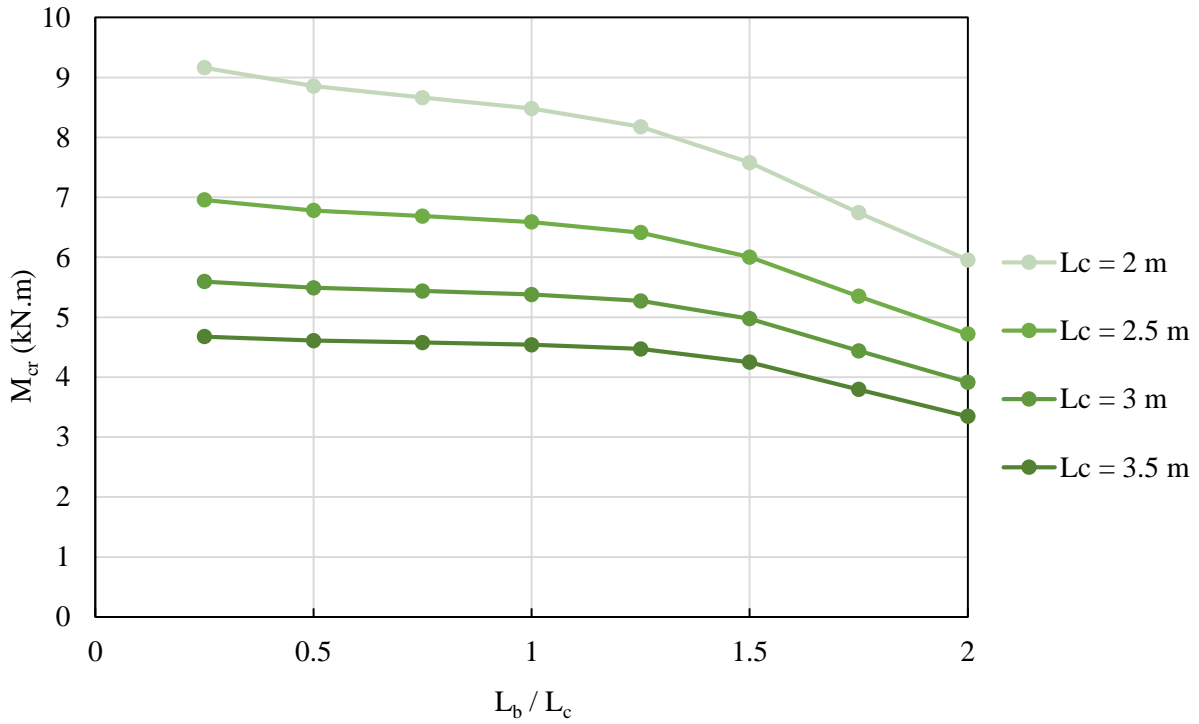
APPENDIX A: FE ANALYSIS RESULTS

IPE$_{AA}$100:

Figure A.1: Critical buckling moments for IPE$_{AA}$100 overhang beam with shear centre loading.
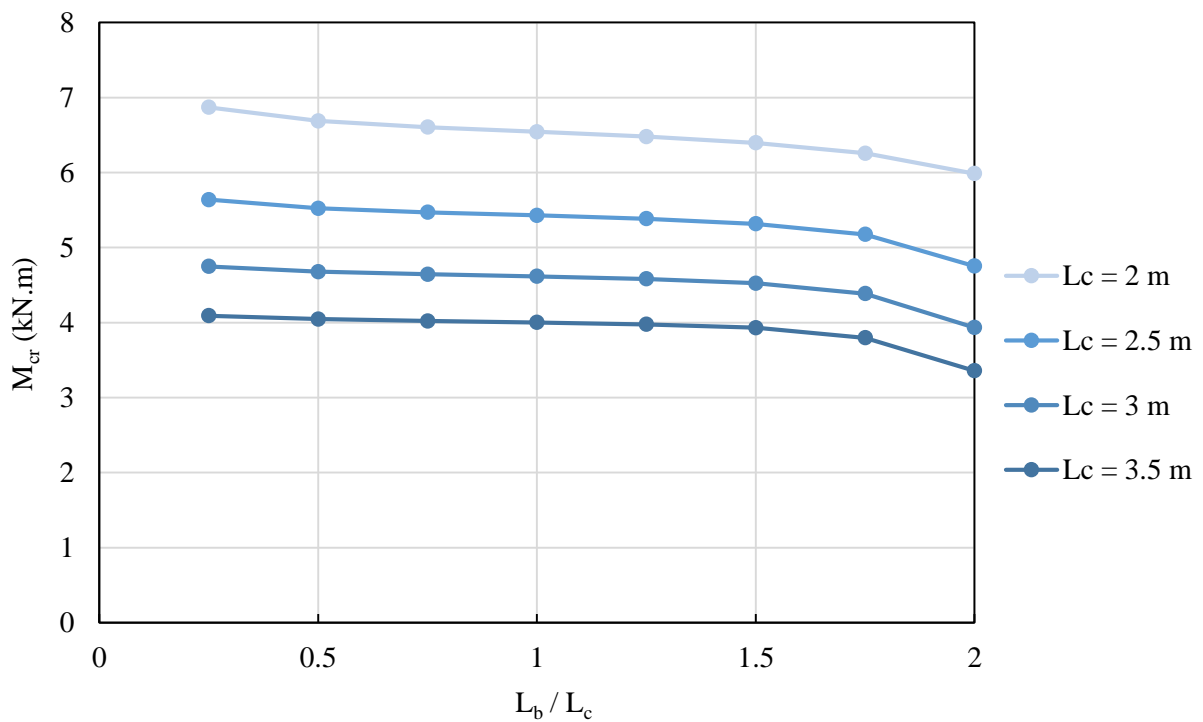

Figure A.2: Critical buckling moments for IPE$_{AA}$100 overhang beam with top flange loading.
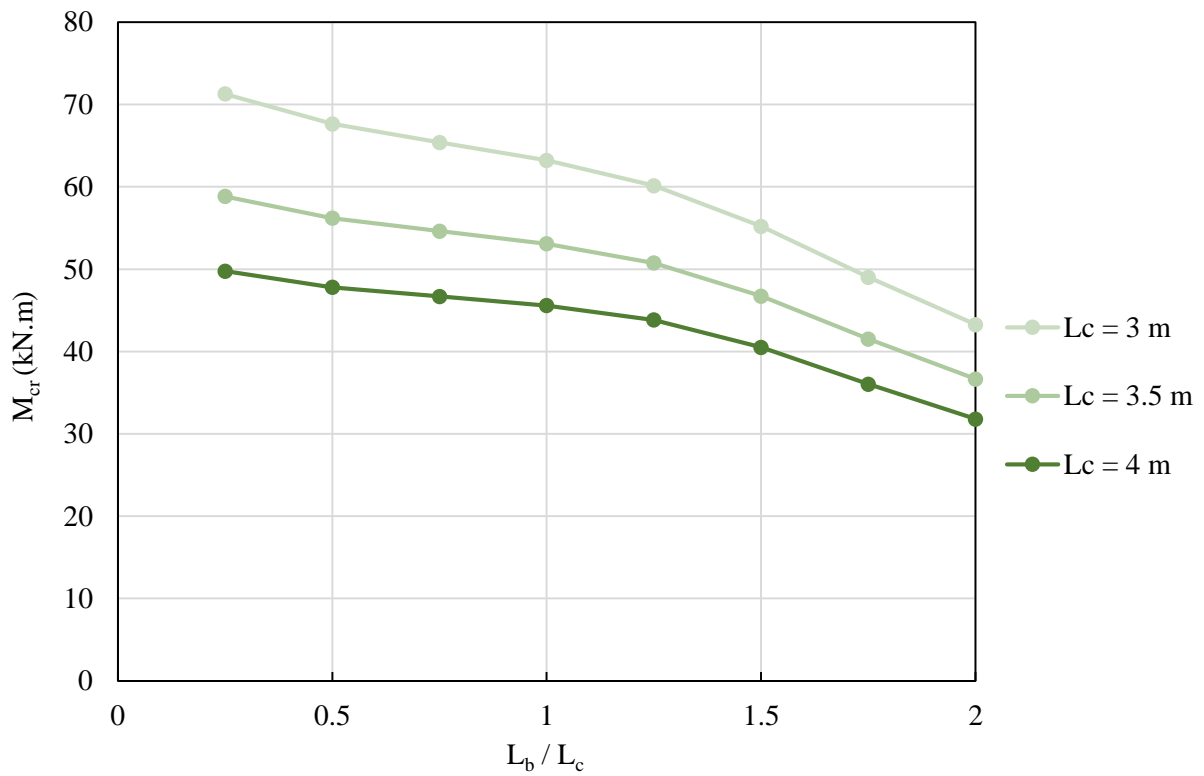
IPE 200:

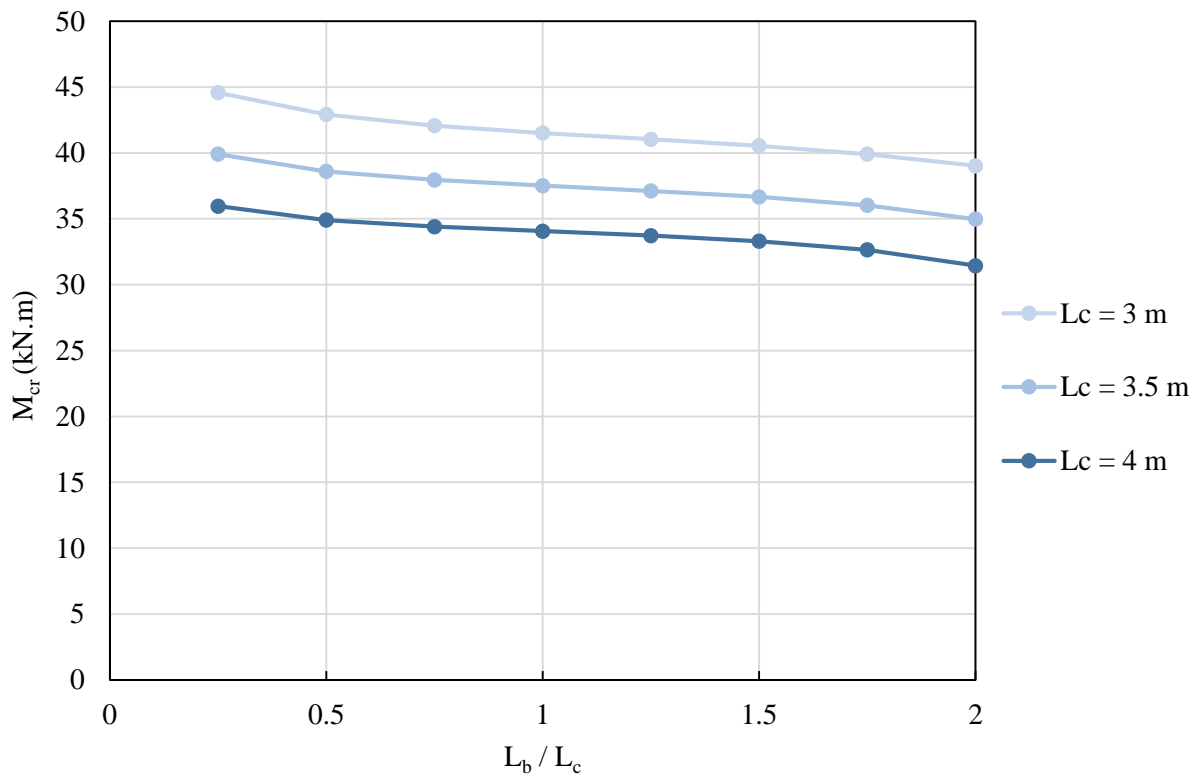Figure A.3: Critical buckling moments for IPE 200 overhang beam with shear centre loading.

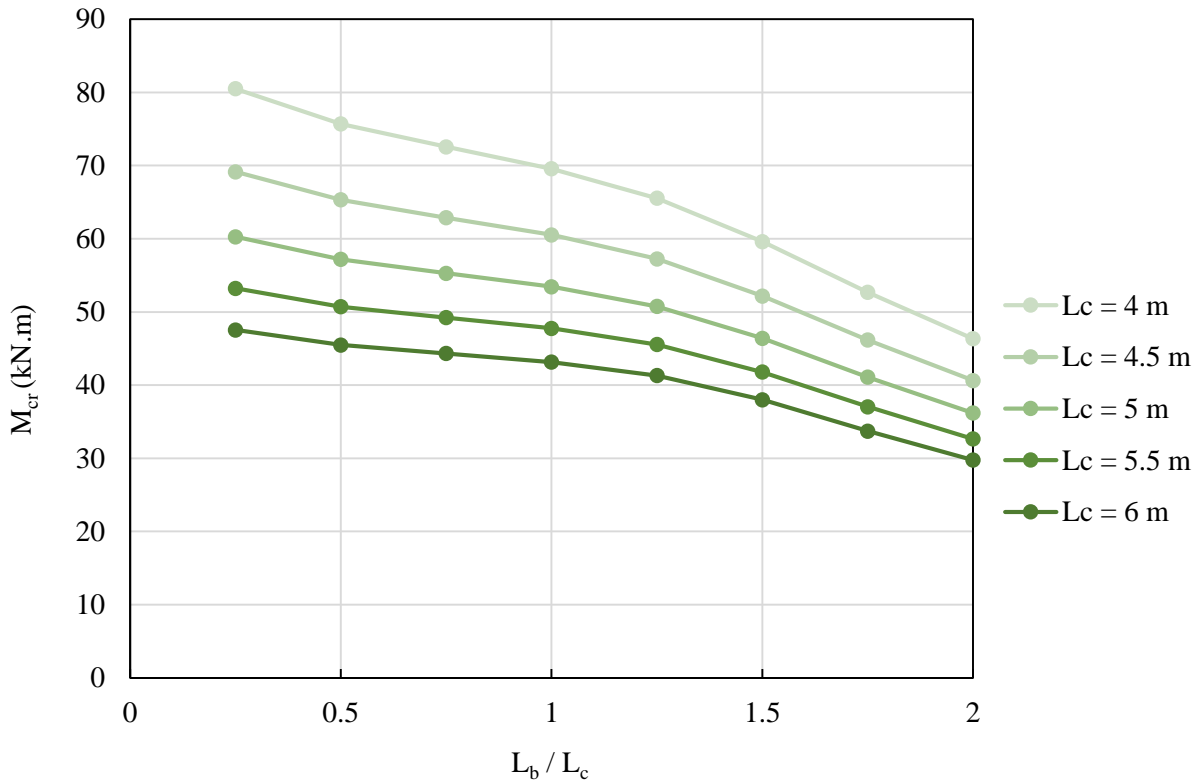Figure A.4: Critical buckling moments for IPE 200 overhang beam with top flange loading.

203x133x25:

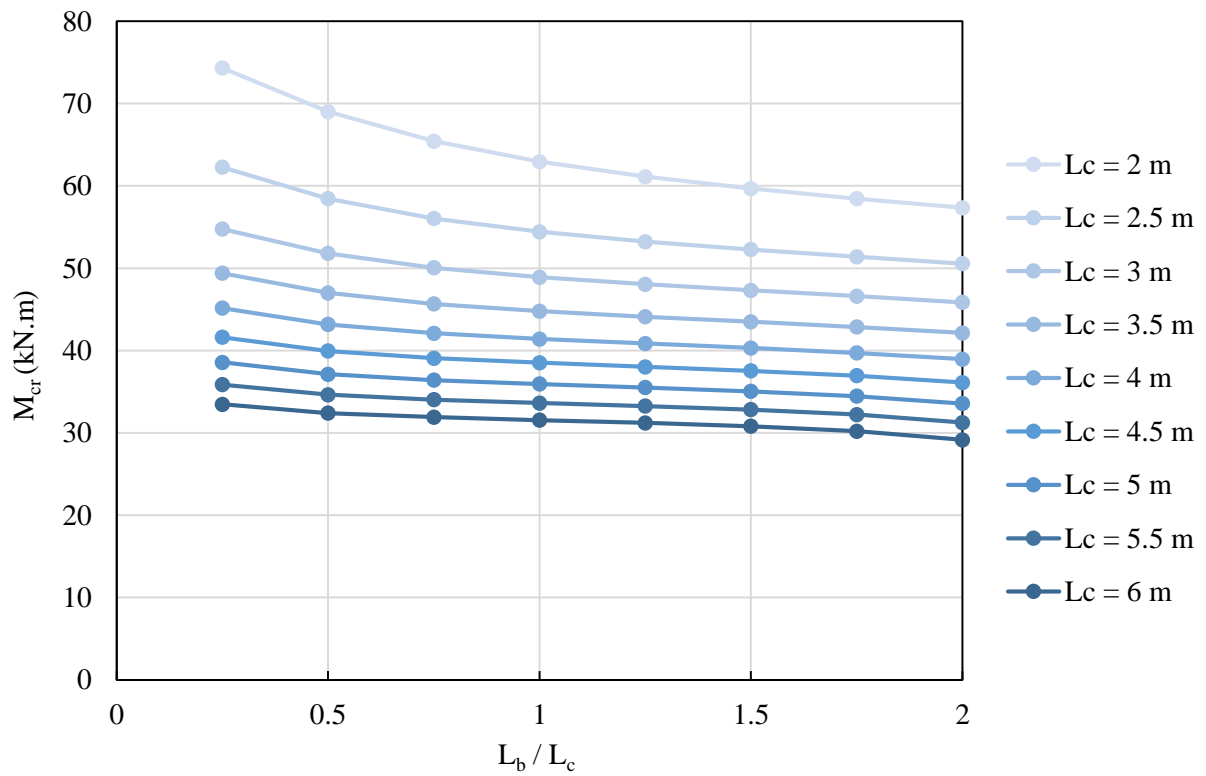Figure A.5: Critical buckling moments for 203x133x25 overhang beam with shear centre loading.

Figure A.6: Critical buckling moments for 203x133x25 overhang beam with top flange loading.
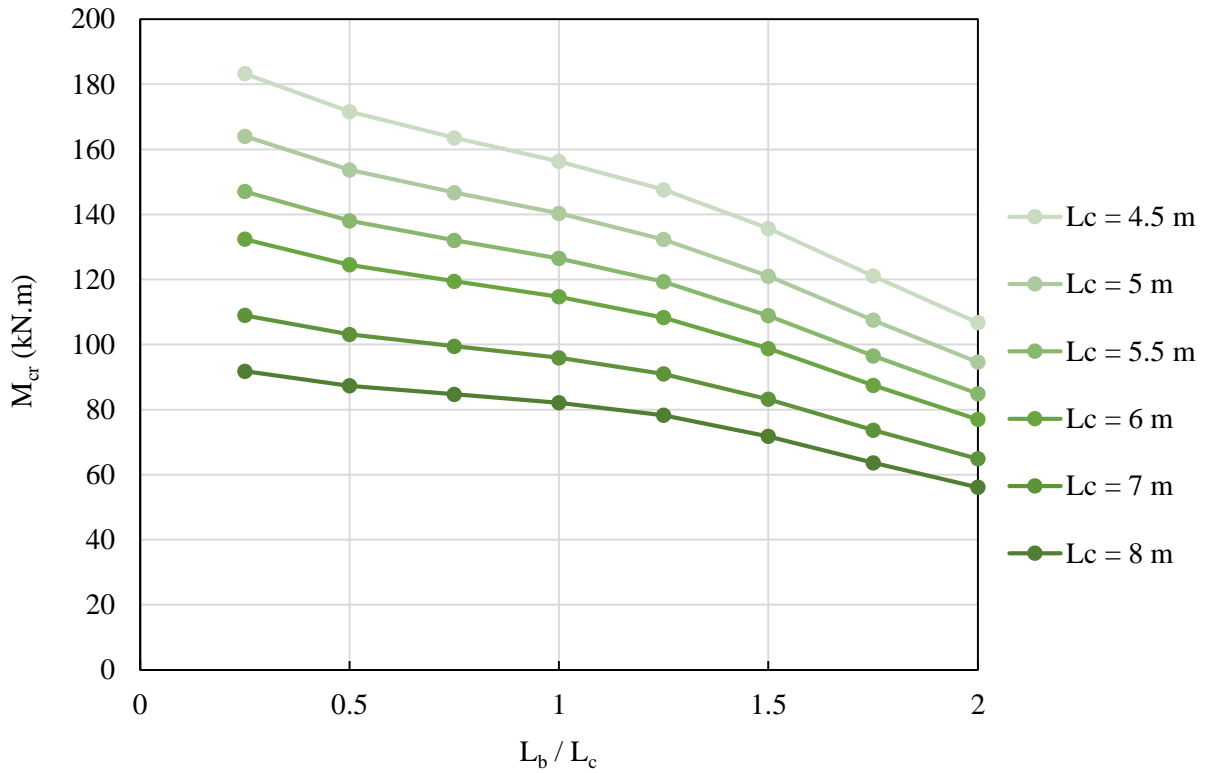
305x165x40:

Figure A.7: Critical buckling moments for 305x165x40 overhang beam with shear centre loading.
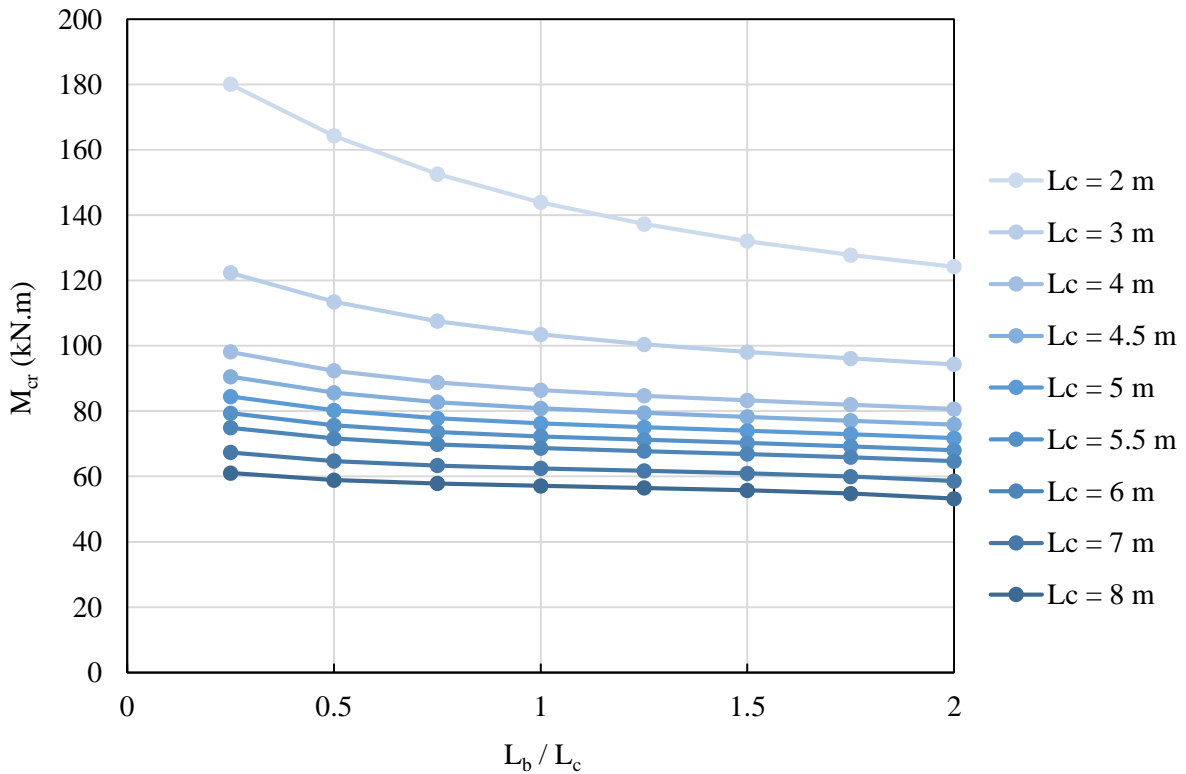

Figure A.8: Critical buckling moments for 305x165x40 overhang beam with top flange loading.
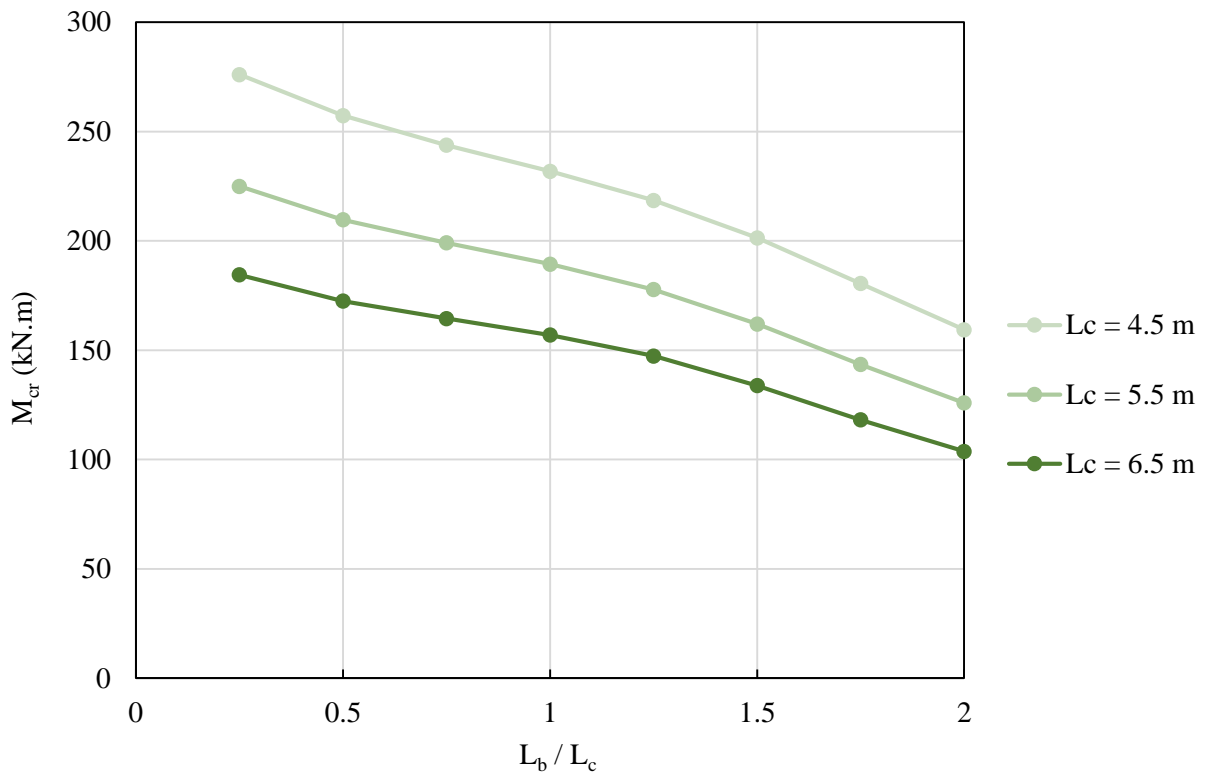
406x178x54:

Figure A.9: Critical buckling moments for 406x178x54 overhang beam with shear centre loading.
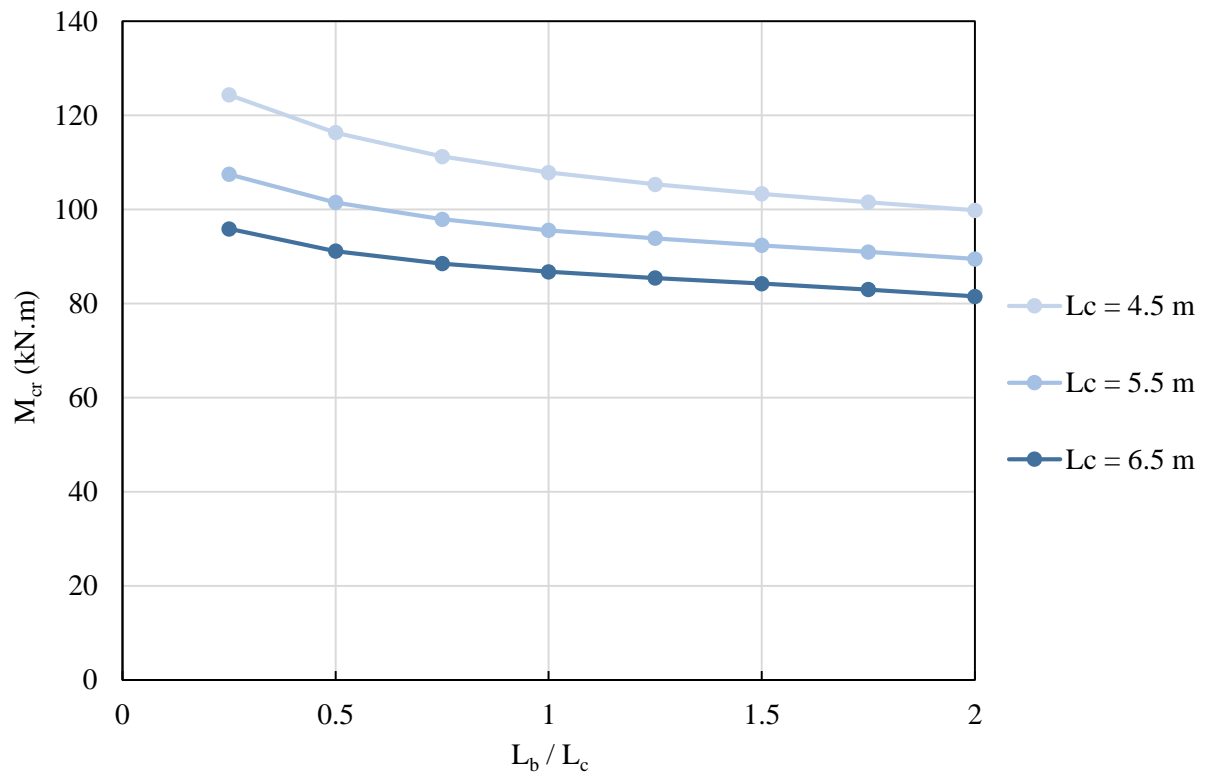

Figure A.10: Critical buckling moments for 406x178x54 overhang beam with top flange loading.
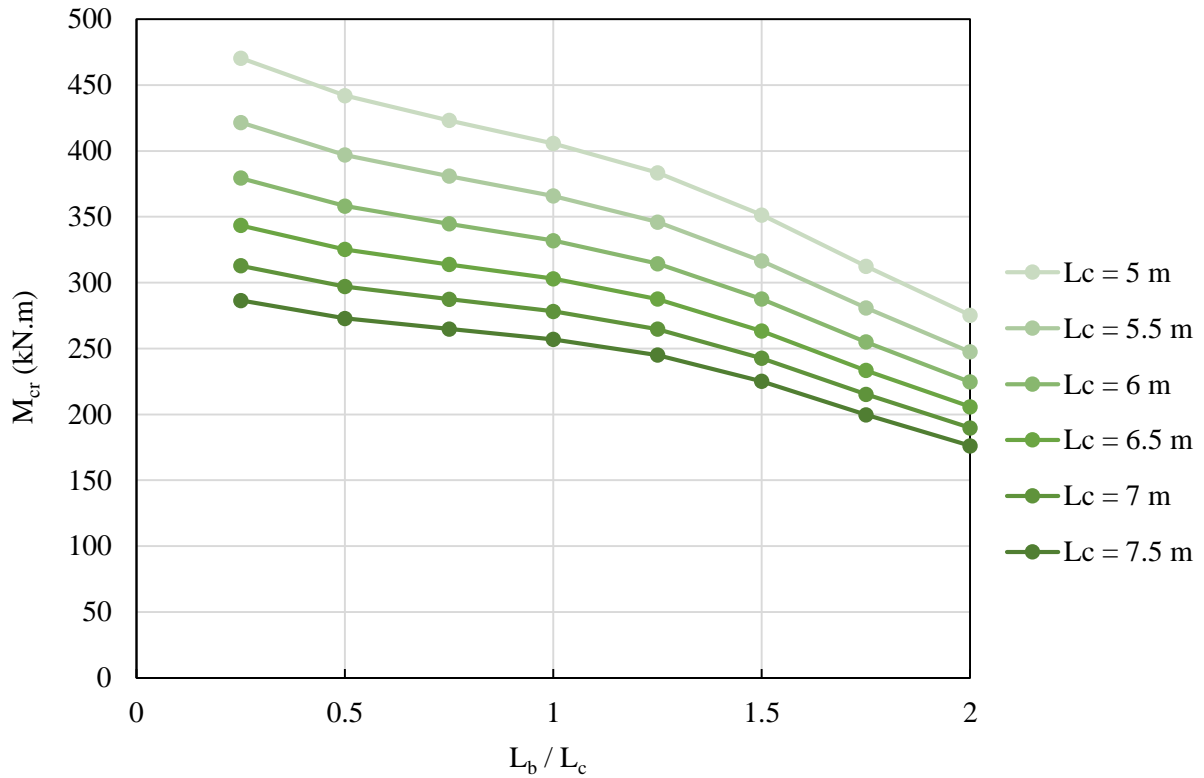
406x178x74:

Figure A.11: Critical buckling moments for 406x178x74 overhang beam with shear centre loading.
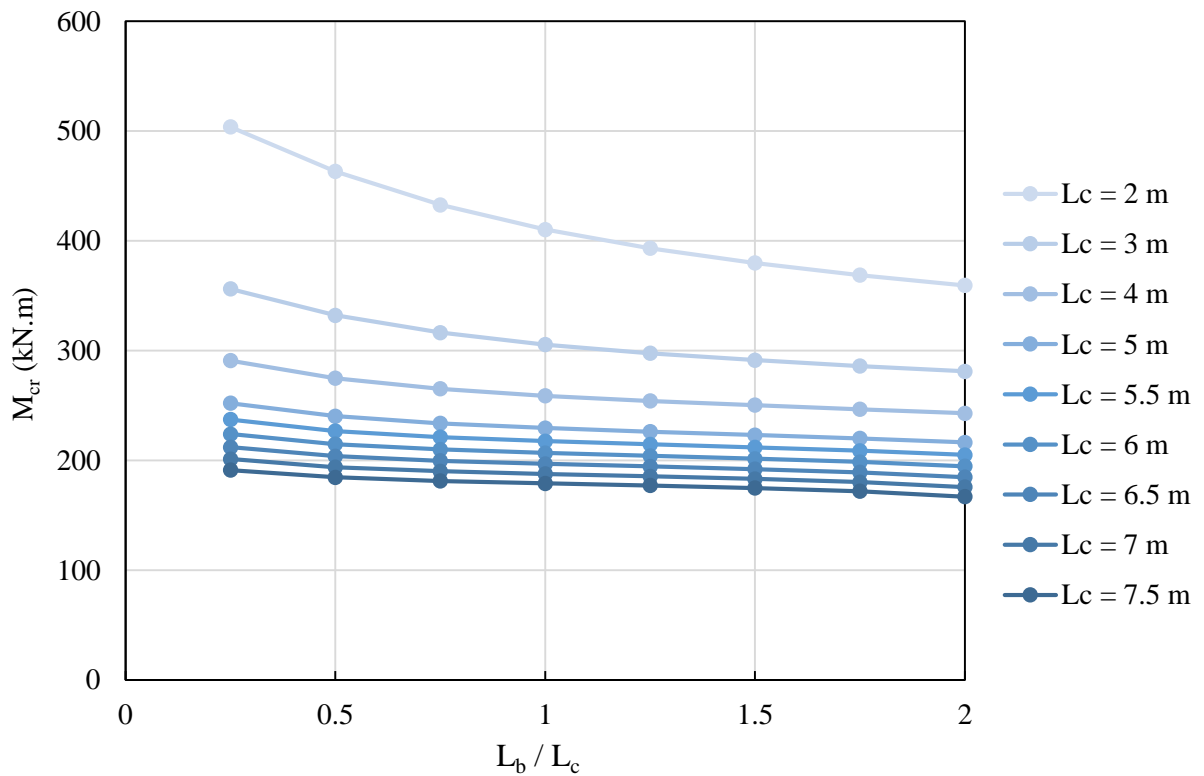

Figure A.12: Critical buckling moments for 406x178x74 overhang beam with top flange loading.

533x210x82:

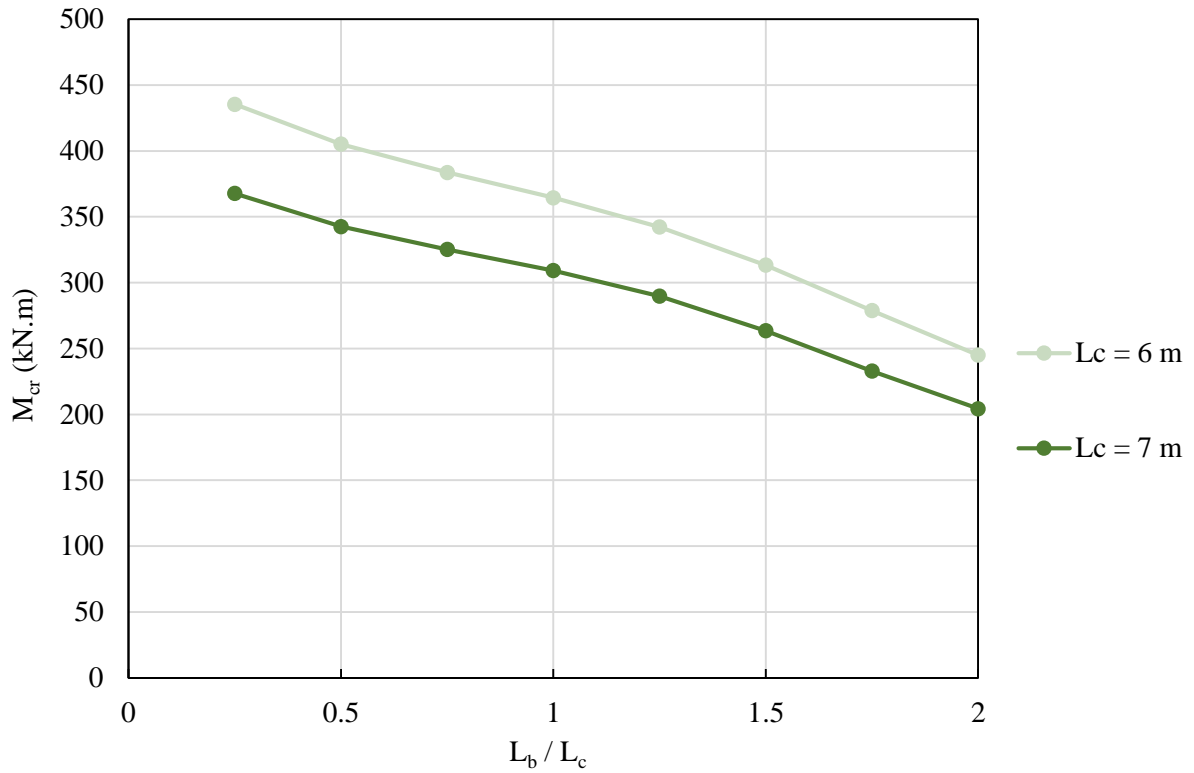Figure A.13: Critical buckling moments for 533x210x82 overhang beam with shear centre loading.
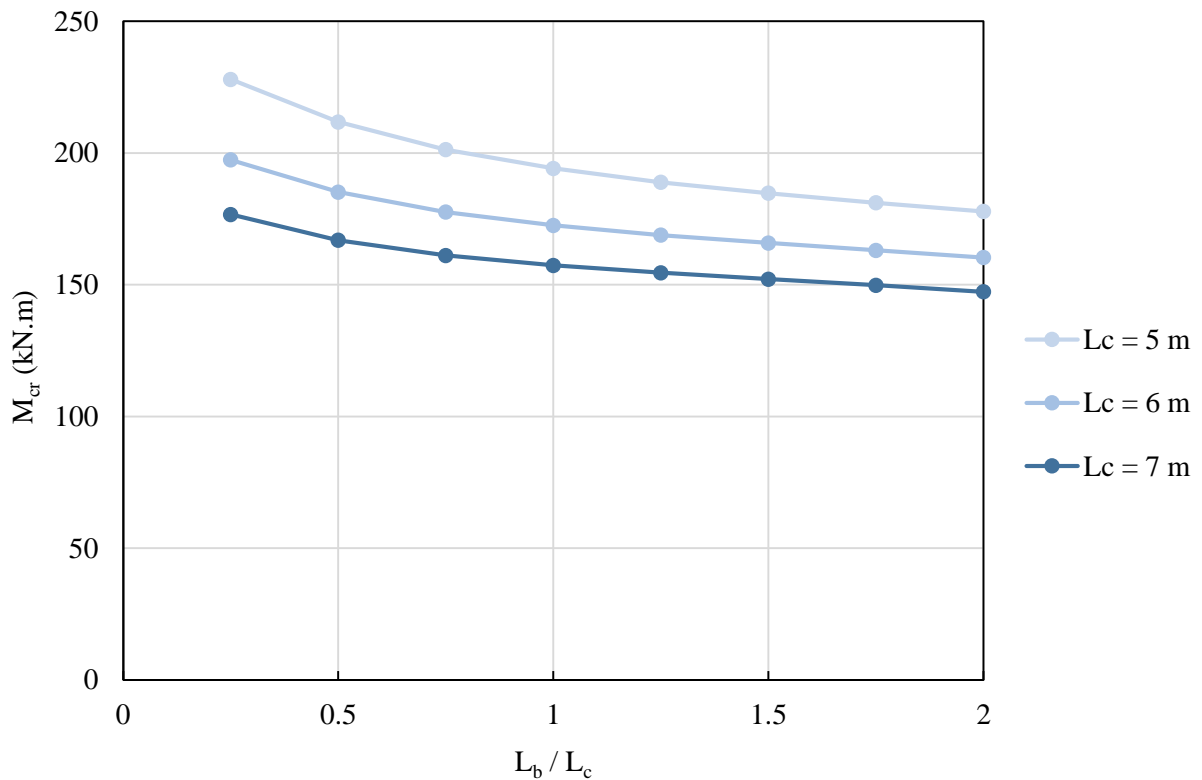

Figure A.14: Critical buckling moments for 533x210x82 overhang beam with top flange loading.
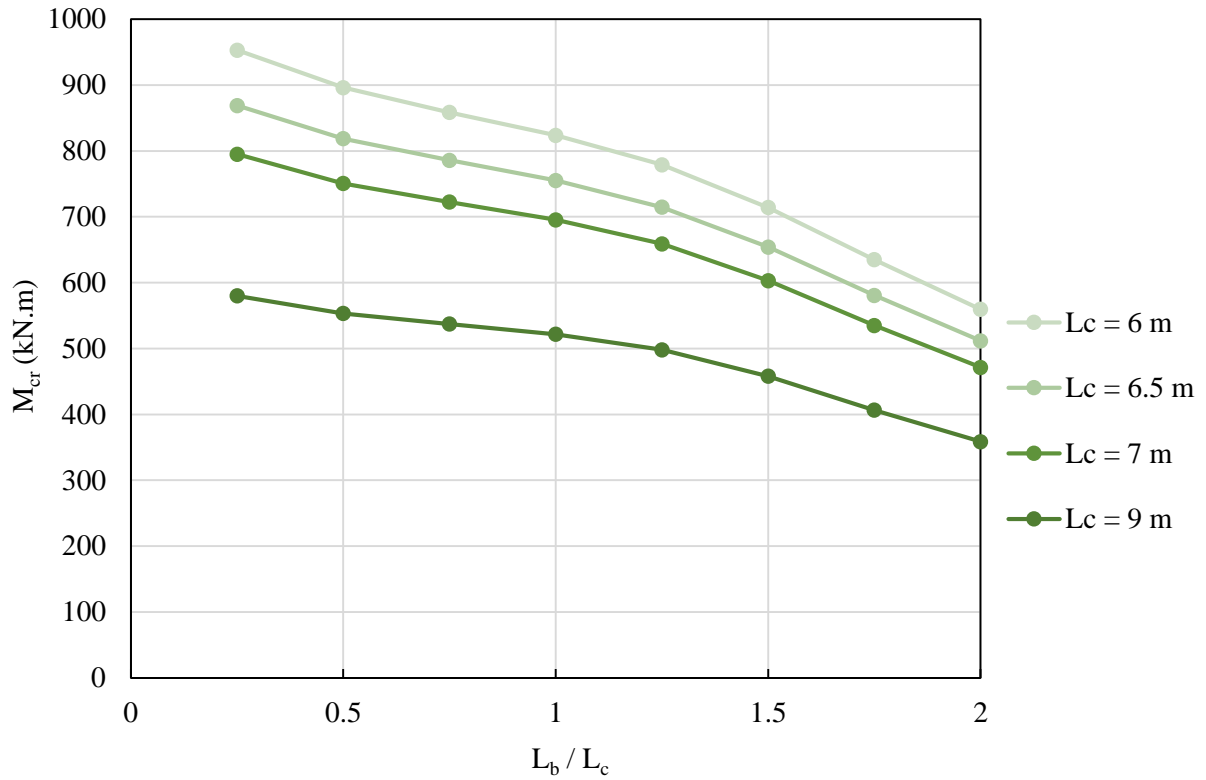
533x210x122:

Figure A.15: Critical buckling moments for 533x210x122 overhang beam with shear centre loading.
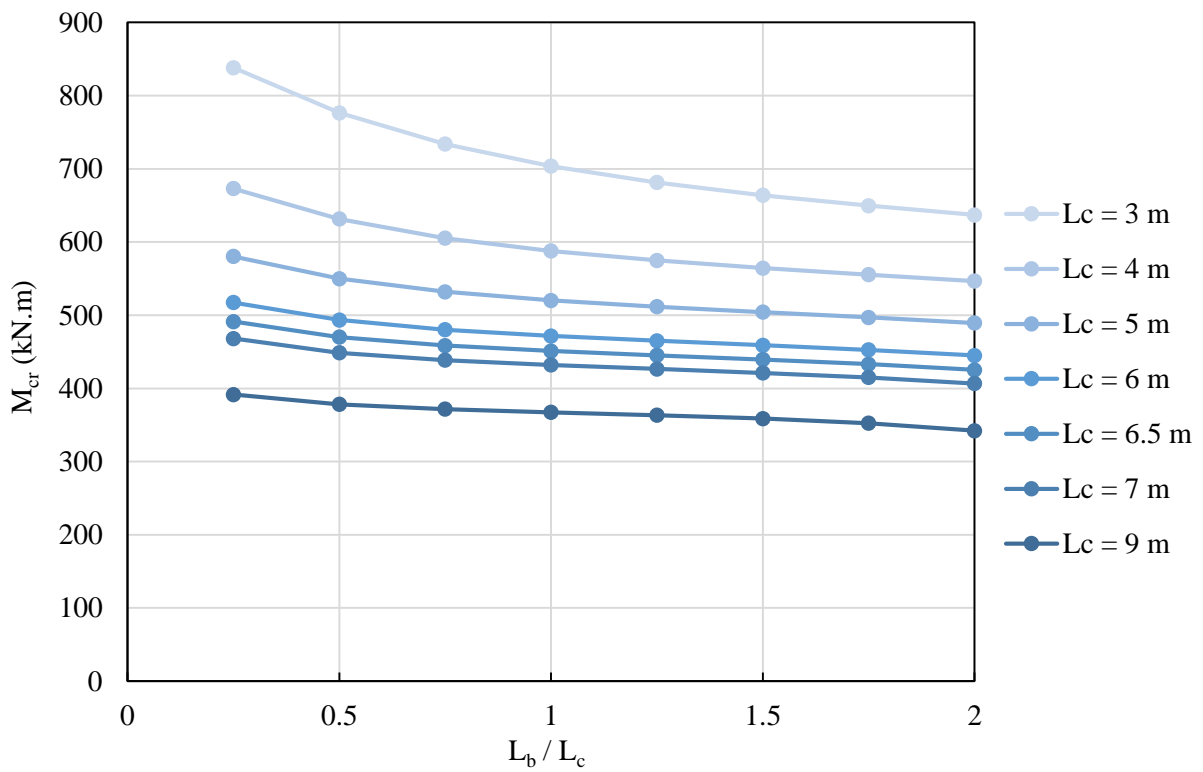

Figure A.16: Critical buckling moments for 533x210x122 overhang beam with top flange loading.

APPENDIX B: THE SANS 10162-1 METHOD

The following Appendix is an excerpt from the South African code 'SANS 10162-1'.

The South African National Standard for the use of structural steel (10162-1) specifies that the critical moment of an unbraced member be:

$$M_{cr} = \frac{\omega_2 \pi}{KL} \sqrt{EI_y GJ + \left(\frac{\pi E}{KL}\right)^2 I_y C_w}$$

Where:

M_{cr} = Critical elastic moment of an unbraced member.

ω_2 = Equivalent moment factor.

K = Effective length factor.

L = Length of beam between restraints.

E = Elastic modulus of steel.

I_y = Moment of inertia about y-axis.

G = Shear modulus of steel.

J = St. Venant torsion constant of a cross-section.

C_w = Warping torsional constant.

It should be noted that this equation is based on a simply supported beam. To account for built-in cantilevers and overhang beams, effective length factors are used. These effective length factors are provided in Table B.1. In addition, L shall be taken as the projecting length.

Table B.1: Effective length factors for built-in cantilevers and overhang beams (SABS, 2011).

Restraint conditions		Loading conditions	
At support	At tip	Normal	Destabilising [a]
Built in laterally and torsionally	Free	0.8L	1.4L
	Lateral restraint only (at compression flange)	0.7L	1.4L
	Torsional restraint only	0.6L	0.6L
	Lateral and torsional restraint	0.5L	0.5L

	Free	1.0L	2.5L
Continuous, with lateral and torsional restraint	Lateral restraint only (at compression flange)	0.9L	2.5L
	Torsional restraint only	0.8L	1.5L
	Lateral and torsional restraint	0.7L	1.2L
Continuous, with lateral restraint only	Free	3.0L	7.5L
	Lateral restraint only	2.7L	7.5L
	Torsional restraint only	2.4L	4.5L
	Lateral and torsional restraint	2.1L	3.6L
[a] The destabilising loading condition applies when the load is applied to the tension flange of the beam and both the load and the flange are free to move laterally.			

The equivalent moment factor ω_2 is equal to 1.0 for cantilevers and overhang beams as there are no effective lateral support for the compression flange at one of the ends of the supported length.

The factored moment resistance of doubly symmetric class 1 and 2 sections are as follows:

i)　　　When $M_{cr} > 0.67 M_p$

$$M_r = 1.15 \, \phi M_p \left(1 - \frac{0.28 M_p}{M_{cr}}\right) < \phi M_p$$

ii)　　　When $M_{cr} \leq 0.67 M_p$

$$M_r = \phi M_{cr}$$

Where:

ϕ　　　= 0.9, Resistance factor for structural steel.

M_p　　　= Plastic moment.

M_r　　　= Factored moment resistance.

M_{cr}　　　= Critical elastic moment.

APPENDIX C: NOMINAL DIMENSIONS OF BEAMS

The following Appendix tabulates the nominal dimensions of the beams used throughout this study. The dimensions are based on SASCH (2013).

Table C.1: Nominal dimensions of beams (mm).

Beam designation	h	b	t_w	t_f	r_1	h_w
IPE$_{AA}$100	97.6	55	3.6	4.5	7	74.6
IPE 200	200	100	5.6	8.5	12	159
203x133x25	203.2	133.2	5.7	7.8	7.6	172
305x165x40	303.8	165.1	6.1	10.2	8.9	266
406x178x54	402.6	177.6	7.6	10.9	10.2	360
406x178x74	412.8	179.7	9.7	16.0	10.2	360
533x210x82	528.3	208.7	9.6	13.2	12.7	476
533x210x122	544.6	211.9	12.8	21.3	12.7	477

h = Height of beam.

b = Width of flange.

t_w = Thickness of web.

t_f = Thickness of flange.

r_1 = Radius of fillet.

h_w = Height of web.

APPENDIX D: WORKED EXAMPLE

The following Appendix is a worked out example using the proposed design method. In addition, the proposed method is compared to the current SANS 10162-1 method using an equal spanned overhang beam (first example). The beam properties used for the examples are summarised in Table D1.

Table D1: Properties of beams.

Beam size	IPE$_{AA}$100	406x178x74
Load height	Top flange	Shear centre
Overhang length L_c	2.5 m	6 m
Backspan to overhang ratio L_b/L_c	1	1.5
Moment of inertia about y-axis I_y	0.126x10^6 mm^4	15.5x10^6 mm^4
Torsional constant J	7.33x10^3 mm^4	642x10^3 mm^4
Warping torsional constant C_w	0.272x10^9 mm^6	610x10^9 mm^6

Example 1: IPE$_{AA}$100:

Proposed design method:

For top flange loading: $A = +0.069(1)^2 - 0.225(1) + 1.12 = 0.964$

$$B = +0.121(1)^2 - 0.266(1) - 0.99 = -1.135$$

$$K = \sqrt{\frac{\pi^2 \times 200 \times 10^3 \times 0.272 \times 10^9}{77 \times 10^3 \times 7.33 \times 10^3 \times 2500^2}} = 0.39$$

$$S = AK^{(B+1)} = 0.964(0.39)^{(-1.135+1)} = 1.0947$$

$$M_{cr} = S\frac{\pi\sqrt{EI_yGJ}}{L_c} = 1.0947 \times \frac{\pi\sqrt{200 \times 10^3 \times 0.126 \times 10^6 \times 77 \times 10^3 \times 7.33 \times 10^3}}{2500}$$

$M_{cr} = 5188031$ N.mm

$\boldsymbol{M_{cr} = 5.2}$ **kN.m**   (Abacus = 5.4 kN.m)

SANS 10162-1 method:

$K = 2.5$ (Effective length factor)

$\omega_2 = 1$

$$M_{cr} = \frac{\omega_2 \pi}{KL} \sqrt{EI_y GJ + \left(\frac{\pi E}{KL}\right)^2 I_y C_w}$$

$$Mcr = \frac{\pi}{2.5(2500)} \times \sqrt{200 \times 0.126 \times 77 \times 7.33 \times 10^{15} + \left(\frac{\pi(200 \times 10^3)}{2.5 \times 2500}\right)^2 \times 0.126 \times 0.272 \times 10^{15}}$$

$Mcr = 1918634$ N.mm

$\boldsymbol{Mcr = 1.92}$ **kN.m**

The current SANS 10162-1 underestimates the buckling capacity significantly by enforcing a large effective length factor of 2.5 for top flange loading.

Example 2: 406x178x74:

Proposed design method:

For shear centre loading: $A = -0.121(1.5)^2 - 0.2(1.5) + 1.89 = 1.31775$

$B = +0.044(1.5)^2 - 0.205(1.5) - 0.7 = -0.9085$

$C = +0.033(1.5) + 0.016 = 0.0655$

$$K = \sqrt{\frac{\pi^2 \times 200 \times 10^3 \times 610 \times 10^9}{77 \times 10^3 \times 642 \times 10^3 \times 6000^2}} = 0.8226$$

$$S = AK^{(B+1)} + C = 1.31775(0.8226)^{(-0.9085+1)} + 0.0655 = 1.36$$

$$M_{cr} = S \frac{\pi \sqrt{EI_y GJ}}{L_c} = 1.36 \times \frac{\pi \sqrt{200 \times 10^3 \times 15.5 \times 10^6 \times 77 \times 10^3 \times 642 \times 10^3}}{6000}$$

$M_{cr} = 278760512$ N.mm

$\boldsymbol{M_{cr} = 278.8}$ **kN.m**   (Abaqus = 287.5 kN.m)

SANS 10162-1 method:

$K = 1$ (Effective length factor)

$\omega_2 = 1$

$$M_{cr} = \frac{\omega_2 \pi}{KL} \sqrt{EI_y GJ + \left(\frac{\pi E}{KL}\right)^2 I_y C_w}$$

$$Mcr = \frac{\pi}{1(6000)} \times \sqrt{200 \times 15.5 \times 77 \times 642 \times 10^{15} + \left(\frac{\pi(200 \times 10^3)}{1 \times 6000}\right)^2 \times 15.5 \times 610 \times 10^{15}}$$

$Mcr = 265403681$ N.mm

$\boldsymbol{Mcr = 265.4}$ **kN.m**

Table D2: Summary of results (kN.m).

Beam	Proposed design method	SANS 10162-1 method	Abaqus FE model
IPE$_{AA}$100 (Top flange)	5.2	1.92	5.4
406x178x74 (Shear centre)	278.8	265.4	287.5